BERICHTE
aus dem Fachbereich Geowissenschaften
der Universität Bremen

Nr. 113

Ziebis, W.

THE IMPACT OF THE THALASSINIDEAN SHRIMP CALLIANASSA TRUNCATA ON THE GEOCHEMISTRY OF PERMEABLE, COASTAL SEDIMENTS

Berichte, Fachbereich Geowissenschaften, Universität Bremen, Nr. 113,
158 Seiten, Bremen 1998

ISSN 0931-0800

BERICHTE
aus dem Fachbereich Geowissenschaften
der Universität Bremen

Nr. 113

Ziebis, W.

THE IMPACT OF THE THALASSINIDEAN SHRIMP CALLIANASSA TRUNCATA ON THE GEOCHEMISTRY OF PERMEABLE, COASTAL SEDIMENTS

Berichte, Fachbereich Geowissenschaften, Universität Bremen, Nr. 113,
158 Seiten, Bremen 1998

ISSN 0931-0800

Die "Berichte aus dem Fachbereich Geowissenschaften" werden in unregelmäßigen Abständen vom Fachbereich 5, Universität Bremen, herausgegeben.

Sie dienen der Veröffentlichung von Forschungsarbeiten, Doktorarbeiten und wissenschaftlichen Beiträgen, die im Fachbereich angefertigt wurden.

Die Berichte können bei:

Frau Gisela Boelen

Sonderforschungsbereich 261

Universität Bremen

Postfach 330 440

D 28334 BREMEN

Telefon: (49) 421 218-4124

Fax: (49) 421 218-3116

angefordert werden.

Zitat:

Ziebis, W.

The impact of the thalassinidean shrimp *Callianassa truncata* on the geochemistry of permeable, coastal sediments. Berichte, Fachbereich Geowissenschaften, Universität Bremen, Nr. 113, 158 Seiten, Bremen, 1998.

ISSN 0931-0800

THE IMPACT OF THE THALASSINIDEAN SHRIMP *CALLIANASSA TRUNCATA* ON THE GEOCHEMISTRY OF PERMEABLE, COASTAL SEDIMENTS

DISSERTATION
zur
Erlangung des Grades eines
Doktors der Naturwissenschaften
- Dr. rer. nat.

dem Fachbereich 5 der
Universität Bremen
vorgelegt von

Wiebke Ziebis

1997

Tag des Promotionskolloquiums: 11. 07. 1997

Erster Gutachter: Prof. Dr. B. B. Jørgensen (MPI)
Zweiter Gutachter: Prof. Dr. H. D. Schulz (FB 5)

Erster Prüfer: Prof. Dr. W. Arntz (FB 2)
Zweiter Prüfer: Prof. Dr. V. Spieß (FB 5)

PREFACE

Prof. Dr. B. B. Jørgensen encouraged and supervised this study which was supported by the Max-Planck-Society. Dr. Stefan Forster and Dr. Markus Huettel were put in charge to guide and supervise the different projects. This thesis consists of several chapters which have either been published or submitted for publication in international scientific journals.

Stefan Forster, Markus Huettel and I started together as the so called `flume group´ at the Max-Planck-Institute during its initial phase. As a sub-group of the biogeochemistry department we were interested in hydrodynamically and biologically influenced transport processes and geochemical processes in permeable sea beds. All three of us were interested in the advective transport of matter in permeable sea beds and the Mediterranean sediment inhabited densely by *Callianassa truncata* offered several ideas for detailed investigations. Studies in laboratory flow channels need the effort and enthusiasm of a group, thus investigations and experiments were carried out together with one person being in charge of the project.

The field investigations on the ecology and biology of the shrimp, the studies of the burrow system, in-situ measurements and sampling were carried out by myself. Underwater field work can not be carried out alone but is dependant on the help and assistance of others. Thus, at different stages of this study several people helped to carry out the underwater investigations, which is greatly acknowledged. Especially mentioned is the contribution of Thomas Pillen and Boris Unger who helped in constructing and deploying the diver observatory for in-situ investigations.

In the following I state my own contribution and that of my colleagues to the different chapters of this thesis. I was in charge of the project of advective oxygen transport described in chapter 1. The flow channel had been constructed by Markus Huettel with some modifications made. The experimental design was discussed with Markus Huettel and Stefan Forster. I carried out the experiments, the analytical work and wrote the manuscript. As a consequence of the first, the second project evolved, the investigation of the total oxygen uptake of the permeable sediment, which is described in Chapter 2. Stefan Forster was mainly responsable for carrying out the experiments and the analyses, he also wrote the manuscript. My contribution consisted in helping to establish the experimental design, assisting in laboratory work and contributing to the manuscript. Parallel to the studies of advective oxygen transport of project 1 and 2, Markus Huettel was investigating the advective particle transport in permeable sediments. I assisted with the experimental design and

contributed to the investigations and the preparation of the manuscript for Chapter 3. As the natural sediment inhabited with *Callianassa truncata* was kept under constant flow in a flow channel during the time between the projects, we made the observation of precipitates forming at the sediment surface adjacent to biogenic structures of mounds and funnels. This lead to the fourth project, the investigation of advective metal and nutrient transport, which was carried out by the three of us together. The effort of the experiments and the analytical work were shared. Dr. George Luther visiting our institute at the time of experiments contributed volumetric electrode measurements to this study. The writing was done by Markus Huettel with contributions of Stefan Forster and me.

Chapter 5 is a summary of the main aspects of the impact of the investigated shrimp on the geochemistry of the sea floor. This study focused on the deeper sediment layers. I carried out the in-situ investigations, measurements and sampling as well as the analytical work. Markus Huettel, Stefan Forster and Prof. Jørgensen critically supervised the work. I wrote the manuscript with constructive contributions of Prof. Jørgensen. In chapter 6 the technical aspects of direct measurements and in-situ sampling in subsurface sediments are described in detail. I was in charge of this project. Thomas Pillen and Boris Unger were constructing and deploying the diver observatory and helped with under water field work. I wrote the manuscript. The last chapter, was written by me and contains different aspects of the ecology and biology of *Callianassa truncata* . I conducted the field work, sampling, in-situ investigations, laboratory studies and analytical work.

TABLE OF CONTENTS

	Page
Introduction	1
1. Impact of biogenic sediment topography on oxygen fluxes in permeable sea beds Wiebke Ziebis, Markus Huettel, Stefan Forster	4
2. Impact of boundary layer flow on oxygen utilisation in coastal sediments Stefan Forster, Markus Huettel, Wiebke Ziebis	24
3. Flow-induced uptake of particulate matter in permeable sediments Markus Huettel, Wiebke Ziebis, Stefan Forster	45
4. Advective transport affecting metal and nutrient distribution and interfacial fluxes in permeable sediments Markus Huettel, Wiebke Ziebis, Stefan Forster, George Luther III	67
5. Complex burrows of the mud shrimp *Callianassa truncata* and their geochemical impact in the sea bed Wiebke Ziebis, Stefan Forster, Markus Huettel, Bo Barker Jørgensen	101
6. A diver observatory for in-situ studies in sublittoral sediments Wiebke Ziebis, Thomas Pillen, Boris Unger	111
7. Aspects of the biology and ecology of *Callianassa truncata* (Decapoda,Thalassinidea) from the Mediterranean Sea Wiebke Ziebis	124
Literature cited	142
Summary	156

INTRODUCTION

The exchange of particulate and dissolved matter between the sediment and the water column is fundamental to biological and geochemical processes in the ocean. The transport processes at the sediment-water interface play an important role in the remineralisation cycles of a marine environment. In a classical view the biogeochemical processes and associated microbial communities in the sea floor are stratified and depend on vertical transport processes. Among the chemical species being transferred between the water column and the sediment oxygen plays a key role. It is essential for aerobic life within the sediment and is energetically the most valuable electron acceptor for the mineralisation of organic compounds and the oxidation of reduced products from anaerobic mineralisation. In coastal sediments oxygen penetrates only a few millimeters into the sediment. In cohesive sediment the penetration depth is regulated by the dynamic balance between diffusion from the overlying water and the rapid consumption in the sea bed. Macrofauna organisms inhabiting the sea bed strongly affect the sediment structure and thus influence the chemical zonation pattern and the exchange processes across the sediment water interface. The animal-generated ventilation of burrow systems introduces oxic water into deeper sediment layers and the transport of solutes across burrow walls affects the geochemistry below the sediment surface.

The presence of macrofauna organisms determines also the surface topography of soft sea beds, which are thus very seldom smooth. Benthic animals create mounds, funnels, pits and trails that are exposed to horizontal bottom currents. Even a small roughness element at the sea floor alters the small-scale flow regime at the interface. As the horizontal water current passes over an obstacle, for example a sediment mound, the flow velocity is locally increased or decreased. The velocity gradients generate pressure differences that are the driving forces for advective pore-water transport. In contrast to diffusion, advection is a directional transport and is depending on the flow velocity of the bottom current and the number and dimensions of the obstacles. The permeability of the sediment is a crucial factor for advective pore-water transport. In cohesive sediments diffusion dominates the transport across the sediment-water interface while advective transport processes gain significance in sandy, permeable beds. Permeable sediments permit pore water flows which transport dissolved and suspended matter through the interstitial pore space. Most coastal areas and also shelf areas are characterized by permeable sands, where advective

transport processes can dominate the exchange processes between sediment and water column.

Thalassinidean shrimp (Crustacea, Decapoda) are found abundantly in nearly every tropical and temperate coastal region. Their presence is usually very conspicuous because they transport sediment to the surface forming volcano-shaped mounds. Though abundant their ecological signifcance and their impact on the physical structure and the geochemistry of the sea-bed has been little investigated. This is due to the fact that they live in permanent or semi-permanent burrow systems several centimeters to some meters below the sediment surface. It is very difficult to collect these animals and has been almost impossible to investigate their influence on the sea-bed without disturbing the sediment structure.

The influence of the thallassinidean shrimp *Callianassa truncata* on the geochemistry of a coastal sediment was investigated in a shallow-water marine environment in the Mediterranean Sea. This species occurs in high densities and constructs elaborate burrow systems. By burrowing it creates a sediment surface topography of mounds and funnels covering the permeable sea bed.

The interaction of sediment topography and boundary layer flow was investigated in laboratory flow channels. A natural sediment core was exposed to varying flow conditions and the alteration of the small-scale flow regime at a sediment mound was shown. The resulting advective transport of solutes across the sediment-water interface was documented by detailed measurements of oxygen penetration into the sediment (Chapter 1). The effect of the increased oxic sediment volume on the total oxygen uptake (TOU) of the sediment as a consequence of topography induced solute transport was investigated in the same experimental set-up. Experiments were carried out demonstrating the effect of different flow velocities, sediment permeabilities and sediment surface structures on the oxygen demand of the sediment (Chapter 2). Parallel to the studies of solute transport across the sediment-water interface, different tracers were used to document advective particle transport in the permeable sediment (Chapter 3). The topography induced pressure gradients not only generate an intruding of supernatant water into the sediment but lead in the low pressure areas to an upward transport of pore water from deeper sediment layers. The up- and downwelling of pore water and the impact of the infacial transport on the geochemical zonation pattern in the permeable sediment was documented by investigating the fluxes and the distribution of nutrients and metals in the permeable sediment (Chapter 4).

Below the sediment surface elaborate burrow systems are constructed by *Callianassa truncata* . The architecture and the functionality of the burrows as well as the consequence of the burrowing activity on the sediment structure were studied in-situ. The animals produce a ventilation current through their burrows, actively flushing deeper sediment layers with oxygenated water. It was investigated how deep oxygen is actually transported into the sediment and how this bioirrigation affects the geochemistry of the surrounding sediment (Chapter 5). So far it had been nearly impossible to measure inside intact burrow system several centimetres to metres below the sediment surface without disturbing the sediment structure. With the construction of a diver observatory buried in the sea bed, in-stu sampling of burrow and pore water and measurements with microelectrodes below the sediment surface were possible (Chapter 6). Thalassinidean shrimp construct species-specific burrows and exhibit a variety of different burrowing and feeding modes. To estimate the overall impact of these macrofauna organisms on the sedimentary environment and the geochemistry of the sea bed, it is necessary to gain also knowledge on the biology and the ecology of the organisms (Chapter 7).

The impact of biogenic sediment topography on oxygen fluxes in permeable seabeds

Wiebke Ziebis, Markus Huettel, Stefan Forster

Max-Planck-Institute for Marine Microbiology, Celsiusstr.1, D-28359 Bremen

Marine Ecology Progress Series 140: 227-237, 12 September 1996

ABSTRACT: Boundary layer flows, interacting with roughness elements at the sediment surface, alter the small-scale flow regime. Consequently, pressure differences are generated, that are the driving forces for advective pore water flow. We in-vestigated topography-induced transport of oxygen in a permeable coastal sediment from the Mediterranean Sea (Isola del Giglio, Italy). The sediment surface was char-acterized by a high abundance (120 m^{-2}) of sediment mounds (average height: 4 cm) built by the mud shrimp *Callianassa truncata* (Decapoda, Thalassinidea). Boundary layer flow velocities recorded *in-situ* ranged between 2 and 16 cm s^{-1}. Detailed ex-periments were performed in a recirculating laboratory flow channel. A natural se-diment core, 20 cm deep with a surface area of 0.3 m^2 was exposed to a uni-directional flow of varying current velocity (3 cm s^{-1}, 6 cm s^{-1}, 10 cm s^{-1}). The alter-ation of the small-scale flow regime at a sediment mound was documented by vertical velocity profiles measured in 1 mm-resolution with temperature-compensated thermistor probes. Oxygen distribution in the sediment was investigated with Clark-type microelectrodes. At a smooth surface, oxygen penetration depth in the perme-able sediment did not exceed 4 mm, independent of flow velocity. In contrast, the topography-induced advective oxygen transport increased significantly with current speed. Oxygen reached down to almost 40 mm at the upstream foot of a 1-cm high sediment mound at a flow velocity of 10 cm s^{-1}. Thus, the oxic sediment volume increased locally by the factor 4.8 compared to the oxic zone underneath a smooth surface. At a natural abundance of 120 mounds m^{-2} the oxic sediment volume per m^2 seabed was calculated to be 3.3-fold higher than in a seabed with a smooth surface. In a parallel experiment advective solute transport was also demonstrated in a less permeable sediment ($k = 5 \times 10^{-12}$ m^2) from the North Sea intertidal flat. Due to the lower permeability the effect on O_2-transport was less than in the Mediterranean sand, but oxygen penetration depth increased locally two-fold at a sediment mound under a flow velocity of 10 cm s^{-1}. The experiments showed the high spatial and temporal variability of oxygen

distribution in a coastal seabed depen-ding on sediment surface topography, boundary layer flow velocities and sediment permeability.

INTRODUCTION

Among the chemical species being transferred between the water-column and the sediment, oxygen plays a key role for biological and geochemical processes. The supply of oxygen to the seabed is essential for aerobic life within the sediment. Among the electron acceptors in marine sediments oxygen is energetically the most valuable for the mineralization of organic compounds and the chemical or bacterial oxidation of reduced products from anaerobic mineralization. It affects also the avail-ability of respiratory electron acceptors within the sediment column used in anaerobic microbial processes. Nitrate and sulphate for example are regenerated from am-monia and sulphide through the oxidation by O_2. The extent of the oxic (containing oxygen) and oxidised zone (having positive redox potential) regulates the distribution of bacterial and protozoan communities (Fenchel 1969, Blackburn 1987, Giere 1993, Berninger & Epstein 1995, Fenchel & Finlay 1995). In turn, the zonation of microbial activity has a strong influence on the organic matter degradation, mineral cycling and nutrient release from the sediment (Fenchel & Blackburn 1979, Meyer-Reil et al. 1987, Mackin & Swider 1989, Jørgensen & Revsbech 1989).

In-situ investigations revealed that in coastal environments oxygen penetrates by diffusion from the overlying water usually not deeper than 2-5 mm into the sediment (Revsbech et al. 1980, Andersen & Helder 1987). Burrowing macrofauna transport supernatant water to deeper sediment layers by irrigating their tubes and burrows. Dissolved substances, like oxygen, diffuse through the burrow walls (Aller 1983, Forster & Graf 1992) into the ambient sediment. The enlargement of the sediment-water interface can considerably increase the solute exchange between the seabed and the overlying water (Hylleberg & Henriksen 1980, Aller 1982, Kristensen 1985, Huettel 1990) depending on the density of organisms and their bioturbation and bio-irrigation behaviour (Forster & Graf 1995).

In areas exposed to tidal waves and strong bottom currents hydrodynamic forces can resuspend and thereby oxygenate surficial sediment or flush the interstices with oxygen-rich water (Riedl et al. 1972, Malan & McLachlan 1991). Coastal environ-ments are characterised by biogenic structures (mounds, pits, tracks and funnels), created by infauna and epifauna organisms and by geological features (ripples) in a variety of morphologies and sizes. These structures strongly affect the small-scale

flow regime at the interface, as flow velocity is locally increased or decreased (Vogel 1983, Schlichting 1987, Yager et al. 1993). The velocity gradients generate pressure differences that constitute driving forces for an advective solute transport across the interface of permeable seabeds (Thibodeaux & Boyle 1987, Huettel & Gust 1992). Thus, the topography of the sea-floor can be of importance for the interfacial solute exchange in coastal sediments.

We investigated the role of advective oxygen transport at the sediment surface caused by the interaction of biogenic sediment topography with boundary layer flows. We investigated the distribution of oxygen with polarographic microelectrodes in a natural sediment core characterised by biogenic mounds created by the mud shrimp *Callianassa truncata* (Decapoda, Thalassinidea). Our results show that advective oxygenation effects can reach several centimetres sediment depth, depending on the surface topography, the flow velocity of bottom currents and the sediment permeability.

MATERIALS AND METHODS

Study site and origin of sediments

The sediment core for the laboratory flume experiments originated from the bay of Campese at the west coast of the Island Giglio in the Mediterranean Sea (Fig. 1). As part of the Tuscany Archipelago, the island is situated ca. 150 km north-west of Rome (42° 20' N, 10° 52' E) off the west coast of Italy and has an area of 21 km^2 with 28 km coastline. The sediment surface in the shallow bay is characterised by conspicuous mounds created by the mud shrimp *Callianassa truncata* (Decapoda, Thalassinidea) (Fig. 2). Thalassinids are burrowing crustaceans that are common and often abundant in soft sediments of temperate and tropical coastal environments (Dworschak 1983, Griffis & Suchanek 1991). While constructing and maintaining its burrow *C. truncata* ejects excavated sediment in a fountain-like manner through a burrow opening at the sediment surface, thus the volcano-shaped mounds are formed. They have an average height of 4 cm (maximum 9 cm). These biogenic features are abundant throughout the shallow part of the bay (2-25 m water depth) and cover the sediment surface in an average density of 120 mounds +/- 43 per m^2 (n = 240) (Ziebis in prep.). The mounds are rebuilt within 1-2 h if erased by wave action when storms occasionally occur. Prevailing regional currents passing the island in South-North direction generate a clock-wise gyre within the bay (Fig. 1). From May to August predominant wind directions are NW and W, with 70 % of the recorded wind speeds being in the range of 1-3 bft. The bay is sheltered from southerly strong winds prevailing in late autumn, winter and early

spring. Boundary flow velocities and directions were measured in the month from May to August using a mechanical current-meter (Mini Air-Water 2, Schiltknecht) connected to a tripod which was lowered onto the sediment surface at stations 1, 2, 3, (indicated in the map) at 5 m, 7 m and 12 m water depths. At each depth the flow velocity was re-corded 5 cm above the sediment surface for periods of 12 hours and recorded by a 12 bit data-logger in intervals of 2 s. Flow velocities ranged between 2 and 16 cm s^{-1} with an average current speed of 8.4 cm s^{-1}. The flow changed little in direction (max. 45°) and intensity during one deployment.

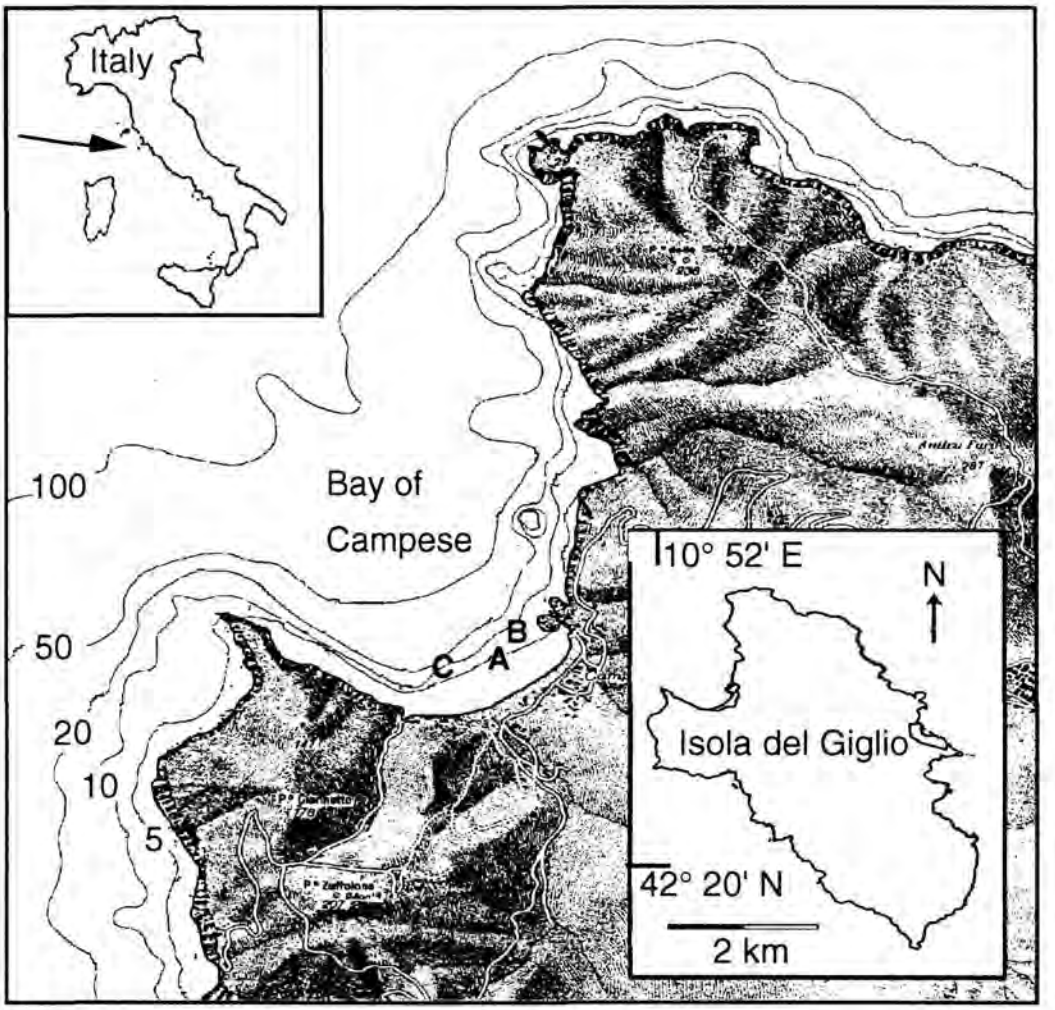

Fig. 1. The island of Giglio is situated in the Thyrrenean Sea. The study site and sampling area was in the bay of Campese at the west coast of the island. Locations 1, 2, 3 were in 5 m, 7 m and 12 m water depth respectively.

Sediment characteristics. Analyses of grain size composition within the upper sedi-ment layer of 10 cm showed that the sediment throughout the shallow part of the bay (2-15 m water depth) was well sorted, 70 to 95 % dry weight consisted of medium sand (200-630 µm). Sediment cores for the experimental set-up were

recovered at site 1 (Fig. 1) in 5 m depth using acrylic cylinders of 20 cm diameter pushed 30 cm into the sediment. At the same site, samples for the analyses of sediment parameters were taken. The median grain size (MD) was 350 µm, the average porosity (water content) 0.4 +/- 0.08 (n = 5) and the organic content 0.8 % of dry weight (loss upon ignition at 540 °C for 12 h). Permeability (k) was determined with a constant head permeameter (Means & Parcher 1964) to be 5.1 x 10^{-11} m^2. Animals were collected separately because within their deep burrows the shrimps are hardly caught by conventional sampling methods.

To investigate the impact of sediment permeability on interfacial exchange processes we used less permeable North-Sea sediment originating from the intertidal flat (Sahlenburg, Germany) for a parallel experimental set-up. The sediment consisted of muddy sand, had a median grain size of 200 µm and an average porosity of 0.38 +/- 0.02 (n = 5). The organic content was 1.2 % of dry weight. The permeability (k = 5.4 x 10^{-12} m^2) was one order of magnitude lower than determined for the Mediterranean sediment.

Fig. 2. The sediment surface topography at 5 m water depth in the bay of Campese. The mounds are built by the mud shrimp *Callianassa truncata*. They had an average height of 4 cm (max. 9 cm) and covered the sediment surface in an average density of 120 mounds per m^2.

The experimental set-up. Two identical recirculating laboratory flow channels similar to the one described by Vogel (1983) were used to simulate *in-situ* conditions. The open, acrylic channel of the flume was 200 cm long, 30 cm wide and 12 cm deep. The drop box (20 cm deep, 30 cm wide and 60 cm long) holding a sediment core with a surface area of 0.3 m^2 exposed to flow was located 90 cm downstream. The sediment recovered from the two study sites was filled into the boxes and the re-maining channel-floor was covered 1 cm high with natural sediment flush with the core surface. Flow was produced by a rotating propeller situated in the return conduit. Flow velocity was controlled by a mechanical flow-meter (Mini air-water 2, Schilt-knecht) located 5 cm above the sediment. The flow speed was regulated by adjusting the voltage of the electric motor. The recirculating water was kept at a constant temperature of 19 °C by means of a cooling coil in the return conduit. Each flume contained a volume 160 l sea water, which had been transported from the sampling sites. The salinity was 37 ‰ for the Mediterranean set-up and 35 ‰ for the North-Sea system.

Prior to the experiments, the sediment in both systems was allowed to equilibrate for a period of 6 weeks at a flow velocity of 10 cm s^{-1}. Before and between experiments, the channels were protected against light and the overlaying water was aerated to keep the oxygen saturation at 97 % air saturation. The Mediterranean sediment core contained 7 individuals of *C. truncata* that constructed 7 mounds (22 mounds m^{-2}) which were maintained throughout the experiment. We chose a mound situated on the centre line and 110 cm downstream for the measurements to avoid side wall effects. Because in the North Sea core a biologically produced topography similar to the Mediterranean sediment was lacking, an artificial sediment mound of similar dimensions was built by hand on the centre line 110 cm downstream.

Small-scale flow velocity profiles were measured using temperature-compensated thermistor probes (LaBarbabera & Vogel 1976) with a tip diameter of 0.8 mm and a 12 cm-long slanted shaft with a maximum diameter of 1.2 mm. The flow sensors had a response time of 0.1 s. For the vertical profiles of flow velocity, the probes were moved by a micro-manipulator from the water-column towards the sediment-water interface. Ten velocity profiles were measured in the Mediterranean set-up along the centre line of the flume starting 4 cm upstream of the *Callianassa* mound and continuing in flow direction. Starting at 20 mm height above the sediment surface the flow velocities were measured in 1 mm intervals. For each step the data was re-corded for a time of 30 s. The free flow velocity 5 cm above the sediment surface was 6.5 cm s^{-1}.

Oxygen profiles were measured using Clark-type oxygen-microelectrodes with a built-in reference and a guard cathode (Revsbech 1989). They had a tip diameter of 10 µm, a 90 % response time of 1 s and showed no stirring sensitivity. Signals were amplified by a picoammeter and recorded on a strip-chart recorder or by a 12 bit data-logger. There was no drift in signal during the measurements. The electrodes were calibrated in air-saturated sea water of known oxygen concentration (Winkler titration) and in N_2-purged, oxygen-free sea water. The sensors were moved along X, Y and Z axes by a micro-manipulator. Vertical profiles were measured in intervals of typically 100 to 250 µm. The position of the sediment-water interface was determined visually through a dissecting microscope as the first contact of the electrode with the sediment surface. The precision of surface detection was in the range of one sand grain (+/- 350 µm Giglio sediment; +/- 200 µm North Sea sediment).

At a constant current speed of 10 cm s^{-1}, 8 profiles of oxygen concentration were measured in an area with a smooth surface in the Mediterranean core, to determine the penetration depth of oxygen in the absence of biotopography. To assess the effect of topography on oxygen penetration depth, 14 oxygen profiles were measured along a transect starting 10 cm upstream of the 1-cm high mound to 10 cm down-stream. At 4 positions, two upstream and two downstream, oxygen profiles along lines perpendicular to the main transect were measured, in order to document the lateral extension of oxygen intrusion.

To estimate the influence of boundary layer flow velocity on advective solute transport in a permeable seabed with biogenic surface topography, the same series of 14 oxygen profiles along the centre line was measured at flow velocities of 3 cm s^{-1} and 6 cm s^{-1}. After a change in velocity the sediment was left for 12 h to equilibrate. Parallel measurements were carried out in the North-Sea sediment to assess the impact of sediment permeability on solute exchange across the sediment-water interface. Three series of 14 oxygen profiles were measured at current speeds of 3 cm s^{-1}, 6 cm s^{-1} and 10 cm s^{-1} along a transect cross-sectioning the artificial mound.

RESULTS

Small scale flow regime at a mound

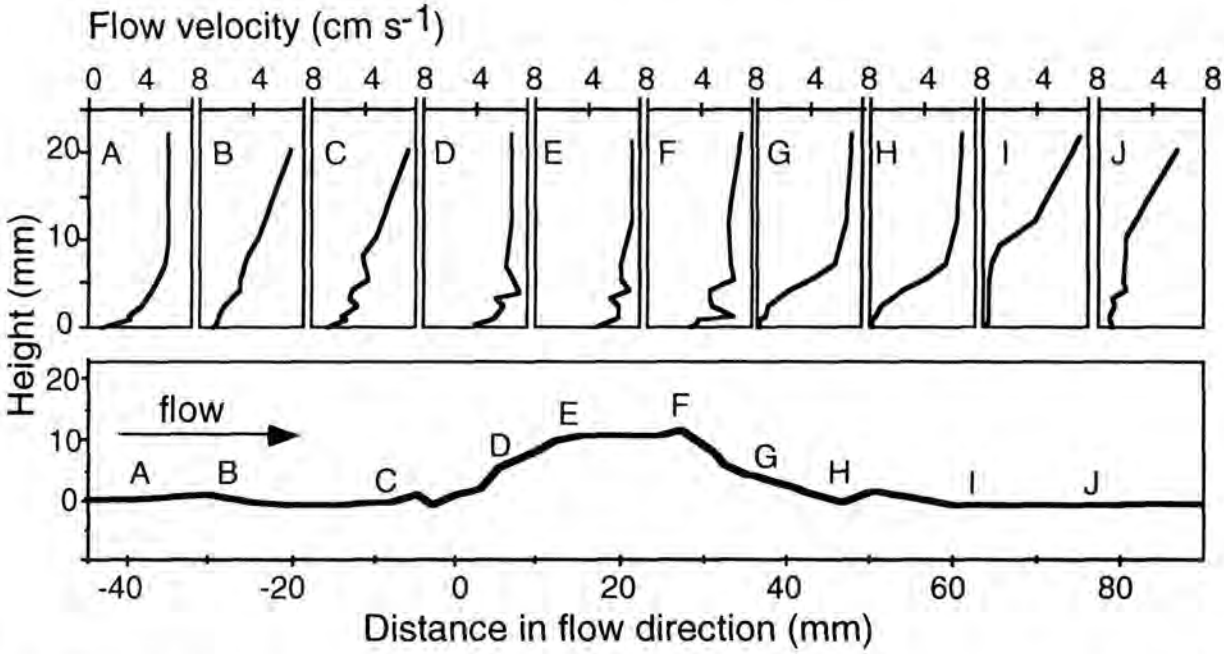

Fig. 3. Velocity profiles at a 1-cm high *C. truncata* mound were measured in a laboratory flow channel. The lower graph shows the cross-section of the mound, which was situated on the centre-line of the channel. The letters A - J indicate the po-sitions of the measured flow profiles. Current velocity was measured in 1 mm intervals using a thermistor probe. The free flow velocity was 6.4 cm s^{-1}. Standard deviations for the measurements at positions A, B and G, H, I, J ranged between 0.05 cm s^{-1} and 0.2 cm s^{-1}. Whereas at positions C, D, E and F, the standard deviations below 10 mm water height were 0.25 cm s^{-1} to 0.35 cm s^{-1}, reflecting a more turbulent water flow.

Fig. 3 shows the flow velocity profiles of the unidirectional flow, as it passed over a 1cm-high *Callianassa* mound. Mean values of the flow velocity recordings for periods of 30 s in 1 mm intervals were used to draw each profile. 4 cm upstream of the mound (position A) the flow was undisturbed and the velocity profile was charac-terised by an increase of flow speed as the logarithm of distance from the sediment surface. Closer to the mound (B, C) flow decreased in velocity below 10 mm height above the sediment surface, the same height as the roughness element. As the flow passed over the mound (D, E, F) it accelerated according to the principle of continuity and turbulent fluctuations close to the interface occurred. The maximum disturbance and flow separation were observed at the downstream edge of the mound (position F). At the downstream slope, flow slowed down, low velocities ($U < 4$ cm s^{-1}) were measured up to 5 mm above the sediment-water

interface (positions G, H). There was an almost stagnant condition at the lee-side of the mound (position I). Due to these velocity gradients, pressure differences built up, with a low pressure area above the mound and high pressure areas upstream and downstream of the mound.

Effect of biogenic topography on oxygen transport

At a smooth sediment surface the average oxygen penetration under a current with a velocity of 10 cm s^{-1} was 3.6 mm +/- 0.57 mm (n = 8). Six of the measured profiles are shown in Fig. 4. Whereas, close to the mound the oxygen penetration changed in relation to the position and distance to the roughness element (Fig. 5). 60 mm upstream of the mound, the steep decline of oxygen was similar to the smooth - surface profiles and the penetration depth of 6 mm was only slightly deeper. Starting in 50 mm upstream of the mound oxygen penetrated deeper and the shape of the profiles changed. The gradients measured at the positions 10 mm in front (x = -10), at the foot (x = 0) and at the slope of the mound (x = +10) showed oxygen penetration depths of up to 36 mm, with high values continuing from the overlying water into the sediment. In 20 mm sediment depth there were still concentrations of 120-150 µmol oxygen l^{-1}.

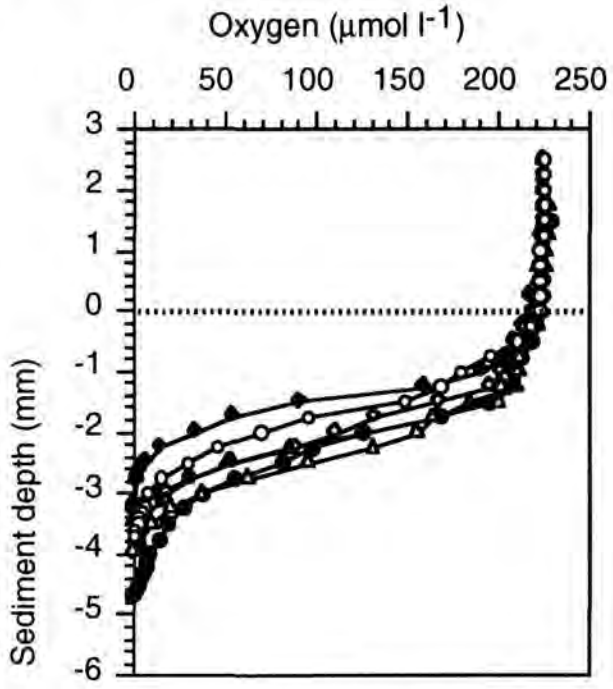

Fig. 4. At a smooth surface, at eight positions along the centre line of the flume oxy-gen profiles were measured under a current velocity of 10 cm s^{-1}. Six profiles are shown here. The average penetration depth of oxygen was 3.6 mm +/- 0.57 mm (n = 8).

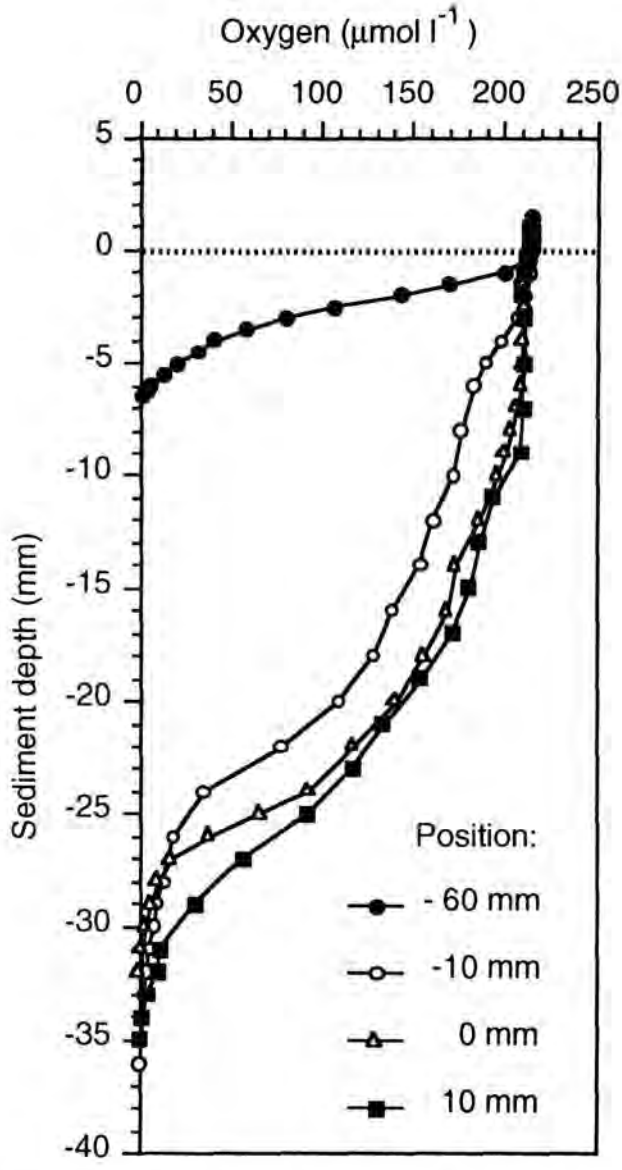

Fig. 5. Fourteen oxygen profiles were measured along a transect, cross-sectioning the mound (shown in Fig. 3) in flow direction, under a current velocity of 10 cm s^{-1}. Four selected profiles are shown here. The positions are given as distances in mm, where x = 0 is the position at the upstream foot of the mound. Negative values are further upstream, positive values are further downstream.

The topography-induced oxygen distribution is illustrated in Fig. 6. In the high press-ure areas up- and downstream of the mound, overflowing water was forced into the sediment and the pore space was flushed with oxygen-rich water. In the downstream area the flushing effect was less intensive, but oxygen still reached down to 17 mm sediment depth. In the low pressure area, on top of the mound, anoxic pore-water from deeper layers was transported upward. Consequently a minimum of oxygen penetration was measured at the downstream edge.

We estimated the total oxic volume adjacent to the mound from the oxygen profiles measured along the main transect and along the 4 transects, perpendicular to it (positions: -30 mm, -10 mm, 60 mm, 75 mm), in the high pressure areas up- and downstream of the mound. Assuming a three-dimensional geometry of an elliptical half sphere,

$V = (4/3\ \pi\ a\ b\ c)/2$ (with a, b, and c being the half axes of an ellipsoid; a as the lateral extension, b as the distance along the centre line and c as the maximum penetration depth), the oxic sediment volumes were estimated as:

$V1 = (4/3\ \pi * 30\ mm * 37{,}5\ mm * 34\ mm)/2 = 80\ cm^3$ upstream and

$V2 = (4/3\ \pi * 20\ mm * 25\ mm * 17\ mm)/2 = 18\ cm^3$ downstream of the mound.

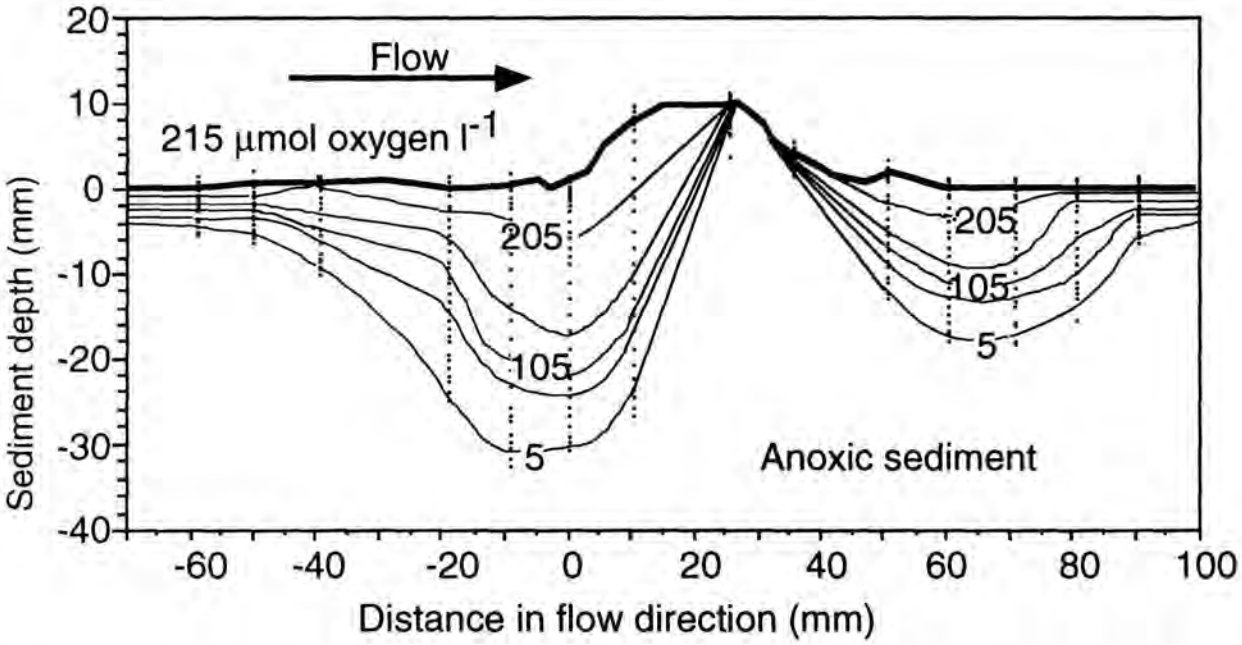

Fig. 6. Points of equal oxygen concentration were connected to illustrate the oxygen distribution underneath the sediment mound exposed to a flow velocity of 10 cm s^{-1}. Isopleths are shown in 50 µM intervals. Vertical dotted lines indicate the fourteen measured oxygen profiles.

Effect of varying flow and sediment permeability

In the sandy Mediterranean sediment the penetration of oxygen in an area with a smooth sediment surface showed very little variation with flow velocity (Fig. 7). The penetration depth ranged from 4.3 mm at a current speed of 3 cm s^{-1} to 4.5 mm and 3.9 mm at current speeds of 6 cm s^{-1} and 10 cm s^{-1} respectively. Considering an accuracy of +/- 0.35 mm of surface determination (grainsize: 350 µm), there was no significant increase of oxygen with current speed. The penetration depth of oxygen

under stagnant conditions varied between 3 mm and 8 mm with a mean value of 4.8 mm (n = 6).

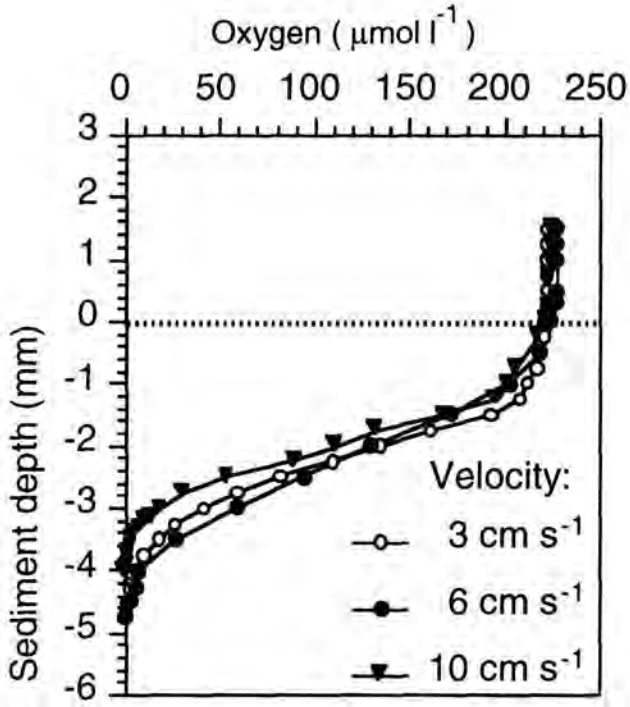

Fig. 7. At a smooth surface, oxygen profiles were measured at the same position, under three different flow conditions of 3 cm s^{-1}, 6 cm s^{-1} and 10 cm s^{-1}.

In contrast, the topography-induced solute transport varied essentially with flow velocity (Fig. 8). The maximum oxygen penetration measured at the same position (x = 0) in the high pressure area upstream of the mound ranged from 10 mm at 3 cm s^{-1} to 22 mm at 6 cm s^{-1} and reached 31 mm at 10 cm s^{-1}. Consequently the sediment volume supplied with oxygen was also clearly increasing with flow speed. In the North Sea sediment, which consisted of less permeable, muddy sand, the pene-tration depth at a smooth surface under a flow of 10 cm s^{-1} was 4 mm +/- 0.65 mm (n = 8). At the sediment mound there was no apparent effect on solute transport at current speeds of 3 cm s^{-1} and 6 cm s^{-1} (fig. 9). Only at a flow velocity of 10 cm s^{-1} a two-fold increase in penetration depth of oxygen was recorded in the high pressure area, upstream of the structure. There was no obvious effect on oxygen penetration in the area downstream of the mound. With a height of 8 mm, the artificial mound was slightly lower than the mounds built by *C. truncata* in the Giglio sediment.

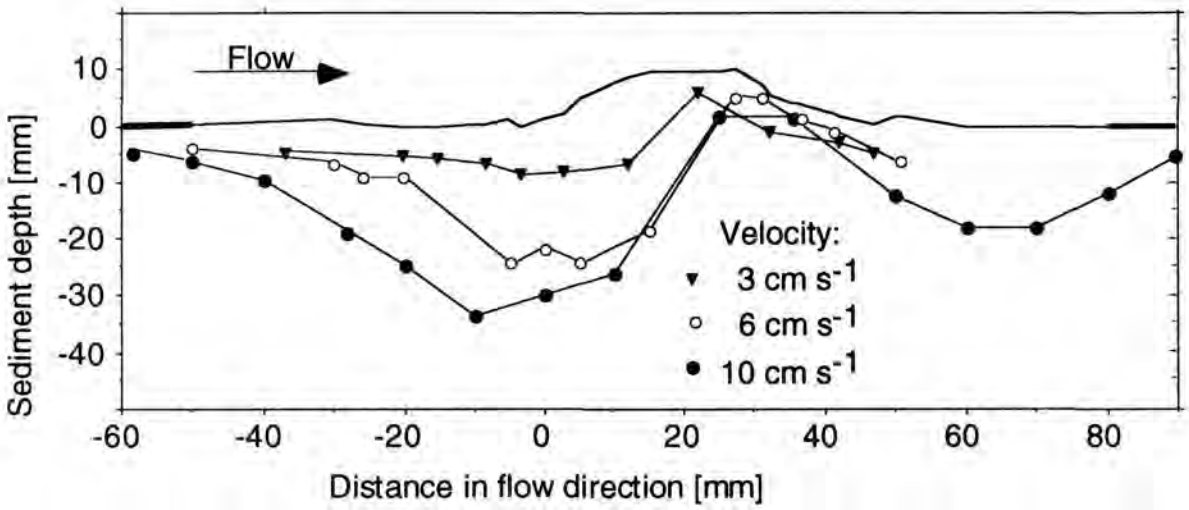

Fig. 8. Data points of the maximum oxygen penetration depths at the *Callianassa mound were connected (solid lines) to illustrate the oxygen penetration and* distribution under three different flow velocities of 3 cm s^{-1}, 6 cm s^{-1} and 10 cm s^{-1}.

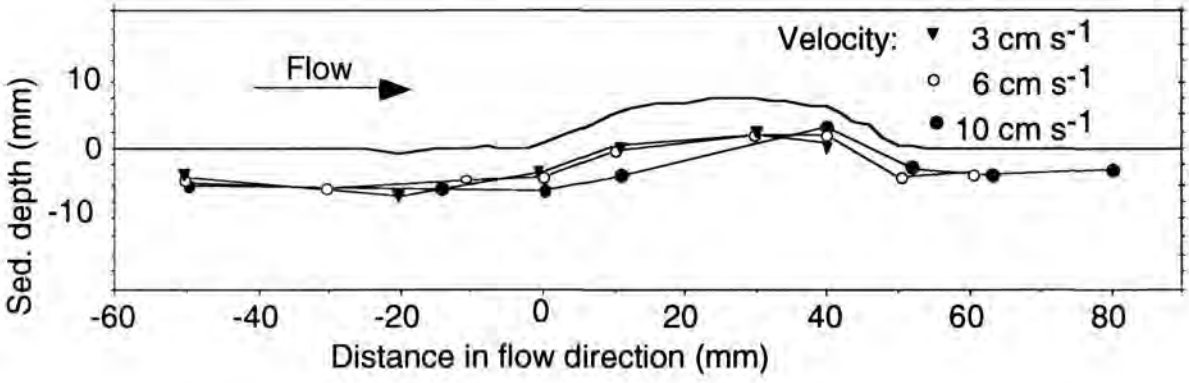

Fig. 9. The maximum oxygen penetration depths near a North Sea sediment mound, measured in a parallel set-up, are illustrated as solid lines for the three different current velocities of 3 cm s^{-1}, 6 cm s^{-1} and 10 cm s^{-1}. The North-Sea sediment was less permeable (k = 5. 1 x 10^{-12} m^2) than the Giglio sand (k = 5. 2 x 10^{-11} m^2).

Dynamics of advective oxygen transport at a mound

Because in the natural environment flow conditions can vary, we were interested in the time scale of advective oxygen supply to a certain sediment depth after a change of flow velocity. Two electrodes were positioned at fixed sediment depths of 3 mm and 20 mm at the upstream foot of the mound (x = 0) to follow the oxygen concen-tration at these particular depths under varying flow conditions (Fig. 10). After equi-libration of the oxygen flux at a flow velocity of 10 cm s^{-1} the flume motor

was switched off and the decrease of oxygen concentration in the respective sediment depths were recorded by a data logger at intervals of 1 second. As a steady state of oxygen concentration was reached, the motor was switched on again. At the beginning of the experiment the oxygen concentrations at 3 mm and 20 mm were 210 µmol oxygen l^{-1} and 115 µmol oxygen l^{-1} respectively, these values corresponded to the oxygen profile measured at this location (x = 0), at a current speed of 10 cm s^{-1} (Fig. 5). As the flow was turned off, the oxygen value in 20 mm sediment depth declined to zero within 2 h. In the upper sediment layer, in 3 mm depth, oxygen decreased to a concentration of 10 to 15 µmol l^{-1}, which was main-tained over a period of 8 hours under no-flow conditions. As the water flow was started again, this oxygen sensor's signal increased almost instantaneously (within 30 s). The initial value of 210 µmol oxygen l^{-1} was stable after 50 min and stayed constant. At the depth of 20 mm this effect was delayed, after a time of 1 h 48 min an increase of oxygen was measured. It took another 1 h and 20 min until a concen-tration of ca. 90 -100 µmol l^{-1} was reached.

The oxygen uptake or respiration (R) in the respective depth could be estimated from the initial (after 30 s) decrease (∂ C) of oxygen with time (∂ t): $R = \partial C / \partial t$. In 3 mm the respiration was 7×10^{-6} µmol O_2 cm^{-3} s^{-1} and slightly higher than the oxygen uptake of 5×10^{-6} µmol O_2 cm^{-3} s^{-1} in 20 mm sediment depth.

DISCUSSION

Advective transport of oxygen

Diffusive oxygen flux across the sediment-water interface is driven by a concentration gradient between overlying water and the pore water. It is dependent on the oxygen concentration in the supernatant water (Rasmussen & Jørgensen 1992) and the diffusion coefficient of oxygen in the water and the sediment. The oxygen penetration depth depends on the oxygen uptake of the sediment (Revsbech & Jørgensen 1986, Reimers & Smith 1986) and thus on the organic content. As the O_2-concentration decreases with depth due to biological and chemical consumption (Cranck 1983) the microscale measured profiles may show a change in the gradient, that allows the calculation of the oxygen uptake in a defined zone (Crank 1983, Nielsen et al. 1990). The oxygen gradients we measured in the permeable sand, underneath a smooth surface are according to the oxygen profiles measured in other coastal regions. The penetration depth was ca. 4 mm and a typical curvature of nearly parabolic shape indicated a steep

decline of oxygen with depth. At a plane surface the change of the boundary layer flow velocity did not significantly affect the oxygen transport across the interface (Fig. 4), although minor changes were possibly not detected due to the error of sediment surface detection. The penetration depth of oxygen under stagnant conditions was in the same range of ca. 4 mm. In early investigations, Fenchel (1969) also demonstrated that a moderate current of 8 cm s^{-1} above natural sands of in-creasing permeability did not result in advective pore water movements below 4 mm sediment depth.

In high-resolution measurements, Jørgensen & Des Marais (1990) showed that oxygen penetration increased 3-fold (from 0.5 mm to 1.5 mm) in a bacterial mat as the flow speed was increased by the factor 25 (0.3 cm s^{-1} to 7.7 cm s^{-1}). Their explanation was a reduced thickness of the diffusive boundary layer (DBL). The DBL is a thin layer of water, typically only 0.2 mm to 1 mm thick (Boudreau & Guinasso 1982, Gundersen & Jørgensen 1990, Jørgensen & Revsbech 1985), covering the sediment surface. Within the DBL the viscous forces exceed the turbulent, and molecular diffusion is the dominant transport mechanism. Oxygen decreases linearly as the sediment surface is approached. With increasing current velocity the thickness of the DBL decreases and as a result oxygen concentration directly at the interface is higher and the solute penetrates deeper into the sediment. In our experiments, in the sandy sediment (MD: 350 µm) from the Mediterranean Sea, the measured profiles do not show the formation of a DBL. One explanation might be the insufficient resolution of the measurements. We assume that the formation of this layer was most likely affected by the sediment surface roughness. Obstacles protruding more than half of the DBL thickness into the overlying water can influence the formation of this laminar layer (Vogel 1983). The absence of a diffusive boundary layer might indicate some advectice flow in the upper mm of the sediment even in the case of a "smooth" surface. The average oxygen penetration under stagnant conditions was 4.8 mm (n = 6), so that we assume that advective transport rate at a plane surface of the sandy sediment was comparable to the diffusive flux of oxygen across the sediment-water interface.

In contrast, hydrodynamic forces determined the interfacial solute transport at the roughness element in the permeable sediment. In vicinity of the small biogenic mound (1 cm high) the small-scale flow field was altered (Fig. 3) and as a consequence pressure differences were generated. Within the high pressure fields oxygen reached not only down to deeper layers but the profiles showed a characteristic change in shape (Fig. 5). High concentrations persisted up to 20 mm deep into the sediment. The curvature of the profile indicates that the oxygen supply is

higher than the concurrent uptake at the respective sediment depths. The deep oxygen penetration can not be explained by diffusional pathways but is due to advection. Consequently, the O_2-uptake can not be calculated from the profiles shape, as it is possible for diffusive oxygen gradients by using Fick´s first law of diffusion. ($J = - D_S \cdot \partial C / \partial x$, where J is the diffusion flux, D_S the apparent diffusion coefficient in the substrate and $\partial C / \partial x$ is the slope of the concentration profile at depth x).

In contrast to dyes, used as conservative tracers in experiments designed to show advective transport (Huettel & Gust 1992), oxygen is one of the most reactive species. While being transported it is also consumed in biological and chemical processes, thus the measured profiles describe a dynamic balance between oxygen supply and consumption in the specific depth. In dye experiments under similar flow conditions and a structure of comparable size, the solute reached down to more than 5 cm sediment depth (Huettel & Gust 1992). The depth distribution of oxygen at the obstacle was a function of flow velocity. Penetration depth and thus the sediment volume oxygenated, was greatest at the highest flow velocity used in our experiments (10 cm s^{-1}), a current speed commonly observed in the natural environment. A total volume of ca. 98 cm^3 of sediment was calculated to be oxic next to this mound of 10 mm height. This compares to 20 cm^3 of sediment supplied with oxygen by diffusion, considering an equivalent area (51 cm^2) of a smooth sediment surface. Thus the oxic volume increased locally by the factor 4.8. This means a significant increase of oxygen availability for aerobic respiration and oxygen-dependent chemical reactions. In the natural environment the sediment volume supplied by advection with oxygen is related to the density of biogenic structures in a given area. At the observed natural density of 120 callianassid mounds per m^2, a 3.3-fold increase of oxygenated sediment, compared to a smooth surface could be expected, under the assumption of a uniform shape of mounds (10 mm height) and a steady unidirectional flow of 10 cm s^{-1}. Concerning the dimensions of the structures, we showed a minimum effect, as the height of the mound used in the experiment was of relative small size compared to the average height (4 cm) of structures at the study site. Oxic zones of greater dimensions probably occur in the field. Furthermore, we considered only the con-spicuous mounds for our estimations, but besides other irregularities of the interface, twice the number of funnel-shaped depressions (3 cm deep) than mounds charac-terised the sediment surface at the Mediterranean study site (240 m^{-2}). Here boundary layer flows are altered in a similar way and generate pressure differences that add to the importance of advective oxygen transport (Huettel & Gust 1992). In the investigated area the sediment surface topography was mainly characterized by the

burrowing activity of the thalassinid shrimp. In other coastal areas sedi-mentological structures, such as ripples may influence the boundary layer flow and thus contribute to an enhanced exchange of dissolved and particulate matter between the water column and the sea bed (Huettel & Gust 1992, Huettel et al. 1996). On the other hand, wave-induced bottom stress has to be considered when evaluationg sediment-water exchange processes in coastal areas. Frequent resus-pension of the upper sediment layer might have a greater influence on oxygenation effects in some areas than biologically mediated oxygen transport. Detailed informa-tion on the boundary layer flow conditions as well as on abundances, shapes and dimensions of biogenic or geological structures are necessary to assess the magnitude of advective interfacial solute exchange.

Physical sediment properties, such as grain size composition and porosity determine the permeability of a seabed. Permeability is a crucial factor for solute transport in sediments and strongly depends on the actual size of sandgrains (in contrast to porosity) and on the degree of sediment sorting. The North Sea sediment had a similar porosity and amount of organic content as the Giglio sediment, but was characterised by a smaller grain-size and thus a lower permeability. In this less permeable sediment there was a two-fold increase in oxygen penetration at the upstream side of the mound at a current velocity of 10 cm s^{-1}, suggesting an advective solute transport. Huettel & Gust (1992) stated that in sediments with a permeability of $K > 2 \times 10^{-11}$ m^2 pressure gradients at the sediment surface would generate advective pore-water flow across the interface. The permeability of the North Sea sediment ($K= 5 \times 10^{-12}$ m^2) was lower than this value. It is also likely that a diffusive boundary layer existed at this finer grained sediment surface. When the DBL was compressed, because of the higher current velocity, it allowed a deeper reaching solute transport, that would explain the increased oxygen penetration depth.
Our experiments show, that the effect of interstitial solute transport, produced by pressure gradients, is strongly dependent on the sediment permeability.

Variability of the oxic zone

In a permeable sediment with biogenic topography the oxic zone below the depth of diffusional transport is controlled by boundary flow velocities. Advective transport is initiated as soon as flowing water is deflected by the roughness element and is much faster than diffusional transport. In our experiment, after a change from stagnant water to a boundary layer flow of 10 cm s^{-1} (Fig. 10), it took ca. 3 h until the sediment layer in 20 mm depth was continuously supplied with oxygen. For a

comparison, the time required for a solute to overcome a distance by diffusional transport can be approximated by using the equation: $t = z^2 / 2 D$, derived from the definition of a 1-dimensional diffusion coefficient, where t is the time in s, z is the distance or sediment depth in cm and D the diffusion coefficient of a solute in water at a given salinity and temperature. The diffusion coefficient for oxygen in sea water with a salinity of 37‰ and a temperature of 19 °C would be D = 1.9214 *10-5 cm^2 s^- 1.

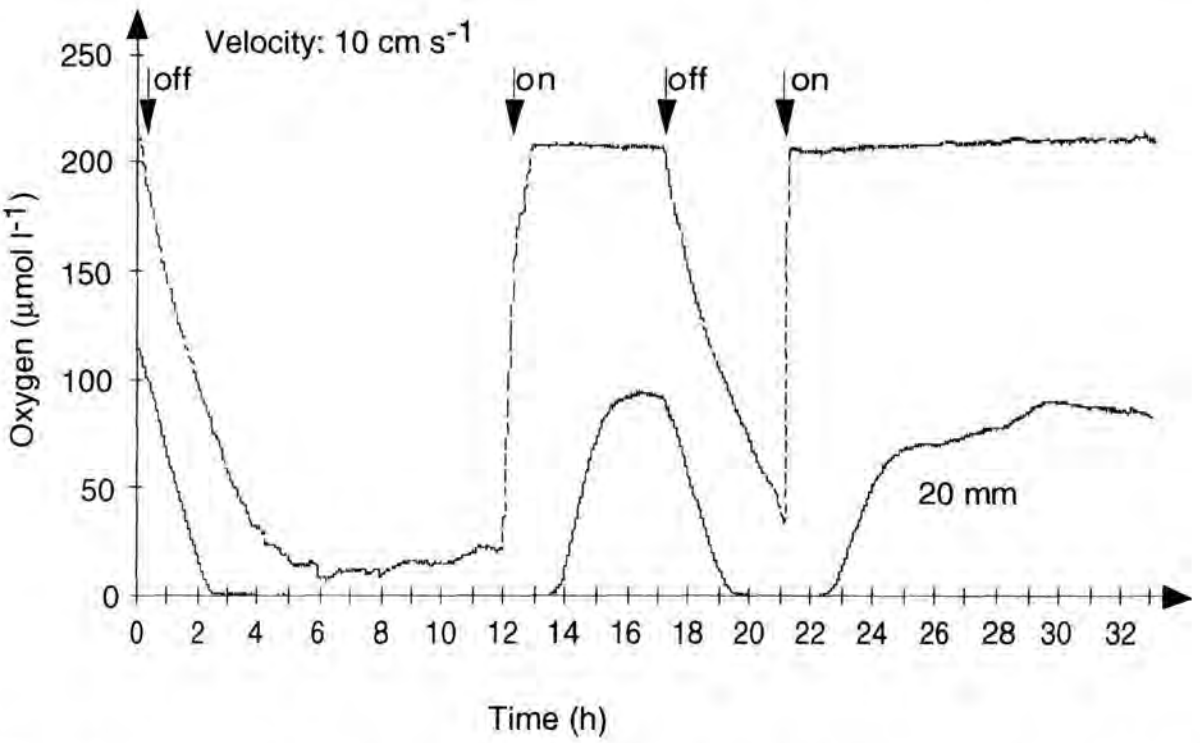

Fig. 10. Oxygen concentrations were continuously measured in 3 mm and 20 mm sediment depth for a time of 32 h at the same position (x = 0) at the upstream foot of the *Callianassa* sediment mound. The initial current velocity of 10 cm s^{-1} was turned on and off twice. The time resolution was 1 second.

According to this calculation it would take 29 h for an oxygen molecule to overcome a distance of 20 mm in sea-water by molecular diffusion. In the sediment the time required would be prolonged (ca. 3-fold) due to the porosity and tortuosity effects (Berner 1980, Iversen & Jørgensen 1989). Underneath an irregular surface and within a few centimetres sediment depth the availability of oxygen can change rapidly with varying flow conditions. Furthermore, the topography of the sea floor is not per-manent but varies with faunal activity, which is often seasonal because it is stimulated by the input of organic carbon from the water column and reflects generation cycles. Most biogenic structures are not stable but change in size and are erased by strong currents. In turn, high boundary layer flow velocities not only

render the sediment more permeable but can generate ripples that produce similar advective transport processes (Thibodeaux & Boyle 1987).

Another important aspect of topography-induced solute transport is the upwelling of reduced pore water due to the low pressure field above a mound or ripple. The isopleths (Fig. 6) show that the oxic zones, upstream and downstream of the mound, are separated by an anoxic region underneath the mound, where reduced solutes reach the sediment surface. Pore water, from as deep as 20 cm, can be transported to the sediment surface by this suction effect (Huettel & Gust 1992). The presence of this oxygen-free zone next to oxic environments further complicates the zonation pattern and creates horizontal gradients of oxygen concentration within the upper sediment layer. The oxygen distribution in natural environments is heterogeneous and highly variable, thus many factors have to be considered when estimating solute exchange rates.

Implications for the sedimentary environment

Advective oxygen transport can play an important role for the ecology of coastal sediments. Many coastal areas and a large part of the continental shelf (40%) are covered by permeable sediments that are exposed to boundary layer flows and are populated by infauna organisms or are characterised by ripples. Thus advective transport processes take place that can expand the oxic sediment volume far beyond the zone supplied by diffusion. The increase of free oxygen available for aerobic respiration enhances the mineralization of organic matter and the subsequent release of regenerated nutrients can be of importance for the ambient environment. Reduced substances are oxidised within the flushed regions or locally at the sediment interface where anoxic pore water is transported upward due to the low pressure on top of elevations. Parallel to the advective solute transport, organic particles are transported into the interstices of the permeable sea bed (Huettel et al. 1996). The co-occurring input of oxygen and organic matter further promotes microbial carbon oxidation and accelerates remineralisation processes within the upper sediment. The oxygen used in surplus during advective transport compared to diffusional supply for respiration and chemical or biological oxidation must also be reflected in the total oxygen uptake (TOU) of the sediment (Forster 1996, same issue). Next to food availability, oxygen is the predominant factor determining the habitat conditions for aerobic micro- and meiofauna. The existence of anaerobic life forms is also not possible in isolation from oxic regions, as the essential chemical energy is provided by the processes that take place in the oxic zones. Anaerobic life has therefore been found to be most abundant in the vicinity of aerobic habitats

(Fenchel & Finlay 1995). In sandy sediments the numbers of protozoans are highest at the transition zone from anoxic to oxic conditions (Giere1993). This is also the region where bacterial activity is often found to be highest (Fenchel & Blackburn 1979). Many protozoans are microaerophilic, but are sensitive to higher O_2-concentrations, which can be toxic for them. The results of this investigation show that due to topography-induced flow effects the oxic-anoxic transition becomes three-dimensional, offering an enlarged habitat for gradient organisms. We showed that this region is also characterised by a high spatial and temporal variability. This implies, that the organisms have to react with high mobility to meet their metabolic needs or to escape unfavourable conditions, if they are not able to tolerate the changing conditions (Alve & Bernhard 1995). Classification of micro-organisms according to the sediment depth where they have been found is only reliable in combination with the exact description of chemical gradients. Foraminifera, for example, have been observed in 'anoxic' habitats, but species with anaerobic metabolism do probably not exist (Bernhard 1989, Bernhard & Reimers 1991). An explanation would be the supply of oxygen to deeper sediment layers. The observed downward migration in Foraminifera as a response to flow (Palmer & Molloy 1986) might be an indication for this.

The presence of biogenic structures at a permeable seafloor, exposed to moderate boundary layer flows induces a high spatial and temporal variability of oxygen concentration within the upper layer of the sediment and may also affect the exchange of other dissolved substances between the water-column and the sediment. The advective supply of oxygen to a permeable seabed far exceeds diffusional trans-port and may essentially affect mineralization processes within the sediment and the distribution of benthic meiofauna and micro-organisms.

ACKNOWLEDGEMENTS: We thank Anja Eggers, Gabriele Eickert and Anni Glud of the microsensor laboratory of our institute for the construction of oxygen microelectrodes. The study was financially supported by the Max-Planck-Society.

Impact of boundary layer flow velocity on oxygen utilisation in coastal sediments

Stefan Forster, Markus Huettel, Wiebke Ziebis

Max-Planck-Institute for Marine Microbiology, Celsiusstr.1, D-28359 Bremen

Marine Ecology Progress Series 143: 173-185, 14 . November 1996

ABSTRACT: Small pressure gradients generated by boundary flow-topography interactions cause advective pore water flows in permeable sediments. Advective pore water exchange enhances the flux of solutes between the sediment and the overlying water, thus generating conditions for an increased utilisation of oxygen. We contrast a less permeable ($k=5 * 10^{-12}$ m^2) with a permeable sediment ($k=5 * 10^{-11}$ m^2) typical for coastal and shelf sediments. Total oxygen utilisation (TOU) in incubated sediment cores was measured in ten laboratory experiments using recirculating flow tanks (33 runs). TOU was a function of flow velocity in permeable sediment where advective pore water flow occurred. TOU increased with the increasing volume of sediment flushed with oxygenated water. We found TOU increased by 91±23 % in a coarse sand when flow increased from 3 to 14 cm s^{-1} (38 mounds m^{-2}, height: 10-30 mm, flow measured 8 cm above the sediment). Addition of fresh algal material caused a stronger stimulation of TOU in the coarse sand than in the fine sand (4 additional flume runs). After the addition intensive oxygen consumption reduced the oxygen penetration depth in the advectively flushed zone of the coarse sediment. However, counteracting this process, advective flow maintained an oxic sediment volume still larger than in the less permeable sediment. Flow enhanced oxygen utilisation is potentially effective in permeable beds of coastal and shelf regions contrasting the situation in cohesive sediments limited by predominantly diffusive oxygen supply.

INTRODUCTION

The flux of oxygen across the sediment-water interface accounts for almost the entire remineralisation in deep sea oligotrophic environments (Aller 1990, Rutgers van der Loeff 1990). In coastal and shelf sediments other respiratory pathways like denitrification, iron, manganese, and sulphate reduction contribute considerably to the oxidation of carbon (Thamdrup et al. 1994, Jørgensen & Revsbech 1989). Within

the sediments the reoxidation of the reduced end products occurs to a large extent via oxygen (Canfield et al.1993, Thamdrup et al. 1994). The total flux of oxygen into the sediment (total oxygen utilisation, TOU) depends on the O_2-concentration in the water, the sedimentary organic carbon content available for bacterial metabolism, the concentration of reduced chemical species in the sediment reflecting bacterial activity, and animals present in the sediment.

The sedimentary oxygen uptake is limited by the rate of oxygen transport across the sediment-water interface. Generally, three different transport modes may be distinguished: molecular diffusion depending on the existence of concentration gradients, biopumping (irrigation) of oxygenated water by macrofauna through their burrows, and advective pore water flow driven by differential pressure gradients at the sediment-water interface. Molecular diffusion dominates transport at the sediment surface, in cohesive sediments, microbial mats and at burrow walls (Aller 1983, Jørgensen & Revsbech 1985, Revsbech & Jørgensen 1986), with a diffusive boundary layer often controlling the flux (Gundersen & Jørgensen 1990, Jørgensen & Des Marais 1990, Glud et al. 1994). Irrigation facilitates flux of solutes across burrow walls thus affecting solute distribution below the sediment surface (Aller 1983, Kristensen et al. 1985, Forster & Graf 1992, Marinelli 1994).

Advective transport occurs when biogenic or physical sediment roughness impedes boundary layer flow at the sediment-water-interface. Advective pore water flow in the sediment depends on boundary layer flow velocity, on the abundance and shape of topography structures and the permeability of the sediment (Huettel & Gust 1992, Ziebis et al. 1996). In the presence of irrigation, the relative contribution of diffusive oxygen flux across the sediment-water interface to the total amount of oxygen supplied decreases (Lindeboom et al. 1985, Rasmussen & Jørgensen 1992, Glud et al. 1994, Forster & Graf 1995). Furthermore TOU increases after sedimentation of fresh algal material (Hansen & Blackburn 1992, van Duyl et al. 1992).

In this study we report a laboratory investigation on the effect of unidirectional flow on total oxygen utilisation in natural permeable sediments with surface topography. Comparing the measurements of TOU from a highly permeable medium sand to a fine silty sand with lower permeability, we investigate the magnitude of the stimulation of total oxygen utilisation by pressure-driven advective pore water flow.

METHODS

Experimental setting

Experiments were conducted in two identical flumes (channel length: 200 cm, width 30 cm, depth 10 cm) recirculating 160 l of sea water. A schematic of the flume design is given in Huettel et al (1996a). Within each flume channel a natural sediment core of 36 dm^3 volume (core size: 60 x 30 x 20 cm, L x W x H) was placed. A 1-cm thick layer of sediment covered the acrylic sheet between the collimators-cm at the up- and downstream end of the channel and the sediment core. The water depth was 10 cm. The propeller driven free flow velocity was calibrated against the voltage of the motor using neutrally buoyant swimmers at the water surface ($r = 0.987$, $n = 18$) corresponding well to flow sensor measurements (Huettel et al. 1996b). Free flow velocities were set between 2 and 14 cm s^{-1}. At these velocities the open channel flow in our flumes was turbulent with Reynolds numbers ranging from 5,000 to 30,000 (Giles 1976). Temperature was controlled and regulated through an external cooling unit and oxygen concentration in the water was monitored with an oxygen electrode (WTW 90). Sediments were collected from two locations (Table 1) and left to equilibrate for 6 weeks. Sand from the nearshore sublittoral off the island of Giglio, Italy in the Mediterranean Sea (Ziebis et al. 1996), below referred to as 'coarse' permeable sediment, was used in experiments performed in flume 1. Flume 2 contained the less permeable sediment from an intertidal sand flat at Sahlenburg, Germany at the North Sea, referred to as ' fine' sediment. Experiments performed in the 2 flumes are listed for an overview in Table 2.

Table 1. Characteristics of the fine and coarse sandy sediment used in this study. Grain size distribution is given with the first, second and third weight quartile.

Sediment type Origin	Porosity	Grain size distrib. (µm) Q_1	(Q_2)	Q_3	Permeability (m^2)	C org (% dry wt)
Silty fine sand Sahlenburg, North Sea, Germany	0.4	130	200	320	$5 \cdot 10^{-12}$	1.2
Coarse sand Giglio island, Mediterranean Sea, Italy	0.4	270	350	450	$5 \cdot 10^{-11}$	0.8

Sea water was collected at the North Sea tidal flats, filtered for removal of planktonic algae, and salinity adjusted to 35 permil by addition of artificial sea salt, if needed (compare Table 3).

Table 2. Experiments carried out in this study. Two identical flumes containing 1 sediment type each were used, both with and without (controls) topography structures.

Flume 1	**Flume 2**
Coarse Giglio sediment	Fine North Sea sediment
Dye penetration experiments	
1 run with topography	1 run with topography
Total oxygen uptake (TOU)	
Exp. 1.1, 5 runs with natural topography Exp. 1.2, 7 runs with natural topography Exp. 1.3, 8 runs with artificial topography Exp. 1.4,4 runs with smooth surface (control)	Exp. 2.3, 5 runs with artificial topography Exp. 2.4, 4 runs with smooth surface (control)
Total oxygen uptake after addition of algae	
Exp. 1.5, 1 run with artificial topography Exp. 1.6, 1 run with acrylic sheet (control) Exp. 1.7, 1 run with smooth surface (control)	Exp. 2.5, 1 run with artificial topography

Table 3. Experimental conditions for the measurement of total oxygen utilisation, including number of runs in each experiment, the range of free flow velocities in the runs performed, mass of particulate organic carbon (POC) added, temperature, salinity, and abundance, dimensions and type (A: artificial; N: natural) of surface topography structures present.

					Topography			
	No. runs	Flow velocities (cm s^{-1})	POC added (mmol C m^{-2})	Temp. (°C)/ Sal. (PSU)	Height (mm)	Diameter (mm)	Type	Abund. (m^{-2})
total oxygen uptake								
Flume 1, coarse								
With topography								
Exp. 1.1	5	2.5 - 13.5	-	20 / 37	8 - 25	40 - 80	N	22
Exp. 1.2	7	2.5 - 13.5	-	20 / 37	8 - 25	40 - 80	N	22
Exp. 1.3	8	2.5 - 13.5	-	20 / 37	14 (8 - 25)	60 (40 - 80)	A (+N)	24 (+14)
Smooth control								
Exp. 1.4	4	2.5 - 11.5	-	20 / 37	-	-	-	-
Flume 2, fine								
With topography								
Exp. 2.3	5	2.0 - 12.0	-	12 / 33	14	60	A	24
Smooth control								
Exp. 2.4	4	3.0 - 12.5	-	12 / 33	-	-	-	-
Algae additions								
Flume 1, coarse								
With topography								
Exp. 1.5	1	8	60	16 / 34	10.5	55	A	33
Control								
Exp. 1.6	1	8	40	16 / 34	acrylic sheet	-	-	-
Smooth control								
Exp. 1.7	1	8	40	16 / 34	-	-	-	-
Flume 2, fine								
With topography								
Exp. 2.5	1	8	60	16 / 34	9.0	55	A	33

Oxygen profiles were measured using micro-manipulator operated microelectrodes equipped with a guard electrode (Revsbech 1989) with a stirring sensitivity <1%. A two-point calibration was made between the anoxic sediment layer and the overlying water. The steepest slope of the concentration gradient (μM mm^{-1}) at the sediment-water interface and the penetration depth of oxygen were used for comparison of profiles at the smooth sediment surfaces.

Permeabilities of both sediments were measured with a constant head permeameter (Means & Parcher 1964) using cores taken from the flumes after the experiments. We calculated sand grain surface area for both types of sediment from data of grain size distribution according to the Wentworth scale (<63, <125, <250, <500, <1000, and ≥1000 μm), obtained by dry sieving, assuming spherical geometry. Water

content and loss on ignition (C_{org}) were determined from samples dried at 60°C for 24 h and heated at 550 °C overnight.

The macrofauna in the Mediterranean sediment was dominated by a thalassinidean shrimp (*Callianassa truncata*, 22 ind m^{-2}), the North Sea sediment by polychaetes (*Heteromastus filiformis, Scoloplos armiger*). Sediment cores were allowed to equilibrate for 4 weeks in the flumes at in situ temperatures and in the dark (20 ±1°C and 12 ±1°C, respectively). During this time period the shrimps produced a distinct topography ('natural topography') on the sediment surface composed of mounds (22 m^{-2}, height: 1 - 3 cm) and funnels (44 m^{-2}, depth: 1 cm). Infauna in the intertidal North Sea sediment did not produce topography structures of significant height or abundance. Therefore we constructed artificial structures of defined abundance and geometry by gently pouring sediment from a syringe onto the surface of the sediment ('artificial topography', for dimensions see Table 3).

Dye experiments

The contribution of advective pore water flow to sediment-water exchange was investigated using inert dye (Rhodamine WT, DuPont, Delware, USA). Two flume experiments, one with 'impermeable' and one with 'permeable' sediment, were set up with otherwise identical flow conditions (5.2 ± 0.8 cm/s) and topography. In these experiments a sediment ripple aligned perpendicular to the flow and across the whole width of the core represented the surface topography. The dimensions were such that the cross-section visible at the transparent walls of the flume (height: 14 mm, base length: 85 mm) was directly comparable to that of the mounds used in the oxygen utilisation experiments (see below). Velocity and penetration depth (precision ± 1 mm) of the red solute front in the two sediments was calculated from enlarged photographs taken through the transparent side walls of the flumes at 1 h intervals over a period of 12 hours.

We calculated sediment volumes (V_S) affected by stained pore water flow for mounds of 14 mm height and an abundance of 24 mounds per m^2. We assumed the geometry of two rotational ellipses up- and downstream of a mound (Fig. 1; $V_S = 0.5\ V = 2/3\ \pi\ a\ b^2$, with the volume (V) of the ellipses, the half-axes (a) and thus the longitudinal rotation axes (2a) oriented along the axes of the flume, and the axes (b) equal to the penetration depth of the dye). Due to the error associated with the measured distances (± 0.1 cm) the result is affected by 3%.

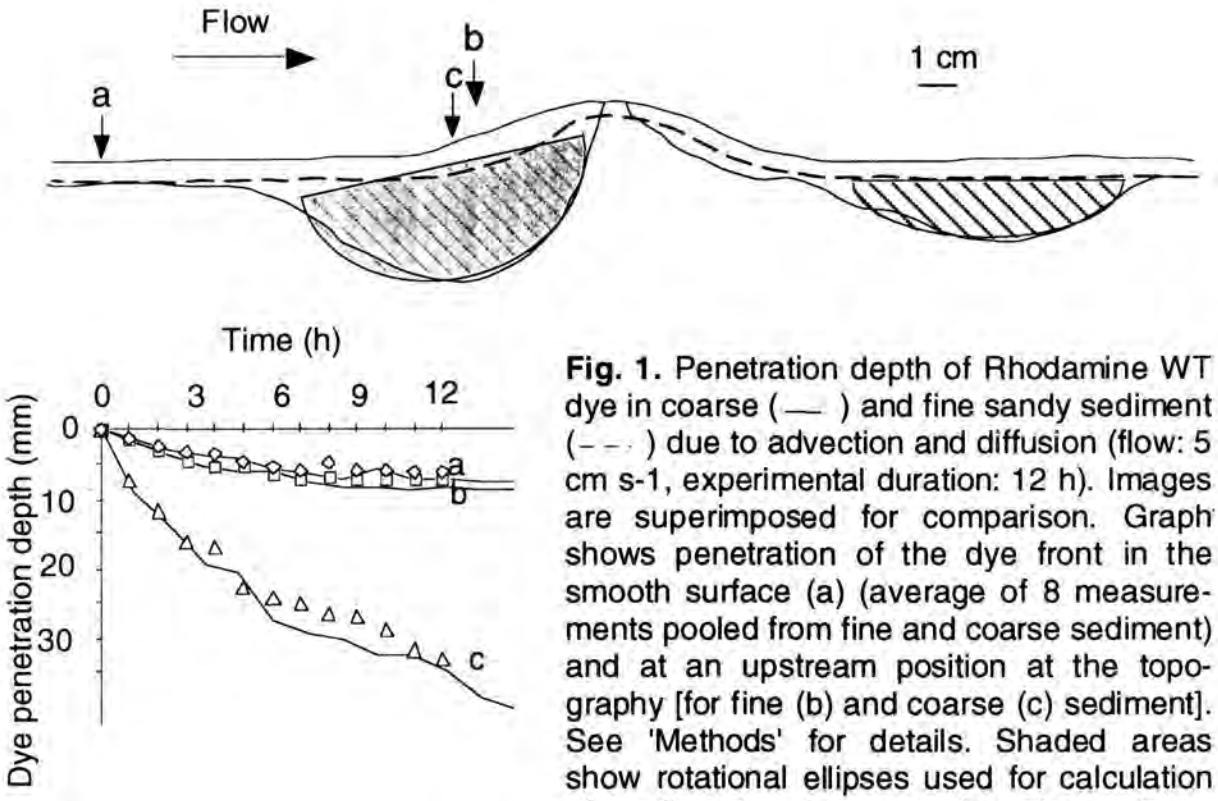

Fig. 1. Penetration depth of Rhodamine WT dye in coarse (—) and fine sandy sediment (- -) due to advection and diffusion (flow: 5 cm s-1, experimental duration: 12 h). Images are superimposed for comparison. Graph shows penetration of the dye front in the smooth surface (a) (average of 8 measurements pooled from fine and coarse sediment) and at an upstream position at the topography [for fine (b) and coarse (c) sediment]. See 'Methods' for details. Shaded areas show rotational ellipses used for calculation of sediment volumes and grain surfaces affected by stained pore water flow.

TOU measurements

The effect of flow on TOU in the two sediment types was investigated by increasing the flow velocity between consecutive runs of 6 experiments listed in table 2. Each experiment included 4 to 8 runs. A 12-hour period was given between changing the flow velocity at the end of one run and the start of TOU measurements in the next one. Prior to each TOU measurement the water was kept above 90 % air saturation by bubbling with air. The flumes were closed with acrylic lids and water was added until no air was left in the system. Light penetration into the flumes was prevented to avoid interfering photosynthetic activity. The initial decline in oxygen concentration during a 4 hour period 2 hours after sealing the flume was used to calculate total oxygen utilisation. Typically the concentration declined from e.g. 190.9 µM to 183.4 µM within 4 hours. Based on the temperature variations and the accuracy of the sensor readings we assign an accuracy of ±1.5 mmol oxygen m^{-2} d^{-1} to TOU values reported. We measured the oxygen consumption of the flume system including collimators, acrylic walls, etc., in a control run with the sediment core covered by a thin acrylic sheet in order to prevent oxygen supply to the sediment. In this case the oxygen consumption was 3 mmol oxygen m^{-2} d^{-1}.

With the coarse sediment we conducted two experiments (1.1, 1.2) with topography structures constructed by the infauna and one experiment (1.3) with artificial topography. Control experiments with smooth sediment surfaces ('smooth control') were performed without topography and without macrofauna present (Exps. 1.4 and 2.4). The macrofauna was removed by sieving (coarse sediment only). To eliminate the topography, the sediment surfaces were carefully smoothed with an acrylic sheet (roughness height $\leq$ 0.3 mm). Finally, in order to compare the effect of sediment permeability in the presence of topography, artificial mounds were built on the fine sediment (Exp. 2.3). In order to test the response of the two sediment types to an addition of particulate organic carbon (POC) we conducted four experiments at a constant flow velocity of 8 cm s^{-1} and with the same salinity and temperature in both flumes (34‰, 16°C, Table 3). A suspension of living planktonic algae (Dunaliella spec., not washed) from a batch culture was added to the flumes and TOU measured during a period of 6 days thereafter.

In experiment 1.6 the coarse smooth sediment core was covered with an acrylic sheet, which made the deposition of algae on the sediment impossible and served as a measure of algal oxygen consumption in the water. In experiment 1.7 we measured the TOU-response to the deposition of POC on a smooth surface of the coarse sediment. In parallel experiments 1.5 and 2.5 both sediment types with the same topography (Table 3) were subjected to identical additions of algae in order to directly compare the effects of topography on POC degradation. The impact of advective pore water flow was assessed from oxygen microprofiles determined prior to and after experiment 1.5 and 2.5. We measured chlorophyll *a* (chl *a*) content (5 replicates; Jeffrey & Humphrey, 1975) and the C/N-ratio (Carlo-Erba Model 1500) in 0.4 µm filtrates from water samples to assess the amount of algal material in suspension (Exps. 1.5-1.7 and 2.5, Table 3). A C/N ratio of 15 found in our fresh algae suspensions was used to convert chlorophyll *a* measurements to carbon-equivalents.

RESULTS

Sediment type and advective water flow

The two sandy sediments used for the comparison were similar in content of water and organic carbon, but they differed in their grain size distribution and permeability (Table 1). Calculated grain surface areas were 208 cm^2 per cm^3 wet sediment in the fine North Sea sand and 115 cm^2 cm^{-3} in the coarse Giglio sand. The experiments with Rhodamine WT dye demonstrated advective transport of water in the coarse

sediment. Intrusion of stained water is depicted in figure 1, a superimposed image derived from the view through the acrylic wall in two tracer experiments. In the more permeable coarse sediment the red colour had penetrated to a maximum of 32 mm in the upstream region of the topography structure after 12 hours of exposure to a free flow of 5.2 ± 0.8 cm s^{-1} (n=11). In the smooth areas of the coarse bed, transport of dye reached a depth of 7.2 ± 1.2 mm (n= 4). Accordingly, the calculation of sediment volume affected by advective flow was 2187 cm^3 relative to a sediment volume of 7200 cm^3 stained predominantly due to diffusion (at 24 mounds m^{-2}) (Table 4). Upwelling of reduced clear pore water from below was marked by the discontinuous distribution of dye on the topography. In the fine grained sand penetration of dye was slightly higher upstream of the topography (6.9 mm) as compared to the smooth surface areas (6.1 ± 0.6 mm, n= 6) after 12 h and at a flow of 5.2 cm s^{-1}. Here the sediment volume affected by advective flow was 68 cm^3 and considerably smaller than the volume stained predominantly by diffusive transport of dye.

Table 4. Sediment volumes and corresponding total sand grain surfaces affected by advection and diffusion (all numbers given for surfaces with 24 mounds of 14 m height per m^2) based on intrusion of dye after 12 h of flow at 5 cm s^{-1}.

	Sediment affected by dye intrusion			
	Fine		Course	
	Diffusive	Advective	Diffusive	Advective
Volume (cm^3 m^{-2})	6100	68	7200	2187
Grain surface (m^2 m^{-2})	127	0.7	83	25

Total oxygen utilisation

The results of the 33 flume runs are summarised in figure 2. TOU increased with boundary flow velocity in the permeable sediment when surface topography was present. Slopes of the regression lines in all three cases are significantly different from zero (student-t test; Exp. 1.1: r = 0.842, p = 0.1; Exp. 1.2: r = 0.652, p = 0.1; Exp. 1.3: r = 0.879, p = 0.005). The increase of TOU with flow for a 10 cm s^{-1} velocity increment amounted to 63%, 55%, and 167% in experiments 1.1, 1.2 and 1.3 respectively. On average TOU increased by 91 ± 23 % (r = 0.782, pooled data, n = 20). There was a difference in topography structure between runs with coarse sediment and natural topography (Exps. 1.1, 1.2) on the one hand and those with artificial topography (Exp. 1.3) on the other hand. Burrowing activity of the infauna

organisms added mounds in the latter experiment (Table 3), some of considerably larger dimensions than the artificial ones. Comparing the intercept of regression lines, a higher value at 0-flow velocity is observed in experiment 1.4, after removal of the macro-organisms and mixing of the sediment during sieving, than in exps. 1.1 to 1.3.

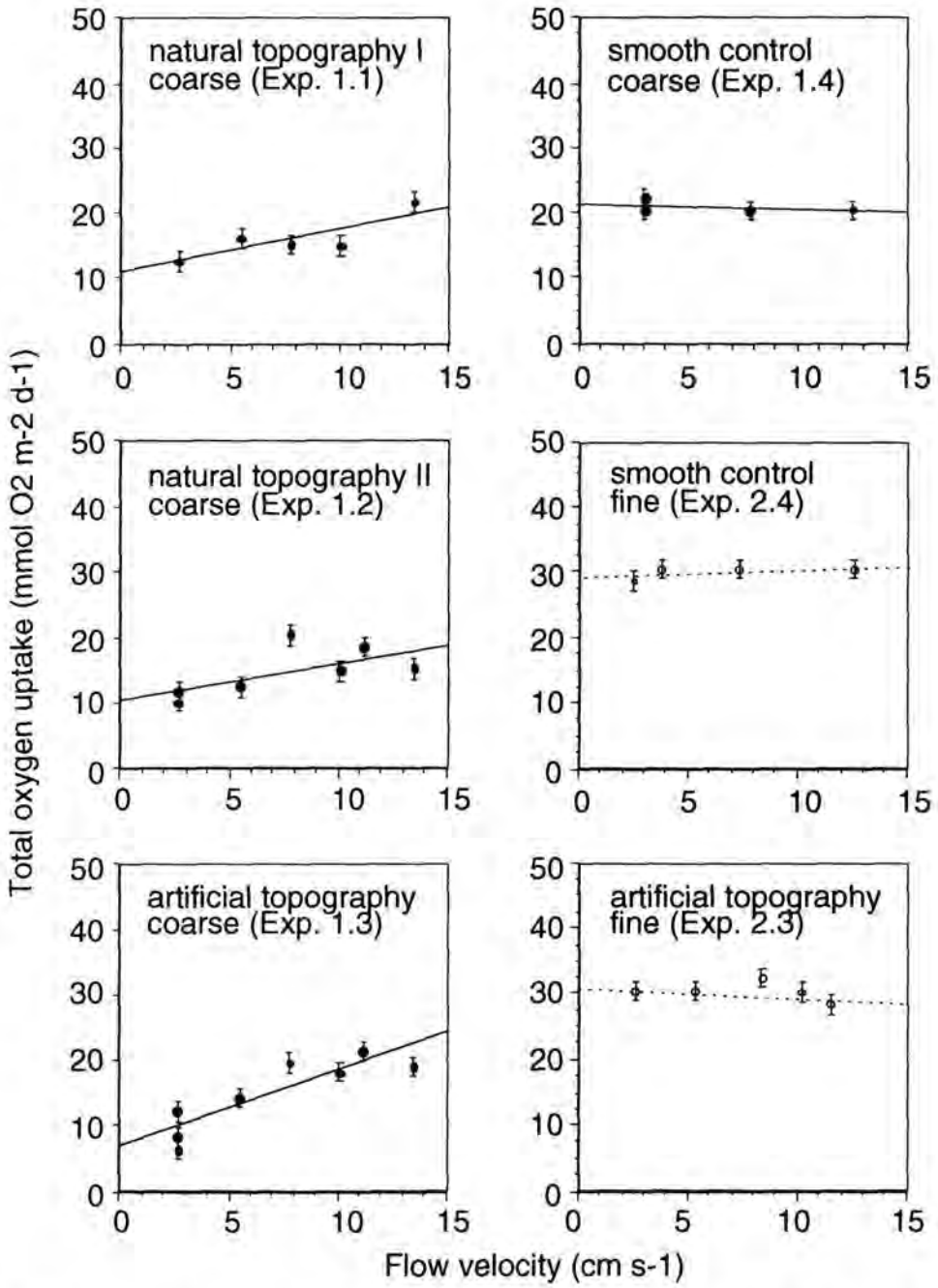

Fig. 2. Total oxygen utilisation (TOU) as a function of flow velocity in sediment cores with different permeabilities and surface topographies. The column on the left includes experiments where advective transport of pore water makes TOU a variable of flow. On the right sediments show no flow-dependency, either because topography structures are lacking or the sediment permeability is too low to show effects of flow on TOU. Error bars show ±1.5 mmol m^{-2} d^{-1}.

There was no detectable flow effect on TOU in the smooth control experiment using coarse sand. The fine sediment core exhibited no dependence of TOU on flow, neither with or without topography added. Oxygen penetrating into the smooth sediment surfaces predominantly by diffusion reached a depth of 4.2 to 4.4 mm on average. The oxygen microprofiles measured at three different flow velocities did not show a significant dependency on flow velocity in either sediment type (Table 4, Fig. 5). Though oxygen penetration depths were similar, oxygen concentrations were higher in the upper millimetre below the sediment-water interface of the coarse sand compared with the fine sediment. Concentration gradients and penetration depths of oxygen are given in Table 5.

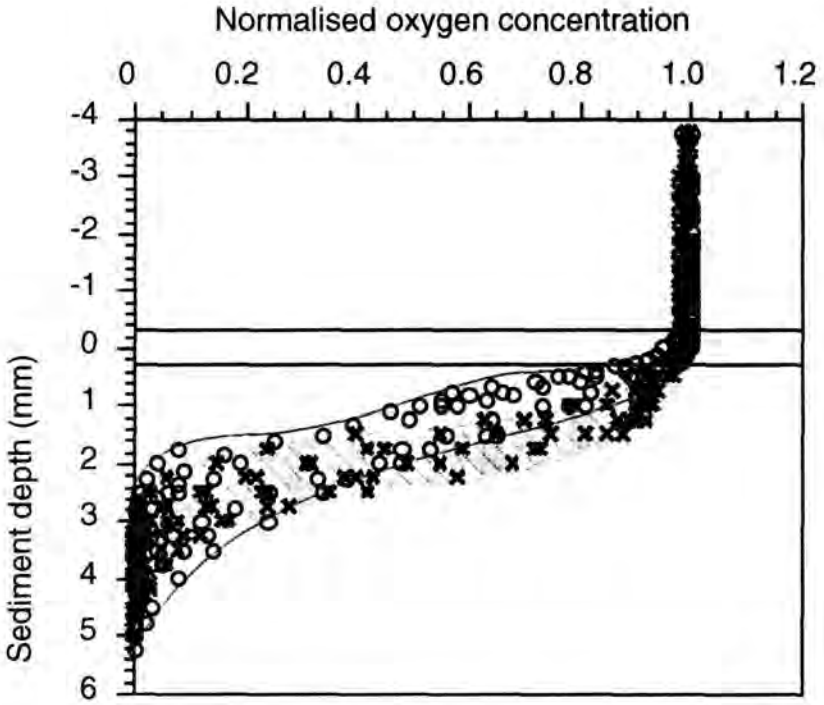

Fig. 3. *Comparison of the oxygen profiles in smooth surface of coarse* (x, hatched area) and fine (o, outlined area) at a flow velocity of 10 cm s^{-1} (Expts. 1.4 and 2.4). Seven concentration profiles are given for each sediment type. For better comparison concentrations are normalised to the overlying water O_2-concentration, which was > 90 % air saturation in each case. Horizontal lines indicate the position of the sediment-water interface within ± 300 µm as determined independently by visual inspection and by the first decline in concentrations by more than 5% of the values in the water column.

Table 5. Steepest oxygen concentration gradient (± s.d.) and penetration depth of oxygen (± s.d.) at smooth sediment surfaces of fine and coarse sand. The values are given for 3 different flow conditions and as average values of all oxygen microprofiles measured. Dye penetration depth at smooth sediment surfaces measured after 12 h at a flow velocity of 5 cm s^{-1} are given for comparison (see Fig. 1).

	Flow velocities (cm s^{-1})			Average
	3 cm s^{-1}	6 cm s^{-1}	10 cm s^{-1}	
Coarse				
Gradient (µM mm^{-1})	0.95 ± 0.18	0.85 ± 0.20	1.15 ± 0.11	1.05 ± 0.30
Penetration (mm)	4.2 ± 0.6	5.3 ± 1.1	3.8 ± 0.5	4.4 ± 1.0
n	6	5	7	18
Dye penetration (mm)		7.2 ± 2.8		
Fine				
Gradient (µM mm^{-1})	1.09 ± 0.27	1.18 ± 0.15	1.30 ± 0.28	1.18 ± 0.26
Penetration (mm)	4.6 ± 0.3	4.1 ± 0.4	3.9 ± 0.9	4.2 ± 0.7
n	5	5	7	17
Dye penetration (mm)		6.1 ± 0.6		

At a constant flow velocity of 8 cm s^{-1} and with POC addition, oxygen penetration depth in the coarse sediment decreased in the upstream region of the mounds within 6 days by 5 mm from 19 to 14 mm (Fig. 4 a). In the fine sand oxygen penetration decreased by only 1 mm to 6 mm in the corresponding locations (Fig. 4 c). No significant changes were recorded in the smooth surface control oxygen profiles of either sediment type (Fig. 4 b, d).

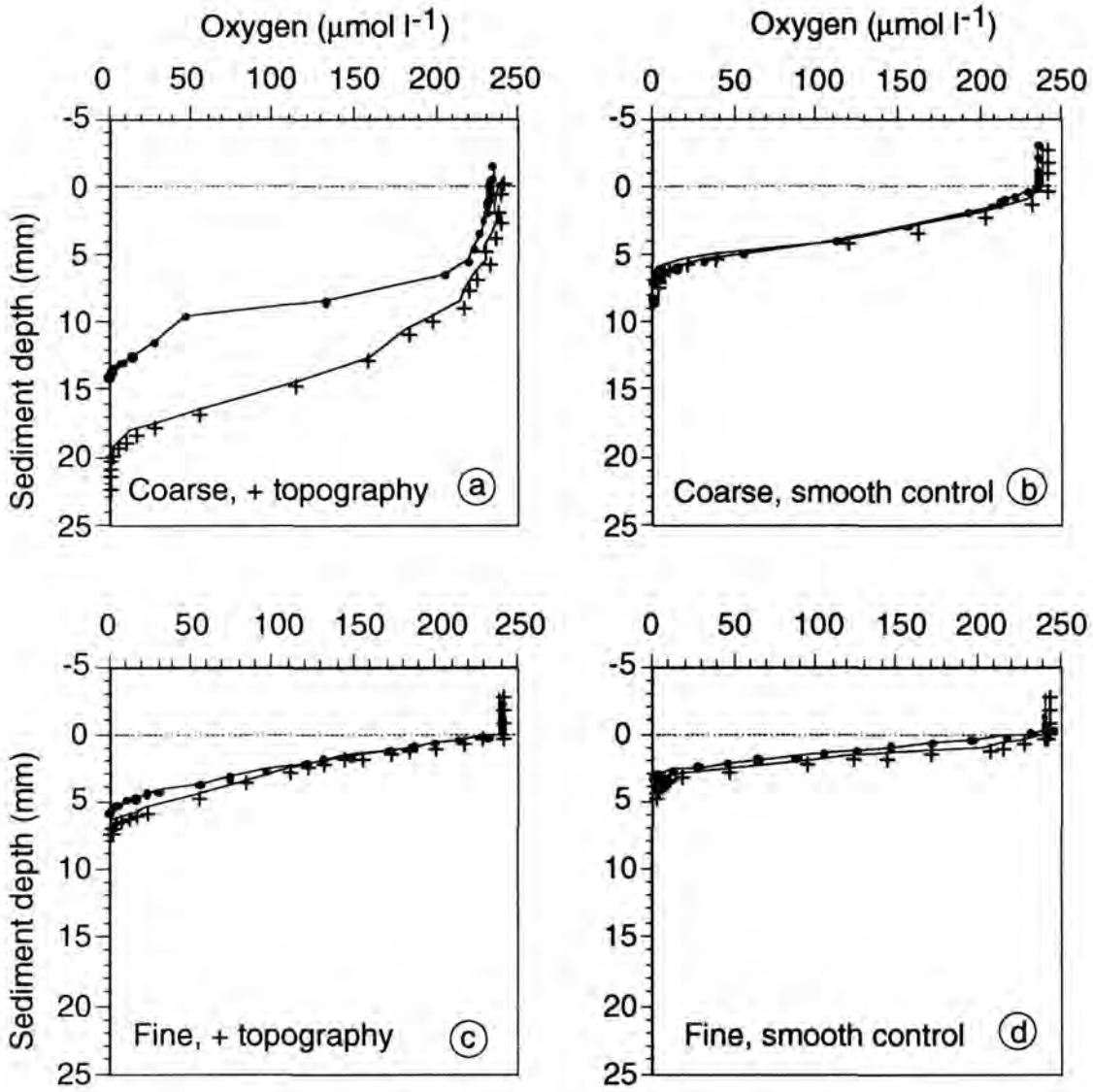

Fig. 4. Penetration of oxygen in coarse (a, b; Exp. 1.5, table 2) and fine sandy sediment (c, d; Exp. 2.5) at selected sites before (+) and 6 days after (•) addition of particulate organic carbon. The profiles in graphs (a) and (c) ('topography') were taken at the site of maximum penetration depth of oxygen upstream of the mound. Profiles (b) and (d) are from smooth control areas in the same flume.

Total oxygen utilisation increased in each of the experiments (Fig. 5). An addition of POC to the flume without deposition on the sediment surface (control experiment 1.6: sediment covered with an acrylic sheet) lead to a short response lasting three days only. Oxygen consumption in the water, presumably by the algal respiration, increased TOU by a total of 6 mmol O_2 m^{-2}. In contrast, algae settling on a smooth sediment surface (experiment 1.7) caused an increase in O_2 utilisation lasting 4 days with a total of 23 mmol O_2 m^{-2}.

In experiments 1.5 and 2.5 the algae settled within 5 days as traced by declining chlorophyll *a* concentrations in the water column equivalent to an organic matter

addition of 60 mmol C m^{-2}. This material initiated a TOU increase which lasted longer than the 6 day period given for measurements. A minimum estimate from the data in Fig. 4 of the additional TOU is and 30 mmol O_2 m^{-2} in the fine and 50 mmol O_2 m^{-2} in the coarse sediment.

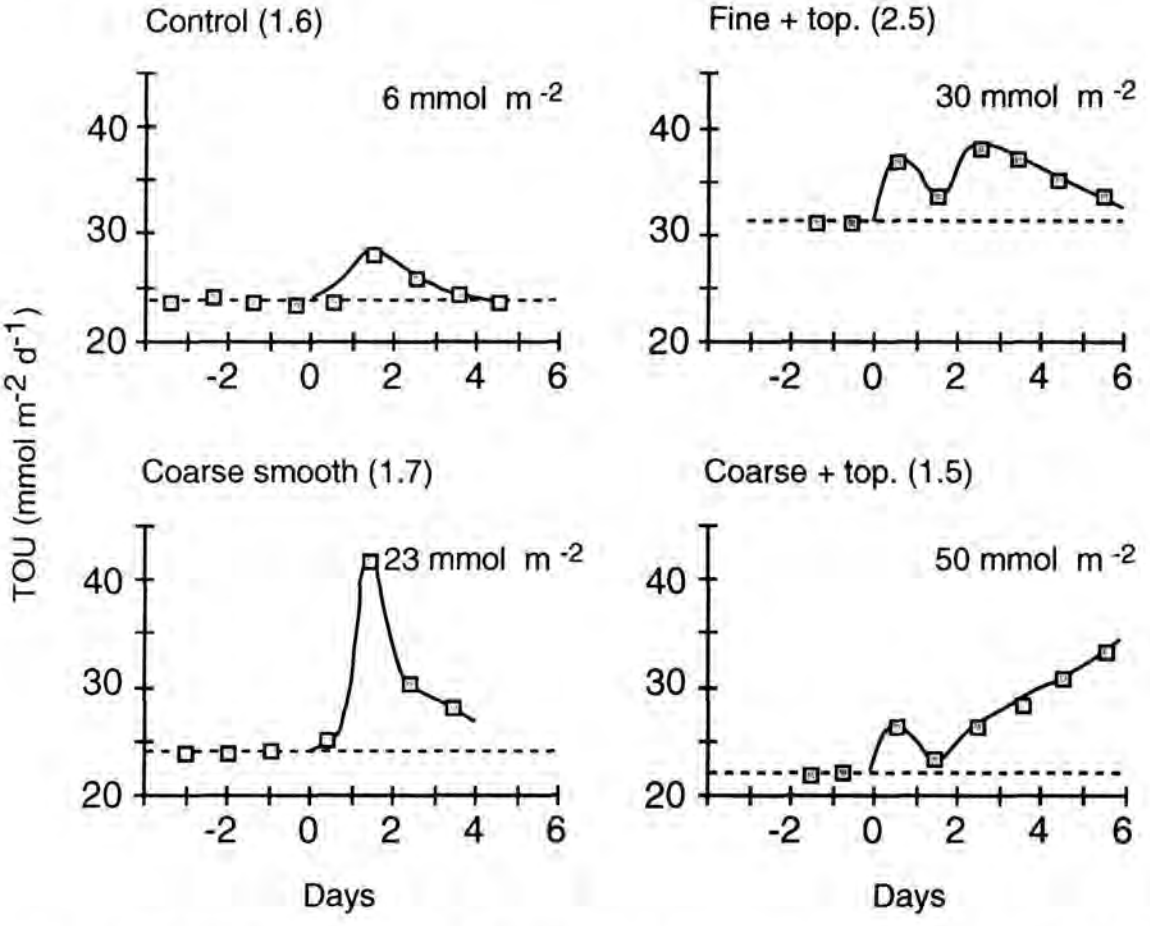

Fig. 5. Time courses of TOU after addition of particulate organic carbon (POC) at day 0. TOU readings were taken once a day with an accuracy of ±1.5 mmol m^{-2} d^{-1}, as indicated by the dimension of the squares. Dashed lines indicate the level of TOU assumed without POC addition. Additional TOU due to POC is calculated by integrating the area between both lines (given in mmol O_2 m^{-2} in each graph). Experiment 1.6 (control): sediment covered with acrylic at t = 0 in order to prevent deposition of algae on the sediment; experiment 1.7: deposition of algae on the smooth surface of the coarse sand; experiment 2.5: effect of deposition of algae on the fine sediment; experiment 1.5: combined effect of advective oxygen transport and POC-input in permeable coarse sand.

DISCUSSION

Flow plays a major role in controlling flux of oxygen and other solutes across the sediment-water-interface (Pamatmat 1971, Bowmann & Delfino 1980). The transformation of organic matter in cohesive sediments is limited by diffusion as the dominant transport process of electron acceptors available for the remineralisation of organic matter by bacteria (Froelich et al. 1979). Biological and hydrodynamical mechanisms enhancing solute fluxes across the sediment-water interface thus increase the potential for mineralisation (Aller 1980, Huettel & Gust 1992, Webster & Taylor 1992, Forster & Graf 1995). Ziebis et al. (1996) investigated the distribution of oxygen in the same coarse sediment in relation to the mechanism driving pore water flow. They demonstrated dramatic changes of oxygen penetration depth with changing flow velocity. The present study focused on the combined effect of surface topography interacting with boundary layer flow on the utilisation of oxygen (TOU).

The advective flow

A linear increase of TOU was observed in the permeable sediment with surface topography present and flow velocities varying between 2 and 14 cm s^{-1} (Fig. 2). This increase is a result of a combined effect of permeability and topography. Permeability differed by one order of magnitude between the coarse and the fine sediment. The effect of permeability on advective flow is apparent in the comparison of fine and coarse sediment of regions adjacent to the topography structure (Fig. 1). The higher permeability of the coarse sand ($k = 5 \times 10^{-11}$ m^2) facilitated flushing of pore space in the vicinity of the topography (Fig. 1, Fig. 3). Water penetrated 32 mm deep into the sediment reaching sediment grain surfaces that were left anoxic at the corresponding depth in the fine sediment. Judging from our experiments with flow of 5 cm s^{-1}, 30 % more particle surface area was exposed to dye due to advection in the coarse sand than in the fine sand. In contrast, in the smooth surface of both coarse and fine sediment, an increase in stained sediment with increasing flow speed was not detectable. In a smooth sediment surface, dye penetration depth after 12 h agreed with average O_2-penetration in steady-state profiles for both sediment types (Table 5). Here, no effect of permeability can be seen in our data. With a permeability of $k = 5 \times 10^{-12}$ m^2 the fine sediment allowed for only little stained water intrusion in the upstream region of the topography structure (Fig. 1), which is documented in a one millimetre increase in dye penetration depth.

A calculation of the particle surface areas yields 127 m^2 m^{-2} in the surface layer of the fine sandy sediment stained by dye (6.1 mm penetration depth, 208 cm^2 particle

surface area per cm^3 wet sediment). The corresponding value in the coarse sand was 83 m^2 m^{-2} if no flow effects were present, that is assuming a dye penetration of 7.2 mm throughout the entire sediment surface (7.2 x 115 cm^2 cm^{-3}). This indicates that there are potentially more bacteria present in the stained fine sand volumes, since most bacteria in sediments adhere to sediment particle surfaces (Meyer-Reil 1986). However, due to topography-flow interaction, in a coarse permeable sediment the total grain surface in contact with oxic water from the sediment-water interface increases with flow, an effect not seen in the fine sediment. Exposed particle surface area in the coarse sand increased from 83 at assumed 0 cm s^{-1} to 108 m^2 m^{-2} (83 m^2 + 25 m^2 in advection areas) at flow of 5 cm s^{-1}, if calculated for mounds of 14 mm height and an abundance of 24 m^{-2}. At higher flow velocities or with more pronounced topography present, more particle surface area with associated bacteria is supplied with oxygen in a permeable bed than in a fine-grained sediment where diffusion is the limiting transport for oxygen from the overlying water.

We conclude that the sediment volume affected by advective pore water flows is negligible in the fine sediment. Pronounced advective transport can be observed in permeable sands, with the sediment volume and grain surface affected by advection increasing with flow velocity and topography present.

Processes increasing TOU

Flow influences the thickness of the diffusive boundary layer (DBL) of the sediment surface making it a rate limiting step in the interfacial transport of oxygen (Morse 1974, Gundersen & Jorgensen 1990, Jørgensen & Des Marais 1990). This effect is most pronounced in organic rich sediments where concentration gradients at the interface are steep. In our oxygen microprofile measurements at the smooth sediment surfaces, the DBL could not be resolved with the spatial resolution used. We therefore could not detect an increase in oxygen gradient with flow velocity (Table 5) indicating that these smooth surface areas did not contribute to the observed positive relation of TOU and flow above coarse sand in our experiments 1.1, 1.2, and 1.3. In any case, we consider the effect of DBL depression on TOU minor in the relatively organic poor sands used. There are, however, indications that the oxygen distribution at the smooth surface of the coarse sediment is different from that in fine sand. In Fig. 3, oxygen profiles taken from the coarse sediment show a slower decline of concentration with depth within the first millimetre of the sediment compared to the fine sediment profiles. Microprofiles of this sigmoidal shape reveal advective transport in the uppermost sediment layer (Revsbech et al. 1980), suggesting that flow in our flume systems potentially affected oxygen distribution

even at the smooth surface of this coarse sediment. The extent to which oxygen flux at this surfaces is possibly enhanced due to flow is below the resolution of our TOU measurements. This issue awaits further investigation.

In contrast to the situation at the smooth surface, boundary flow significantly increases the volume of oxic sediment in the vicinity of surface topography as demonstrated by Ziebis et al. (1996). The authors measured the distribution of oxygen in the advective flow zone of a mound and report an additional oxic volume of 98 cm^3 in the coarse sediment generated by a single mound (height: 10 mm, flow velocity: 10 cm s^{-1}). Adopting this number as the average effect of mounds in our experiments, we can calculate the increase in oxic sediment volume through flow and relate this volume to the oxic surface layer of 4.4 mm thickness present without flow. The estimated oxic volume increase, thus, lies between 49 % (98 x 22/4400) and 85 % (98 x 38 / 4400) with 22 to 38 mounds per m^2 present. The observed increase in TOU of 55 to 167 % in TOU in the coarse sediment experiments is in the same range as the sediment volume flushed by oxic water through the advective flow. Deviations in size from the 10 mm standard mound assumed in the estimate above may account for the differences in the percentages, since sediment volume affected by advective flow increases exponentially with size of the mounds (Huettel & Gust 1992). Natural topography in the experiments constructed by *Callianassa truncata* consisted of mounds of approximately 1 to 3 cm height and 3 to 6 cm diameter, and funnels of 1 to 2 cm diameter 1 cm depth. In the fine sediment an equivalent estimate yields an oxic volume increase ≤ 0.5%, impossible to detect in our TOU measurements.

Other oxygen consuming processes included in the coarse sediment experiment with natural topography (Exps. 1.1, 1.2, 1.3) were irrigation and respiration by the shrimp. We did not measure these. However, their contribution to TOU is a function of the metabolism of the organisms themselves. Therefore a linearly increasing relation with flow velocity is not to be expected. Such a relation could be observed in the case of relict burrows flushed by boundary velocity induced secondary flows (Ray & Aller 1985), or in the case of a faunal irrigation activity stimulated by boundary layer flow, a mechanism which to our knowledge has not been reported so far. TOU increased as a function of the abundance of mounds (Exps. 1.1 and 1.2 vs Exp. 1.3) with the same number of animals present in all experiments. This further supports the conclusion that advective flushing of sediment interstices rather than irrigation was responsible for the positive relation of flow and TOU. Reduced sediment expelled from the burrow may have contributed to the scatter observed in the TOU data of both sediment types. However, burrowing activity can neither explain the

observed linear increase in TOU with flow velocity nor differences between fine and coarse sediment.

TOU was in the range of 30 mmol O_2 m^{-2} d^{-1} for all measurements performed in the fine sediment core. In the coarse sediment TOU was lower (intercept at zero flow around 10 mmol O_2 m^{-2} d^{-1}). This observation is in agreement with a lower activity generally associated with low organic carbon content in sandy environments (Keil et al., 1994). TOU in the coarse sediment control experiment 1.4, however, showed a higher level (20 mmol O_2 m^{-2} d^{-1}) after complete mixing of the sediment in order to remove the macrofauna. This mixing destroyed the stratification of bacterial distribution within the sediment and altered microbial activity. It also brought in contact reduced sediment layers with former surface sediment and possibly facilitated the oxidation of minerals, for instance FeS_2, in the oxic layer. After a week of equilibration TOU was measured and remained constant for 5 days on a high level, reflecting a new steady state of microbial processes. An important result is that oxygen flux was not a function of flow velocity.

In addition to increasing the oxic sediment volume, the advective flows depicted in Fig. 1 also enlarge the interface between oxic and anoxic sediment and channel a flow of reduced pore water upwards to the sediment surface (Huettel et al.1996b, Ziebis et al. 1996). The latter mixes with the recirculating water of the flume and an unknown amount of oxygen, equivalent to the reduced solute content of the upwelling water, is utilised. Presumably the contribution of upwelling pore water was of minor importance in our experimental set-up with relatively little anaerobic activity at low sediment carbon content. This is also indicated by the agreement between the sediment volume flushed and the TOU increase. Processes at oxic-anoxic interfaces and effects of upwelling reduced pore water may be more pronounced in sediments rich in organic carbon.

Within the limits of accuracy, the TOU increase observed in the coarse sediment experiments is related to the oxic volume enlargement of sediment at the topography structures. This result is in agreement with oxygen consumption being a 0-order process with respect to oxygen at concentrations above 10 µM (Hao et al. 1983, Rasmussen & Jørgensen 1992). With TOU dependent on advective interfacial pore water flow, one more mechanism for enhanced O_2-uptake is presented. The result indicates that in-situ oxygen utilisation data from sandy beds have to be interpreted in context with the flow conditions and topography maintained during the measurements.

Effects of fresh carbon input

Oxygen is consumed at higher rates in sediments that are rich in degradable organic material and after sedimentation events (Graf et al. 1983, Hansen & Blackburn 1992). In our TOU-experiments, we assumed the organic matter to be associated with particle surfaces in both sediment types, that is, a distribution as a monolayer on the particles (Mayer et al. 1985, Mayer et al. 1988). However, in most cases of high fresh carbon input, dissolved organic carbon and organic rich large particles are dominant in the pool of carbon and a fixed relation of organic carbon to particle surface area does not exist (Mayer 1989).

The experiments showed that oxic respiration in the flumes is enhanced when POC deposits on the sediment. A minor increase in oxygen consumption owing to the presence of algae in the flume water (6 mmol O_2 m^{-2}) is maintained for a short time only and cannot account for the TOU responses obtained in the subsequent experiments. POC deposited on the smooth surface of the coarse sediment (Exp. 1.7) was available for aerobic processes with predominantly diffusive supply of oxygen and caused 23 mmol O_2 m^{-2} of additional TOU. A similar value was obtained in fine sediment with topography present (Exp. 2.5, 30 mmol O_2 m^{-2}), but the highest additional consumption of oxygen clearly resulted in the combination of POC addition and advective oxygen supply (Exp. 1.5, 50 mmol O_2 m^{-2}).

Increased oxygen utilisation may reflect decomposition of a certain percentage of the carbon input and is calculated assuming complete aerobic respiration and a respiratory ratio of 0.85 (moles of CO_2 evolved per mole O_2 consumed, Schmidt-Nielsen 1983). Additional oxygen utilised in our experiments thus corresponds to 71 % in the coarse and 43 % the fine sediment of the carbon added to the flumes. This indicates that particulate carbon is remineralized quite effectively under flow conditions and more so in the coarse sediment. Monitoring oxygen uptake in an algae addition experiment, Hansen and Blackburn (1992) found an equivalent of less than 20 % of the carbon added within 5 days.

The amount of POC added (60 mmol C m^{-2}) is roughly equivalent to twice the daily export production to the sediment in the North Sea given as 38 mmol C m^{-2} y^{-1} by Wollast (1991) (170 g C m^{-2} y^{-1}). Sedimentation events in the field and additions in bloom simulation experiments often involve much higher masses of carbon than our addition. Hansen and Blackburn (1992) added algae equivalent to 686 mmol C m^{-2} to incubated sediment cores triggering a response in increased oxygen uptake lasting 13 days. From an addition experiment with *Phaeocystis spp.* equivalent to 2000

mmol C m^{-2}, van Duyl et al. (1992, 1993) reported 10 days of increased bacterial production. Graf et al. (1983) observed a bloom of 960 mmol C m^{-2} settling in the field and a response in heat production in the sediment indicating complete utilisation of that bloom material within 13 days. In view of the relatively small additions the duration of responses found in our addition experiments fits reasonably well. There is a further increase in TOU after 6 days in the coarse sediment such that the ratio of additional oxygen utilisation in the coarse over the fine sediment (50 mmol O_2 m^{-2} / 30 mmol O_2 m^{-2}) would have been even higher after some more days.

When particulate carbon in the form of algae deposits on the sediment, cells release exudates, open by lysis or due to meiofauna feeding in the sand (Jensen 1987). Organic material deposited on the sediment surface or components thereof (DOC) is also found in the sediment below (Graf 1992, Sun et al. 1994). Deposition of algae is increased in the vicinity of roughness elements (Yager et al. 1993) and advective pore water flow carries POC into the interstices at the sites of maximum oxygen penetration (Huettel et al. 1996b). Intense oxygen respiration decreased the oxic sediment volume in our experiments, as reflected in O_2-microprofiles (Fig.4). However, advective transport of oxygen remained constant throughout the experiments at 8 cm s^{-1} and oxygen was supplied at a rate sufficient to sustain an oxic sediment layer thicker than in the control area. A decrease in oxic volume after POC input implies that rates of utilisation of oxygen per unit volume was stimulated to an even higher degree by advective transport in the presence of easily degradable carbon. This is also evident in the comparison of coarse sediment with and without advective flow. Additional TOU in the coarse sediment was twice as high with topography and larger oxic sediment volume than without advection at the smooth sediment surface (Exp. 1.5: 50 mmol O_2 m^{-2}; Exp. 1.7: 23 mmol O_2 m^{-2}). The data show that permeable sediments do have a high potential for aerobic oxygen utilisation.

Implications for the field

The predominant regions where advective transport of pore-water oxygen potentially increases TOU are well-sorted sands with low fine sand fraction of the intertidal and subtidal areas of the shelves. In shallow waters permeable sediments, wave action, and currents contribute to flushing of the pore space (Riedl et al.1972, Webster 1992, Webster & Taylor 1992). Ripples on the order of several centimetres height develop on sandy grounds to tens of meters water depth (Jenness & Duineveld 1985) and to >100 m depth due to heavy storms (Bedford & Abdelrhman 1987). Abundant biogenic topography structures ranging from 20 to 120 m^{-2} are reported from many

shelf and coastal sea beds (Suchanek 1985, Huettel 1988, Witbaard & Duineveld 1989, Cadée 1976, Griffis & Suchanek 1993, Ziebis et al. 1996).

Our experiments demonstrate that advective pore water flow is effective in stimulating sedimentary total oxygen utilisation with potential effects on nutrient and pollutant cycling (Kersten et al. 1988, Walsh 1991). When comparing our findings with the field caution is warranted since the mechanisms active produce an overall effect on TOU which depends on a number of variables, among others abundance and type of topography, sediment permeability, and the carbon available for mineralisation. This paper probably describes minimum effects on TOU, since flushing of pore space increases with boundary layer flow velocity (Huettel & Gust 1992), and velocities in our experiments were at the lower end of the range possible. As indicated by the carbon addition experiment, advective transport enhances TOU even more when easily degradable organic carbon is available (Shum & Sundby 1996). Particularly in shallow marine environments a substantial portion of fresh carbon deposition is observed in episodic events (Smetacek et al. 1978, Graf et al. 1983, Graf 1992, Walsh 1991). The impact of boundary layer flow on remineralisation of carbon may therefore be more pronounced following sedimentation events. Moreover, organic poor sands apparently have a higher capacity for mineralisation than previously thought (Shum & Sundby 1996). In these sediments the combined effects of fresh carbon supply and advective oxygen transport provide a mechanism by which carbon utilisation is enhanced.

ACKNOWLEDGEMENTS: We would like to thank S. Wenck for her help with the flume work and U. Bathmann for letting us use the CHN element analyser at the Alfred-Wegener Institute. There was valuable support from G. Herz, O. Görg, V. Meyer and G. Kothe from the machine and electronics shop during this early experimental phase with the flumes. Oxygen microelectrodes were skilfully constructed by A. Glud, A. Eggers, and G. Eickert from the microsensor group. We are grateful for U. Berninger's help both in the experiments and discussion of results. The manuscript benefited from constructive criticism of anonymous reviewers. This work was supported by the Max-Planck-Society, Germany.

Flow-induced uptake of particulate matter in permeable sediments

Markus Huettel, Wiebke Ziebis, Stefan Forster

Max-Planck-Institute for Marine Microbiology, Celsiusstr.1, D-28359 Bremen

Limnology and Oceanography 41 (2): 309-322, February1996

ABSTRACT: We demonstrate the fast transfer of suspended particles from the boundary layer into the upper strata ($z < 4$ cm) of permeable sediments with topography-related interfacial water flows. The transport is driven by pressure gradients ($D P < 3$ Pa) that are generated when bottom flows ($u \leq 10$ cm s^{-1}) are deflected by small surface structures ($z < 3$ cm) of hydrodynamical or biological origin. Acrylic pigment grains of 1 and 10 µm diameter traced the intrusion of particulate matter into sandy sediment ($k > 2 \times 10^{-11}$ m^2) incubated in a laboratory flume. Increased pressure up- and downstream of small mounds ($z = 2.5$ cm) drove water 5.5 cm into the core, carrying suspended particles (1 µm) down to 2.2 cm sediment depth within 10 h. Simultaneously, decreased pressure at the downstream slope of the protrusions drew pore fluid from deeper layers ($z \leq 10$ cm) to the surface. In the sediment, friction reduced the velocity of the particulate tracers resulting in size fractionation and layers of increased particle concentration. Ripple topography (0.8-2.8 cm height) enhanced interfacial particle (1 µm) flux by a factor 2.3 when compared to a level control core. The pathways of the particle and solute tracers below a sediment ripple are explained using a source-sink-model that describes the pore flow velocity field. Our results suggest that bed-form-induced interfacial flows are important for the uptake of particulate organic matter into permeable shelf sediments.

INTRODUCTION

In shelf environments up to 50% of the primary production can settle through the water column (Riley 1956; Jørgensen et al. 1990). Most of this particulate organic material (POM) is mineralized in the sediment and its decomposition products are returned to the water column (Canfield et al. 1993; Nedwell et al. 1993). The seabed thus acts as a site of substantial nutrient recycling (Berner 1980).

The transfer of suspended particulate matter into sediments involves two steps: first, the removal of the suspended matter from the boundary layer, and second, the

transport of the particles into the sediment. Gravitational settling (Deuser et al. 1981), filtration activities of benthic animals (Hargrave 1976; Risk & Moffat 1977), and aggregation at the sediment-water interface (Stolzenbach et al. 1992) withdraw particles from the bottom water. Progressing sedimentation (Smetacek et al. 1978), lateral sediment flows (Jenness & Duineveld 1985) and bioturbation (Huettel 1990; Boudreau 1994) then transfer the deposited materials from the aerobic interface to deeper, possibly anaerobic sediment layers.

In addition to these sedimentological and biological processes we propose that a hydromechanical mechanism can enhance the transfer of suspended particles into permeable marine sediments. The driving forces for this transport are pressure gradients, generated when boundary layer flows interact with sediment topography. Soft seabeds are characterized by a variety of surface structures of biological, hydrodynamical or geological origin. Foraging of benthic organisms create mounds, funnels and trails, while current-induced lateral sediment transport generates ripples on the beds (Heezen & Hollister 1971; Smith et al. 1993). Despite its relatively small size (the majority of these structures does not exceed 5 cm height), this topography affects existing bottom flows.

On the shelf, the water overlying the sediment rarely is stagnant. Wind, waves, tides and density gradients generate water currents reaching down to the shelf bed (Davies 1993; Van Weering et al. 1993). The resulting bottom flows are deflected by the seabed topography. Flow obstruction by structures protruding the sediment surface causes pressure increase at the slopes opposing the flow. Pressure decreases where the flow accelerates while passing over the elevated structures i.e., the Bernoulli principle (Batchelor 1967; Schlichting 1987), Fig. 1. In sediments with permeabilities $k > 2 \times 10^{-11}$ m^2 (permeability $k = Km/rg$, K = hydraulic conductivity, m = dynamic viscosity, r = density, g = gravity), the resulting horizontal pressure gradients produce fluid transport across the sediment-water interface and related pore water flows (Huettel & Gust 1992).

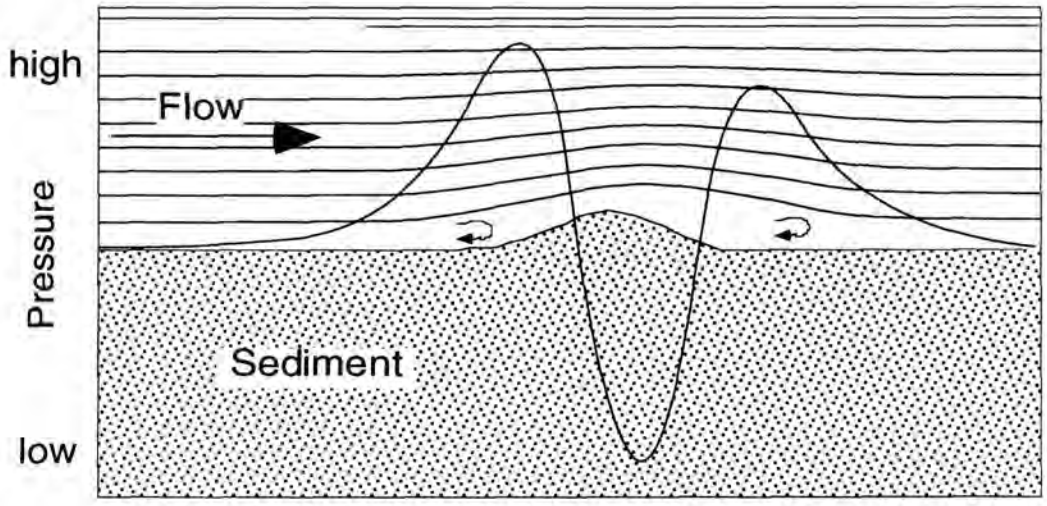

Fig. 1. Water flow (thin lines), deflected by protruding topography, produces pressure changes (thick line) at the sediment-water interface.

Wave induced oscillating bottom currents, river and tidal flows have been shown to generate such advective pore water circulation in sediments with topography (Webb & Theodor 1968; Thibodeaux & Boyle 1987; Savant et al. 1987). In flume experiments, flow over sandy sediment with simulated biogenic surface structures increased interfacial fluid exchange up to seven-fold (Huettel & Gust 1992). The question arises, whether these interfacial fluid flows contribute to the flux of particulate organic matter. In this article we present an investigation of the co-transport of fluid and particles through the sediment-water interface caused by the interaction of bottom flows and sediment topography.

MATERIAL AND METHODS

Three laboratory flume experiments with permeable sediments were designed to assess the intrusion of tracer particles at small mounds and depth range of the advective transport processes with time (Exp. 1), the extent of the advective transport processes for different sized particles caused by mounds of different heights (Exp. 2), and the enhancement of particulate matter flux due to ripples on the sediment surface (Exp. 3).

The recirculating flume used for these experiments was made of clear acrylic and had an open-channel section of 200 cm length, 30 cm width, and 12 cm height. A drop box, located 90 cm downstream in the channel, contained the experimental sediment core (60 cm long, 30 cm wide, 20 cm deep). The sediment consisted either of sieved quartz sands or natural beach sand (Table 1). The permeabilities and the

retardation factors of the particulate tracers in these sediments were determined with a constant head permeameter, as described by Means and Parcher (1964). The ratio of the particle velocities and fluid velocity in the permeameter column yielded the retardation factors.

Before each experimental run, the sediment was compacted by applying low frequency vibrations, and the surface was carefully smoothed. Then the small mounds (experiments 1 and 2, Fig. 2) or ripples (experiment 3, ripple heights 0.8 to 2.8 cm, wavelength 10-15 cm) were built on the surface.

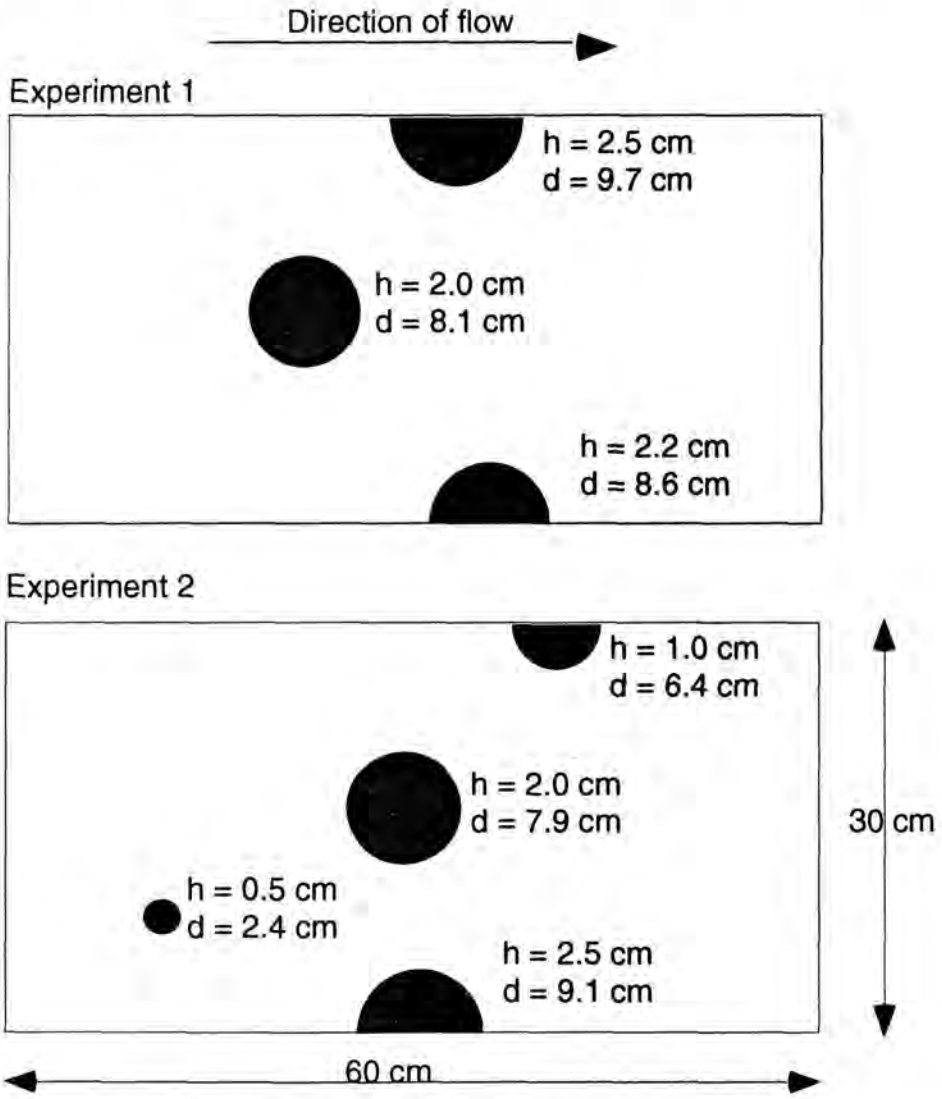

Fig. 2. The positions and dimensions of the mounds in experiment 1 and 2. The rectangles represent the sediment surfaces seen from above, the dark circles indicate the locations of the mounds, h = height, d = diameter.

The flume was filled with 160 litres of freshwater. Cooling coils located in the return pipe of the flume held the water temperature at 20° C. An axial pump, controlled by a

flow sensor (MiniWater 2, Schiltknecht), recirculated the water at the selected flow velocity of 10 cm s^{-1} at 8 cm above the sediment. The water depth of 10 cm above the sediment core was maintained by adjusting the height of a weir at the end of the open channel section and the flume tilt. Flow velocity profiles above the smooth surface and topography were measured with thermistors (LaBarbera and Vogel 1976). A sensitive differential pressure gauge (Effa Ga 63), connected to gauze-covered pressure ports located 0.5 mm below the sediment surface, recorded the pressure differential between protruding topography and the level sediment surface (Huettel & Gust 1992).

To trace particle transport into the sediment, we added non-soluble acrylic pigment grains (black: 1 ± 0.8 µm, $r = 1.48$ g cm^{-3}, 10^5 ml^{-1} (experiments 1, 2, 3); blue: 10 ± 7 µm, $r = 1.45$ g cm^{-3}, 10^4 ml^{-1} (experiment 2) to the flume water at the beginning of the experiments. Interfacial solute transport was traced using the fluorescent red dye, Rhodamine WT (3.5 µm), mixed either into the pore water of the sediment core (experiment 1) or into the recirculating flume water (experiments 2 and 3). In experiment 2 the pore water of two horizontal sediment layers, the upper at 7 to 9 cm depth, the lower at 13 to 15 cm depth, were also stained with Rhodamine to trace pore fluid transport at depth. The intrusion of particles and fluid into the sediment could be observed through the transparent side walls of the flume. Time-lapse photography and video recordings documented the progress of the advective transport processes and permitted the calculation of their velocities. The concentration decrease of tracers in the recirculating flow was monitored by spectrophotometrical analysis of water samples. Experiment 1 lasted 120 h, experiment 2: 16.5 h and experiment 3: 5 h. At the end of the experiments the water was drained. Sequential removal of 2-mm-thick horizontal layers of sediment from the core with a vertically adjustable sharp blade revealed the solute and particle pathways inside the sediment. After experiment 2, we digitized the picture of each exposed layer and separated the RGB signals (red, green, blue value of each pixel) to outline the zones affected by the different tracers. The line was drawn where the respective color intensity exceeded that of the average background value for that color. With these outlines the program "MacStereology" (Moss 1993) reproduced a three-dimensional transparent view of the tracer intrusion zones and calculated their depths, surface areas and volumes.

RESULTS

The flume flows

With Reynolds numbers of Re ≈ 12,000 to 19,200 our open channel flow was turbulent [Re = 4 H u ρ / μ (Giles 1976), where hydraulic radius, H = 0.06 m, average velocities, u = 0.05 to 0.08 m s^{-1}, density, ρ = 1000 kg m^{-3}, dynamic viscosity, μ = $1x10^{-3}$ kg m^{-1} s^{-1}]. The length of the channel did not allow full development of the boundary layer at the selected free-flow velocity of 10 cm s^{-1} and 10 cm water depth. Velocity profiles measured above the smooth control core indicated that the thickness of the boundary layer grew from 4 cm at the upstream end to 5 cm at the downstream end.

Internal boundary layers created by the protruding structures dominated the flow regime over the surfaces with topography. The velocity profiles depicted in Fig. 3 reflect reduced flow speeds with enhanced turbulence up- and downstream of the mound and accelerating flows above the protrusion. This acceleration caused a pressure decrease at the top of the mound, e.g. by 1.2 Pa for a mound of 2.2 cm height exposed to a current velocity of 10 cm s^{-1} (Fig. 4). The resulting pressure differentials altered the hydraulic gradients within the core thereby generating advection across the sediment-water interface.

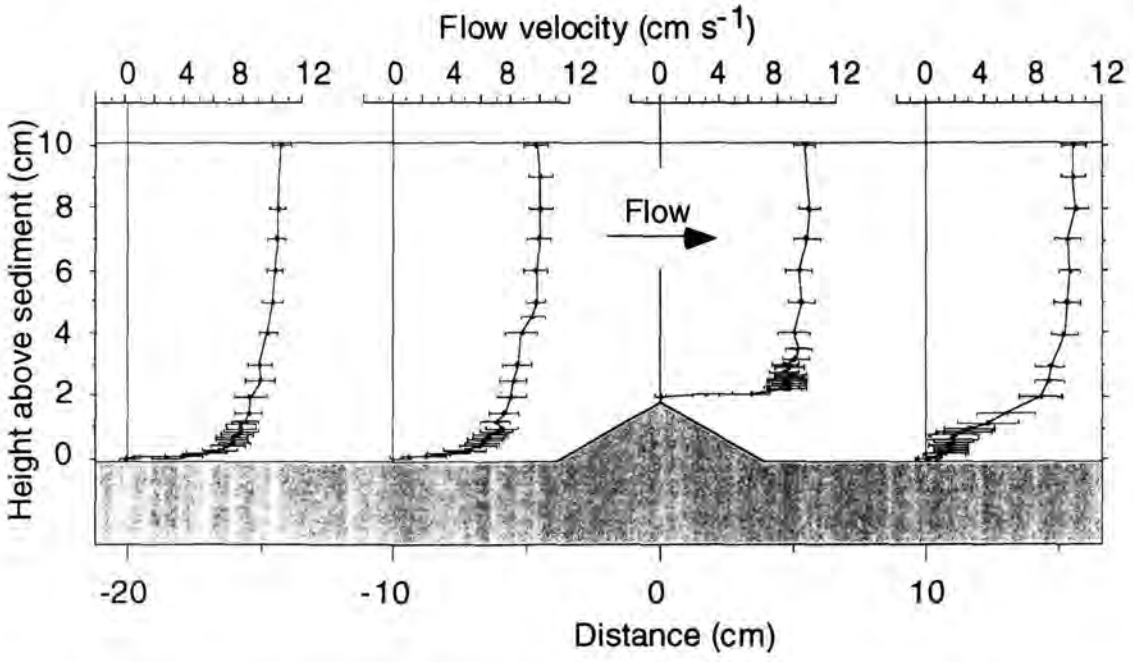

Fig. 3. Flow velocity profiles recorded at a mound 2.0 cm high (slopes 30°). The sediment consisted of quartz sand (md = 250 μm). Error bars, SD (n = 5).

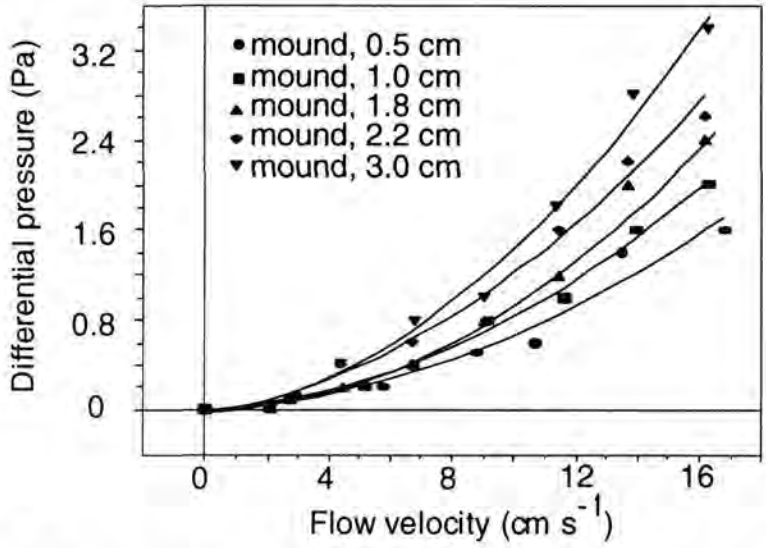

Fig 4. Pressure gradients measured at mounds of different heights (slopes 30°) at selected flow velocities. The pressure ports were located below the top and at the upstream edge of the elevations. The water depth was 10 cm.

Results of experiment 1

Our first experiment demonstrates the fast transport of suspended acrylic particles into permeable sediment with the topography related interfacial fluid flows (Table 2, Fig. 5). Immediately after starting the flume flow, a color change in the upstream slope of the mounds and the sediment areas up- and downstream adjacent the protrusions revealed fluid intrusion into the stained core. Visible penetration of black particles could be detected in these areas after only 2 min.

Table 2. Experiment 1. Intrusion of fluid and 1 µm organic particles into sandy sediment caused by mounds on the sediment surface. The table lists the sizes of the fluid intrusion areas (cm^2), maximum penetration depths (cm) of fluid and particles and the volumes (cm^3) of the intrusion zones. Sediment volumes affected by fluid or particle intrusion at the half-mounds build close to the sidewalls were multiplied by 2. Therefore, the calculations for the level surface (last row) are based on an extended sediment surface area of 60 x 50 cm = 3000 cm^2. Sediment: md = 250 µm, k = 4.5 x 10^{-11} m^2, flow velocity: 10 cm s^{-1}, duration of the experiment: 5 d

				Intrusion zones			
						1-µm particles	
Location of	Mound (cm)		Fluid intrusion	Fluid Max.		Max.	
intrusion zone	Ht	Diam	area	depth	Volume	depth	Volume
Upstream							
mound center	2.0	8.1	148.0	9.0	853.0	2.6	98.5
mound side 1	2.2	8.6	173.2	10.5	925.0	2.8	120.9
mound side 2	2.5	9.7	228.6	12.0	1,149.0	3.1	156

Location of intrusion zone	Mound (cm) Ht	Diam	Intrusion zones: Fluid intrusion area	Fluid Max. depth	Fluid Volume	1 µm particles Max. depth	1 µm particles Volume
Downstream							
mound center	2.0	8.1	177.6	5.5	401.0	2.2	55.8
mound side 1	2.2	8.6	259.8	5.8	419.0	2.3	63.7
mound side 2	2.5	9.7	297.2	6.8	558.0	2.4	72.4
Average depths ort otal volumes							
mound center	2.0	8.1	325.6	7.3	1,254.0	2.4	154.3
mound side 1	2.2	8.6	433.0	8.2	1,344.0	2.6	184.6
mound side 2	2.5	9.7	525.8	9.4	1,707.0	2.8	228.4
level surface area unaffected by pressure gradients	0.0	0.0	1,715.6	0.5	857.8	0.2	343.1

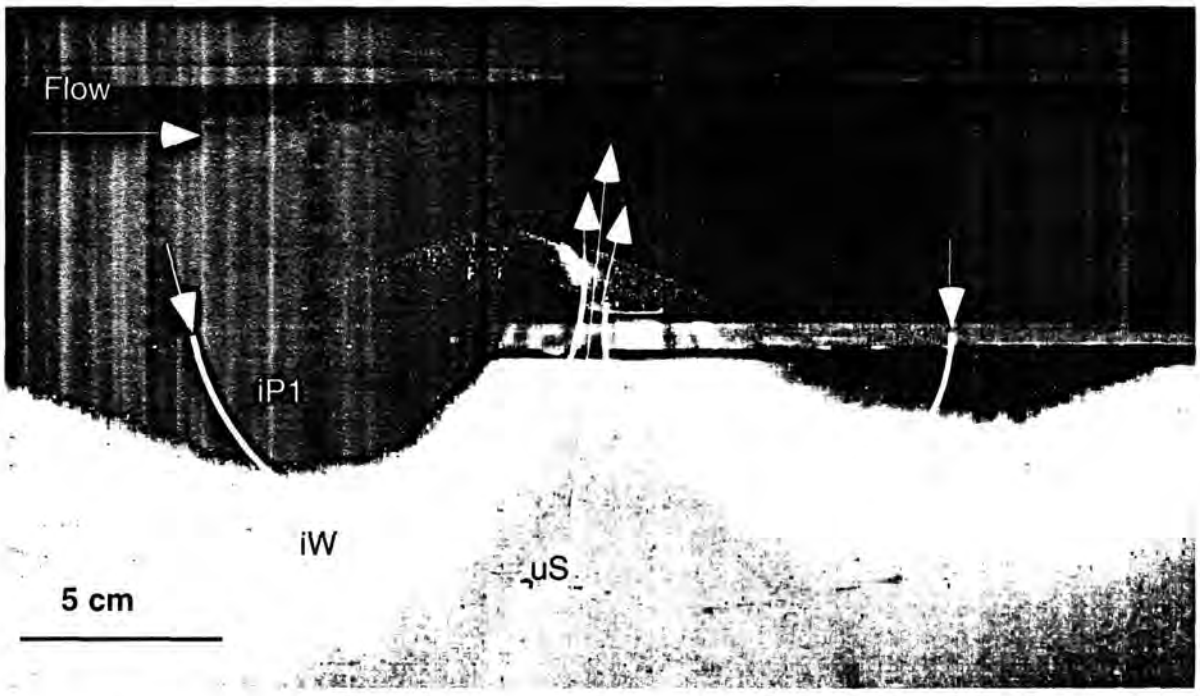

Fig. 5. Experiment 1. Intrusion of black particles into permeable sandy sediment at a mound 2.5 cm high (md = 250 µm, k = 4.5×10^{-11} m^2). iP1: intruding 1-µm particles, iW: intruding water, uS upwelling solute (red porewater). In the cross-sectional view the white arrows indicate the observed flow trajectories of pore fluid. The flow velocity was 10 cm s^{-1}. Duration of the experiment was 5 d. The thick horizontal bar running through the picture is the upper rim of the box containing the sediment core.

Intruding fluid moved faster through the interstices than the particles. The ensuing filtration process separated clear flume water and black pigment grains, generating two distinct fronts moving at different velocities through the sediment. At the tallest mound (2.5 cm) we measured initial (0-60 min) vertical intrusion velocities of 2.5 cm h^{-1} for the fluid and 1.3 cm h^{-1} for the 1-µm particles. After an initial phase (0-10 h) of

fast tracer penetration, the fluid and particle fronts progressed at low velocities continuously deeper into the sediment. Ten hours into experiment 1, intruding fluid had reached 5.5 cm and particles 2.2 cm sediment depth, and the velocities decreased to 0.3 and 0.1 cm h^{-1} for fluid and particles, respectively (Fig. 6).

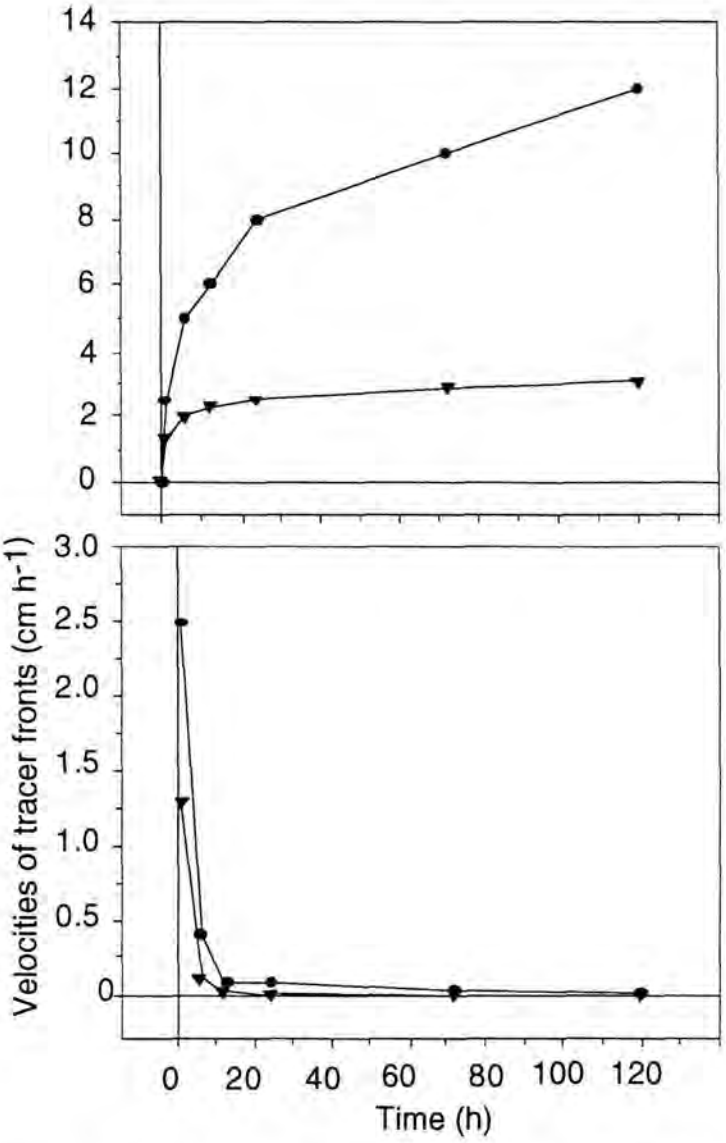

Fig. 6. Experiment 1. The vertical progress of the intruding water and particle (1 µm) fronts upstream from mound 2.5 cm high with time. The upper graph shows the penetration depths, the lower graph the vertical velocities of the intruding fronts. Black dots represent the water front, triangles the particle front (md = 250 µm, k = 4.5×10^{-11} m^2).

In contrast to the smooth front produced by the intruding water, the particle fronts were uneven. The pigment grains funnelled through the largest interstitial spaces, producing fine particle streaks following the streamlines of the advective pore water flows. These streaks showed that the tracers followed a curved path from the up- and downstream intrusion areas to the downstream slope of the mound (Fig. 5). From the

latter area, a continuous flow of red pore fluid emerged during the entire span of the experiment.

At the end of the experiment (day 5) the advective processes had not attained a steady state. The intruding fluid front was still progressing deeper into the sediment at a rate of 0.02 cm h^{-1}, and the particle front had slowed to 0.002 cm h^{-1} (2.5-cm mound). Newly intruding particles accumulated in the zone already blackened by pigment grains. Fluid and particle penetration depths upstream of the 2.5-cm mound had reached 12 cm and 3.1 cm depth, respectively (Table 2). In the areas of the core that were unaffected by pressure gradients, the intrusion of tracers by vertical diffusion did not exceed 0.5 cm for fluid and 0.2 cm for particles. The final dissection of the core revealed that approximately 13% of the sediment volume that had been percolated by the advective flows (1,707 cm^3, 2.5-cm mound, Table 2) was stained by black particle grains (228 cm^3).

Results of experiment 2

The second experiment demonstrated the impact of topography height and particle diameter on the advective transport processes (Table 3). The black pigment grains (1 µm, retardation factor 0.7) moved faster through the interstices than the blue ones (10 µm , retardation factor 0.2), resulting in particle separation (Fig. 7).

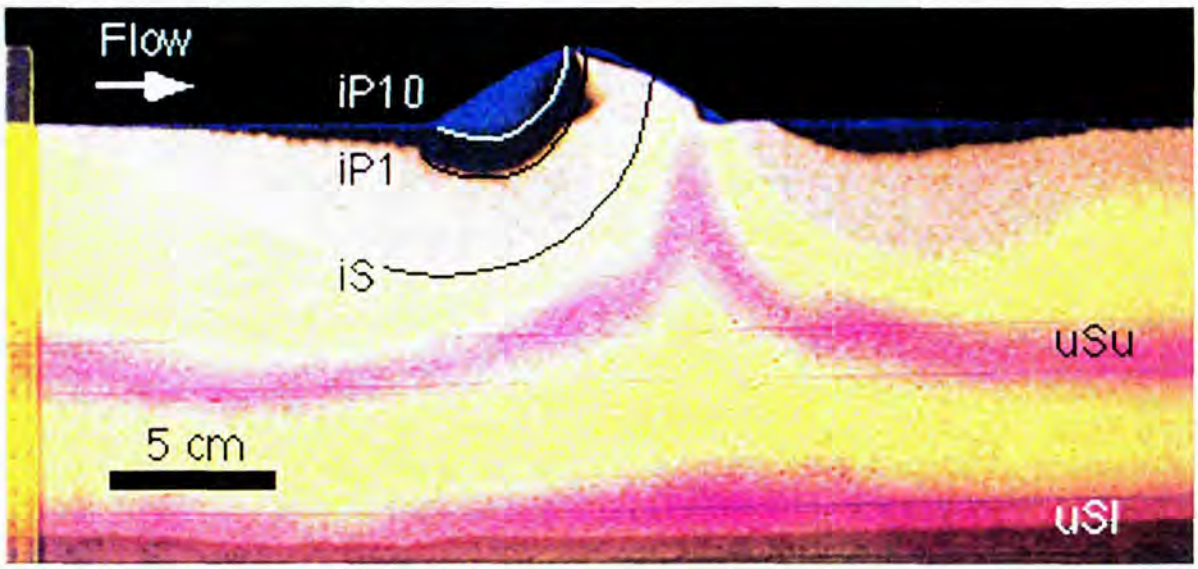

Fig. 7. Experiment 2. Tracer intrusion into sandy sediment at a mound 2.5 cm high. iP10: 10-µm particle intrusion, iP1: intruding 1-µm particles, iS: intruding red solute, uSu: upwelling red solute, upper layer, uSl: upwelling red solute, lower layer. The curved lines indicate the locations of the intruding tracer fronts after 16.5 h. The straight parallel lines show the initial positions of the stained porewater layers at 7 to 9 cm and 13 to 15 cm sediment depth. The flow velocity was 10 cm s^{-1} (md = 300 µm, k = 2.9×10^{-11} m^2).

In the upper sediment layer (0-0.3 cm), the vertical velocities of the resulting tracer fronts ranged from 3.3 cm h^{-1} for the solute to 0.5 cm h^{-1} and 0.1 cm h^{-1} for 1-µm and 10-µm particles, respectively (at 2.5-cm mound, Fig. 8). The pressure decrease at the downstream slope of the mound drew the red-dyed pore fluid layer, initially at 7-9 cm depth, to the sediment surface within 16 hs. Upwelling solute velocities reached 1.2 cm h^{-1} in the upper sediment layer (Fig. 8). Pore water flows connecting intrusion and emergence zones produced horizontal velocities of 0.8 cm h^{-1} at 1-cm sediment depth.

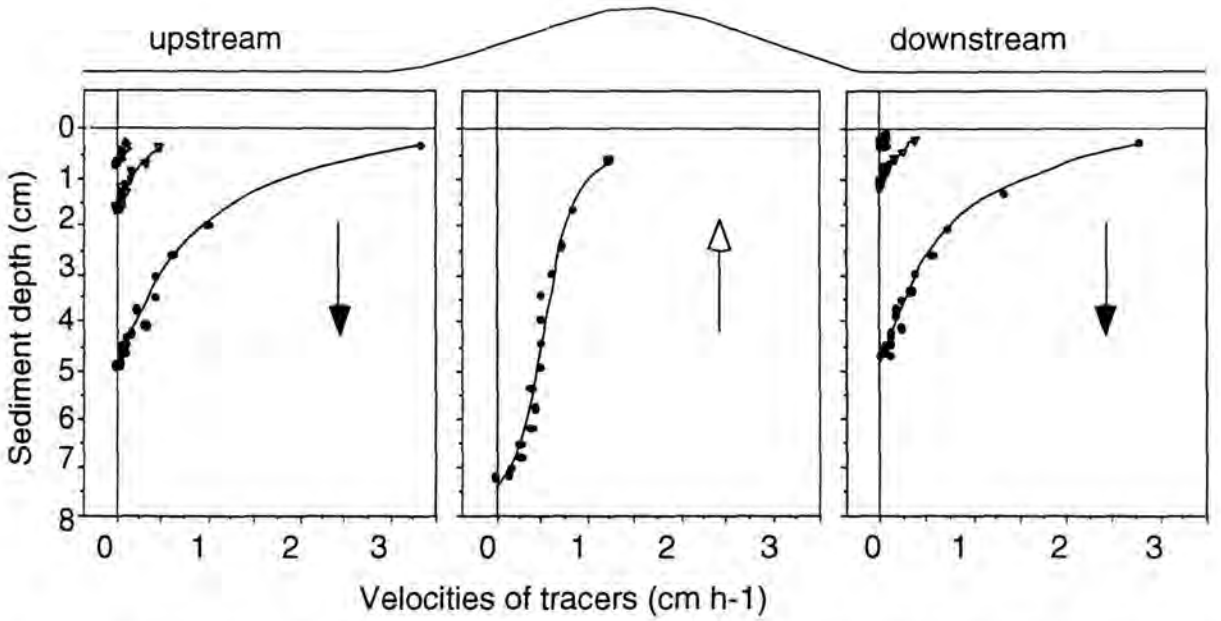

Fig. 8. Experiment 2. Vertical intrusion and upwelling velocities of solute (circles) and particle tracer fronts (diamonds: 10-µm particles, triangles: 1-µm particles) recorded for the 2.5 cm mound. Upwelling velocities (middle graph) could only be measured for red solute.

Horizontal slicing of the sediment core at the end of the experiment (total duration 16.5 h) revealed the three-dimensional extent of the tracer intrusion zones at the four different mounds. Computer-aided transparent reconstruction of the core (Fig. 9 A) demonstrates the impact of the advective transport processes on the distribution of solutes and particles within the sediment. The downstream intrusion zones are more elongated than the upstream, approximately circular, intrusion zones (Fig. 9 B). Fig. 9 C depicts the cone-shaped deformation of the upper horizontal stained pore water layer caused by upwelling.

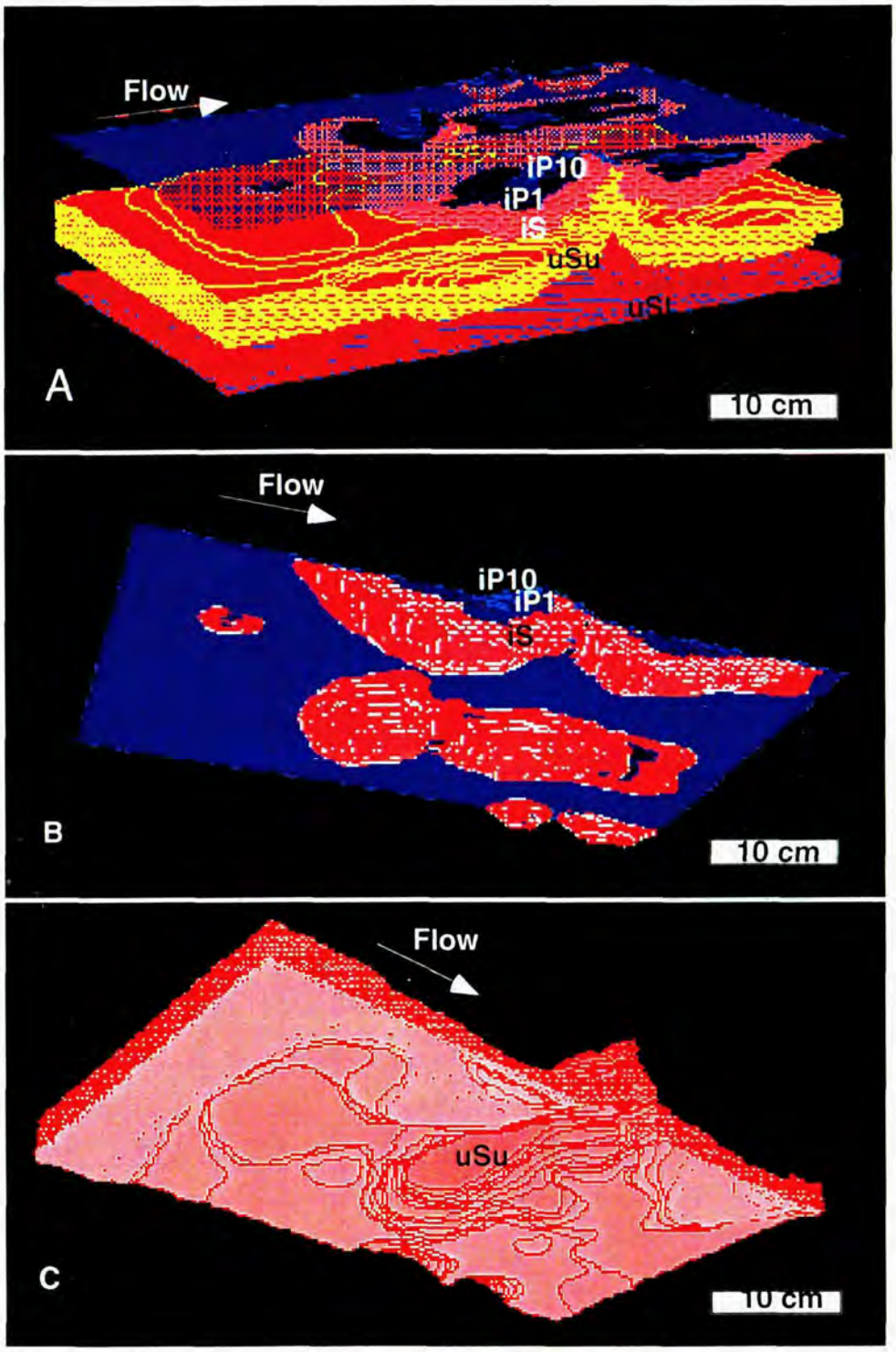

Fig. 9. Experiment 2. 3-D transparent view of the sediment core showing tracer intrusion zones and porewater upwelling. The core was reconstructed using digitized pictures of 2-mm-thick horizontal sediment slices. Sediment areas with tracers are color coded. iP10 (blue): intruding 10-μm particles, iP1 (black): intruding 1-μm particles, iS (pink): intruding red solute, uSu (orange): upwelling red solute, upper layer, uSl (red/blue): upwelling red solute, lower layer (md = 300 μm, k = 2.92×10^{-11} m^2). Graph generated using MacStereology by V. A. Moss.

The analysis of the sliced core showed that the depth of tracer intrusion increased linearly with the height of the mounds (Table 3, Fig. 10). Maximum depth of particulate tracer penetration upstream of the 2.5-cm mound was 2.3 cm for the 1-µm particles and 0.8 cm for the 10-µm particles, while the solute had penetrated down to 4.5 cm depth.

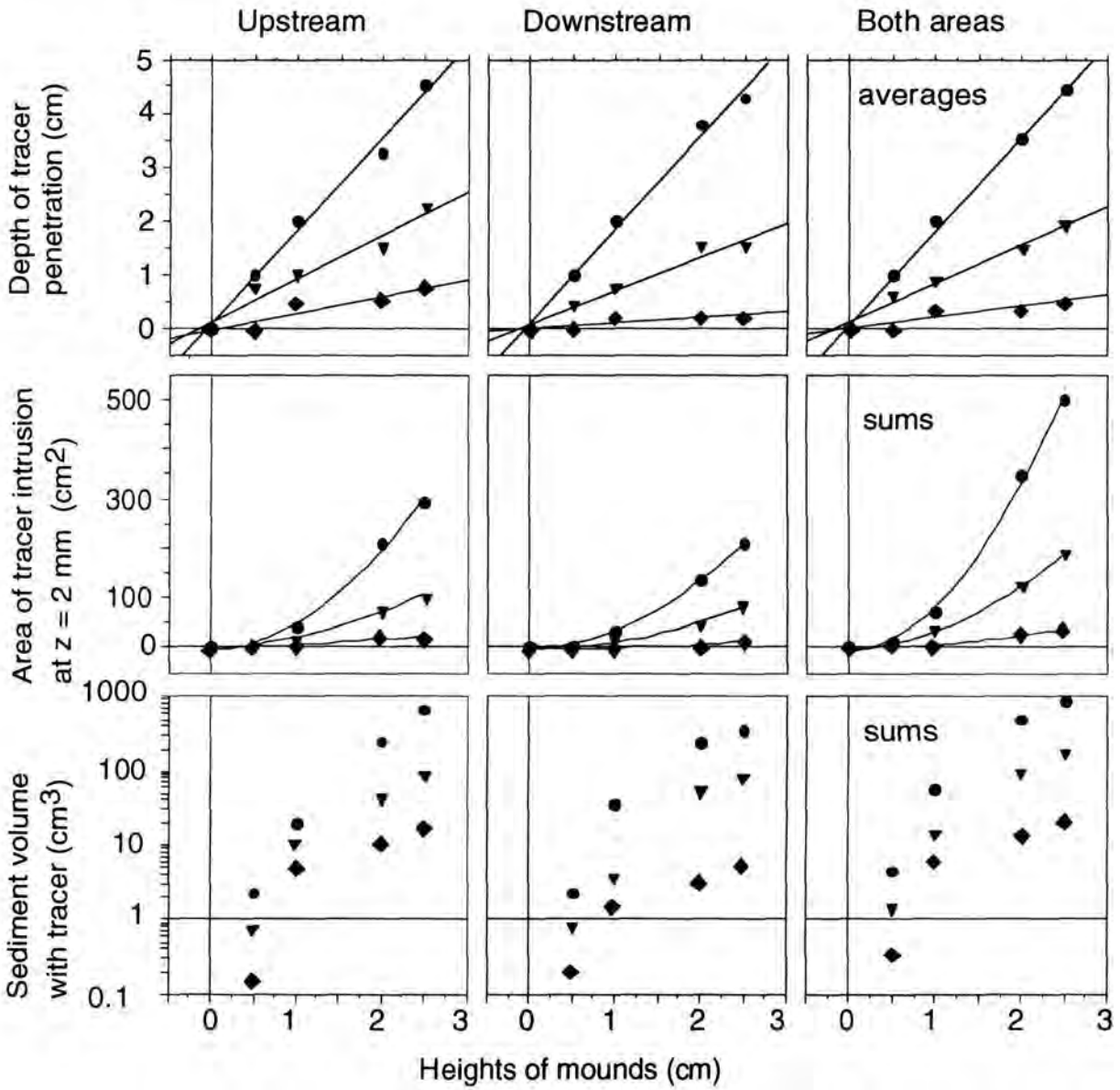

Fig. 12. Experiment 2. Depths, surface areas and volumes of sediment affected by intruding tracers. Dots represent solute, triangles 1-µm particles and diamonds the 10-µm particles. R^2 values for regressions: upper graphs: solute > 0.99, 1 µm > 0.95, 10 µm > 0.70, middle graphs: solute > 0.99, 1 µm > 0.99, 10 µm > 0.90. The sizes of the areas of tracer intrusion were measured 2 mm below the surface of the core.

Forty-five percent of the sediment surface was affected by the intruding water flows induced by the four mounds. The area affected by the pressure gradients at a given elevation increased exponentially with height and grew from 11 cm^2 at the mound 0.5 cm high to 499 cm^2 for a mound 2.5 cm hight (Table 3, Fig. 12). A single mound caused fluid staining in 4.5 cm^3 to 812 cm^3 of sediment, depending on its size. The sediment volumes containing tracer particles reached 4% (10-µm particles: total 49 cm^3) and 18% (1-µm particles: total 246 cm^3) of the volume percolated by red solute (1,357 cm^3, Table 3, Fig. 9). Comparison of tracer intrusions at the different mounds showed that sidewall effects, reducing the flow velocity close to the acrylic walls of the flume, had no significant impact on tracer penetration into the core (Table 3, Figs. 9).

Results of experiment 3

Sediment topography, represented by sand ripples, enhanced the interfacial flux of acrylic particles. Red flume water and black pigment grains (1 µm) intruded into the core in the ripple valleys and increased the sediment volume with tracer by a factor of 2.1 (solute) to 2.2 (particles) compared to a level control core (Table 4, Fig. 11).

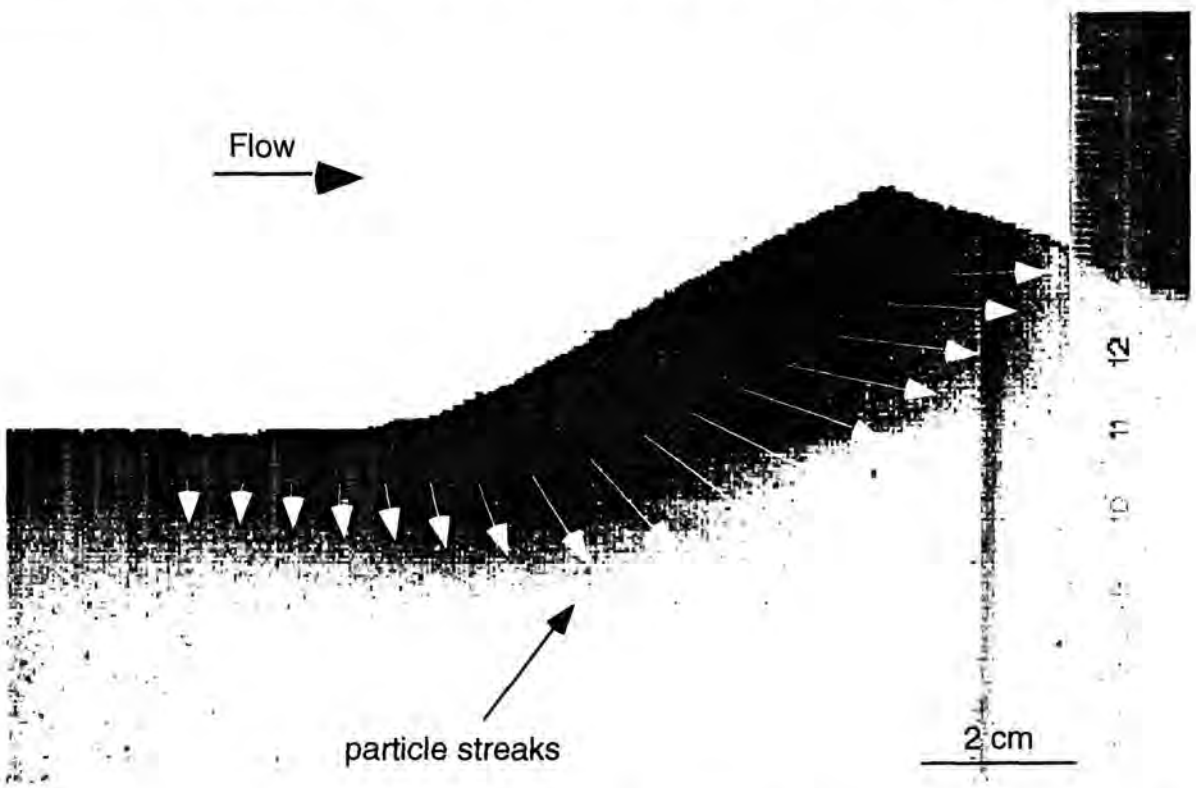

Fig. 11. Experiment 3. Intrusion of 1-µm particles at a sediment ripple (2.8 cm height, md = 300 µm, k = 2.9 x 10^{-11} m^2). White arrows indicate the direction of the particle streaks following the streamlines of the advective porewater flows.

The tracer concentration decrease in the flume flows reflected the advective removal of particulate matter from the boundary layer (Table 4, Fig. 12). During the first hour, the concentration of 1-µm particles in the water over the rippled bed decreased 2.3 times faster than in the control run (215 mg m^{-2} h^{-1} vs. 95 mg m^{-2} h^{-1}). The apparent solute flux, measured as the decrease of Rhodamine concentration in the water, was enhanced by a factor of 1.9 (6.8 l m^{-2} h^{-1} vs. 3.5 l m^{-2} h^{-1}). This smaller factor is explained by recycling of pore fluid. Dye that intruded the sediment was partly released at the downstream slope of the ripples during the experiment. Intruding pigment grains did not reach the emergence areas within the duration of the experiment.

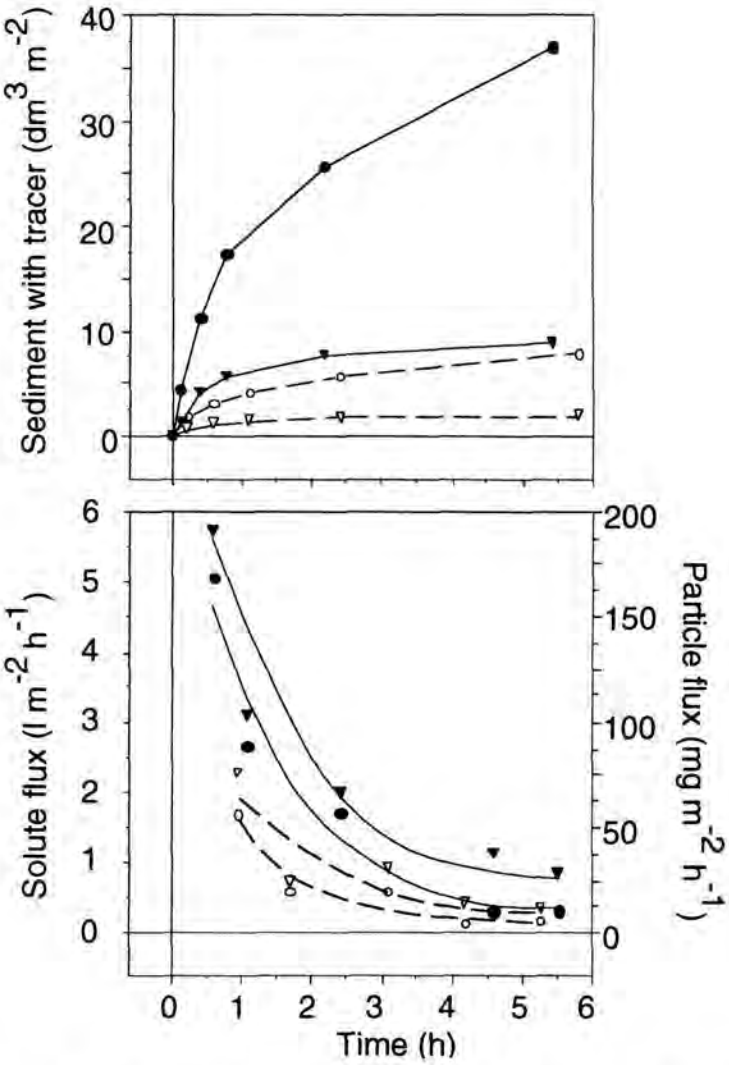

Fig. 12. Experiment 3. The upper graph shows the sediment volumes affected by intruding solute (circles) and 1-µm particle (triangles) tracers under a level (open symbols, broken lines) or rippled (2.8-cm-ripple height, solid symbols) sediment surface. The lower graph depicts the fluxes calculated from the tracer concentration decreases in the flume water. Duration of the experiment 5 h.

Discussion

The size distribution of suspended matter in ocean waters reveals that the deposition and mineralization of small particles are significant processes of geochemical cycling in marine sediments. Approximately one third of the total organic carbon in seawater is colloidal and smaller than 1 μm (Sharp 1973; McCave 1984a). Up to 60% of the particles larger than 1 μm in surface waters are between 1 and 10 μm, and only 10% are larger than 100 μm (Mullin 1965). With settling velocities of less than 1 m day^{-1} (McCave 1984b), deposition modes other than simple sedimentation gain importance for the incorporation of these particles into the seabed.

Our experiments demonstrate that boundary layer flows can interact with surface topography to remove small particles from suspension and transport them into permeable sediments. The lift force created by protruding surface structures is a consequence of the pressure gradients that drive water and suspended particles into and out of the seabed. This lift force, (F_L), at a protrusion is given by :

$$F_L = C_L (\rho u^2 / 2) A$$

where C_L = lift coefficient, ρ = density, u = flow velocity at height of the protrusion, A = surface area exposed to the flow.

If we use a lift coefficient of 0.30 to 0.47 (for half sphere-shaped objects similar to our mounds, Vogel 1981; Middleton & Southard 1984), the lift force at the 2.5-cm mound is 7×10^{-3} to 10×10^{-3} N ($\rho = 1 \times 10^3$ kg m^{-3}, u = 0.08 m s^{-1}, A = 6.9×10^{-3} m^2). Dividing this force by the surface area exposed to the flow yields a pressure drop of 1.0 to 1.5 Pa at that mound, which agrees with our flume measurements (Fig. 4). Darcy's law relates the pore water transport velocity (q) to the pressure (P) that forces water through a sediment of known permeability (k) (Batchelor 1967):

$$q = k\ 1/\mu\ (P/L)$$

where μ = dynamic viscosity and L = length of flow path.

If we assume a flow path of 10 cm (length of a curved path connecting the center of the intrusion areas to the center of the upwelling area), the calculated average transport velocity (q) is 0.10 cm h^{-1} to 0.16 cm h^{-1} (Δ P = 1.0 to 1.5 Pa, k = 2.9×10^{-11} m^2, $\mu = 1 \times 10^{-3}$ kg m^{-1} s^{-1}). Much higher velocities (up to 1.2 cm h^{-1}) were reached near the surface in close proximity to the high and low pressure centers at the mound (Figs. 1, 8), which is explained by the structure of the velocity field in the sediment (see below).

For mounds with 30° slopes the size of the sediment area where upwelling red pore fluid stained the surface of the core (downstream slope of the mounds and adjacent sediment areas) was similar in size to the base area of these mounds (e.g. 58 cm^2 for the mound 2.5 cm high). The interstitial space where fluid is actually exuded was approximately one third (36 ± 3%) of these stained surfaces. With a measured upwelling velocity of 1.2 cm h^{-1}, the 2.5-cm mound released 25 cm^3 h^{-1}. With an abundance of 50 biogenic mounds per m^2, as found in intertidal sandflats along the German North Sea coast (Huettel 1990), pore water would be released at a rate of 1,250 cm^3 m^{-2} h^{-1} ≈ 30 liters m^{-2} d^{-1} (the sediment permeability, flow speeds, and dimensions of mounds in these intertidal sand flats are similar to those in our flume experiments).

The release of pore water at a protrusion is balanced by the same volume of bottom water entering the sediment upstream and downstream of the surface structure. These interfacial flows removed particles from the boundary layer as suspended pigment grains intruded into the sediment along with the fluid. This co-transport is a consequence of the coupling between the suspended grains and the intruding fluid motion. At particle Reynolds numbers of 4.1×10^{-5} to 4.2×10^{-6} ($Re = u\,L\,r\,/\,\mu$, where $u = 2.8 \times 10^{-6}$ m s^{-1}, $L = 1 \times 10^{-6}$ m and 10×10^{-6} m, r = 1,480 kg m^{-3} and 1,450 kg m^{-3}, for black particles and blue particles, respectively, and $\mu = 1 \times 10^{-3}$ kg m^{-1} s^{-1}) gravity and inertia have little impact on the pathway of the suspended grains, and their motion is mainly governed by the transporting fluid (Purcell 1977). This assumption is justified by our observation that the large and small tracer particles moved along the same streamlines through the sediment as the solute tracer.

The directions and velocities of the fluid flows through the interstitial space are controlled by the pressure field caused by flow deflection at the protruding surface topography. With the simplifying assumptions that the flow is steady and irrotational, and that the sediment is homogenous, we can generate a scalar function (φ), the velocity potential, which allows us to calculate the streamline vectors at a given location (X) in this flow field.

To model the approximate pore water flow field associated with the pressure disturbance at a sediment ripple, we placed two line sources at the high pressure centers (approximate centers of eddies up- and downstream of the ripple, 1 cm above the surface, Figs. 1, 13) and one line sink at the center of the low pressure zone (downstream slope of the ripple, Fig. 13). A line source is considered to be a line of infinite length running in the z direction (in our case parallel to the ripple) that emits material at the same rate in any direction of the x-y plane. Analogously, the

line sink collects material from all directions (Batchelor 1967, Williams & Elder 1989). Combination of the two line sources and the line sink generates the flow field where the fluid volume emitted by the two sources equals the volume collected by the sink. For this two-dimensional model only the lower part of the flow field extending into the sediment is of interest.

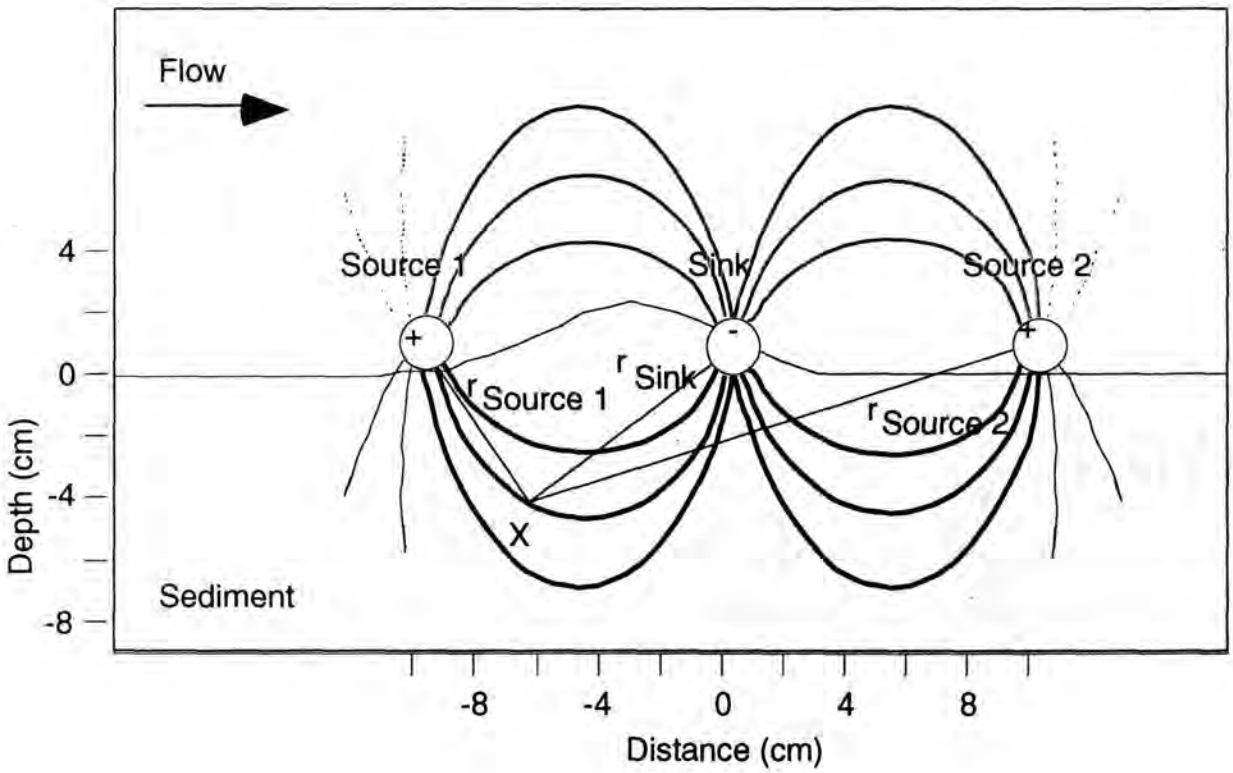

Fig. 13. The location of the sources and sinks used to model the velocity field. Only the lower part of the field is used to calculate the flow trajectories.

The velocity potential φ for the line source is given by:

$\varphi_{source} = -(Q_{source}\ 2/\pi)\ \ln r$ (Williams & Elder 1989)

where Q_{source} = volume of fluid emitted per unit time per unit length of the line source and r = distance of a point X from the source.

The velocity components (u, v) at the point of interest are given by:

$u_{source} = -\delta\varphi/\delta x = (Q_{source}\ 2/\pi)\ (x/r^2)$ and $v_{source} = -\delta\varphi/\delta y = (Q_{source}\ 2/\pi)\ (y/r^2)$.

Analogously for the line sink:

$\varphi_{sink} = (Q_{sink}\ 2/\pi)\ \ln \rho$, $u_{sink} = -\delta\varphi/\delta x = -(Q_{sink}\ 2/\pi)\ (x/r^2)$, and

$v_{sink} = -\delta\varphi/\delta y = -(Q_{sink}\ 2/\pi)\ (y/r^2)$. By adding the velocity potentials for the two line sources and the line sink, we obtain the velocity potential for the velocity field under the ripple: $\varphi_{ripple} = \varphi_{source\ 1} + \varphi_{sink} + \varphi_{source\ 2}$

with the velocity components: $u_{ripple} = u_{source\ 1} + u_{sink} + u_{source\ 2}$ and

$v_{ripple} = v_{source\ 1} + v_{sink} + v_{source\ 2}$.

The volume of fluid intruding the sediment at the selected ripple (2.8 cm high) was calculated from the decrease of tracer concentration in the flume water, i.e. (initial flux rippled bed - initial flux level bed) x (sediment volume with tracer at 2.8-cm ripple / total sediment volume with tracer at all ripples). In accord with the ratios of sediment volumes percolated by solute tracer upstream and downstream of the ripple, this volume was divided between the two sources in a ratio of 1.2 to 1. When calculating Q, only the lower part of the flow field was used.

Fig. 14 A shows the pore water velocity field at a ripple 2.8 cm high predicted by the source-sink model. The velocity vectors show the upwelling of the pore water under the ripple and the water intrusion upstream and downstream. In the upwelling zone, the vertical pore fluid velocities reach 1 cm h^{-1}, which agrees with the velocities we observed in our experiments. The diagram shows that the horizontal velocities in the upper sediment layer, close to the edges of the protrusion, reach values comparable to the highest vertical water movements. The recorded velocities of horizontal tracer flow through the flume sediments reached 0.8 cm h^{-1}. Topography-related advective pore water flows, thus, enhance lateral transport within the sediment to a degree similar to the vertical transport.

The flow-trajectory plot (Fig. 14 B) computed with the velocity vectors reproduces the pore water flow pattern observed in the ripple experiment. Observed particle streaks (Fig. 13), which traced the pore water streamlines, confirm the calculated trajec-tories connecting the intrusion areas and the emergence area. Using the retardation factor for the 1-µm pigment grains, we calculated the theoretical particle intrusion zones for the flow field generated by the 2.8-cm ripple (Fig. 14 B). The modeled penetration depth of the tracers reaches 2.0 cm after 5 h. This smaller than that measured in the flume core (2.7 cm), suggesting an additive effect of neighbouring ripples.

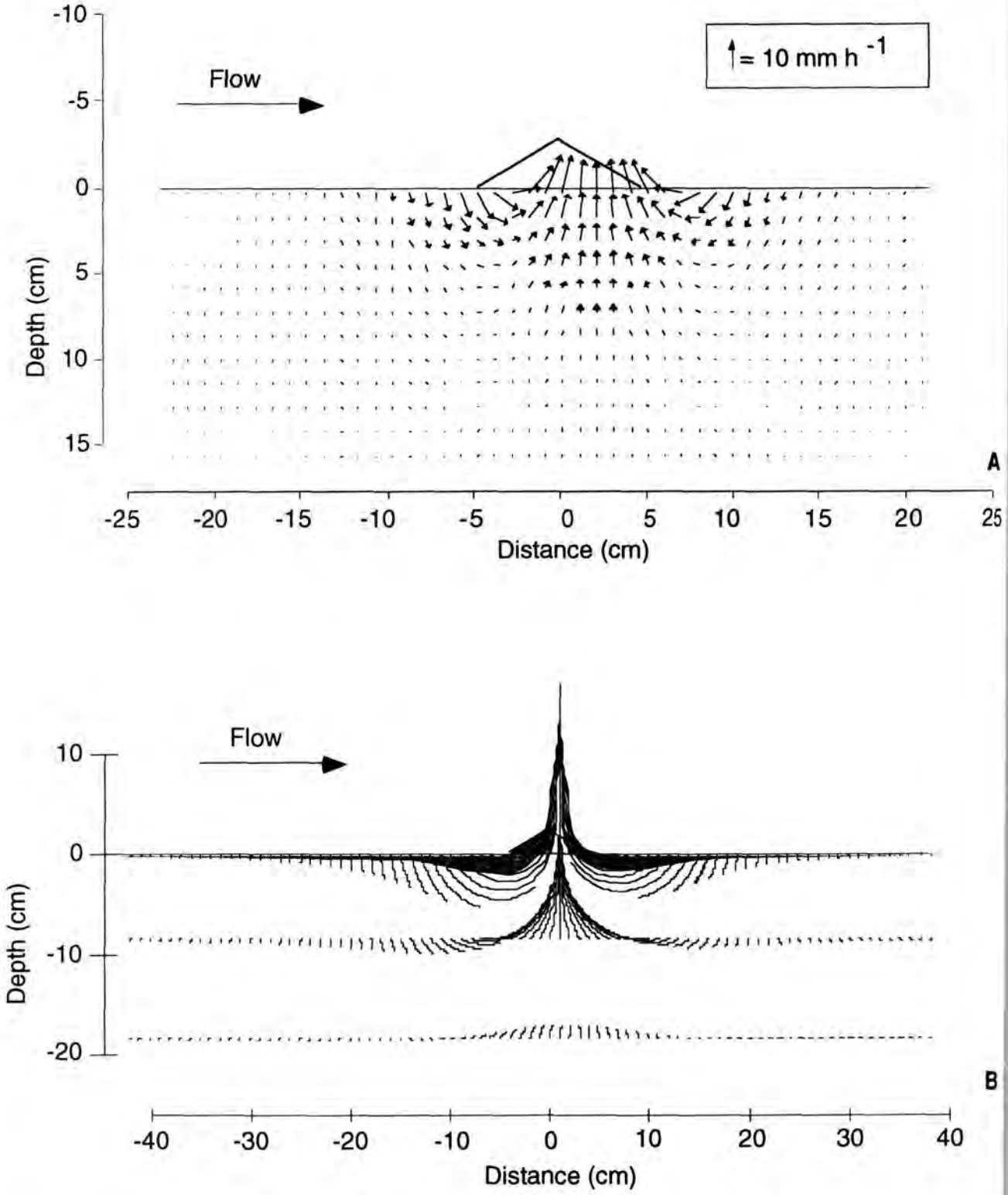

Fig. 16. Upper graph: Porewater velocity vectors generated using the source-sink model for the flow field at a ripple 2.8 cm high. Lower graph: Flow trajectories of red solute and the black particle (1 μm) accumulation zones in permeable sand at a 2.8 cm ripple calculated using the velocity vectors. The upper trajectories show the pathways of intruding solute and particles while the lower ones trace the movement of the pore fluid at depth.

In experiment 2, size-dependent retardation separated black (1 µm) and blue (10 µm) pigment grains, producing tracer fronts that moved at different velocities through the interstitial space. The pressure field creates a gradient with pore water velocities decreasing inversely with distance from the centers of the high pressure and low pressure, respectively (Fig. 15, 16). Pigment grains accumulate where the fluid velocity drops below the threshold necessary to overcome the retention forces acting on the moving particles. Concentric layers of particle accretion form around the intrusion areas. These layers decrease the permeability of the sediment and result in a feedback process that promotes particle accumulation. Percolated perpendicularly by the advective pore water flows, these layers may produce zones of ehanced microbial decomposition activities.

The optimal particle size for transport through permeable sediment can be predicted by the theoretical minimum of the collector efficiency of the porous medium (Rajagopalan & Tien 1976). For the sands used in our experiments this optimal size was 0.5 - 1 µm, similar to the size of our black particles. The majority of the particulate material in seawater thus fits into the size range (0-2 µm, see above) that can be carried into sandy sediments with interfacial suspension flows. As it ranges from a fraction to a few micrometers, the size of bacteria is ideal for transport through the interstitial space of sandy coastal sediments. Martin & Noonon (1977) and Sinton (1980) showed that bacteria can be carried over several hundred meters through permeable sediments with groundwater flows. For particles smaller than 0.5 µm the chances of being caught grow because Brownian motion and with it the likelihood that particles contact stationary surfaces increase (Shimeta 1993).

Along with density and size, the surface characteristics of the particles affect their transport through the interstitial space. When a particle collides with a stationary sediment grain, the physical, chemical, and biological properties of the contacting surfaces determine whether the particle is reversibly adsorbed or permanently caught (Mayer et al. 1985; Harvey et al. 1993). Exopolymers secreted by bacteria, algae or benthic animals produce coatings on the sand grains that bind particulate matter and reduce sediment permeability (Dade et al. 1990; Yallop et al. 1994). Ion exchange and electrostatic interactions cause adsorption and desorption (Wang & Lee 1993). As a consequence of these processes, up to 90% of the POM in coastal sediments is adsorbed to the inorganic surfaces of sand grains (Suess 1973; Mayer et al. 1988; Keil et al. 1994).

Sorption makes the penetration depth of particulate material, in contrast to that of an inert solute, dependent on the particle concentration in the intruding suspension.

For our tracers, sorption was negligible and high concentrations of pigment grains in the water confirmed that particle concentrations were never a limiting factor.

The ecological relevance of advective interfacial particle transport is related to sediment permeability and the organic particle load of the bottom water. In our experiments, significant particle transport by current-induced pore water flows was restricted to sediments with permeabilities exceeding $2x10^{-11}$ m^2. Typically, such sediments are found on the shelf, where strong wind, wave or tide-driven currents frequently resuspend the upper sediment layers (Johnson & Stride 1969; Nittrouer & Wright 1994).

After redeposition advective transport provides the fast initial pathway for the particulate matter into the seabed. Similarly to a filtration process, the topography related interfacial fluid flows remove suspended matter from the bottom water, loading the winnowed sediment layers with 'fresh' degradable particles. In contrast to simple deposition, the advective flows transport organic matter through the sediment-water interface, providing a fast pathway for energetically rich particles into deeper sediment strata. By increasing the flux of organic matter and electron acceptors into the sediment and enhancing the release of decomposition products from the bed, this hydro-mechanical process promotes sedimentary mineralization and nutrient recycling. We conclude that the topography related interfacial particle transport is a key process for organic matter uptake and cycling in seabeds with sand-like permeabilities.

ACKNOWLEGDEMENTS: Without the support of B. B. Jørgensen it would not have been possible to realize this work. We thank B. Boudreau, M. E. Holmes, U. Berninger, A. Khalili, and two anonymous reviewers for their comments and constructive criticism on the first version of the manuscript. Thanks also to S. Klöser, V. Meyer, G. Herz, O. Görg, G. Kohte, J. Lamers, and the microsensor group for technical assistance during this project. This study was supported by the Max-Planck-Society.

Advective transport affecting metal and nutrient distribution and interfacial fluxes in permeable sediments

Markus Huettel[1], Wiebke Ziebis[1], Stefan Forster[1], George Luther III[2]

[1]Max- Planck-Institute for Marine Microbiology, Celsiusstr. 1, 28359 Bremen, Germany

[2]College of Marine Studies, University of Delaware, Lewes DE 19958, USA

accepted for *Geochimica et Cosmochimica Acta , October 1997*

ABSTRACT: In laboratory flume experiments we demonstrate that advective pore water flows produce biogeochemical reaction zones in permeable sediments causing specific and reproducible patterns of iron, manganese and nutrient distribution. Oxygenated water, forced into the sediment when boundary flows are deflected by protruding sediment structures, generated distinct zones of enhanced nitrification and ferric iron precipitation. This inflow was balanced by ammonium-rich porewater ascending from deeper sediment layers thereby creating an anoxic channel where dissolved ferrous iron and Mn^{2+} could reach the surface. Between the zones of ferric iron precipitation and ferrous iron upwelling a layer with increased manganese oxide and solid phase Fe(II) concentrations formed, indicating redox reaction between these components. The establishment of topography on the previously smooth sediment surface reversed the interfacial flux of solutes. While the smooth control core was a sink for metals and nutrients, the sediment with mounds acted as a source for these substances. Our experiments show that in permeable sands with oxidized surface layer reduced metal species can be released to the water column by flow topography interactions. We concluded that advective transport processes constitute an important process controlling biogeochemical zonations and fluxes in permeable sea beds.

INTRODUCTION

Physical and biological transfer mechanisms link the mineralization processes in the sediments to the production processes in the overlying water column. Transport of dissolved and particulate substances across the sediment-water interface governs the uptake and release rates of the sea bed and thus the biogeochemical processes and diagenesis of the sediment (Berner 1971). By controlling the distribution of reactive substances and microorganisms within the sediment, these transport processes are also important in setting the chemical and biological

environment in the sea bed. Interfacial and in-bed transport processes depend largely on the composition of the sediment and the activities of the benthic fauna (Aller 1983; Aller 1982; Aller 1984; Forster & Graf 1995; Huettel 1990; Ziebis et al. 1996a). In this study, we focus on the impact of hydrodynamically induced advective transport in permeable sediment.

While diffusion is the major transport mechanism for solutes in muddy, cohesive sediments (Berner 1980) advective transport processes gain significance in sandy, permeable beds (Huettel & Gust 1992a). Permeable sediments permit pore water flows which act as vehicle for directional transport of dissolved and suspended matter through the interstitial space. The transport rate through the sediment then is proportional to the permeability and the pressure gradient driving the interstitial flow (Darcy's Law, (Darcy 1856)). Such gradients may be generated by bottom currents, propagating waves or bottom water density changes (Huettel & Gust 1992a; Shum & Sundby 1996; Webster et al. 1996).

The pressure pattern at the sediment water interface creates up- and downwelling zones within permeable beds (Savant et al. 1987; Thibodeaux & Boyle. 1987; Webb & Theodor 1968). Pressure gradients as small as 1 Pa cm^{-1} generated when bottom flows are deflected by small sea bed topography can force water several centimeters into such sediments and draw pore fluid from more than 10 cm depth to the surface (Fig. 1) (Huettel & Gust 1992a). Velocities of these pore flows may reach 1-3 $cm\ h^{-1}$ in the upper centimeter of sandy sediment (Huettel & Gust 1992a). Due to this process, sediment ripples or a few scattered small mounds may affect pore flows within the entire upper layer of the sediment (Huettel et al. 1996b).

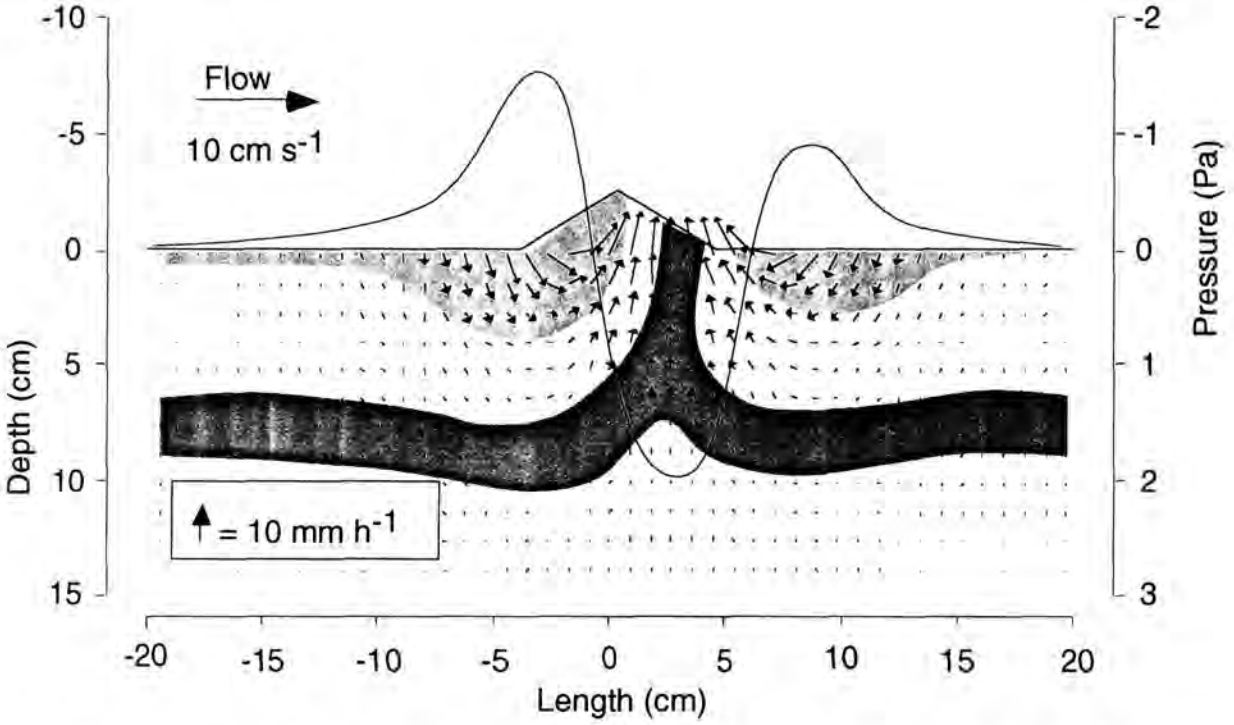

Fig. 1. The pressure distribution at a small mound on the sediment surface exposed to boundary layer flow and the resulting pore water flow velocity field (modified after Huettel et al. 1996b).

Such advective processes will have an impact on the diagenesis of the sediment. However, geochemical processes and pore water solute distributions in non-accumulating sandy beds are not well studied due to the many difficulties in sampling. Laboratory studies can circumvent some of these methodological problems. In flume experiments, (Ziebis et al. 1996b) and could show, that advective flows can enhance the depth of oxygen penetration into natural sandy sediment by a factor of 10. (Forster et al. 1996) demonstrated that interfacial water flows can significantly enhance sedimentary oxygen consumption and organic matter mineralization. Using a similar experimental set-up, we investigated in this study the impact of advective pore water flows on the transport and distribution of trace metals (Fe, Mn) and nutrients (NH_4^+, NO_2^-, NO_3^-, PO_4^-, $Si(OH)_4$) in sandy sediments.

Manganese and iron play important roles in the biogeochemical cycles of carbon, sulfur, phosphorus and several trace elements (Burdige 1993; Millward & Moore 1982; Murray 1975) and sedimentary bacteria decomposing a wide range of organic substrates gain energy from the reduction of nitrate or Mn and Fe oxides (Lovley & Phillips 1988; Madigan et al. 1997; Myers & Nealson 1988). In marine sediments, nitrate, manganese and iron reduction associated with organic matter

decomposition are referred to as sub-oxic remineralization processes which have been shown to be important especially in shelf beds with higher organic carbon input (Aller & Blair 1996; Canfield et al. 1993a; Canfield et al. 1993b; Jørgensen & Sørensen 1985; Thamdrup et al. 1994b).

Based on free energy considerations manganese reduction is less efficient for microbial carbon oxidation than denitrification but more favourable than iron reduction. The metal species available for the microbial degradation process exist as solid amorphous minerals (e.g. ferrihydrite) and dissolved ions (Skinner & Fitzpatrick 1992). The minerals may dissolve when they are subjected to reducing environments in deeper anoxic sediment layers while the dissolved species can be adsorbed or precipitate out of the pore water as sulfide, carbonate and phosphate phases or solid (hydr)oxides when reaching oxidized sediment surface layers (Burdige 1993). Upon transition between oxidizing and reducing environments they are subject to complex dissolution, adsorption and precipitation processes (Burdige 1993).

Despite the important role of iron and manganese for the decomposition processes in coastal sediments, it is neither well understood how the variable sedimentary oxygen microdistribution affects the metal oxidation and distribution nor to which extent iron and manganese are retained in the sea bed (Thamdrup et al. 1994b). Previous research indicated that advective transport processes may gain significance in sandy shelf sediments (Huettel & Gust 1992a; Riedl et al. 1972; Riedl & Machan 1972; Webb & Theodor 1968; Webb & Theodor 1972). Our flume experiments show the complex effect of advective pore water flows on manganese, iron and nutrient dynamics in permeable sediments, the interfacial fluxes of theses substances, and the interaction of the metal redox reactions and microbial degradation processes

METHODS

Sediment

The sediment used for our experiments originated from a shallow bay at the island of Giglio, Italy (42° 20' N ; 10° 52' E). The sediment in this bay is inhabited by a dense population of the thalassinidean shrimp *Callianassa truncata* with an average abundance of 120 ± 43 individuals per m^2 (Ziebis et al. 1996b). These burrowing shrimps cause strong bioturbation and produce a distinct sea bed topography with small funnels and mounds of up to 8 cm height (average 4 cm). The sediment consists of well sorted sand with a median grain size of 350 µm and has a

permeability of 5.1 x 10^{-11} m^2, a porosity of 0.4 and a low organic content of 0.2 %. From May to August bottom currents in this bay range from 2 to 16 cm s^{-1} with water temperatures of 19 to 24°C.

Flume

The sediment core (60 cm long, 30 cm wide, 20 cm deep) was incubated in a laboratory acrylic flume with an open-channel section of 200 cm length, 30 cm width, and 12 cm height. 160 l of sea water (salinity 38) were recirculated in the flume by an axial pump producing a flow velocity of 10 cm s^{-1} measured at 8 cm above the sediment core. The water depth was held constant at 10 cm above the core. Water temperature was kept at 20.0 ± 0.1°C by a cooling unit. An opaque PVC foil covering the flume prevented algal growth and evaporation. A detailed description of the flume system is given by (Huettel et al. 1996a).

Experiments

We conducted three flume experiments to investigate the impact of advective flows on the distribution of iron, manganese and nutrients in permeable sediment and one experiment to assess the impact of advection on sediment-water flux of these constituents (Table 1). For all experiments the same natural sediment was used.

Table 1. Overview of the experiments

Expt No. run	Sediment	Topography	Sampling and analyses
Expt 1 1 run	Giglio sand	Natural topography created by 6 *C.truncata*	- Anal. of metal oxide surface precipitates - Micrographs of *Gallionella* colonies
Expt 2 2 runs	Giglio sand	Artificial topography 1 mound on surface	- 2 transects of sediment cores - Anal. of solid phase metal conc. and pore water nutrient conc. (2nd run)
Expt 3 2 runs	Giglio sand + org. matter	Artificial topography 1 mound on surface	- 2 transects of sediment cores - Anal. of solid / liquid phase metal conc. and pore water nutrient conc. (2nd run)
Expt 4 2 runs	Giglio sand + org. matter	Artificial topography 10 mounds on surface	- Sampling of flume water - Anal. of iron, manganese and nutrients
Expt 5 1 run	Giglio sand + org. matter	Artificial topography 1 mound on surface	- voltammetric measurements to detect dissolved oxygen, iron and manganese

In **Experiment 1** we investigated the formation of metal precipitates at the sediment surface caused by advective processes at natural biogenic topography. 6 small shrimps (approx. 2 cm long) of the species *Callianassa truncata* build their burrows in the flume core and produced mounds and funnels at the sediment surface. Once constructed, the burrows were semi-permanent and the mounds and funnels were maintained at the same positions. After 4 months surface sediment samples (0-1 mm depth) were collected at 4 different locations: 1) in smooth reference areas unaffected by pressure gradients related to topography, 2) in areas 3 cm upstream of mounds, 3) at the downstream slopes of mounds and 4) in areas 3 cm downstream of the mounds. The sediment samples (sample volumes 0.5 to 1 cm^3) were collected with plastic spatula and immediately transferred to nitrogen flushed serum vials and frozen until analyses for iron and manganese (see below). Regardless of porewater or seawater ice still adhering to the sand grains, we will further on call metal concentrations derived from wet sediment samples 'solid' or 'particulate'. Metal concentrations thus are quoted in $\mu mol\ cm^{-3}$ of wet sediment volume. The volumes of the wet sediment samples were calculated from the wet weight divided by the average density of the wet sediment.

Experiment 2 was designed to assess whether advective processes also cause zones of metal precipitation within the sediment thereby changing the geochemical zonation of the bed. For this investigation the shrimps were removed from the sediment to exclude effects of bioturbation and bioirrigation. After thorough homogenization, the sediment core was levelled and a small mound (2.5 cm high, 10 cm diameter) was built in the center of the smooth surface using the same sand. After 2 months, we took 7 sediment subcores along a transect cross-sectioning the mound in flow direction and 7 subcores along a line paralleling this centerline transect (distance between lines = 50 mm). The subcores (26 mm diameter, 100 mm long) were sectioned immediately after retrieval (in vertical steps above surface (mound): 19, 17, 15, 13, 11, 9, 7, 5, 3, 1, 0 mm, and -1, -3, -5, -7, -9, -15, -25, -35, -45, -55, -65, 75, -85, -95 mm below surface). A subsample from each slice was transferred to nitrogen-flushed vials and frozen until analyses for particulate iron and manganese (see below). This experiment was repeated mainly in the same manner once, only that the depth intervals for sampling were slightly altered: (vertical steps 19.5, 9.5, 6.5, 5.5, 4.5, 3.5, 2.5, 1.5, 0.5, 0, -0.5, -1.5, -2.5, -3.5, -4.5, -7.5, -9, -15, -25, -35, -45, -55, -65, -75, -85, -95 mm). Additionally, nutrient concentrations (nitrate, nitrite, ammonium, phosphate and silicate) in the different depth intervals were investigated in pore water extracted by centrifugation. To gain sufficient pore water, we pooled the sediment of the layers 2.5 to 0 mm, 0 to -2.5 mm, -2.5 to -7.5 mm, and -7.5 to -15 mm.

Experiment 3 was similar to experiment 2 but prior to the run we mixed pulverized algal and sea grass debris (ca. 50 g dry mass) into the sediment in order to enhance microbially mediated processes affecting metal dissolution and nutrient generation. Sediment topography consisted again of one central artificial mound (2.5 cm high, 10 cm diameter). After 2 months 2 x 7 subcores were taken along centerline and parallel line and sliced (vertical steps 4.5, 3.5, 2.5, 1.5, 0.5, 0, -0.5, -1.5, -2.5, -3.5, -4.5, -7.5, -9, -15, -25, -35, -45, -55, -65, 75, -85, -95 mm). Subsamples were analyzed for particulate iron and manganese concentrations as well as for nutrients as described above. In a second run, repeating this experiment, Fe^{2+} and Mn^{2+} were analyzed in the pore water extracted from 14 cores taken after two months along the centre and the parallel transect. The cores were sectioned in 10 mm intervals down to 160 mm sediment depth and pore fluid was extracted by centrifugation under nitrogen atmosphere.

Experiment 4 was designed to assess the impact of surface topography on the sediment-water fluxes of iron, manganese and nutrients. We levelled the surface of the sediment core, filled the flume with artificial sea water (S = 38) and set the free stream flow velocity to 10 cm s^{-1}. During the following 4 days we collected flume water samples (50 ml), the water volume removed from the flume was replaced by the same artificial sea water of the initial flume filling. On the fifth day, the flow was stopped and 10 mounds (2.5 cm high, 10 cm diameter, 55.6 mounds m^{-2}) were built on the sediment, distributed evenly in a manner that blockage of flow between mounds was minimized. This was done by pouring 40 cm^3 dry, clean sand of the same sediment type through a small funnel at the position where the respective mound had to be built. After restarting the flow (10 cm s^{-1}), water samples (50 ml) were taken on each of the following 18 days. The water removed was replaced as described above. All samples were analyzed for their iron, manganese and nutrient concentrations (see below). This experiment also was repeated once, only that in this second run the mounds were established 7 days after the surface of the core had been levelled.

For **Experiment 5** the sediment core was prepared as described for experiment 3 but after the set up the core was kept under stagnant water for a period of 3 weeks to allow the build up of reduced metal species in the pore water. Then the pump was switched on and the flow was adjusted to 1 cm s^{-1} and measurements were started one week thereafter. In this experiment, solid state voltammetric microelectrodes were used to detect dissolved O_2, Fe and Mn and we applied this method to trace the interfacial flux of iron (Brendel 1995). The voltammetric cell arrangement consisted of the gold amalgam microelectrode of 100 µm diameter, a

500 µm diameter platinum wire as counter electrode, and a saturated calomel electrode as reference electrode. The microelectrode, held by a 3-axis micro-manipulators, was placed 2 mm above the downstream slope of the mound and interfaced to an Analytical Instrument Systems, Inc. model DLK-100 voltammetric analyzer. The voltage range scanned was typically from -0.1 V to -2.1 V. For linear sweep voltammetry, we scanned at 200 mV s^{-1} and for square wave voltammetry, we used a pulse height of 15 mV, step increments of 2 mV, a frequency of 100 Hz and also a scan rate 200 mV s^{-1}. The electrode was standardized according to (Brendel 1995). Precision for replicates of Fe^{2+} at a given depth was 2-5% with a minimum detection limit of 5 µM. The electrodes can also detect a soluble Fe(III) phases over the voltage range -0.2 to -0.9 V (Brendel 1995). These Fe(III) phases are similar to those observed when dissolved Fe(II) is added to tris buffer (pH=8) in the presence of O_2 (Von Gunten 1989; Von Gunten 1991). Tris stabilizes Fe(III) in solution by forming complexes which age. Within the voltage scan, two well defined peaks occur at about -0.5 V and -0.9 V, and on aging the peak ratio (-0.45 V/ -0.9 V) decreases. However, Fe(III) cannot be readily quantified in sea water because so far there is no standard available for saline media.

Analyses

Iron

HCl extractable Fe(II) and the amorphous, poorly crystalline fraction of the Fe(III) minerals, were measured by following the procedures as described by (Lovley & Phillips 1987) with the modifications of (Kostka & Luther III 1994). 200 mg sub-sample (wet sediment) of each sediment section was added to 10 ml of 0.5 M HCl in a preweighed plastic vial. After mixing for 1 hour on a shaker, the sample was centrifuged for 5 minutes at 4000 rpm. Then 100 µl of the supernatant were added to 5 ml of Ferrozine (1 g l^{-1}) in 50 mM HEPES buffer at pH 7 and Fe^{2+} was determined spectrophotometrically at 562 nm (Stookey 1970). To determine the concentration of Fe^{2+} + Fe^{3+}, a second subsample (100 µl) of the acidic super-natant was added to reducing Ferrozine solution (Ferrozine with 1% hydroxylamine hydrochloride) and measured after 3 h reaction time spectrophotometrically (Chao & Zhou 1983; Phillips & Lovley 1987; Thamdrup et al. 1994a). The Fe^{3+} concentration was calculated as the difference between the (Fe^{2+} + Fe^{3+}) and Fe^{2+} concentrations.

To asses the content of the total amount of free iron oxides (except magnetite) in our sediments, we used the extraction with dithionite as described by (Thamdrup et al. 1994a). Through this procedure, both Fe(II) and Fe(III) dissolve as Fe^{2+} (Wallmann et al. 1993). For this extraction ca. 200 mg wet sediment were transferred to

preweighed plastic vials with 10 ml of citrate/acetic acid buffer (pH = 4.8), then 0.5 g sodium dithionite powder was added. After 1 h extraction at room temperature on a shaker, the vial was centrifuged 5 min at 4000 rpm. The decanted supernatant was stored for some days to allow oxidation of the remaining dithionite (to avoid interference with the Fe determination), then the concentration of Fe^{2+} in a 100 µl subsample was measured using Ferrozine as described above. From the resulting total concentration of free iron oxides, we subtracted the concentrations of the hydroxylamine extractable iron. The remaining iron oxide concentration was assumed to be the iron oxide fraction not available for microbial processes and will be called in the following text Fe-min (mineral bound iron).

Manganese

The manganese concentration in the HCl extracts and in the porewater samples was analyzed by flame absorption spectroscopy (Perkin Elmer) (Thamdrup et al. 1994b).

Nutrients

Nitrate, nitrite, ammonium, phosphate and silicate in flume- and pore water where analyzed after centrifugation (5 min at 4000 rpm) according to (Grasshoff et al. 1983)

Voltametric microelectrode measurements

With proper calibration, voltametric microelectrodes can detect colloidal Fe(III) over the voltage range -0.2 to -0.7 V (Brendel 1995; Brendel & Luther 1995) and we applied this method to trace interfacial flux of iron. The voltammetric cell arrangement consisted of the gold amalgam microelectrode standardized for Fe as measuring electrode (Brendel & Luther 1995), a 0.5 mm diameter platinum wire as counter electrode, and a saturated calomel electrode (SCE) as reference electrode. The microelectrode, held by a 3-axis micro-manipulators, was placed 2 mm above the downstream slope of the mound (Exp. 3) and interfaced to an Analytical Instrument Systems, Inc. (AIS) model DLK-100 voltammetric analyzer. The voltage range scanned was typically from -0.1 V to -2.1 V. For linear sweep voltammetry, we scanned at 200 mV sec^{-1} and for square wave voltammetry, we used a pulse height of 15 mV, step increments of 2 mV, a frequency of 100 Hz and also a scan rate 200 mV sec^{-1}. Precision for replicates of Fe^{2+} and Fe^{3+} at a given depth was 2-5%.

RESULTS

Surface precipitates of iron and manganese caused by pore water advection (Experiment 1)

In experiment 1, the effect of advective processes on the geochemical zonation was visible at the sediment surface. Once burrow construction of *C.truncata* had reached a stage of burrow maintenance after a period of ca. 6 weeks, mounds and funnels were quasi permanent structures. Here the interaction of flow and sediment topography produced conspicuous reddish metal precipitates at the downstream slopes of the mounds. First, two reddish spots appeared left and right from the center line, then these spots grew larger until they merged to a band (0.5 to 1.5 cm wide) crossing the slopes horizontally.

Iron analyses showed a 2.7-fold enhanced Fe(III) concentration in the precipitates relative to the smooth reference area while particulate Fe(II) concentrations did not show any significant change when comparing all sampling areas (Fig. 2). Below the approximately 1 mm thick layer of the reddish iron oxide minerals and on the sediment surface downstream of the mounds, we found a thin layer (<1 mm) of dark brown precipitates. The analyses showed that these brown precipitates contained manganese oxides, although only in the downstream area Mn concentrations were significantly higher (factor 1.5) than in the reference areas (Fig. 2). In the areas where the color of the reddish surface precipitates was most intense, we observed the formation of small red fluffy spheres with up to 2 mm diameter. Microscopical inspection of these spheres revealed colonies of *Gallionella spec.*, an iron oxidizing bacterium.

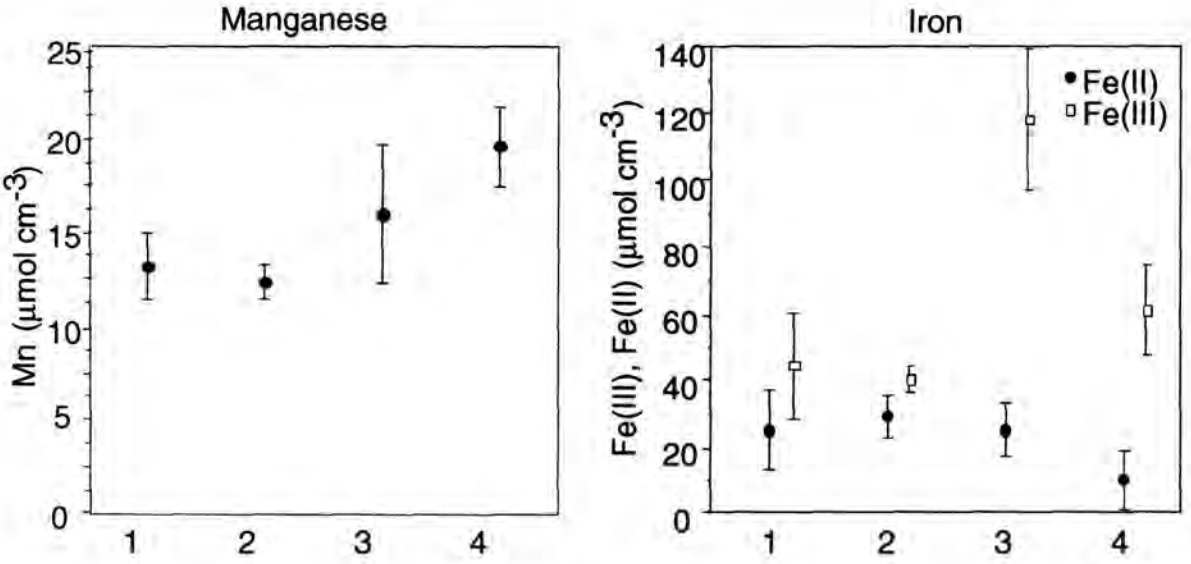

1: Reference, 2: Upstream, 3: Mound, 4: Downstream

Fig. 2. Experiment 1: Concentrations of Mn (left graph) and Fe(III) and Fe(II) (right graph) in metal-oxide precipitates collected from the surface of the sediment core (0-1 mm depth). (Units: µmol cm^{-3} wet sediment)

It is possible, that the pumping activity the shrimps also affected the formation of the precipitates, but we did not quantify this impact. However, experiments 2, 3 and 4 demonstrated, that the surface precipitates also formed as intensely at artificial topography when *Callianassa* and bioirrigation were excluded (see blow).

Advective control of particulate metal-oxide distribution within the sediment (Experiment 2)

The results of experiment 2 demonstrated, that the advective pore water flows caused not only metal precipitation at the sediment surface but also strongly affected the geochemical zonation within the core (Fig. 3). We found a reproducible pattern of particulate Fe(III), Fe(II) and Mn shaped by advective processes down to a sediment depth of 8 cm. The ranges of iron and manganese concentrations measured in this experiment are listed in Table 2. In most cases, the metal distributions along the centerline transect, were very similar to those along the parallel transect. We therefore will only present those data from the parallel transect which interestingly deviated from the centerline transect.

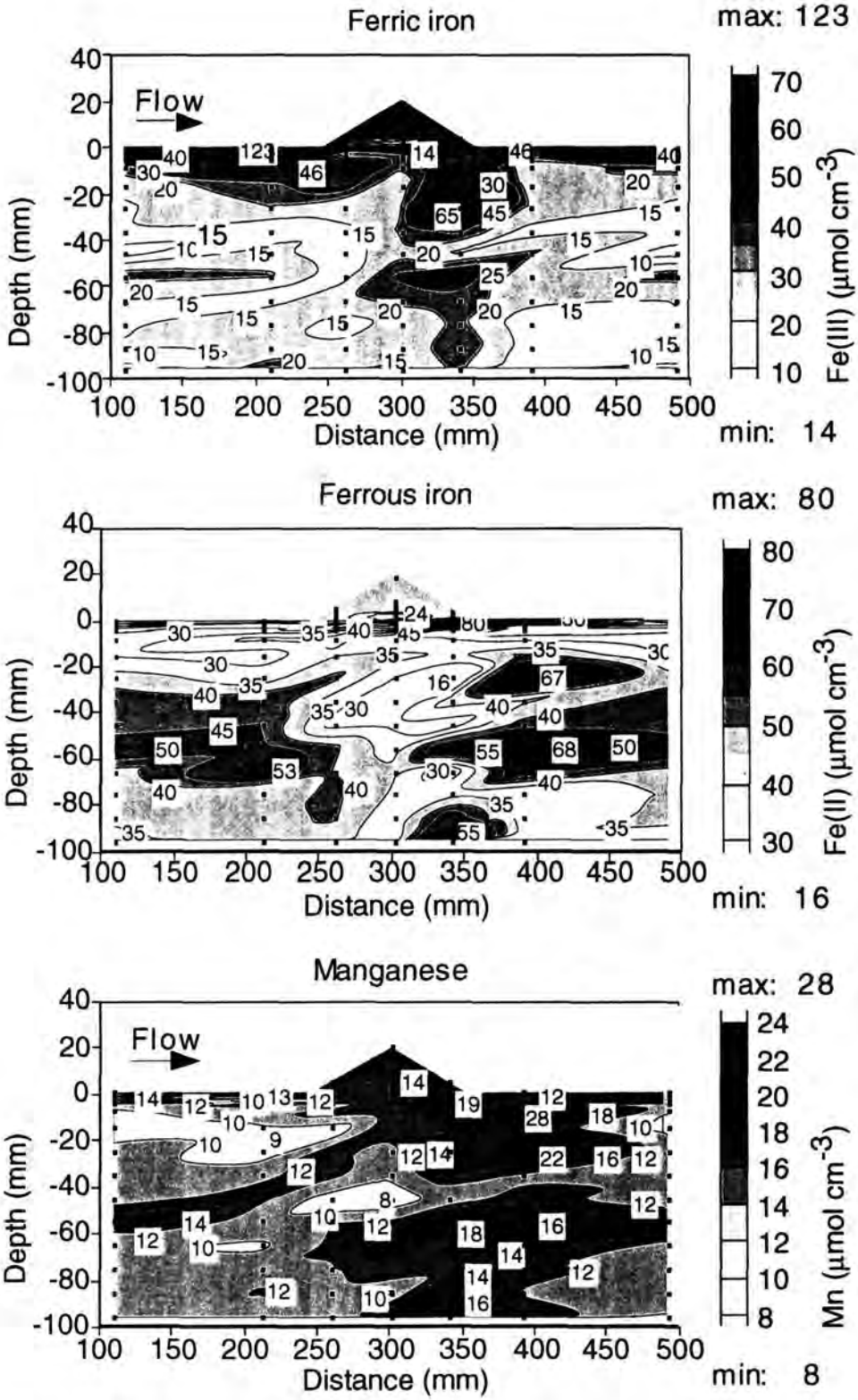

Fig. 3. Experiment 2, second run: Isoline diagrams depicting the concentrations of solid phase Fe(III), Fe(II) and Mn recorded in the sediment core (Units: µmol cm^{-3} wet sediment)

Table 2. Comparison of maximum nutrient, iron and manganese concentrations recorded in experiment 2 and experiment 3

	Expt 2				Expt 3 (+ org. matter)				Differences and ratios					
	Center		Parallel		Center		Parallel		Center		Parallel		Averages	
	min	max	min	max	min	max	min	max	diff	ratio	diff	ratio	diff	ratio
Solutes														
nitrate	0	74	1	79	0	260	0	228	186	3.5	149	2.9	167	3.2
nitrite	0	6	0	13	0	13	0	8	8	2.3	-5	0.6	1	1.5
ammonium	0	147	0	164	10	1428	7	1562	1281	9.7	1398	9.5	1340	9.6
phosphate	0	6	0	8	0	17	0	44	11	2.9	36	5.4	24	4.1
silicate	7	103	7	142	12	177	15	181	74	1.7	39	1.3	57	1.5
solid phase														
Fe(III)	14	123	9	116	0	66	0	49	-57	0.54	-67	0.42	-62	0.48
Fe(II)	16	80	24	58	19	68	4	71	-12	0.85	13	1.22	0.5	1.04
Fe(III)+(II)	30	203	33	174	19	134	4	120	-69	0.66	-54	0.69	-61.5	0.67
Fe min	14	335	70	464	18	214	5	294	-121	0.64	-170	0.63	-146	0.64
Mn	8	28	8	28	6	26	2	28	-2	0.93	0	1.00	-1	0.96

After 2 months a thin layer of increased iron and manganese oxides had formed at the sediment surface (0-3 mm) (Fig. 3). Maximum Fe(III) concentrations were reached at 0 to -1.5 mm depth (Exp. 2, 1st run 1: 100 µmol cm^{-3}; Exp. 2, second run: 123 µmol cm^{-3}). In the high pressure area upstream of the mound, where water intrusion was strongest, the Fe(III) enriched layer extended deeper into the sediment (run 1: 10 mm; run 2: 20 mm), whereas at the downstream slope, reddish precipitates had formed at the surface as observed in experiment 1. Unexpectedly, a Fe(III) maximum was found in both runs at 20 to 30 mm depth just downstream the mound, this maximum was also recorded later in experiment 3. This maximum was most pronounced in the second run of Exp. 2 where 65 µmol cm^{-3} Fe(III) were measured in this zone. The up- and downstream accumulations of Fe(III) were separated by a wedge like zone with lower Fe(III) concentrations reaching from the deeper sediment layers to the surface underneath the mound (1st run: 15 µmol cm^{-3} isoline; 2nd run: 20 µmol cm^{-3} isoline).

The distribution of particulate Fe(II) showed strong similarities to the distribution of the manganese oxides, both were affected by advection. The concentration maxima were again located up- and downstream the mound, but deeper in the sediment (1st run: 40 mm, 2nd run: 60 mm depth) below those of Fe(III). Originating from the upstream deep maxima a zone of increased Fe(II) and Mn concentration (Fe(II): 35 µmol cm^{-3} isolines, Mn 10^{-12} µmol cm^{-3} isolines) bent upwards towards the downstream slope of the mound. In this experiment we measured increased concentrations of Mn (17-19 µmol cm^{-3}) in the reddish precipitates on the downstream slope of the mound. After the second run of experiment 2, a relatively strong

Mn maximum was recorded downstream the mound at 20-30 mm depth. This maximum enclosed the area of both, the Fe(III) as well as an additional Fe(II) maximum observed at that depth.

The Fe-min (iron oxides not available for microbial processes) concentrations in our sediment core were much higher than those of HCl extractable Fe(III) and Fe(II). The Fe-min isolines did not show any reproducible advection related pattern. In general, the Fe-min concentrations in the central part of the sediment core were lower than the concentrations at the upstream and downstream edges of the core.

Impact of advective porewater flows on pore water nutrient concentrations (Experiment 2 and 3)

From the distribution patterns of the dissolved nutrients in the sediment, we expected to gain information not only on the geochemical zonation but also on the effect of advective processes on the microbial degradation processes. The pore water nutrient isolines in the sediment cores of experiments 2 and 3 clearly reflected advective processes and local enhancement of nitrification (Fig. 4). Zones with deepest penetrations of nitrate were found at the up- and downstream edge of the surface topography (experiment 2: >10 µM down to 70 mm), whereas ammonium was depleted in these areas (experiment 2: >10 µM down to 70 mm). Underneath the mound, pore water upwelling produced a wedge of increased ammonium concentrations extending towards the surface. The nitrite pattern was less clear, but highest concentrations (up to 13 µM) were recorded close to the surface in the up-and downstream areas of the mound and at the transitions between the nitrate and the ammonium rich zones. Phosphate and silicate concentrations produced highest concentrations in a thin layer (0 to -10 mm) right underneath the sediment surface and the maxima where located where water intruded the core (phosphate 6.1 µM, silicate: 103 µM) . Below this surface layer, phosphate concentrations were very low (< 2 µM) and did not show any advection related pattern. The addition of organic matter prior to experiment 3 caused a significant increase in all pore water nutrient concentrations (Table 2), however, the distribution patterns of the solutes described above remained more or less the same. With the maximum concentrations rising from 147 µM to 1281 µM ammonium showed the strongest increase (factor 9.7) while nitrate and nitrite increased by factor 3.5 (from 74 µM to 260 µM) and 2.3 (from 5.8 µM to 13.3 µM), respectively. Phosphate maxima showed a stronger increase (from 6.1 to 17.4 µM, factor 2.9) than those of silicate (from 103 to 177 µM, factor 1.7). The silicate distribution in

experiment 3 was very similar to that of nitrate indicating that silicate was also affected by the advective porewater flows.

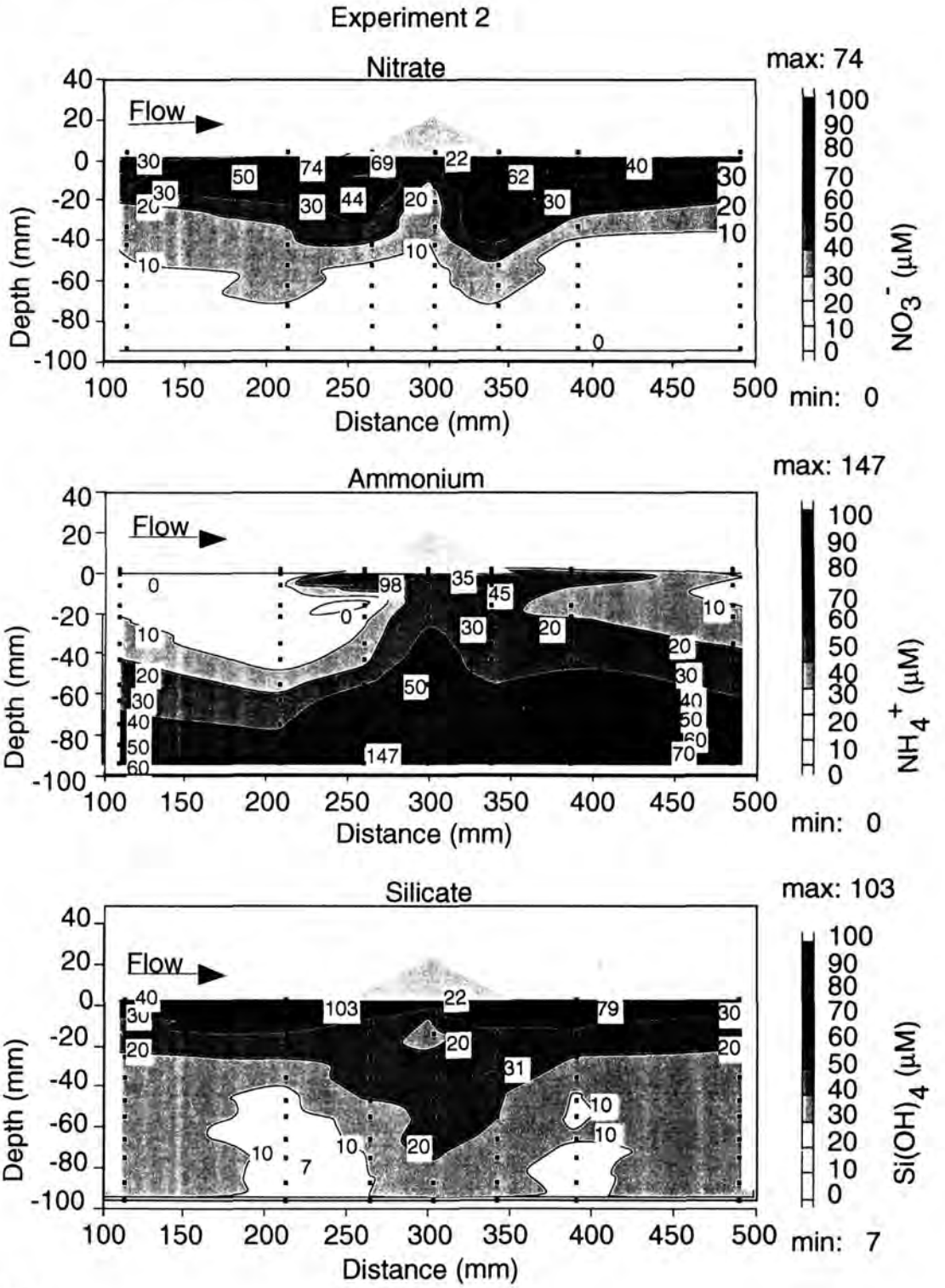

Fig. 4 A.

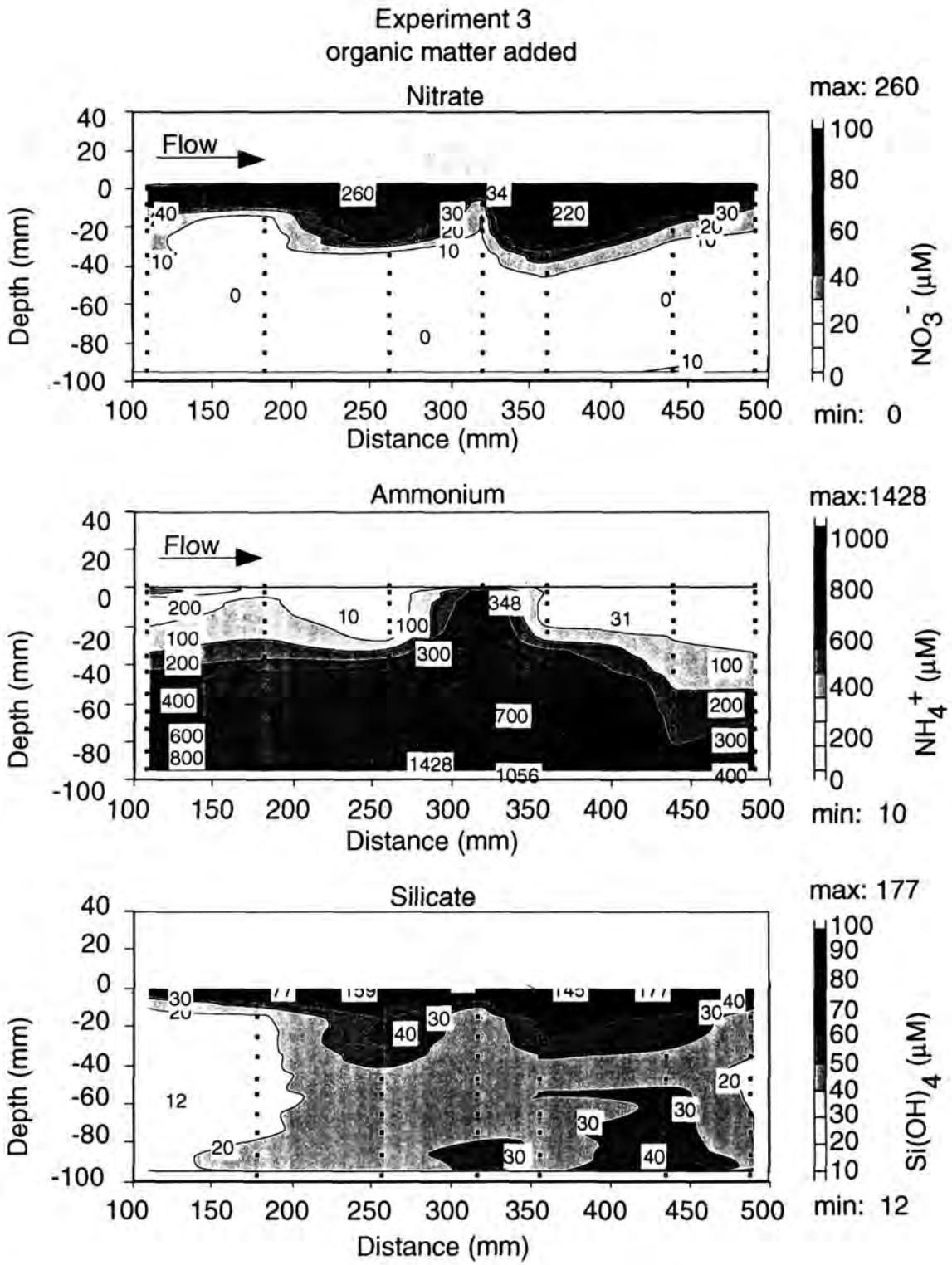

Fig. 4B. Experiments 2 and 3: Pore water concentrations of nitrate, ammonium and silicate recorded in the sediment core after Experiment (no organic matter added,Fig. 4A) and Experiment 3 (organic matter added Fig. 4B).

Impact of organic matter addition on iron and manganese concentrations (Experiment 3)

In the sediment core where organic matter had been added, similar concentration patterns developed for the particulate iron and manganese as found in experiment 2, however, for manganese they were less pronounced. Also, maximum Fe(III) concentrations in the centerline of the core reached only 66 μmol cm^{-3} (parallel line: 49 μmol cm^{-3}) and thus were lower compared to experiment 2, without addition of organic matter (run 1, centerline: 100 μmol cm^{-3}, parallel: 118 μmol cm^{-3}, run 2: centerline: 123 μmol cm^{-3}, parallel: 116 μmol cm^{-3}). The Fe(II), Fe-min and Mn concentration maxima where not significantly different in the cores with and without additional organic matter.

The isoline diagrams of the dissolved Fe^{2+} concentrations in the porewater of the sediment core with organic matter resembled those of ammonium, giving a clear indication of advective pore fluid upwelling underneath the mound (Fig. 5). A thick layer of high Fe^{2+} concentrations (265 to 276 μM) had developed at 100 to 140 mm depth, above this layer the Fe^{2+} concentrations decreased rapidly (within 20 mm) to values < 20 μM. Most pronounced in the parallel transect, the dissolved iron was drawn from the deeper layers to the surface and Fe^{2+} concentrations in the surface layer (0-0.5 mm) here reached 12 μM.

Dissolved Mn concentrations were highest within a layer between 40 and 140 mm sediment depth which was slightly above the Fe^{2+} rich zone but with a considerable overlap. Similar to Fe^{2+}, high concentrations also occurred in the upper sediment layer within the upwelling zone. This again was especially obvious along the parallel transect where 1.9 μM Mn^{2+} were measured in the surface layer (0 to -0.5 mm).

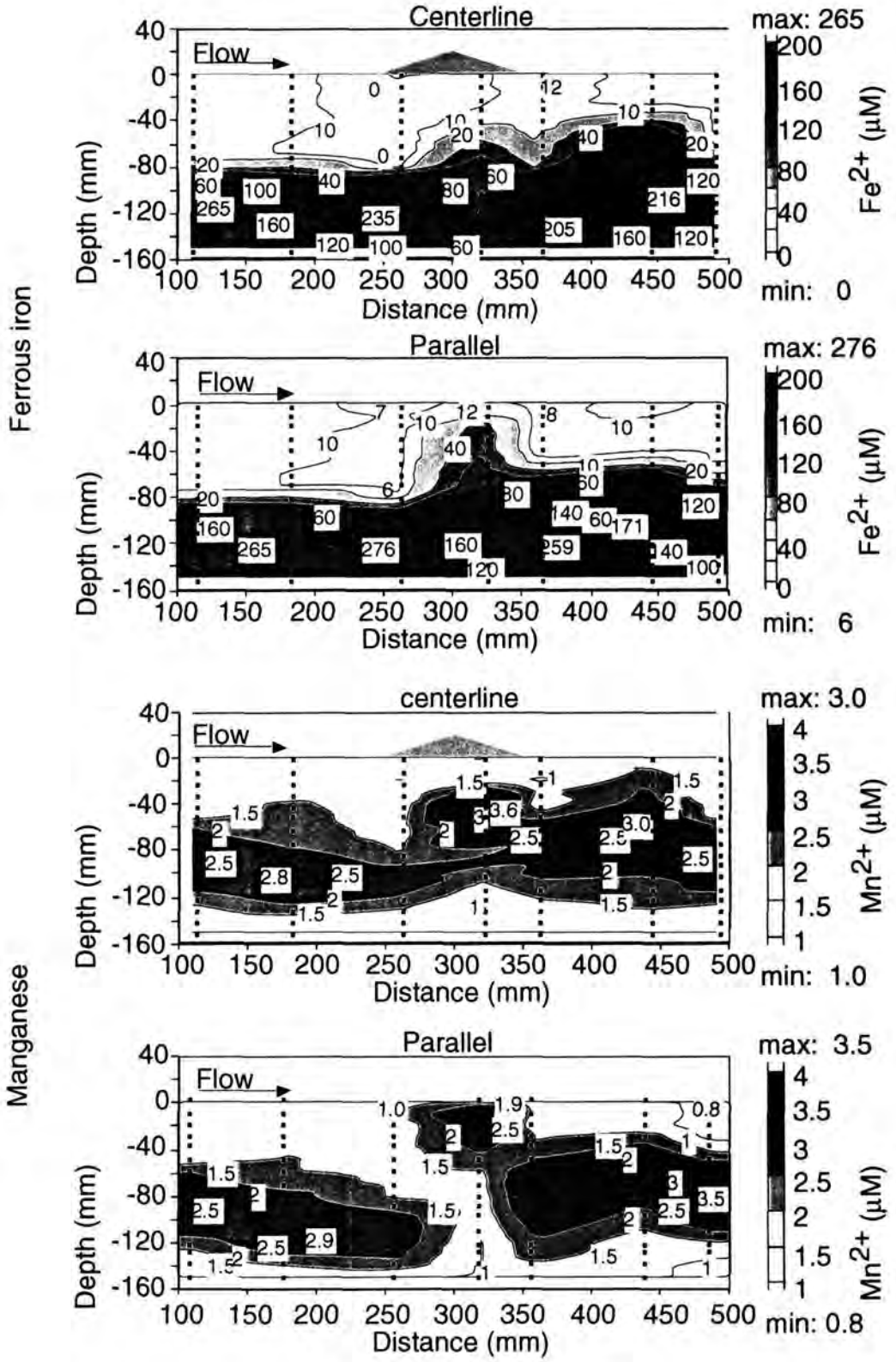

Fig. 5. Experiment 3: Pore water Fe^{2+} (upper panels) and Mn^{2+} (lower panels) concentrations in centerline and parallel transects .

Interfacial fluxes

Boundary flow - topography interaction affected the fluxes of nutrients and metals between the sediment and the overlying water (Table 3). After the sediment core had been placed in the flume and the surface had been levelled, the nutrient concentrations in the flume water decreased steadily (range: -0.16 to -0.44 mmol m^{-2} d^{-1}) and the metal concentrations remained low (< 0.15 µM) (Fig. 6). The establishment of surface topography (10 mounds, 2.5 cm high = 56 mounds m^{-2}) caused an immediate sharp increase of ammonium and silicate concentrations for a short time period of 12 h. After this initial period we recorded a steady increase in nitrate (0.69 mmol m^{-2} d^{-1}) and silicate (1.44 mmol m^{-2} d^{-1}) concentrations and a decrease in ammonium (-0.34 mmol m^{-2} d^{-1}) in the flume water while phosphate concentration remained 0. After one week, reddish precipitates had formed at the downstream slopes of the mounds (Fig. 7). Although the concentrations were very low, we also measured an increase of iron (7.1 µmol m^{-2} d^{-1}) and manganese (14.2 µmol m^{-2} d^{-1}) in the flume water (Fig. 6, Table 3). In contrast to the nutrients, the increase of the metal concentrations in the flume water started only 5 days after the mounds had been build on the surface. The metal concentration increased for 10 days, then they levelled out and started to decrease again.

Table 3. Topography related fluxes of nutrients (mmol m^{-2} d^{-1}) and metals (µmol m^{-2} d^{-1}) calculated from concentation changes in the experimental flume set-up recorded in experiment 4 in two runs. Fluxes across a smooth surface are compared with a rough sediment surface, characterized by sediment mounds.

Nutrients	Run 1			Run 2		
	Smooth	Rough	Difference	Smooth	Rough	Difference
Nitrate	-0.38	0.69	1.08	-0.71	5.29	6.00
Nitrite	-0.16	0.09	0.25	0.00	0.02	0.02
Ammonium	-0.44	-0.34	0.10	-0.18	0.73	0.91
Phosphate	0.00	0.00	0.00	0.00	0.00	0.00
Silicate	-0.31	1.44	1.75	-0.66	0.80	1.46
Metals	Run 1			Run 2		
	Smooth	Rough	Difference	Smooth	Rough	Difference
Iron	-0.89	7.11	8.00	0.00	2.76	2.76
Manganese	3.56	14.22	10.67	-2.22	31.65	33.87

In the second run, we also measured increases of nitrate, nitrite, ammonium and silicate in the flume water after establishment of surface topography. Nitrate fluxes were much higher (5.3 vs. 0.7 mmol m^{-2} d^{-1}, respectively) than in the first run (Table 3). However, the time period with increased fluxes was shorter than in the previous run and lasted only 5 days. In the second run, topography increased the iron concentration in the flume only insignificantly while the apparent manganese fluxes increased from -2.2 to 31.6 µmol m^{-2} d^{-1} for a period of 2 days.

Results of voltammetric electrode measurements

The microelectrode measurements documented the release of iron from the sediment with upwelling reduced pore water flows. With the initial flow rate setting of 1 cm s^{-1} no Fe could be detected by the microelectrode in the diffusive sublayer and the upper 5 mm of the sediment and the flow rate was increased to 8 cm s^{-1}. Two hours later, Fe was found within 3 mm of the surface at the downstream slope of the mound . The flow velocity then was increased to 10 cm s^{-1}. 8 hours thereafter, two red iron (oxy)hydroxide spots of about approximately 1 cm diameter had formed at the downstream slope of the mound (Fig. 7). In these spots (0 to 1 mm depth) Fe(II) and Fe(III) species were found while O_2 was absent. Between the spots, close to the centerline, Fe(II) and Fe(III) were detected to 2 mm above the sediment-water interface and again O_2 was not present here. The Fe(III) peak current decreased exponentially with increasing Fe(II) concentration throughout the profile.

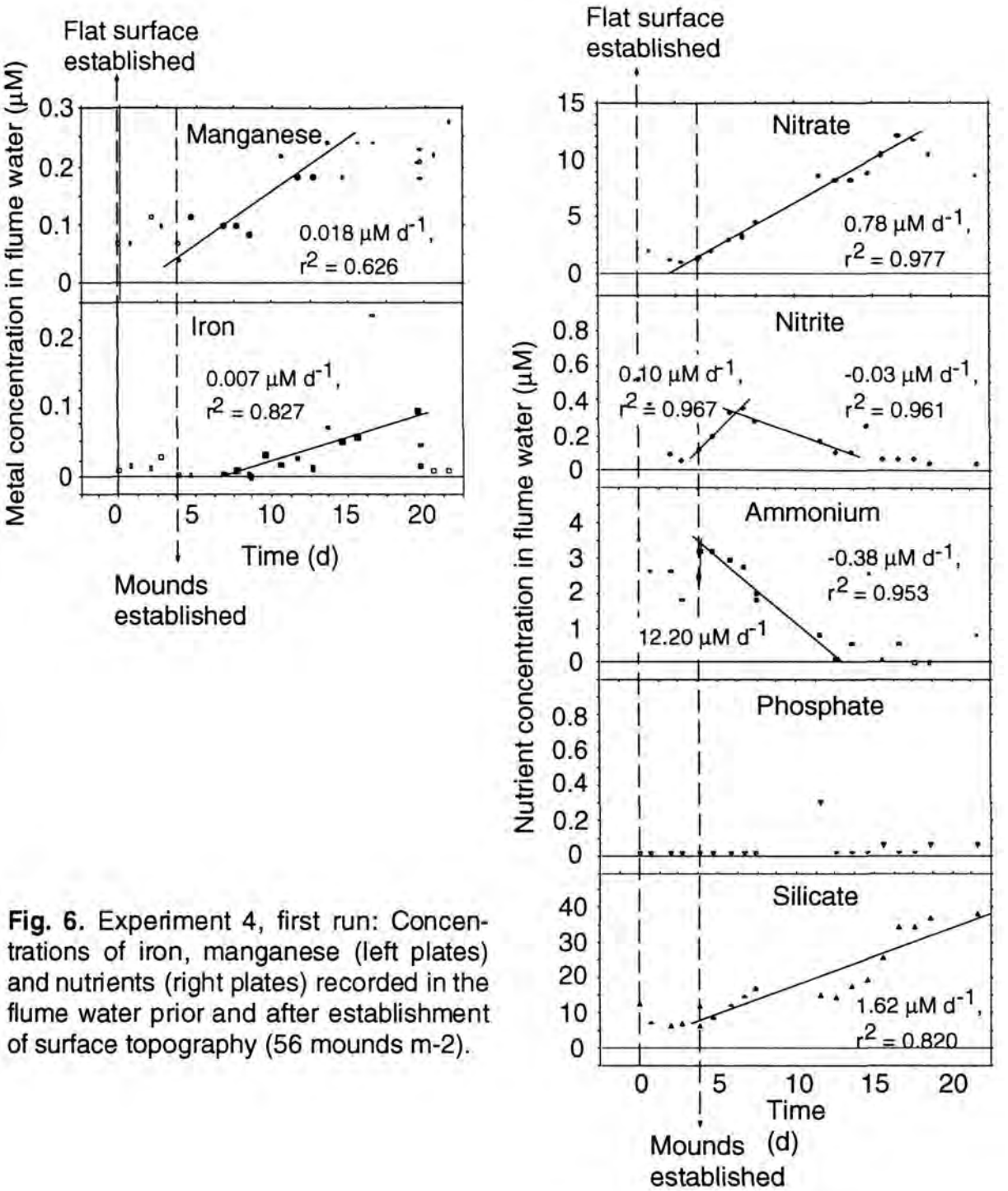

Fig. 6. Experiment 4, first run: Concentrations of iron, manganese (left plates) and nutrients (right plates) recorded in the flume water prior and after establishment of surface topography (56 mounds m-2).

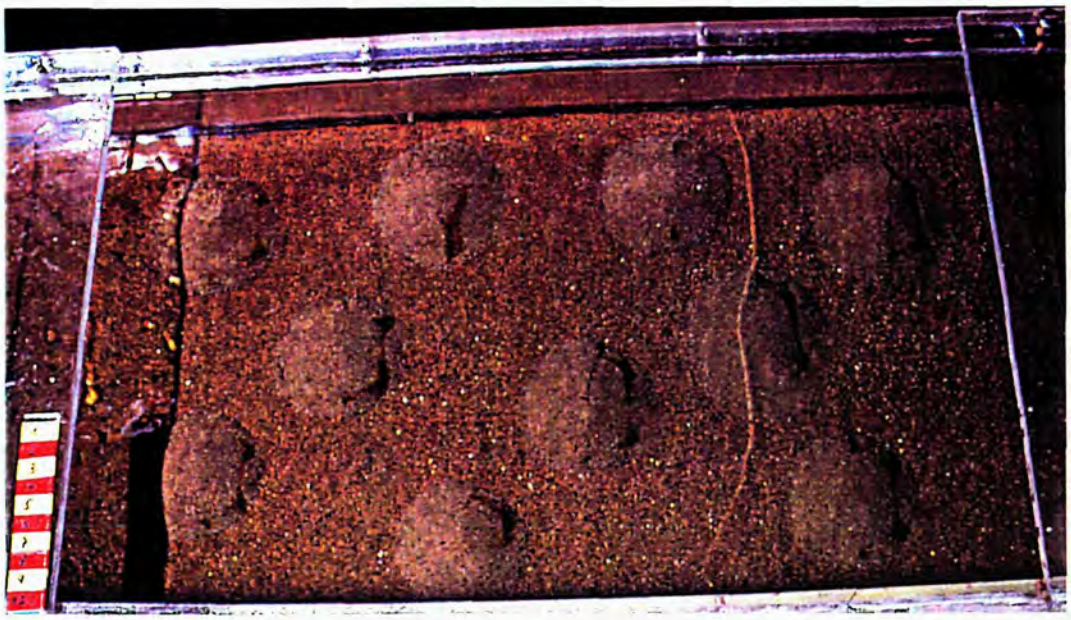

Fig. 7 A.

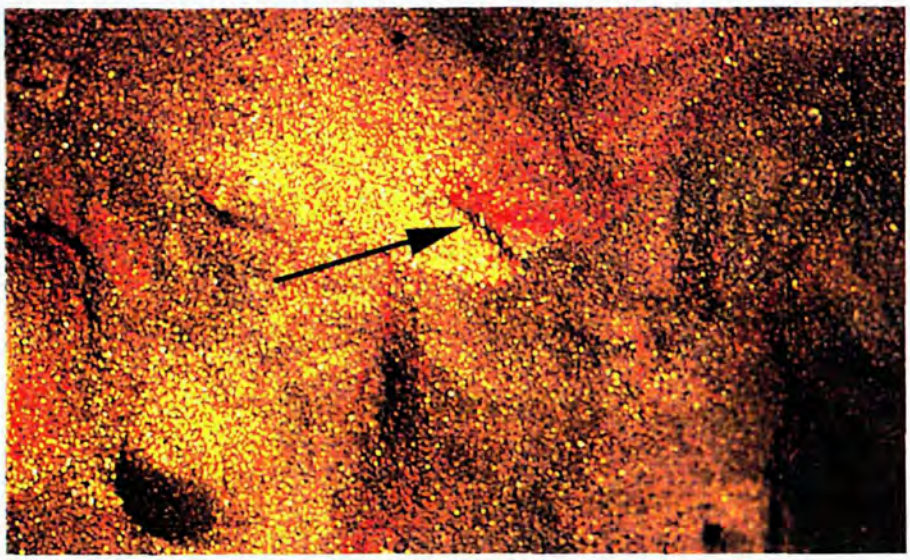

B

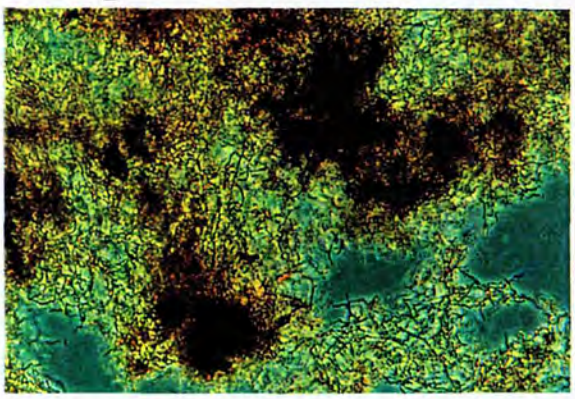

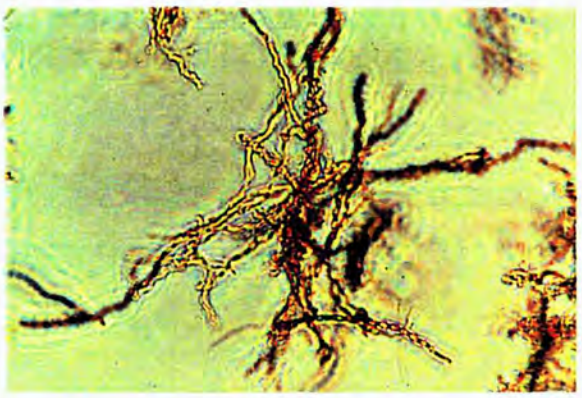

C D

Fig. 7 A: Artificial topography on flume core with metal-oxide precipitates at the downstream side of the mounds. **B**: Mounds created on flume core by *Callianassa truncata*. The fuzzy spheres close to the top of the mounds are colonies of the iron oxidizing bacterium *Gallionella spec.* **C**: Micrograph of the *Gallionella* stalks (magnification: 40 x). **D**: Micrograph of the *Gallionella* stalks (magnification: 400 x).

DISCUSSION

Advection as structuring process

In cohesive sediments a one dimensional horizontal layering of geochemical reaction zones is predominant where a vertical sequence of oxygen, nitrate, manganese oxides, iron oxides and sulfate reducing processes may reflect a balance between diffusional supply and consumption of electron acceptors (Aller 1982). Our experiments demonstrate that this scenario may change dramatically when the sediment is permeable allowing advective transport. In the permeable flume core, advective pore water flows generated a complex three dimensional geochemical zonation. The observed patterns, characterized by two oxidized water intrusion zones and an reduced upwelling area associated with each mound, were reproducible (e.g. Figs. 3, 4, 5) and agreed with previously measured inert tracer and oxygen patterns (Huettel et al. 1996b; Ziebis et al. 1996b). This correspondence identified the advective pore water flows as the cause for the oxide precipitates observed at the surface of our sediment and the uneven distribution of metals and nutrients within the core.

The three dimensional biogeochemical zonation in permeable sediment is controlled by 1) the forcing of water and solutes into the sediment 2) the co-transport of suspended particulate material into the bed with the intruding fluid, 3) horizontal transport of solutes and particles within the sediment and 4) the pumping of pore water from deeper sediment layer to the surface and out of the bed. The depth range of the advective fluid up- and downwelling is directly related to the permeability of the sediment, the size of the surface topography and the bottom flow velocity (Huettel et al. 1996a; Huettel & Gust 1992a). In our flume experiments, advective processes affected the upper 8 cm of the sediment core. Within this depth range, advective pore water flows can provide a transport mechanism much faster than diffusion which can be demonstrated by the following rough comparison. The concentration at a specific depth and time of a solute diffusing into homogenous sediment can be calculated using:

$$C(z, t) = C_0 \, \mathrm{erfc} \, z/2\sqrt{(Ds\, t)} \qquad \text{(Crank 1983)}$$

with $C(z, t)$ = concentration at depth (z) at time (t), C_0 = initial concentration of solute, erfc = complement of error function, D_0 = diffusion coefficient, D_s = apparent diffusion coefficient with:

$$D_s = D_0 \, j/q \text{ and } q = 1\text{-}\ln(j^2) \qquad \text{(Boudreau 1996)}$$

j = porosity, q = tortuosity

Assuming a diffusivity of 1.5 x 10^{-5} cm^2 s^{-1} and sediment with a porosity of 0.3, diffusive transport would take 41 days to reach 10% of the surface concentration at 5 cm depth according to this calculation. In the sandy sediment we used, pressure driven pore water transport covers 5 cm depth difference within a day (Huettel & Gust 1992a; Huettel et al. 1996b). Although diffusion may be relatively fast over distances within the millimeter range, advective transport in permeable sediments thus can be more efficient over larger scales.

There are various ways how the fast, conveyorbelt-like advective transport can affect diagenetic processes. In the sediment, replacement of pore fluid by intruding bottom water changes the concentrations of interstitial solutes and particles shifting redox boundaries and creating new geochemical gradients. Chemical reactions are boosted by the intensified contact of reactants due to the advective mixing while microbial processes are promoted by increased supply of substrates and the rapid removal of waste products. In the following, we will use our results to document the effects of advection and related mechanisms on the geochemical zonation and interfacial fluxes.

Manganese

Although pore water flows influenced the distribution of the solid phase metal-oxides in our flume sediments, the particulate metal isolines did not show the impact of advection as nicely as those of the dissolved metals. This is not surprising, since the sediment, especially after the addition of organic matter, had many small inhomogeneities which caused a wider scatter of iron and manganese concentrations in the small volumes of sediment used for the solid phase metal analyses.

In the oxic surface layer of marine sediments, solid manganese (oxyhydr)oxides occur in the form of amorphous materials and coatings on particles often occur in close association with iron oxides. Below this layer, under conditions of low Eh and pH, manganese is reduced from the oxidation state IV to state II (some soluble Mn^{3+} may also be produced (Luther et al. 1994)), and then may be found dissolved in the pore water as free or organically complexed ion. In addition to microbial manganese reduction, a wide range of organic and inorganic compounds including sulfide, nitrite, pyruvate and oxalate are able to chemically reduce manganese oxides. Because the Mn redox boundary usually is found where oxygen concentrations in the sediment drop to near-zero levels oxygen is assumed to be the primary sedimentary oxidant of manganese (Burdige 1993). However, observed high

reaction rates the suggest that fast Mn oxidation can be microbially catalyzed (Thamdrup et al. 1994b).

In our flume experiments, we found manganese oxides concentrated in the uppermost layer of the sediment but also at 30 to 50 mm depth upstream and downstream the mound (Fig. 3). From the deep maxima, zones of increased manganese oxide concentration reached upwards towards the mound. This pattern can be related to water flows which intruded the sediment up- and downstream of the mound and then moved on a curved flow path towards the downstream slope of the elevation (Fig. 1, (Huettel & Gust 1992a)). As shown by (Ziebis et al. 1996a) these advective pore water flows can transport oxygen more than 30 mm into the sediment upstream of mounds and approximately down to 20 mm on the downstream side (same sediment as in our experiments). The manganese oxide maxima found in the deeper sediment layers thus had formed at the lower boundary of the water intrusion zones and the upward directed layers of manganese oxide followed these boundaries to the surface. Apparently, mobile Mn^{2+} transported upwards from reduced deeper sediment layers was oxidized when contacting the advective water flows and precipitated at the interface of the reduced and the oxygenated sediment.

The distribution of the dissolved Mn^{2+} supported our theory on the formation of the upward directed layers of particulate manganese oxides. The up- and downstream maxima of Mn^{2+} were located just below the concentration maxima of the manganese oxides. Advection and diffusion then transported Mn^{2+} upwards. Under the mound upwelling of reduced pore water allowed the ascent of Mn^{2+} to the upper sediment layers and, in the parallel transect where upwelling was strongest, the release of Mn^{2+} to the water column (for fluxes see below). This manganese then probably re-entered the sediment with the flume water as suspended particulate oxides where it increased the Mn concentrations in the surface layer.

Iron

The distributions of Fe(II) and Fe(III) in the solid phase (Fig. 3) and dissolved Fe^{2+} (Fig. 5) sustain our interpretations of the manganese results. Advective oxygenation up- and downstream the mound lead to ferric iron precipitation in the upper sediment layer while reducing conditions in the diffusion dominated sediment layers below 80 mm depth promoted the build up of dissolved Fe^{2+}. Oxidation of Fe^{2+} by manganese oxides (Myers & Nealson 1988) may have caused the deeper

extension of the downstream Fe(III) zone and the formation of the Fe(III) maximum at 20-30 mm depth.

Also, as demonstrated recently by (Straub et al. 1996) some nitrate-reducing bacteria can grow anaerobically with ferrous iron as the only electron donor or as the additional electron donor in the presence of acetate. This process also may have contributed to the formation of the ferric iron maxima in the nitrate enriched zone. Beneath the mound, upwelling fluid carried ferrous iron towards the surface (Figs. 3, 5). As already seen in the manganese isolines, upwelling of the dissolved metals was strongest in the parallel transect where the 20 µM Fe^{2+} isoline almost reached the surface. The formation of the reddish surface precipitates started exactly in the area where this pore flow hit the surface.

Fe^{2+} is far less soluble than Mn^{2+} and also forms various solid phases with e.g. carbonate, sulfur and phosphate (Berner 1980; Burdige 1993). Scavenging by sulfides may have caused the decrease of the Fe^{2+} concentration below 120 mm depth in our sediment core, a reaction which also may have been responsible for the Mn^{2+} decrease observed in this zone (Burdige & Nealson 1986). Maxima of solid phase Fe(II) were located up- and downstream the upwelling zone, below the Fe(III) enriched zone. This distribution proposed that these concentrations of Fe(II) particles were an intermediary product between the dissolved ferrous iron concentrated in the deeper sediment layers (and the upwelling zone) and the precipitated iron oxides near the surface. The strong similarity between the solid phase Fe(II) and solid phase Mn distribution (Fig. 3) suggests that Fe^{2+} was adsorbed to Mn-oxides, a process which may precede the redox reaction between the two metals.

Most of the geochemical patterns, however, were probably microbially mediated as indicated by Fe-min, the iron oxides not available for microbial reduction (Lovley 1995). The Fe-min distribution did not show any significant reaction to the advective transport processes. Results of experiment 3 support this assumption. Enhanced microbial activity after organic matter amendment resulted in mobilization and redistribution of the microbially available iron and manganese. The ensuing increase of solid phase Fe(III), Fe(II) and Mn concentrations near the sediment surface proposed that iron and manganese were dissolved in the deeper sediment layers and then precipitated again in the upper layers. Also, the reddish surface precipitates at the mounds appeared after only one day while it took up to three weeks for the precipitates to form in the sediment without organic matter addition.

Nutrients

The impact of advection on the sedimentary microbial community was most obvious in the nutrient profiles. Advective percolation produced local zones of enhanced nitrification in the upper sediment layers up and downstream the mound, causing the build up of nitrate (Fig. 4). Elevated concentrations of nitrite, intermediary compound in the microbial oxidation of ammonium or reduction of nitrate, also indicated enhanced microbial activity in these zones. The nitrification zones were identical to the zones of advective oxygenation at sediment topography reported by (Ziebis et al. 1996a) and (Forster et al. 1996). Similar local nitrification zones caused by advective pore water flows can be observed where benthic macrofauna forces oxygenated water through interstitial spaces of the sediment (Grundmanis 1977; Huettel 1990).

While nitrate concentrations in the flume water never exceeded 20 µM, 74 to 260 µM were recorded in the percolated sediment zones, demonstrating that nitrification within the sediment was responsible for this build up. Maxima located at 15 mm (upstream) and 25 mm (downstream) depth (experiment 2, Fig. 4) proved that the vertical extent of the nitrate enriched zones was not solely caused by downward transport of nitrate from the surface sediment but also by nitrification in deeper layers. According to (Berner 1980) nitrate is used for organic matter decomposition when oxygen levels fall to approximately 5% of their concentration in oxygenated water. At the downwelling zones in our flume core this boundary was located at approximately 30 mm depth (Ziebis et al. 1996a; Ziebis et al. 1996b) which agrees with the observed decrease of nitrate and increase of ammonium concentrations below this layer.

Although nitrification and advective flushing removed most of the ammonium from the upper sediment layers, ammonium could reach the sediment surface with relatively high concentrations (experiment 2: 35 µM, experiment 3: 348 µM, Fig. 4) through the upwelling channel. Along the slopes of this anoxic wedge, concentration isolines were compressed between intruding flume water and upwelling pore water. Ammonium as well as the nitrate gradients were steepest here suggesting increased nitrification/denitrification activities in this zone. This again is similar to processes at vertical animal burrows producing zones of enhanced nitrification/denitrification and steep horizontal gradients in an otherwise horizontal geochemical layering (Aller 1983; Aller 1982; Aller 1984; Ziebis et al. 1996a; Kristensen 1985).

After addition of organic matter to our sediment, the pore water concentrations of ammonium and nitrate increased 10 and 3.5-fold, respectively, but the general geochemical zonation persisted. In contrast to these distinct concentration increases, the depth of the nitrification zones decreased relatively little, (70 to approx. 40 mm for 10 µm isoline, factor 1.7, 20 µM isoline remained almost at same depth) indicating that advective flushing could efficiently maintain the oxic/suboxic conditions in the percolated areas after the amendment of organic matter. For this process the advective removal of ammonium and nitrate from the sediment may have been as important as the supply of oxygen to the pore water (Rönner 1985; Williams 1986) (see below).

In contrast to nitrate and ammonium, the advective flows affected dissolved phosphate distributions only very little, concentration in the deeper sediment layers were low and did not show any clear pattern. This may have been causes by iron oxides which strongly adsorb dissolved phosphate and remove it from sediment pore waters (Callender 1982; Griffioen 1994; Krom 1981; Slomp et al. 1996; Van Raaphorst & Kloosterhuis 1994). The relatively high concentrations of iron oxides in our sediment acted as an effective trap for the dissolved phosphate produced by the microbial remineralization. This was most obvious after the addition of organic matter. Assuming Redfield stoichiometry of N:P = 16:1 (Redfield 1934) the average increase of dissolved inorganic nitrogen by approximately 500 µM after POC addition could have caused an increase in phosphate by roughly 30 µM, however, concentrations in the porewater did not change significantly.

To trace the pathways of the missing phosphate, we determined the adsorbed phosphorus in rinsed sediment samples taken before and after the organic matter addition by acid persulfate oxidation (Grasshoff et al. 1983). We found an increase of the phosphorus concentration by ca. 12 µmol cm^{-3} (7.55 ± 2.10 µmol cm^{-3} (n = 3) versus 19.51 ± 10.10 µmol cm^{-3} (n = 3)) which indicates that the phosphate released through the organic matter degradation was partly adsorbed to iron oxides covering the sand grains.

At the end of experiment 3, increased phosphate concentrations were found at the bottom of the sediment core. The addition of organic matter may have caused the build up of sulfides in these layers which reacted with the iron oxides thereby reducing the available adsorption sites (Kostka &Luther 1994, 1995). Likewise, the higher phosphate concentrations in the surface layer may have been caused by the trapping of particulate organic matter in this zone (compare Huettel et al. 1996b) and subsequent development of anoxic microzones. This hypothesis is

strengthened by the increased ammonium concentrations at the upstream edge of the mound we observed in the first run of experiment 2 despite strong percolation of this zone.

The effect of advective pore water flows on dissolved silicate could be seen in experiment 3, where the silicate isolines showed a distribution pattern similar to that found for nitrate. Highest silicate concentrations in the water intrusion zones near the surface, indicated that the enhanced microbial activity in this zone induced increased silicate dissolution. Degradation of protective surface coatings may have enhanced the dissolution of biogenic opal (McManus et al. 1995). The increase of silicate concentrations after organic matter addition emphasises this role of microbial activity for the release of silicate to the pore water. Particle trapping as discussed above for the phosphate dynamics likely also contributed to the high silicate concentrations in the surface layer (Schink 1975).

Fluxes

The isoline diagrams of the dissolved components, especially those of ammonium and Fe^{2+}, proposed that advection enhanced the flux of solutes from the sediment to the water column. The reddish surface precipitates observed in all our experiments were obvious indicators that dissolved metal species reached the sediment surface. Their orange-red color was typical for relatively fast forming ferrihydrites (Schwertmann & Fitzpatrick 1992), poorly crystalline Fe(III) minerals. Analyses of the flume water then revealed that iron and manganese can actually be released from sandy sediment when advective pore water flows create anoxic channels through the oxidized surface layer.

The establishment of mounds on the flat sediment surface caused a reversal of the fluxes of nutrients and metals (Table 3). While the smooth sediment was a sink for metals and nutrients (possibly due to adsorption processes (Van Raaphorst & Kloosterhuis 1994; Van Raaphorst & Malschaert 1996; Van Cappellen & Wang 1996)), the sediment with mounds acted as a source for theses substances. The advective release of pore water produced a steady increase of nitrate, silicate, iron and manganese in the recirculating flume water for 2 to 10 days. The seemingly contradictory decrease of ammonium in the first run of the experiment was probably caused by nitrification in the oxic flume water as suggested by the strong increase of the nitrate concentrations.

The delay between establishment of the mounds and the increase of the metal concentration in the flume water is likely due to precipitation of the reduced metal species in the oxidized surface layer of the sediment. Fully oxidized Mn oxides have a very high affinity to Mn^{2+} (Canfield et al. 1993b; Morgan and Stumm 1964) and also oxidize Fe^{2+} (Myers and Nealson 1988). Therefore Mn^{2+} and Fe^{2+} could not pass the surface layer before saturation of all adsorption sites or reduction of these oxides.

Voltammetric measurements

The microelectrode results confirmed the flux of iron from the sediment to the overlying water. Fe species were detected up to 2 mm above the sediment surface although only small quantities of dissolved Fe could get higher into the overlying water due to the fast oxidation kinetics of Fe(II) (Stumm, 1996). The formation of Fe(III) occurred rapidly as Fe^{2+} approached and escaped the sediment-water interface with consequent precipitation of the Fe(III) on the surface. The voltage scans indicated that there were two different forms of Fe(III) present with the peak potential for Fe(III) being more negative in the overlying water than in the sediments. In contrast to the sharp peaks found by (Von Gunten 1991), we observed broader peaks of Fe(III) in the ranges -0.3 to -0.5 V and -0.6 to -0.8 V. We attribute these broad peaks to a range of dissolved organic material that can stabilize the Fe(III) as a metastable species. The broad peaks of Fe(III) at -0.3 to -0.5 v are typically found only in the upper few mm of sediments. The more negative Fe(III) peaks are found in the overlying water column when Fe^{2+} becomes rapidly oxidized indicating an ageing process of the resulting Fe(III) species (Von Gunten 1991).

The electrodes recorded higher concentration of Fe near the surface compared to Exp. 4 which can be related to the extended period the core was subjected to stagnating water and very low flow velocities (1 cm s^{-1}) prior to the measurements. This period allowed the build up of higher Fe^{2+} concentrations near the surface due to the lack of advective oxygenation of the upper sediment layers. The microelectrode measurements showed significant spatial heterogeneities at the sediment-water interface and in the sediment near the red iron hydroxide spot which also may explain some of the concentration differences between the microelectrode measurements and the pore water analyses data.

A supplemental biological indication that reduced iron was released from the sediment was the growth of the iron oxidizing bacterium *Gallionella spec.* on the

sediment surface. One week into the flux experiment, we observed the formation of small fluffy spheres (Ø up to 2 mm) where the reddish precipitates had formed at the surface (Fig. 7). Microscopical inspection revealed that these spheres were composed of interwoven twisted reddish stalks which are typical for *Gallionella* (Hallbeck & Pedersen 1995; Schmidt & Overbeck 1994) The twisted stalks are organic excretions of the cells and contain ferric hydroxide (Fig. 7) (Houot & Berthelin 1992). These iron oxidizers live where ferrous iron is moving from anoxic to oxic conditions and can grow autotrophycally on CO_2 as sole carbon source via the Calvin cycle (Madigan et al. 1997). *Gallionella* is mostly found in freshwater environments but has also been reported from saline soils (Houot & Berthelin 1992).

However, all the fluxes caused by the bottom flow - surface roughness interaction were relatively small which could be expected for a sediment core composed of coarse sand. For comparison, sediment-water nutrient fluxes in sandy North Sea/Baltic coastal environments may be found in the range of 8.5 - 47.0 mmol m^{-2} d^{-1} NH_4, -16.3 - 3.5 mmol m^{-2} d^{-1} NO_2 +NO_3, 0.4 - 3.3 mmol m^{-2} d^{-1} PO_4, 6.4- 23.8 mmol m^{-2} d^{-1} Si (Gehlen et al. 1995; Hall et al. 1996; Rutgers Van Der Loeff 1980.), manganese fluxes may reach 0.4 mmol m^{-2} d^{-1} (Thamdrup et al. 1994b). To our knowledge iron effluxes from oxidized sandy sediment have not been reported so far. Diffusional flux calculations based on Fe^{2+} pore water profiles by (Thamdrup et al. 1994a) support fluxes in the order of 0.03 - 0.7 mmol m^{-2} d^{-1} for a fine grained coastal North Sea sediment, however, even a thin oxic layer may be an efficient barrier for Fe^{2+} if advective pore water upwelling or bioirrigation are absent. Based on flux data from our smooth sediment core and measured pore water solute concentrations, we can back-calculate the advective component of the fluxes we recorded after establishment of the surface topography.

From our previous experiments with inert solute tracers (Huettel et al. 1996b) we know that the volume of upwelling pore fluid released at a small mound comparable to those we build on the flume core amounts to ca. 25 cm^3 h^{-1} if the sediment consists of clean sand ($k = 2.9\ 10^{-11}$ m^2). The permeability of our natural sediment, however, was reduced in the upwelling zone due to metal precipitates and bacterial growth. The concentration increases of silicate in the flume water after establishment of the mounds suggested a pore water release rate of 14 cm^3 h^{-1} per mound. Flux calculations based on this rate result in solute increases similar to those observed in the flume (Table 4) with the main difference that the rates for nitrate and ammonium are switched. This supports our assumption that ammonium released from the sediment was nitrified in the water column as discussed above. Also,

calculated fluxes of iron were much higher than those recorded in the flume, showing that Fe^{2+} was efficiently trapped at the sediment surface when contacting oxygenated flume water (chemically and biologically), the iron precipitates covering the sediment surface above the upwelling zone documented that process. In contrast to iron, the calculated manganese flux is similar to that measured in the flume. It is well known, that ferrous iron is oxidized much more rapidly than Mn^{2+} in oxygenated seawater (Stumm & Morgan 1981) explaining why manganese was not trapped at the interface to an extent as Fe^{2+} was.

Table 4. Comparison of measured and calculated fluxes (mM m^{-2} d^{-1}) across a smooth and a rough sediment surface. (For details of the calculation see text). (The sediment surface area of the flume core was 0.6 m x 0.3 m = 0.18 m^2. 10 mounds were established for the rough sediment surface. The pore water release rate per mound was calculated to be 14 cm^3 h^{-1}).

	Conc. sediment (µM)	Measured flux Smooth	Calc. flux Rough	Measured flux Rough	Diff.
Nutrients					
Nitrate	34	-0.71	-0.07	5.29	-5.36
Nitrite	2	0.00	0.04	0.02	0.02
Ammonia	348	-0.18	6.32	0.73	5.59
NO_3+NO_2+NH_4		-0.89	6.28	6.04	0.24
Phosphate	17	0.00	0.32	0.00	0.32
Silicate	76	-0.66	0.76	0.80	-0.04
Metals					
Iron	12	0.000	0.224	0.003	0.221
Manganese	2	-0.002	0.037	0.032	0.005

Impact in natural environment

The results of our flume experiments show that advective pore water flows have a distinct impact on the distribution of manganese, iron and nutrients in permeable sediments and the interfacial fluxes of these substances. This poses the questions whether these processes occur also in the natural environment and whether they are important.

The main limiting factor for advective processes is the permeability of the sediment, pore water flows are restricted to sediments with a relatively high hydraulic conductivity (Glud et al. 1996; Huettel & Gust 1992b). Such sediments mainly are found in coastal environments where flow velocities are high and surface wave orbitals reach the sea floor. Strong bottom currents prevent the deposition of fine material and cause resuspension resulting in winnowing and sorting of the bed.

Approximately 40% of the shelves are covered by permeable sands (Reineck 1967; Riedl et al. 1972; Seibold & Berger 1982) but also in the deep sea, in areas with strong bottom currents, well sorted permeable sediments may be found (Driscoll & Tucholke 1983; Heezen & Hollister 1971; Howe & Humphery 1995).

The factors which may cause advective flows in these permeable sediments are highly variable. Sediment topography usually is present but may change on a time scale ranging from a few minutes for smaller structures to months for large ripples or depressions. The velocities and directions of bottom flows may change or they may oscillate due to surface waves or tidal cycles. However, advective pore water flows immediately can transmit these changes in topography and flow to the upper sediment layers (Huettel & Gust 1992a; Ziebis et al. 1996b). The geochemical zonation within permeable beds thus may be subjected to frequent changes in space and in time. Recent in-situ investigations demonstrated these changes in natural environments.

In their recent studies of shelf sediments from the South Atlantic Bight (Jahnke et al. 1996) found patchy zones of oxic remineralization and sulfate reduction revealing that in these non-accumulating sediments diagenetic processes were highly active. Depth profiles of pore water nutrients in this area showed a large variability and indicated episodic flushing of nutrients from the upper 8 to 15 cm of the sediment column (Marinelli et al. 1997). Lohse et al. (1996) found similar anomalies in oxygen pore water profiles measured in sandy North Sea sediments which were characterized by an up to 16 mm thick upper layer of almost uniform oxygen concentration. Based on these profiles the authors calculated transport coefficients exceeding that of molecular diffusion by factor 1.5 to >100. Analogously, oxygen profiles measured in situ on the shelf of the Middle Atlantic Bight showed large temporal concentration variations at sediment depths between 1 and 3.5 cm indicating advective pore water flows (Reimers et al. 1996) Oxygen consumption rates as high as 15 mmol m^{-2} d^{-1} were calculated for these organic-poor sandy sediments, documenting again high diagenetic activity for a non-accumulating sea bed.

An extreme example for sandy shelf sediments are intertidal sand flats. In the Wadden Sea along the German North Sea coast the effects of advective flows can be seen at the sediment surface when exposed during low tide. We found large areas where reddish iron precipitates had formed on the downstream slope of sediment ripples. Sediment analyses revealed a 2-fold increase of the iron concentration in these zones relative to the upstream slope of the ripples. Likewise, we observed accumulations of benthic diatoms on the downstream side of ripples (abundance

increased 3.7-fold relative to upstream side) suggesting that these organisms aggregated where nutrients emerged the sediment. (Fig. 7).

On a larger time scale the advective pore water flows may be regarded as an efficient mixing process linking bottom water and the upper sediment layers. This enhanced vertical and horizontal exchange of matter within the sediment may enhance microbial remineralization and benthic-pelagic coupling while keeping concentrations low through advective flushing. Non-accumulating coastal sand beds thus may function as fast bioreactors where low organic carbon and nutrient concentrations reflect a high turnover rate rather than low activity. Since approximately 30% of the oceanic primary production takes place in the nutrient-rich coastal zone and 25 to 50% of this organic matter is remineralized in shelf sediments (Jørgensen 1996; Wollast 1991) these advective processes could be of general importance for the marine cycles of matter.

ACKNOWLEDGEMENTS: We like to thank S. Menger and M. Schuette for their help in processing the samples and O. Eckhoff, G. Herz, G. Kothe and V. Meyer for technical assistance during this project. This study was supported by the Max-Planck-Society.

Complex burrows of the mud shrimp *Callianassa truncata* and their geochemical impact in the sea-bed

Wiebke Ziebis, Stefan Forster, Markus Huettel, Bo Barker Jørgensen

Max-Planck-Institute for Marine Microbiology, Celsiusstr.1, D-28359 Bremen

Nature 382: 619-622, 15 August 1996

The biogeochemical processes and associated microbial communities in the sea floor are stratified (Berner 1980) and dependent on vertical transport mechanisms. The penetration of oxygen is generally only a few millimeters in coastal sediments (Revsbech et al. 1980), regulated by the dynamic balance between diffusion from the overlying water and rapid consumption within the sea bed. Macrofauna organisms living within the sea bed affect the physical structure of the sea floor, its chemical zonations and the exchange processes across the sediment-water interface (Aller 1982, Boudreau 1994). Thalassinidean mud-shrimps are often abundant in tropical and temperate coastal regions (Aller & Dodge 1974, Griffis & Suchanek 1991, Dworschak 1983) and build burrows with a species-specific architecture. The deepest reported burrows reach down to 2.5 m sediment depth (Pemberton et al. 1976). It is difficult to study the activities of these secretive animals and their effect on sediment biogeochemistry without disturbing the sediment system (Forster & Graf 1995). Here we report the use of a diver observatory within the sea bed, along with *in-situ* measurements, to assess the geochemical impact of the mud-shrimp *Callianassa truncata* Giard and Bonnier (Decapoda, Thalassinidea), a species that commonly inhabits sandy sediments in the Mediterranean sea .

An interesting underwater landscape created by the mud shrimp, *Callianassa truncata*, was found in a shallow bay off the coast of the Italian island, Giglio, in the Mediterranean Sea (Fig. 1). Conspicuous mounds and funnels covered the sea bed at an average density of 120 per m^{-2} (+/- 43, n = 240). One mound and two funnels constitute the surface structure of one burrow system, built and maintained by a single shrimp (Fig. 1).

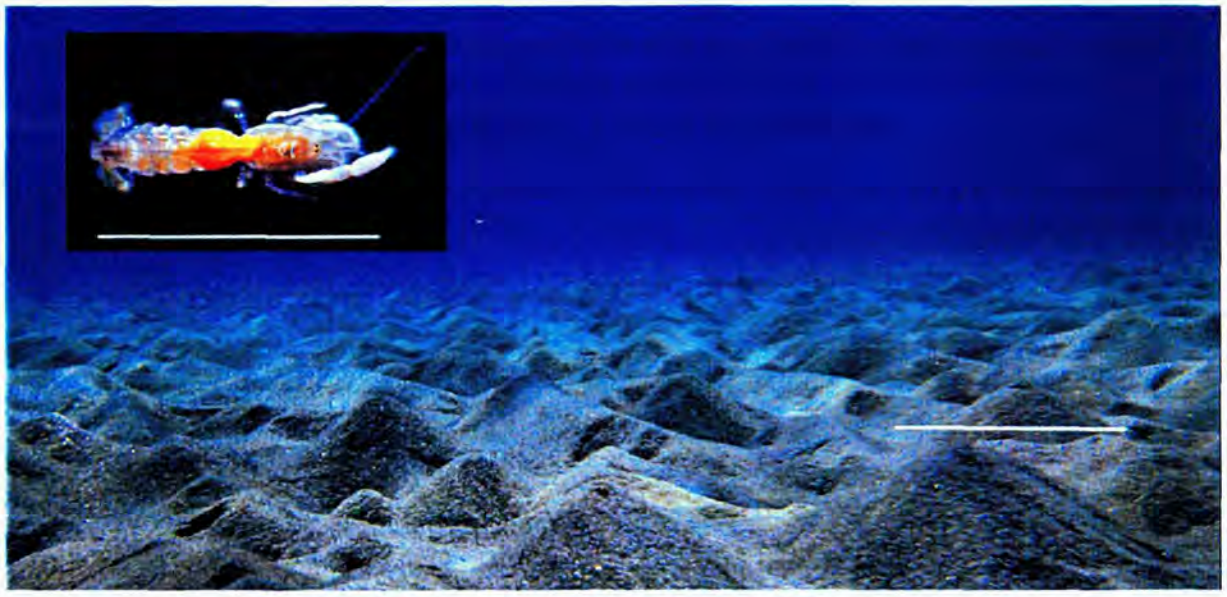

Fig.1. Sediment surface topography at 5-m water depth created by the burrowing shrimp, *Callianassa truncata* (insert), in the bay of Campese, Isola del Giglio, Italy (42° 20' N; 10° 52' E). Conical mounds with an average height of 4 cm (max. 9 cm) and funnel-shaped depressions (average depth 4 cm, max. 6 cm) cover the sea-bed between 2 and 15 m water depth in the entire bay. The upper 10 cm of bulk sediment consists of organically poor sand (0.2 % dry weight) which is well sorted with a median grain-size of 350 μm. The vulcano-shaped mounds consist of finer sand (median grain-size: 200 μm) than the ambient sediment and are created from discarded sediment which is ejected by the animals at the excurrent openings of their burrows. In average 2 - 3 kg of sand per m^2 and day were ejected up to 6 cm high into the bottom water current which ranged in velocity from 2 to 16 cm s^{-1}, as recorded 5 cm above the sea bed in the months from May to August. The scale bars are 10 cm (sediment) and 2 cm (insert). Photograph by Thomas Pillen.

Polyester resin casts revealed that the intricate burrows have a uniform architecture of horizontal galleries interconnected by vertical shafts (Fig. 2 A). The first horizontal gallery is connected to the overlying water (Ray & Aller 1985) and consists of three connected chambers aligned in roughly 10 cm sediment depth (Fig. 2 B). From two funnels, slanted inhalant shafts are leading to the first spherical chamber. The third chamber in the row is elongated and narrows into a thin exhalant tube, which bends at a right angle straight up to the sediment surface and ends at the top of a conical mound. From the central chamber the burrow continues vertically downward with 7-10 galleries, each consisting of 2-5 spherical chambers at regular depth intervals and it ends blindly in a single chamber. Chambers connected by vertical shafts re-present turning chambers where the animals change direction by doing a somersault, whereas blind-ending chambers are used for storage of trapped organic material.

At the observed abundances (120 per m^2) the extensive burrows, with a mean volume of 60 cm^3 (+/- 5 cm^3, n = 14) increase the total area of the sediment-water interface by roughly 400 %. The animals consolidate their burrows with particles cemented by mucus. In the course of burrowing, fine-grained sediment is selectively excavated and ejected to the sediment surface through the thin shaft in the mound. Before ejection, the sandgrains are gleaned for organic matter. Coarse grains, possibly too heavy to be ejected, are transported downward and are used for the construction of the chamber walls at deeper burrow levels (insert in Fig. 2 a). The selective ejection of fine grained sand into the overflowing sea water increases the bulk sediment permeability of the whole inhabited area. As the depth intervals of galleries are very regular for all burrows, the accumulation of coarse sand grains in chamber walls resulted in distinct layers of highly permeable coarse sand. Such high permeability facilitates pore water flow and is thus a crucial factor for solute exchange in sediments.

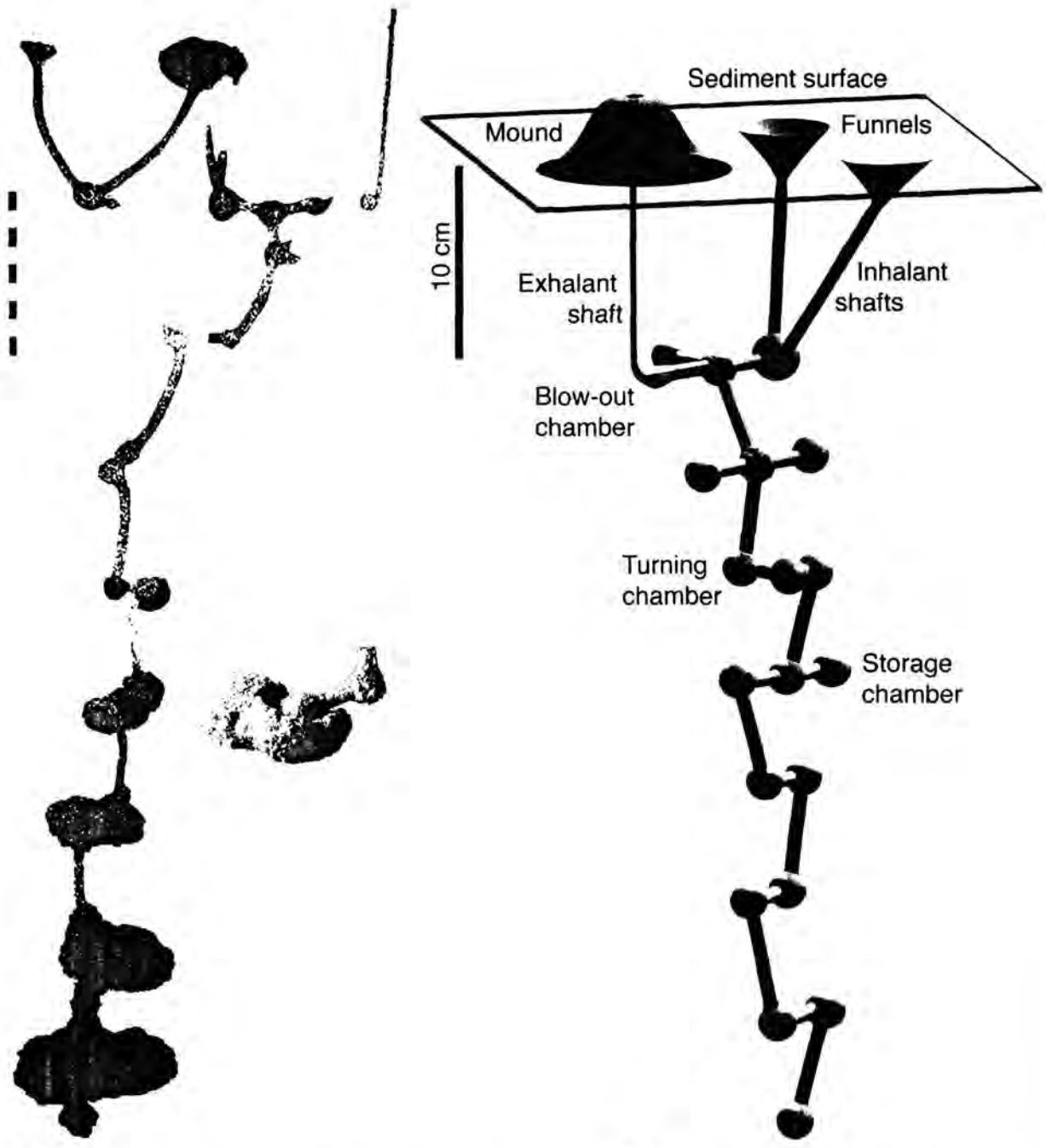

Fig. 2. The burrow system of *Callianassa truncata* in the sandy sea-bed.
A) Polyester resin casts showed the complex but uniform architecture of the burrows. B) Fourteen casts were analyzed to reconstruct the generalized 3D computer image of the burrow systems. The characteristic upper burrow compartment comprises three connected chambers with two shafts leading to the funnels and a thin tube ending in a sediment mound on the surface. The burrow continues downward with chambers at regular depth intervals. Coarse grains are used for the construction of the chamber walls at deeper burrow levels. (These chambers appear too large in the casts because resin penetrated the permeable coarse walls (insert)). The diameters of the spherical chambers (14 mm) were uniform throughout the burrow, except for the larger first chamber in the first gallery (16-17 mm) and the elongated blow-out chamber (8 mm). Shafts have a uniform diameter of 4-5 mm except for the exhalant shaft (2-3 mm). The scale bars are 10 cm.

The biogenic surface topography alters the small scale flow regime of the bottom current (Schlichting 1987). The boundary flow accelerates when passing over a mound but is retarded in the upstream and downstream regions. The resulting lateral velocity gradients cause pressure differences that drive advective pore-water flows (Huettel & Gust 1992, Yager et al. 1993, Vogel 1983). In the high-pressure areas, oxygen-rich supernatant water is forced into the permeable sediment and flows in a curved path towards the lee side of the mound where anoxic porewater emerges due to the lower pressure. Pore-water solutes, such as nutrients or metal ions are thereby released to the water column. The local advective solute transport by far exceeds the molecular diffusion across the sediment-water interface.

The flow pattern and the resulting oxygen distribution was studied around a *Callianassa* mound established in sediment cores from the natural habitat within a laboratory flow channel (Fig. 3). Oxygen was transported roughly 40 mm by the advective pore water flow, whereas oxygen penetration at a smooth surface did not exceed 4 mm. In the area of advective inflow, up- and downstream of the mound, high oxygen concentrations (> 100 µM) persisted to a sediment depth of 20 mm. The sediment volume adjacant to a mound of 1-cm height that was supplied with oxygen under a current of 10 cm s^{-1} was calculated to be 90 cm^3 and thereby increased locally 4.5-fold compared to the oxic zone underneath a flat surface.The availabilty of oxygen for aerobic degradation processes was thus enhanced in the flume sediment with 22 mounds per m^2 by a factor of 1.5. This explained a 1.7-fold increase in total oxygen uptake of this sediment measured in the water column of a gas-tight sealed flume compared to a smooth sediment in a parallel set-up. The lateral velocity gradients of the bottom water flow also caused a passive ventilation (Vogel 1983, Allanson et al. 1992) of the upper part of the burrow system. Because of the low pressure, burrow water was sucked out through the exhalant opening on top of the mound. A compensating inflow of oxygen-rich water occurred through the funnel openings. The hydrodynamically induced water flow had velocities of 0.3 - 0.4 cm s^{-1} in the inhalant shafts and about twice that in the exhalant tube. Organic material, mainly sea grass debris, was physically trapped in the funnels. Laboratory and *in-situ* experiments with stained, decaying seagrass fragments documented that the shrimps either feed directly on the organic material and the associated bacteria or store it in blind chambers of the burrow system for further microbial decomposition. This active downward transport provided a fast burial of organic material into the sea bed.

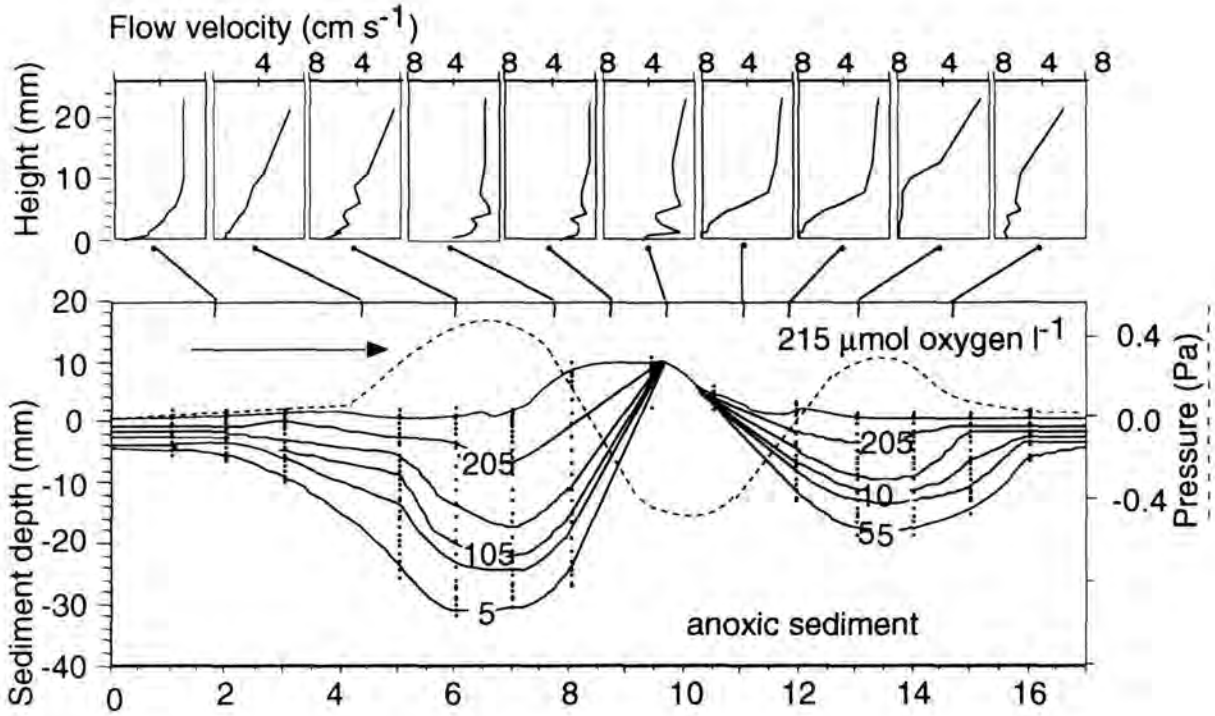

Fig. 3. Water flow and oxygen distribution around a 1-cm high *Callianassa* mound. Upper graph: flow velocity profiles; lower graph: oxygen (isopleths) and hydrodynamic pressure distribution. Measurements were performed in a laboratory flow channel (200 x 30 x 12 cm) containing a natural sediment core (60 x 30 x 20 cm; median grain size, 350 µm, permeability k (defined as a material constant related to the pore size of a sediment by the tortuosity factor (Hsü 1989))= 5.1 x 10^{-11} m^2, porosity, 0.4) inhabited by *C. truncata*. The surface of the sediment core was flush with the channel floor. Flow velocities were measured at 1 mm vertical resolution using a thermistor probe (LaBarbera & Vogel 1976). Fourteen oxygen profiles (vertical dotted lines) were recorded using Clark-type microelectrodes (Revsbech 1989) driven into the sediment at 250 µm depth increments. The isopleths connect points of equal oxygen concentration at 50 µM intervals. Fifteen pressure ports were located at the sediment-water interface and connected to a differential pressure gauge by which the pressure distribution over the mound was measured. Grey arrows indicate the flow paths of water and pore fluid. Oxygen penetrated down to 38 mm, whereas oxygen penetration did not exceed 4 mm in the area not affected by the mound.

In addition to the hydrodynamically induced flushing, the shrimps produce a water current through their burrow system by a regular beating of their pleopods. Until now it was not known how deep oxygen is transported into the burrows by this bio-irrigation and how far it penetrates into the surrounding sediment and thus affected the geochemistry. *In-situ* studies were therefore done. A hexagonal acrylic observatory, large enough to accomodate one or two SCUBA divers, was burried in the sand with its lid level with the sediment surface. Two months after deployment the surrounding sediment had been reinhabited by *C. truncata* at natural densities.

Silicone-filled holes in the acrylic walls allowed direct sampling and measurements in intact burrows. Oxygen micro-electrodes (Revsbech 1989) were inserted horizontally into the burrows and the surrounding sediment using micromanipulators. Continuous oxygen measurements at 26 cm and 48 cm sediment depth revealed that *C. truncata* maintained burrow-water oxygen concentrations at 10-40 % and 3-12 % of air saturation, respectively, at the two depths (Fig. 4 A). Horizontal oxygen micro-electrode profiles measured in steps of 250 µm perpendicular to the burrow showed at both depths that oxygen penetrated 6-7 mm through the highly permeable chamber walls into the ambient sediment, whereas oxygen penetration out from the the vertical shafts was only 3 mm at both depths(Fig. 4 B, Fig. 4 C). An oxic sediment environment of 12-25-mm diameter thus surrounds each burrow. Given the population density of 120 individuals per m^2, each 10 cm x 10 cm area of the sea bed thus contained one complex structure, some centimeters wide, of oxic sediment penetrating down at least half a meter.

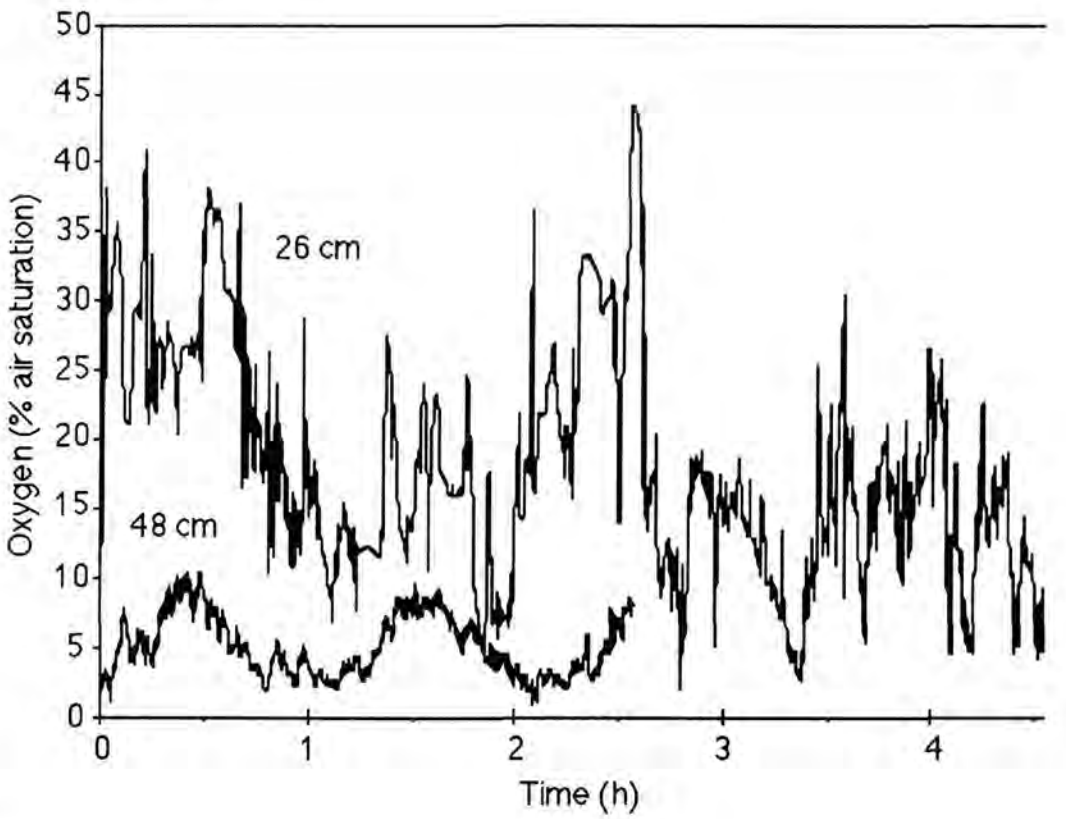

A

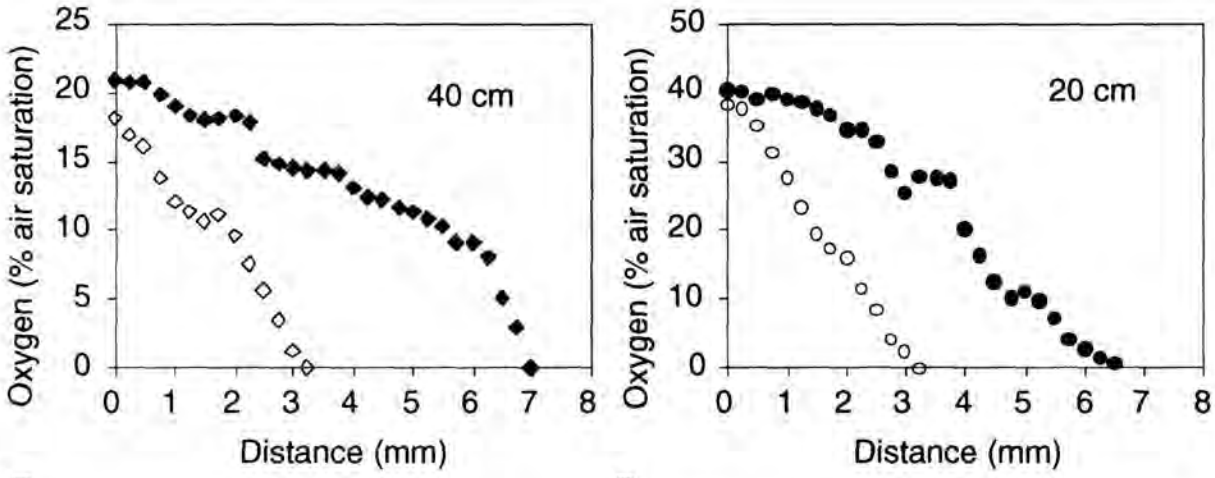

B C

Fig. 4. A) Continuous oxygen measurements within a burrow system at 26 cm and 48 cm sediment depth. B) and C) Oxygen micro-profiles measured at ca. 20 and 40 cm sediment depths from inside the burrow and out through chamber walls (●, ◆) and tube walls (o, o) into the surrounding sediment. These measurements were performed directly *in-situ* from an hexagonal observatory (1.2 m high, 2 m in diameter) deployed in the sea-bed at 5-m water depth. Six acrylic walls allowed direct observations and measurements through silicone-filled holes. Continuous oxygen data were recorded by a 12-bit data logger. The instruments were self-contained in watertight housings. One electrode was inserted into the burrow lumen and a second electrode was introduced into the ambient sediment at the same depth. This control showed that oxygen did not penetrate through the silicone ports and that measurements inside the burrows thus represented true *in-situ* concentrations.

By the active exchange of burrow water, products of organic degradation, such as ammonium, are efficiently transported into the overlying water. The flushing with oxygenated seawater also enhances the bacterial ammonium oxidation and probably other bacterial activities in the sediment (Kristensen 1985). Ammonium concentrations measured inside the burrows were thus low (2-14 µmol l^{-1}) down to a depth of 60 cm. In the pore-water of the surrounding sediment, ammonium was depleted to < 15 µmol l^{-1} at a distance of up to 3-4 cm as compared with 100 µmol l^{-1} in surrounding sediment not inhabited by *C. truncata*.. The depletion affects a sediment column of roughly 10 cm diameter around each burrow. At the observed abundance, the ammonium concentration was thus kept low in the entire sediment down to at least 50 cm depth (Fig. 5). The oxygenation of the sediment due to the bioirrigation by *C. truncata* was also apparent from the marked differences in redox potential existing between inhabited and non-inhabited sediment (Fig. 5).

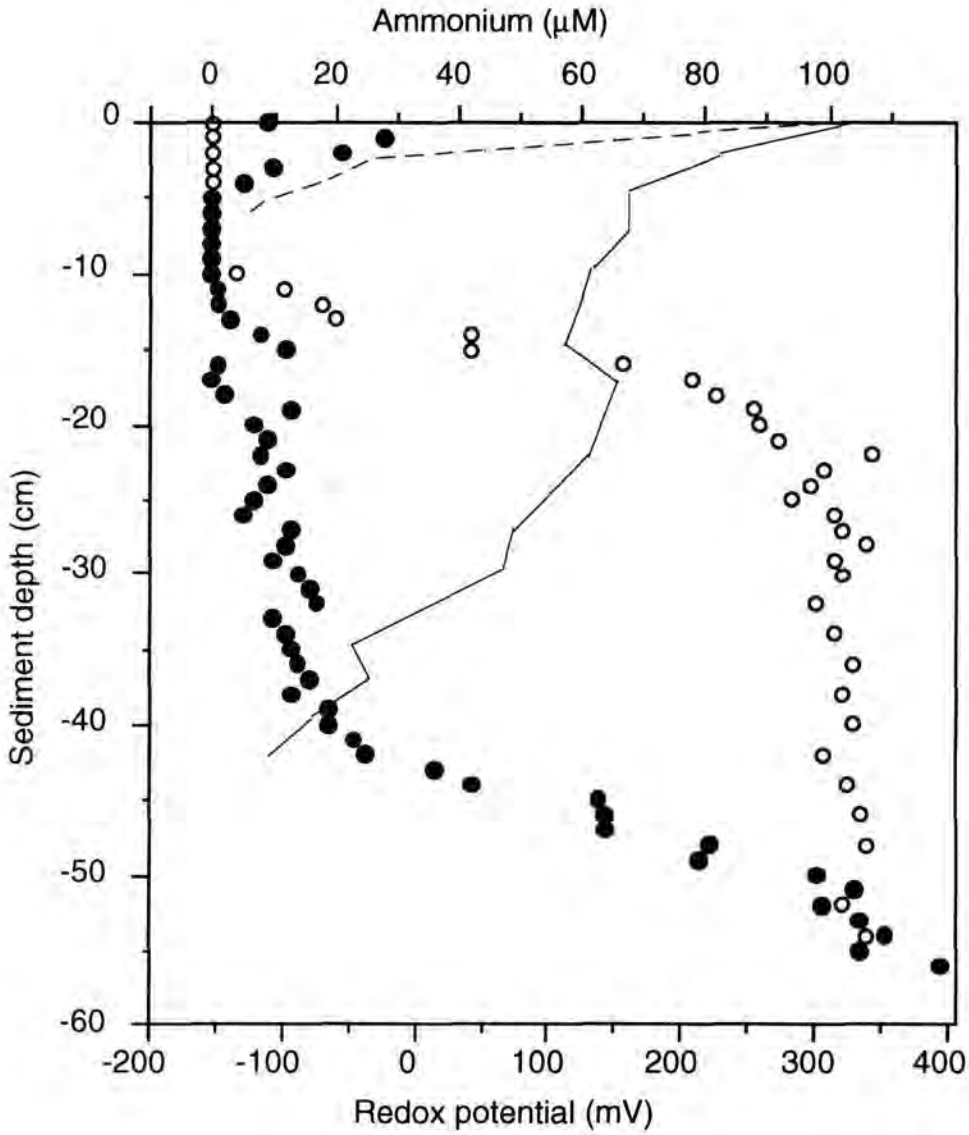

Fig. 5. Redox and ammonium profiles in sediment inhabited (— and ●) by *C. truncata* compared to profiles in a non-inhabited (---- and o) sediment. The latter was established in cages, with 1 mm mesh size to exclude the macrofauna, which were attached to the wall outside the observatory. Ammonium samples were taken with evacuated serum vials closed with silicone stoppers. By two connected syringes with a filter (pore size: 45 µm) in between, small samples (1 ml) were sucked into the vial by inserting one end into the burrow or sediment through the silicone ports in the observatory walls, while the other end penetrated through the silicone stopper into the vial. Samples were analyzed within 24 h by the flow injection method modified for small samples (Hall & Aller 1992). Redox potentials in the bulk sediment were measured using Pt-electrodes inserted through silicone stoppers in the acrylic glass walls at vertical steps of 1 cm down to 56 cm sediment depth.

The *in-situ* studies from our sediment observatory revealed that the mud-shrimp, *C. truncata*, although only 2-cm long, constructs unique burrows of extreme architectural and functional complexity that influence the whole sedimentology and geochemistry of the sea bed. The design of the upper burrow system including mounds, funnels and first gallery, induces a hydrodynamic water exchange in upper sediment layer.

The biopumping of dissolved oxygen down to 60-80 cm sediment depth and the transport of detrital particles to similar depths can strongly accelerates the degradation of organic matter in the sandy sediments.

ACKNOWLEDGEMENTS: We thank T. Pillen and B. Unger for the construction and deployment of the diver observatory and for their help during underwater field work, other members of the Giglio Diving and Research Team: D. Claus, K. Eichstaedt, J. Hass and C. Lott; and A. Eggers, G. Eickert, O. Goerg, A. Glud, G. Herz, G. Kothe and V. Meyer for technical support and the construction of microelectrodes. The study was supported by the Max-Planck-Society.

A Diver observatory for in-situ studies in sublittoral sediments

Wiebke Ziebis[1], Thomas Pillen[2], Boris Unger[2]

[1]MPI for Marine Microbiology, Celsiusstr. 1, D-28359 Bremen, Germany
[2]Institut fuer Meereswissenschaften, Localita Fetovaia 72, I-57034 Marina di Campo/Elba, Italy

Proceedings of The Fourth Underwater Science Symposium, November 1997

ABSTRACT: In marine sediments macrofauna organisms often produce deep reaching tubes or burrows that greatly influence the biogeochemistry of the inhabited sediment (Hylleberg & Henriksen 1980, Aller 1982, Huettel 1990). Among the burrowing organisms thalassinidean shrimps are a group of decapod crustaceans that are often abundant in coastal sediments (Suchanek 1985, Griffis & Suchanek 1992) and build complex burrow systems reaching up to 2.5 m into the sediment (Pemberton 1976). Recent studies focused on the species *Callianassa truncata* that occurs at high densities (120 ind. m^{-1}) in shallow-water sediments off the coast of the Italian island Giglio in the Mediterranean Sea and constructs elaborate burrows to a sediment depth of 80-100 cm (Ziebis et al. 1996a). Like many burrowing organisms it produces a ventilation current through its burrow system. Many attempts to study this ventilation in laboratory systems were difficult due to the constraints of aquariums and the difficulty of measuring inside burrows without destroying the sediment structure (Witbaard & Duineveld 1989, Forster & Graf 1992, 1995). Our interest was to gain information on the in-situ burrowing behaviour and to find out how deep oxygen-rich water is actually pumped into the sediment by bio-irrigation and how this is affecting the sediment chemistry.

We report here the construction of a diver observatory and its deployment in the field for in-situ investigations of deep-burrowing organisms and their effects on the sedimentary environment. The large, hexagonal container (1.2 m high, 2 m in diameter) was built of 6 acrylic glass walls that were held by a stainless steel frame and was covered by a lid made of PVC to avoid light penetration. It was buried in the sediment so that the lid was level with the sediment surface. The sediment from inside was removed to allow divers to enter through a door in the lid in order to perform observations and measurements from inside the observatory into the surrounding sediment. We demonstrate the unique possibilities of observing the

behaviour of burrowing animals in their natural habitat down to a sediment depth of 1 m and show the opportunities of direct sampling of pore- and burrow-water in intact systems as well as detailed in-situ measurements through silicone-filled ports in the walls of the observatory.

INTRODUCTION

It has always been an aim of benthic ecologists to perform investigations and measurements reflecting as close as possible the real conditions in the investigated environment. Therefore many studies have been carried out in aquaria, mesocosms and flow tanks (Kristensen 1985, van Duyl et al. 1992, Huettel & Gust 1992) simulating in-situ situations in order to gain information on the interaction of biological or physical factors with the geochemistry of ocean floors.

In interdisciplinary projects, where parallel field and laboratory studies have been carried out to gain information on a defined marine system, it was realised that there often exists a gap between laboratory and in-situ measurements (Rumohr et al.1987). It was difficult to relate laboratory findings to the environment and a problem to measure directly in the sediment without disturbing the structure. With the introduction of microsensors to the field of marine benthic ecology (Revsbech et al. 1980, Revsbech & Jørgensen 1986, Revsbech 1989) it was possible to gain detailed in-situ information of the geochemistry in the upper layer of the sea-floor by causing negligible disturbance of the sediment (Gundersen & Jørgensen 1990). The development of self-contained lander systems equipped with electrodes to measure profiles at the sediment surface made it possible to perform in-situ measurements even at deep ocean floors (Glud et al.1994, Reimers 1996). The profiles measured from above were usually restricted to the upper 10 cm of the sediment. Although shallow water environments are easily accessible by SCUBA diving it was so far hardly possible to carry out in-situ measurements below the depth of electrode penetration. For the investigation of deeper sediment layers cores were extracted and analysed in the laboratory. Although this is acceptable for many applications there often remains some uncertainty about the results because of the knowledge that the sampling procedure, the transport and the processing of the samples can create artefacts. Also the analysis of an extracted sediment core reflects a stationary condition, although coastal sediments are dynamic systems. Especially when macrofauna organisms mediate the sediment structure by constructing tubes and burrows, the sediment reworking and ventilation of their burrows greatly affects the geochemical processes within the sea bed (Aller 1984).

Mud shrimps of the group thalassinidea are wide spread in coastal environments and are known to often build deep reaching burrows (Griffis & Suchanek 1992). The species *Callianassa truncata* has occurs in high abundances (120 m^{-2}) in shallow water in the Mediterranean Sea and constructs elaborate burrow systems reaching down to at least 80 cm sediment depth. Transport processes at the sediment surface mediated by this species has been studied in laboratory flow channels (Forster et al. 1996, Ziebis et al. 1996, Huettel et al. 1997). Attempts to investigate geochemical processes influenced by mud shrimps also in deeper sediment layers in laboratory system revealed complex interactions (Forster & Graf 1992, 1995) but were fastidious to perform and interpret because of the difficulty to measure with electrodes in deeper sediment layers and the constraints for burrowing organisms in aquaria. The construction of a diver obser-vatory to be buried in the sediment meant to fulfil the long thought idea to be able to enter into the sediment in order to perform in-situ investigations and measurements in a natural habitat, inhabited by a deep burrowing macrofauna organism, without disturbing the sediment layering. The inverse aquarium allowed divers to perform in-situ sampling and to apply microelectrodes several dm below the sediment surface.

MATERIAL AND METHODS

Construction of the observatory

The hexagonal observatory (Fig. 1) consisted of a stainless steel frame holding acrylic glass windows. The windows were 1 m high and 1 m wide. The distance between opposite sides was 1.777 m and the longest inner diameter was 2.05 m. The bottom was open, while the top was closed with a lid made of grey, opaque PVC to prevent light penetration. A metal frame supported the lid placed on the upper rim of the hexagon. A double door in the centre of the lid (each door: 100 cm x 45 cm) allowed access into the observatory from above. When closed the doors were locked with wing nuts. One of the doors was equipped with a removable plate (30 x 30 cm) for the installation of for example a flow-sensor for the recording of bottom water flow velocities, while the meter and data logger in water-tight housings can be safely deployed in the interior of the observatory. Each of the six walls consisted of 3 separate acrylic windows of equal size held in the metal frame between two flat bars (3 mm thick, 50 mm wide). One of the two bars was connected to the frame, the counterpart was then screwed to it. Thus the windows could easily be exchanged in case of damage or to prepare them for different applications. These subdivisions of the walls also provided extra stabilisation of the frame. Each of the walls was constructed as one unit to facilitate the transport. The units were constructed as rectangulars of stainless-steel flat bars (3 mm thick, 40 or 50 mm wide) welded

together, with two flat bars subdividing the wall to hold the acrylic glass plates. At the sides flat bars were welded to each unit at an angle of 60° so that the six parts could be screwed together to built a hexagon. An angle iron (40 x 40 x 4 mm) was welded to the top of the walls pointing to the inside to provide the upper rim. At the bottom an angle iron (20 x 20 x 3 mm) was connected the same way, to hold the acrylic windows. At this lower edge, flat bars (50 x 3 mm) were connected additionally to the outside of the walls at a right angle to provide an anchor of the structure to stabilise it in the sediment.

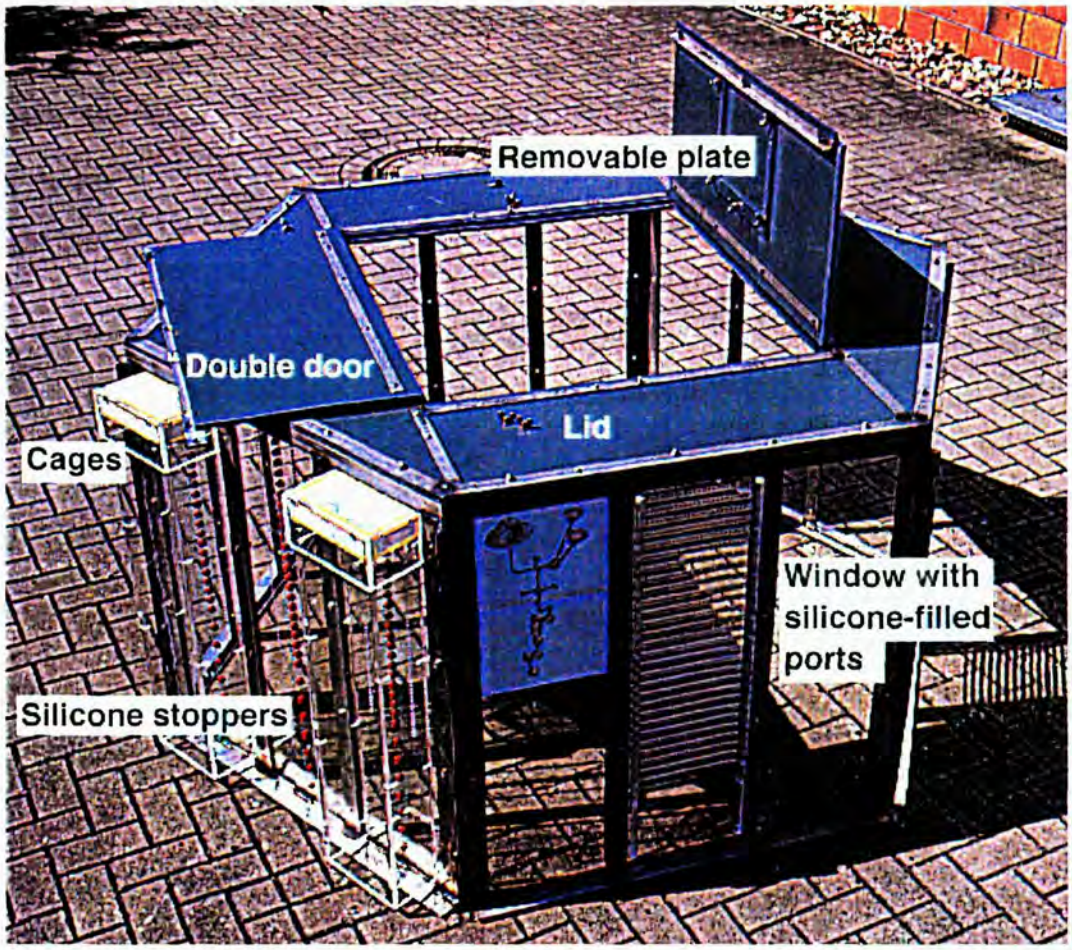

Fig. 1. Hexagonal diver observatory built with a stain-less steel frame holding acrylic glass windows. The lid made of PVC was constructed with a double door to provide an entrance into the observatory from above. A sketch of a burrow system of *C. truncata* is placed in one front window.

Preparation of the acrylic windows

The acrylic glass walls were not only ideal for in-situ observations but could also be easily prepared according to different scopes and interests of research. For our interests, two sub-units of two different walls were especially prepared to provide ports for inserting microelectrodes or syringes. At one side of the 1-cm thick acrylic plates grooves were mill-cut 5-mm deep at vertical distances of 2 cm. From the

other side holes (4 mm diameter) were drilled along these grooves at horizontal distances of 1 cm and also 5 mm deep (Fig. 4). The perforations were filled with sea-water proof silicone and provided a dense grid of ports for in-situ measurements. The special design of the ports was intended to prevent a dislocation of the silicone when inserting electrodes or syringes.

One wall held three acrylic plates that were identically prepared with three rows of horizontally aligned holes to allow measurement of vertical profiles. Two rows consisted of small silicone filled ports (4 mm diameter) in vertical distances of 1 cm. The third and central row consisted of larger holes (12,5 mm diameter) in vertical distances of 2.5 cm that were closed with red silicone rubber stoppers. Later two-way stop-cocks were inserted into the rubber stoppers to allow a penetration also for larger electrodes (Platinum redox electrodes with a diameter of 3 mm) or sampling devices. To the outside of the left and right sub-unit, cages with 1-mm mesh size were attached, that were filled with sieved sediment to exclude macrofauna organisms in order to carry out comparative measurements in inhabited and non-inhabited sediment.

Fig. 2. Acrylic glass window prepared with grooves and holes to provide a dense grid of ports for in-situ measurements and sampling. In the background a glass wall with vertical rows of holes with silicone stoppers and small silicone-filled holes is seen.

Transport and deployment

The study site for the deployment of the observatory was the Bay of Campese at the west coast of the Italian island Giglio in the Mediterranean Sea. Previous investigations showed that in this area the species *Callinassa truncata* (Decapoda, Thalassinidea) is the dominant macrofauna organism occurring in an average density of 120 individuals per m^2 in the sandy sediment of the shallow bay (2-15 m water depth).

The six wall units of the observatory, 18 acrylic glass windows and the lid were transported to the island in a station wagon. Altogether it were approximately 13.5 dm^3 stainless steel, 54 dm^3 acrylic glass and 27 dm^3 PVC with a total weight of roughly 300 kg to be transported. Upon arrival at the study site, the windows were installed and the six units were screwed together using stainless steel screws and the transitions and gaps were sealed with silicone.

After this final construction had been completed the observatory was transported to the shore line with the help of many volunteers. In shallow water it was flooded carefully securing it with ropes to boats and using stabilising it with lifting bags. It was transported slowly, held by two ropes, between two parallel moving boats to the selected position in the bay at ca.4 m water depth. As the specific weight is much less under water, the final positioning could be achieved by two divers. In order to bury the observatory into the sediment, additional weight of roughly 200 kg was put on top, using lead weights. The sediment was continuously excavated from the inside by using a suction sampler that consisted of a 1.50 m long tube with an air hose at the lower end connected to the valve of a 10-litre SCUBA cylinder. To support the burying process, divers were removing sediment from underneath the walls. Thus the hexagon was slowly sinking into the sea-floor. The excavated sediment was brought to distant areas by using buckets. The observatory was buried into the sediment, until the lid was level with the sediment surface (Fig. 3). This was controlled by measuring the water depth at the upper edge of the struc-ture. After successful deployment the site was marked with a buoy. The deployment required approximately 15 h of dive time by three well trained divers and 50 x 10-litre cylinders of compressed air at 200 bar or respectively 100 m^3 air. The sediment surface surrounding the observatory was smoothed. Because the sediment was disturbed, a number of mud shrimps were collected in the bay during the following days and set free close to the walls of the observatory. Prior to first investigations the observatory stayed for 2 months in the sediment. After this time the surrounding area was repopulated to a natural density by *Callianassa truncata*.

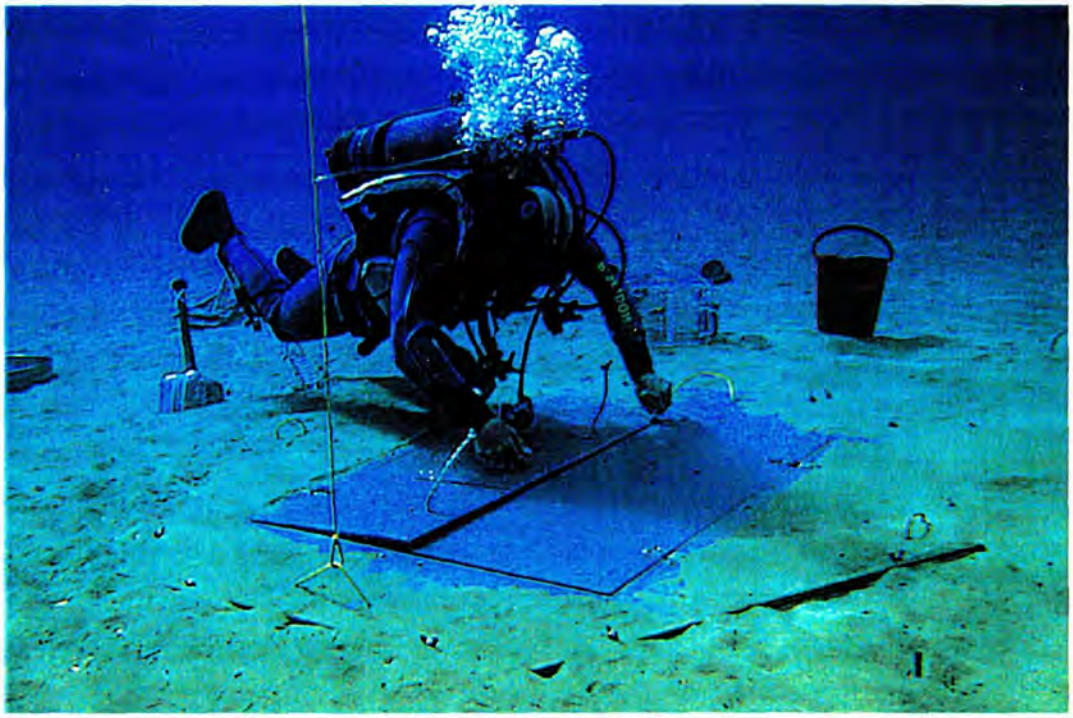

Fig. 3. The diver observatory was buried in the sandy sediment with its lid level with the sediment surface. Divers could enter through the double door to perform measurements and sampling below the sediment surface.

Sampling of pore-water

For the extraction of small volume pore-water and burrow water we used double-sided syringes with a filter (45 μm pore size) in between (Fig. 4.). The sampling system was well known for other application and originally used for taking blood samples. As one end was inserted through the silicone filled port into the sediment or burrow, the other end was still closed by a rubber membrane. The evacuated serum vial was inserted into the syringe holder, with the rubber stopper onto the other end of the injection needle. The protective membrane was pushed back while the needle perforated the rubber stopper. The sample was sucked by the vacuum through the filter into the vial. The filter also produced that the sample was tickling very slowly into the tube thus not disturbing the sediment layering. The sampling could easily be stopped by withdrawing the vial. The perforated walls allowed sampling in vertical profiles but also along horizontal transects starting in a burrow lumen and continuing radial in 1 cm or 2 cm intervals. This sampling method could be used for geochemical analyses of relevant pore-water constituents. The filtered samples were stored safely in the gas-tight vials, which were subsequently collected in bags or racks that were weighted to prevent uplift. We concentrated on pore water and burrow water collection for ammonium and nitrate determination. If not analysed right away the samples were frozen for later analyses. One possibility

is also the addition of chemical preservatives to the vials prior to sampling for special applications or in order to fix the samples immediately. For anaerobic sampling we rinsed the vials with nitrogen and closed them with the stoppers. We evacuated the vials again by inserting an injection needle through the stopper that was connected to a gas-tight tube and applying a vacuum pump. The syringe-filter unit was rinsed and filled with oxygen-free, filtered sea-water prior to sampling to prevent an interference of the sample with oxygen.

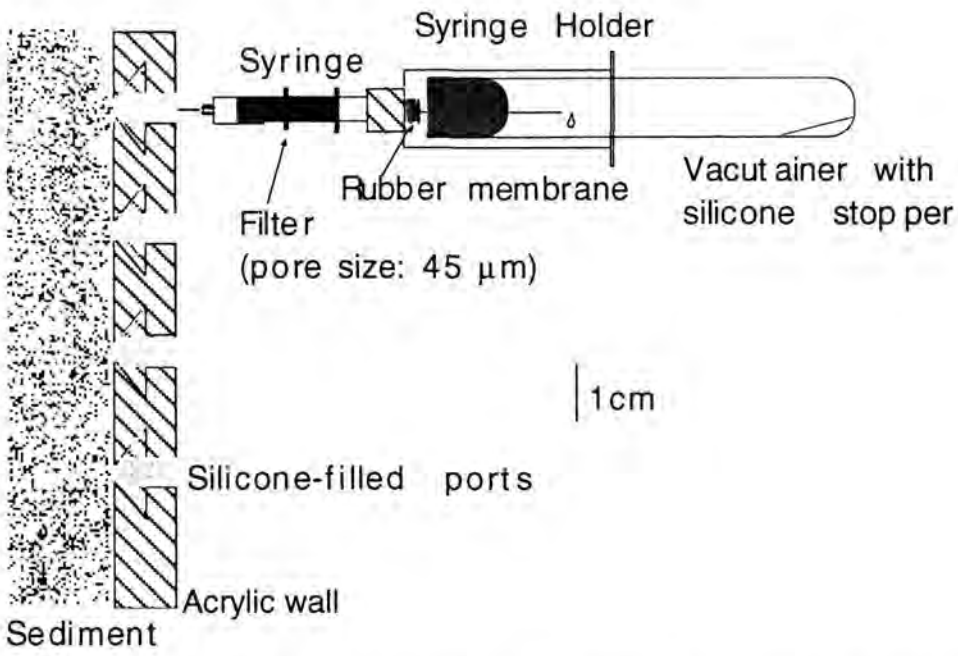

Fig. 4. In-situ sampling of pore-water or burrow water was performed through the silicone-filled holes by using double-sided syringes and evacuated serum vials.

In-situ measurement with microelectrodes

We used Clark-type oxygen microelectrodes with a built-in reference and guard cathode for the measurement of dissolved oxygen in the sediment and within burrows. The electrodes had been especially designed with a long (4 cm) tapered tip and a tip diameter of 50-60 µm. The electrodes showed no stirring effect and had a response time of < 1 s. They were calibrated in oxygen saturated and nitrogen-purged sea water. The wires of the electrode, reference and guard cathode were sealed and combined in one cable that was directly connected to a battery-supplied pico-ammeter in a water-tight acrylic glass housing. Because of the very low signal out-put (picoamps) it was not possible to use plugs to connect the cables from the electrodes to the housing, thus they had to be lead through holes in the housings lid that were then sealed with o-rings and silicone sealant. We used a two-channel instrument for parallel measurement with two electrodes. The signals were transferred to and recorded by a 12-bit data-logger in a separate housing. To avoid

condensation in the housings due to temperature differences on land and under water the housings were flushed with nitrogen before closing. Lead weights put into the housings compensated for uplift.

Commercially available micro-manipulators were attached to holders made of acrylic glass that were equipped with two suckers to attach them to the walls in the observatory. The micro-manipulators were sprayed with silicone oil to prevent corrosion. The electrodes and instruments were secured in a box to transport them to the observatory by SCUBA-diving. In the observatory the micro-manipulators were attached at the desired position by pressing the holder against the wall. By the suction effect they were held in place (Fig. 5). Before mounting the electrodes onto the manipulators we used glass pipettes to test positioning at the selected ports. It was difficult to perceive the exact distances of objects because of the different angles of refraction of water, glass and acrylic glass. The micro-manipulators allowed exact movement in y, x and z direction. After positioning had been achieved the electrode was inserted slowly along the x-axis through the silicone port into the sediment or burrow while the signal was controlled on the display of the pico-ammeter that could be seen through the acrylic glass. We used two electrodes for our measurements. One was inserted into the burrow at a certain sediment depth while the control electrode was inserted at the same depth into the sediment to monitor whether oxygen is penetrating through the silicone stopper from the inside of the observatory and thus influencing the measurement. Long-term measurements of oxygen concentrations at different depths and burrow compartments were performed. Also horizontal profiles in steps of typically 250 µm were measured from the inside of the burrow into the surrounding sediment.

Although some of the walls were densely perforated in advance with holes, the burrowing shrimp would preferably burrow nicely along the wall of the observatory where no ports were present. To solve this problem we drilled holes into the acrylic windows at the sites of interest using a gimlet. The holes were immediately and very quickly sealed with silicone brought under water in a syringe. This procedure did not disturb the burrows or sediment structure because of the advantage that the same hydrostatic pressure existed inside and outside of the observatory. This was very convenient compared to laboratory experiments with aquaria. The only problem was that the shrimp would be alarmed by the noise or vibration of the drilling and upon notice they would immediately close the burrow at the site of the invasion by digging sand into the burrow and thus abandon this part of the system.

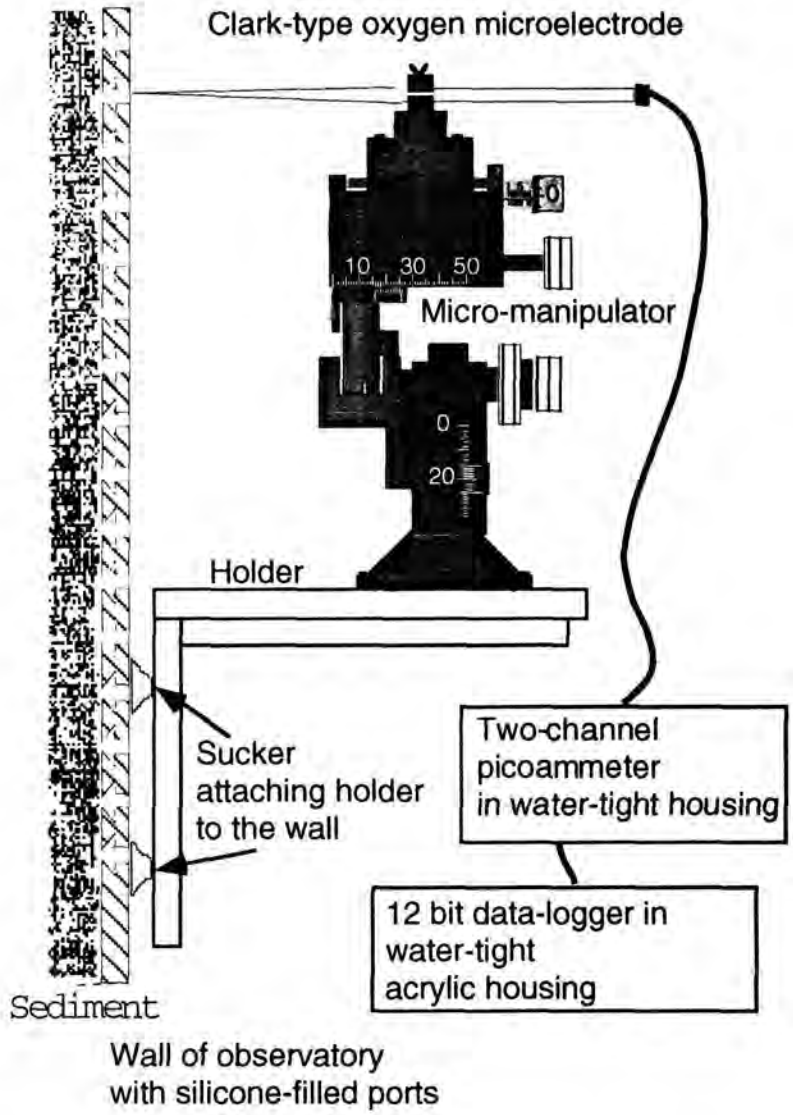

Fig. 5. In-situ measurements of dissolved oxygen in intact burrow systems or undisturbed sediment was carried out using Clark-type microelectrodes mounted on a micro-manipulator attached to a holder that was positioned at the wall and attached by two suckers. The signals were amplified by a self-contained pico-ammeter and recorded by a 12-bit datalogger both held in water-tight acrylic glass housings.

RESULTS AND DISCUSSION

The diver observatory

The design of the observatory proved to be favourable. The hexagon had compared to a cube the advantage of a large volume with a relatively small surface area and provided six walls for investigations and measurements. Taken apart it was still transportable in a conventional car. The construction of six wall units and a lid to be put together at the study site made it possible that it could be still transported in a

normal car. At the same time it was large enough to accomodate two divers with equipment along with sampling devices or instruments. The size allowed also a safe deployment, although the help of many volunteers was needed to transport it to the shore line and two boats with qualified boat handlers were required for the transport to the final position. The presence of a diving base and a compressor was essential for the filling of the large number of cylinders with compressed air to excavate the large volume of sediment by using a suction sampler. The metal frame was essential for the stability. In fact we had built a prototype, a hexagon of the same size, entirely made of acrylic glass that had been destroyed after short time by strong waves during a storm.

It is important that the observatory is buried with its lid level with the sediment surface, otherwise horizontal bottom currents will be deflected by the protruding object and induce advective pore-water flows affecting transport of solutes across the sediment-water interface (Huettel 1992, Ziebis 1996b). Even if it is buried completely, the solid walls of the observatory hinder pore water flows in contrast to the permeable sediment . This can induce an intrusion of water into deeper sediment layers directly at the walls and thus can influence the geochemical conditions. Consequently it is very important to plan the deployment and in-situ investigation for a time period of predominantly calm weather. We conducted our measurements during summer, when bottom current velocities of 3-12 cm s^{-1} were recorded in this area. We were concentrating for our investigation on deeper sediment layers and presumed that the effect of down-welling water at the walls is of minor importance as long as there are no stronger currents. One disadvantage is that these shallow water environments are exposed to strong bottom currents when storms occur. The waves forming by strong winds reach the sea-floor and resuspend the upper layer of the sediment. In this extreme case the observatory in the permeable sediment is an obstacle where these forces can attack. The sand at the walls is eroded until the structure is removed from the sediment. Then it is either damaged by the water forces, broken apart and distributed in the bay (our experience with the first observatory) or it is transported as almost intact structure to the shore line (this happened with the second observatory).

Diving

As the observatory was buried only 200 m away from the shore line, it could be reached by the divers swimming there. When heavy equipment had to be carried, walking without fins over the sea-floor was more convenient. The advantage of a shallow water site is its accessibility and the long time that scientists can stay at

these depths to perform investigations while diving on compressed air. Because the time limit of non-decompression is hardly reached at a depth below 5 m, the risk of diving was fairly low. Although the ambient water temperature in summer was more than 20°C, it was necessary to wear dry suits because of the loss of body heat during long dive times of more than 2 hours.

Sampling procedure

The established technique of using double-sided syringes in combination with vacutainers proved to be an excellent tool for in-situ sampling in an submerged environment. The direct sampling of pore water into the evacuated vials had the advantage of no interference with ambient sea-water. The advantage of directly filtering the sample had also the positive effect that the water was extracted slowly, not disturbing the sediment stucture. Because of the uplift of the vials it is important to have a weighted rack where the tubes can be secured in the order the samples were taken. This reduces also the number of items that have to be handled by the diver. Additionally it is imperative to label the tubes, especially when measuring profiles. Samples for ammonium and nitrate analyses were taken and exhibited distinct differences between inhabited and no-inhabited sediment, as well as inside of the burrows and the surrounding sediment. One disadvantage of this sampling procedure is that the needles and the filters can be blocked by transported particles. It is wise to always bring a set of spare syringes and vacutainers and we recommend that the gauge of the used needles is smaller than the median grain size of the sediment. The vials can be used for different applications and allow an-aerobic and sterile sampling.

In-situ measurements with microelectrodes

The application of oxygen microelectrodes for measurements deep below the sediment surface was done for the first time and was successful. None of the fragile glass electrodes were broken during measurements. The insertion of the only 50-µm wide tip through the 1 cm thick silicone-filled port was surprisingly not a problem. It was convenient that the signal could be monitored at the display of the pico-ammeter during measurements. As the electrode was inserted through the silicone stopper the value decreased from ambient sea-water concentration to zero, when entering an irrigated burrow it increased according to the present concentration. Time series measurements of up to 4 hours were carried out in different burrow compartments at different depths, that were recorded by the data-logger. They revealed an active transport of oxygen down to sediment depths of al-

most 50 cm. The control electrode that was inserted through a port at the same depth into the sediment showed that oxygen is not penetrating through the silicone during this time, thus the measurements represented true in-situ measurements of oxygen transported into the burrows by the activity of the thalassinidean shrimps. A clear indication that an electrode was still working was the immediate increase of the signal when it was withdrawn from the sediment into the ambient sea-water. The direct measurement of oxygen concentrations inside intact burrows gave new and important information on the impact of macrofauna organisms on oxygen supply to deeper sediment layers.

The diver observatory deployed in a shallow-water environment, that was heavily bioturbated by a thalassinidean, shrimp offered the possibility for sub-surface in-situ sampling and direct measurements. The successful application of advanced analytical methods, as well as the use of micro-electrodes gave important and new insight into the interaction of macrofauna activity and biogeochemical processes. These first investigations gave ideas for continuing projects. Further detailed investigations of pore water concentration and geochemical processes can contribute to the understanding of element cycling in a coastal, bioturbated environment. Other interesting studies would be the investigation of the distribution and abundances of interstitial meiofauna in relation to the physical and chemical conditions, as well as the determination of bacteria associated with the deep reaching burrow systems.

ACKNOWLEDGEMENTS: We greatly acknowledge the enthousiastic assistance of the members of the Giglio Diving and Research Team and of many volunteers in transporting and deploying the observatory as well as in under water field work. We are thankful to Gaby Eickert and Anni Glud of the microsensor group at the MPI for the construction of electrodes and Olaf Eckhoff, Gerd Kothe, Volker Meyer and Georg Herz for technical support. We thank Stefan Forster, Markus Huettel and B.B. Jørgensen for critical and constructive supervision of the project. This work was supported by the Max-Planck-Society.

Aspects of the biology and ecology of *Callianassa truncata* (Decapoda, Thalassinidea) from the Mediterranean Sea

Wiebke Ziebis

Max-Planck-Institute for marine Microbiology, Celsiusstr.1, 28359 Bremen, Germany

submitted to *Marine Ecology, November 1997*

ABSTRACT: The thalassinidean shrimp *Callianassa truncata* was investigated in the bay of Campese on the Island Giglio in the Mediterranean Sea, Italy. It occurs in shallow water in sandy, well sorted sediment of a medium grain size of 350 µm. The in this area dominant macrofauna species lives in average densities of 120 ind. m^{-2}. The conspicuous biogenic structures of mounds and funnels created by the burrowing activity of the subsurface living animals characterise the sea floor in the entire area to a water depth of roughly 15 m. By the investigation of the population structure, two communities were distinguished in the month of October. Juvenile shrimp settle out of the water column in the month of June to August to a slightly deeper region. Adult individuals have an average body size of 2 cm and inhabit complex burrow system which penetrate up to 80 cm into the sediment. *In-situ* resin casts revealed the functional and consistent architecture of the burrows. The average volume of the burrow was calculated to be 60 cm^3 with a surface area of 330 cm^2, resulting in a total burrow surface of 4 m^2 under 1 m^2 of sediment surface. During the course of burrowing the animals transport sediment from deeper layers upward and ejected it at the surface. In-situ experiments showed that this sediment is of finer grainsize than the ambient sediment. Coarse sediment to heavy to be ejected is used for the construction of chamber walls in deeper sediment layers. This sediment sorting affects the structure and permeability of the inhabited sediment.

The shrimp actively irrigate their deep reaching burrows in a frequent ventilation pattern. Oxygen was recorded to penetrate at least 50 cm into the sediment, enhancing ammonium oxidation within the burrows and to a distance of 4-5 cm into the surrounding sediment. A the observed densities *Callianassa truncata* is a key species in the investigated area profoundly affecting the geochemistry of the inhabited area down to a sediment depth of 0.5 m.

INTRODUCTION

There is an increasing widespread interest in the dynamics of shallow water environments. The effects of benthic organisms on sediment characteristics has been subject of several investigations (Aller 1982, Aller & Yingst 1985). Thalassinidean shrimp, referred to as mud or ghost shrimp are among the most common burrowing organisms in eu- and sublittoral sediments of tropical, subtropical and temperate regions (Griffis & Suchanek 1991, Dworschak 1983). Because of their secretive life style and their often deep reaching burrows, they have often been overlooked by conventional sampling methods. But their dominant role in the structuring of sediments is becoming increasingly well known. The species-specific morphology of their burrows ranges from simple vertical tubes to complex, elaborate systems (Dworschak 1983, Suchanek 1985, Griffis & Suchanek 1991, Nickell & Atkinson 1995). Their burrowing activity has been documented to have an important impact on the physical and geochemical properties of the sea bed (Aller & Dodge 1974, Ott et al. 1976, Branch & Pringle 1987, Dobbs & Guckert 1988, Forster & Graf 1995).

The species *Callianassa truncata* (Giard and Bonnier) has been seldom investigated since its description 1890 for the gulf of Naples (Moncharment 1980). Its occurence has been described also for the greek seas (Thessalou-Legakis 1986) but investigations on the biology and ecology of this species have so far not been documented.

MATERIAL AND METHODS

The study-site

The island Giglio is situated at the west coast of Italy in the Tyrrhenian Sea. It belongs to the Toskany Archipelago and is next to Elba the second largest Island covering an area of 22 km^2 with a coastline of 48 km. The investigation was carried out in the Bay of Campese at the North-West coast of the Island. The bay has a width of ca. 700 m. The inner part of the bay is very shallow stretching out to a distance of roughly 200 m. From here the water depth increases down a slope to 30 m in 300 m distance. The sea-floor consists of well -sorted quartz sand. Conspicuous biogenic structures of mounds and funnels cover the entire area to a depth of approximately 15 m.

Population density and grain size distribution

The thalassinid shrimp have an average body size of 2 cm. A characteristic morphology is the sexual dimorphism of the first pereiopod. Whereas the male carries a huge chela either at the right or left side, the chelae at the first pereiopod of the female are of equal smaller size (Fig. 1).

A **B**

Fig. 1 *Callianassa truncata* **A** Male with a large chela. **B** Female bearing eggs.

Investigations on population density and distribution and sediment grainsize composition were carried out using SCUBA. Along 4 transects perpendicular to the shore line starting at the water line to a distance of 200 m the density of mounds and burrow openings was determined by randomly throwing a frame covering an area of 1 m^2 at 10 m intervals along the transects. The frame was subdivided in 4 quadrants. 5 parallel frames at each interval were counted. Every 10-m interval a sediment core, 20 cm deep (acrylic glass tube, 7.5 cm inner diameter) was taken for subsequent grainsize analysis.

Attempts to collect the deep burrowing animals by conventional methods using box corers, line corers and suction samplers were not very efficient or meant damaging of the animals. The best method was to extract a sediment core at a mound just in the moment when sediment was ejected in a fountain-like manner. The animals expel excavated sediment through the exhalant shaft ending in the mound by producing an ejection current by vigorously beating with their pleopods. A sediment fountain observed at the sediment surface was an indication that the animal was sitting at the blow-out chamber of its burrow ca. 10 cm underneath the mound. The quickly taken sediment core, which penetrated approximately 20 cm into the sediment was transferred to a sieve of 1 mm mesh size, sieved underwater and the animals were put for transport into small glass containers. In the laboratory specimen were either preserved in ethanol or transferred to aquaria filled with sediment.

Burrow structure

Burrow morphology was determined by resin casting (Atkinson & Chapman 1984) in the field using SCUBA. Casts were made with polyester resin adding 1% by weight of a peroxide catalyst. A curing agent was not added in order to prolong the reaction time. The resin mixture was transferred to 2-l screw-cap plastic bottles. On the sea bed first little of the resin was poured carefully into a funnel-shaped opening to stabilise the surface sediment. A plastic collar was placed around the opening and the resin was added in stages until the burrow system appeared to be completely filled. After a hardening time of 48 h, the resin casts were carefully hand excavated from the sediment, washed and allowed to dry and harden in air, overnight. Morphological measurements were made using digital sliding hand callipers. Surface areas were estimated by visually dividing each cast into a series of geometric shapes. Each shape was measured and the surface area and the volume was calculated. Because the resin penetrated the coarse sediment surrounding the burrow chambers, the sand grains adhered to the cast and the burrow volume could not be estimated by the weight of the cast or displacement of water. The data of 14 complete casts were used to establish a 3D-computer model of the burrow architecture.

Particle transport

Ejected sediment was collected in-situ by the direct entrapment method (Rowden and Jones 1993). 30 plastic collection traps were placed over mounds at the sea floor and the ejected sediment was collected for a period of 2 days. The sediment samples were washed, dried (60°C for 24 h) and sieved for grainsize analysis. To investigate sediment processing by *Callianassa truncata* a cylinder (diameter 20 cm) was filled with natural sediment (35 cm deep) and overlying sea-water. Two 1-cm thick layers of fluorescent-stained sand grains (ø 250-500 µm) were inserted at 8 and 14 cm sediment depth. One shrimp was introduced to the core and immediately constructed a burrow. After 10 days a subcore of 10 cm was taken and cut in 1 cm slices. The surface of each slice was photographed under UV light with a high resolution camera. Supported by an image analysis system particles were counted, their co-ordinates were registered and the images of the different layers were joined together to a 3D image (Teucher 1992).

Fluid transport

The ventilation of a burrow was monitored by inserting a thermistor probe 1 cm deep into the 4 mm wide opening in the mound of a well established burrow in an aquarium (40 x 30 cm, 40 cm deep). The sensor was built after LaBarbera & Vogel (1987), had a tip diameter of 0.8 mm and a response time of 0.1 s. The signal was recorded by a strip chart recorder for a period of 11 hours.

Burrow water chemistry

Burrow water chemistry was investigated for dissolved oxygen and ammonium in-situ using a large diver observatory deployed in the sea-floor with its lid level with the sea floor (Ziebis et al. 1996, Ziebis et al. subm.). The hexagonal observatory consisted of 6 acrylic glass walls (1.2 m high, 1 m wide, 1 cm thick) that were held in a stainless-steel frame. Inside there was enough space for two divers with equipment. Prior to first investigations, the observatory was left for two months in the sediment until the surrounding area was repopulated at natural densities by *C. truncata*. The acrylic walls were prepared with silicone filled holes to allow direct measurements and sampling in intact burrows and the surrounding sediment. For comparative measurements in non-bioturbated sediment, two cages with 1 mm mesh size to exclude the macrofauna were attached to the outside of one wall.

Oxygen measurements were carried out using microelectrodes (Revsbech 1987) mounted on micromanipulators attached to the walls. Signals were amplified by pico-ammeters and recorded by a 12 bit data logger. The self-contained instruments were installed in water-tight housings.

Pore-water and burrow water were extracted using double-sided syringes and evacuated serum vials. One end of the syringe was inserted through the silicone -filled ports while the other perforated the silicone rubber stopper of the vial. Ammonium was analysed by the rapid small volume flow injection method described by Hall & Aller (1992).

Feeding experiments

Seagrass (*posidonia oceanica*) fragments were stained with an inert fluorescent dye for feeding experiments. The organic material was introduced into the funnels at the sea bed. After a period of 2 days the animals were collected and their gut content was analysed using an epifluorescence microscope.

RESULTS

Population density

Ovigerous females, which release planctonic larvae, occurred in April until the beginning of August. Females bearing eyed embryos were first observed in May. The settling of juveniles out of the water-column onto the sediment was observed by the large number of small mounds appearing at the sediment surface took place from June to August. The investigation of the population density was carried out in the month of October. The number of individuals per m^2 was estimated by the counted mounds per area, because investigations had shown that each individual inhabits a single burrow system with one mound and two funnels at the sediment surface. Also the ratio of counted funnels to mounds was roughly 2 ($x = 1.8$, $SD = 0.4$). Adult animals could be distinguished from juveniles by the size of the surface structures. This was also verified by samples taken randomly.The distribution pattern along the four transects was similar. One transect is illustrated in Fig. 2. The average number of individuals in the inhabited area was estimated to be 120 per m^2 (+-43, n=240). The composition of the sediment was described by the fine, medium and coarse sand fractions in the area. At the shore line to 30 m distance coarse to very coarse sand prevented C. truncata from constructing burrows. The sea-floor in the shallow bay (<10 m water depth) consisted mainly (60-80 %) of medium sand with a median grain size of 350 µm. At ca. 200 m distance the water depth increased and down this slope the fraction of the fine sand increased. We could distinguish two cohorts of *C. truncata* at this time of the year in the bay. The adult community occurred in the area characterised by medium sand, while the juveniles, only 2-4 mm in body size, preferred the deeper area of the bay with sediment of a smaller grain-size. In the beginning of the year the cohorts could no longer be differentiated, there was only one community apparent in the shallow zone of medium sand. This suggested that while the animals of the new generation are growing during the year, they move, by continuously reconstructing their burrow systems, towards the shallower part of the bay.

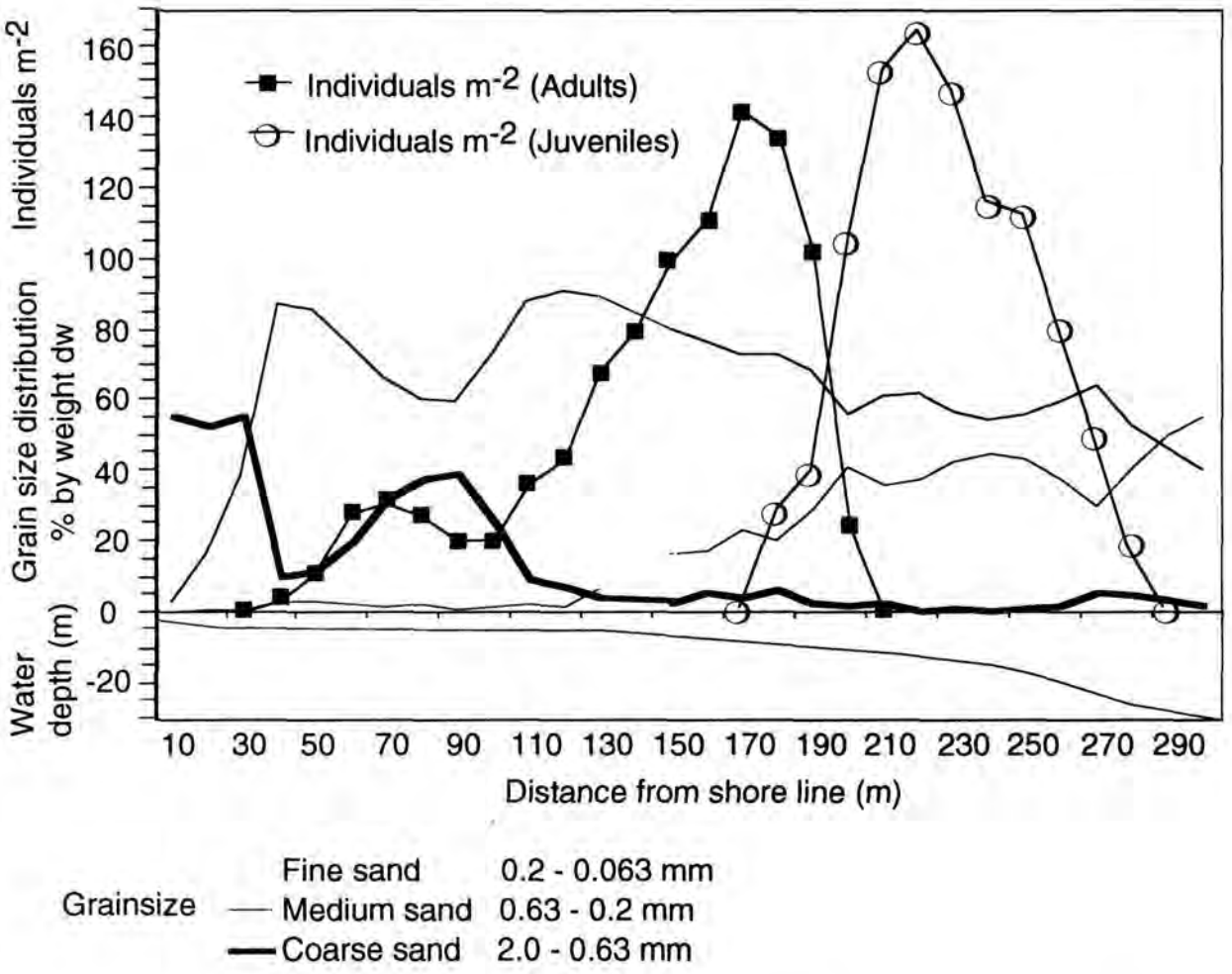

Fig. 2. Grain size distribution and population density along one transect in the bay of Campese.

Burrow structure

More than 30 casts were made that gave detailed reproductions of entire burrows and revealed the consistent and complex burrow morphology (Fig. 3 A). 14 casts of adult shrimp were analysed for surface area and volume determination and to establish a 3-D computer model (Fig. 8).

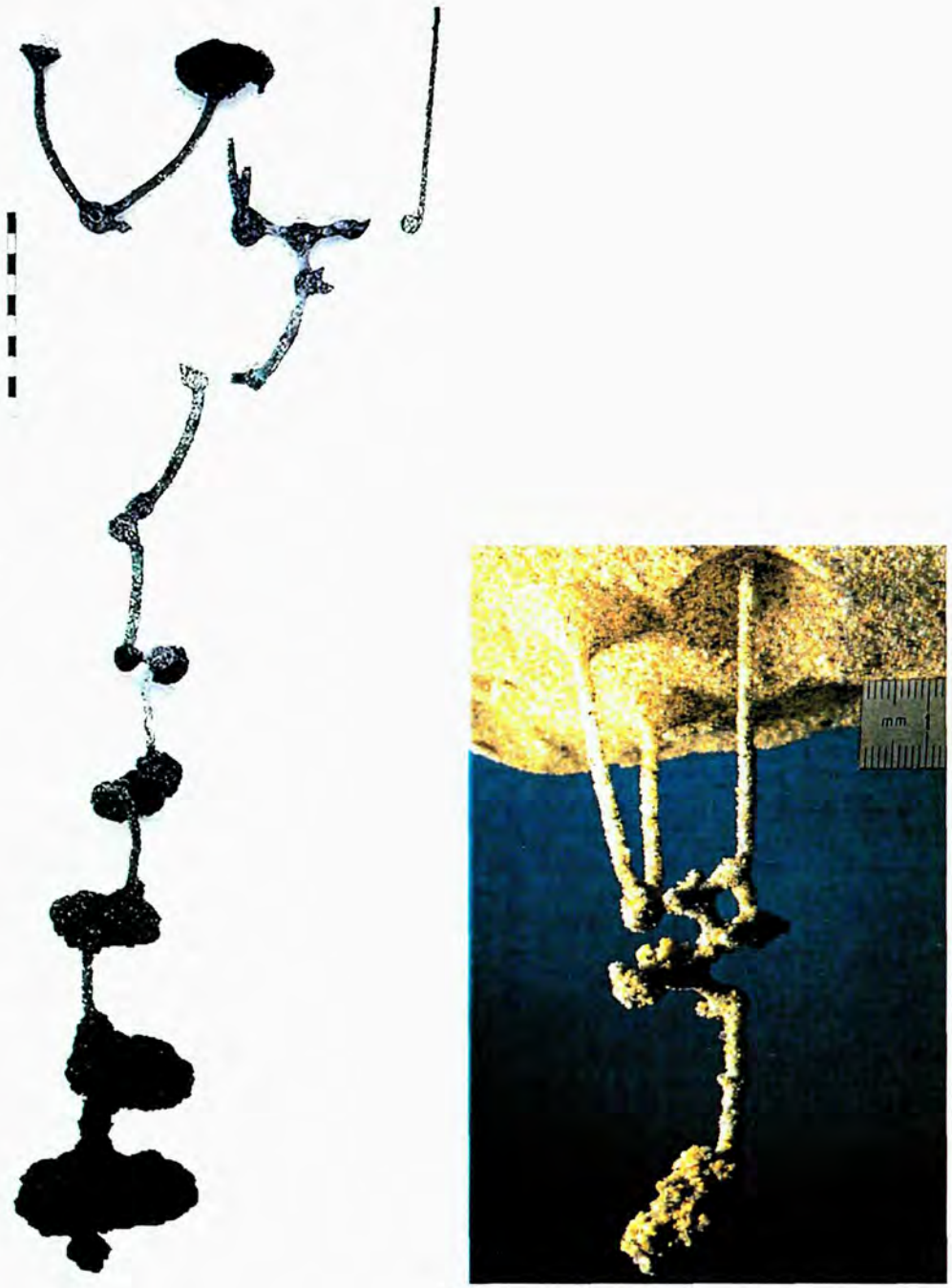

A B

Fig. 3. A Resin cast of a burrow system of *C. truncata* (adult). Scale bar 10 cm. **B** Resin cast of a burrow system of a juvenile shrimp only 4 mm in body size. Scale bar 1 cm.

At the sediment surface one mound and two opposite funnels were the characteristic features of the burrow system (Fig. 4 B). The mounds had an average height of 4 cm and can reach a maximum of 9 cm in calm weather periods. The funnels are roughly 3 cm deep with a diameter of 4-5 cm. The burrows reach down to 80 cm depth with

an average volume of 60 cm^3 with a surface area of 330 cm^2. The sediment-water interface in the inhabited area was thus increased by roughly 400 %.

The first horizontal gallery was connected to the overlying water and consists of three connected chambers aligned in roughly 10 cm sediment depth. From the two funnels, slanted inhalant shafts were leading to the first spherical chamber. The third chamber in the row was elongated and narrowed into a thin exhalant tube, which bent at a right angle straight up to the sediment surface and ended at the top of a conical mound. We called this chamber blow-out chamber (Fig. 4 A). A very similar chamber has been found in burrows of *Callianassa subterranea* (Rowden and Jones. 1995) and was called `expulsion nodule´. From here sediment was expelled to the sediment surface by a jet- stream produced by the ventilation current funnelled through the thin shaft ending in the mound. From the central chamber the burrow continued vertically downward with 7-10 galleries, each consisting of 2-5 spherical chambers at regular depth intervals and it ended blindly in a single chamber or sump. Chambers connected by vertical shafts represented turning chambers where the animals changed direction by doing a somersault, whereas blind-ending chambers were used for storage of trapped organic material. The diameters of the spherical chambers (14 mm) were uniform throughout the burrow, except for the larger first chamber in the first gallery (16-17 mm) and the elongated blow-out chamber (8 mm). Shafts had a uniform diameter of 4-5 mm except for the exhalant shaft (2-3 mm). Shafts connecting galleries have an angle of 65-80° better enabling the animals to move up- and down their burrows. The orientation changed at each level thus the whole burrow system was a straight structure. Juvenile shrimp with only 2-4 mm body size constructed burrows of the same architecture only `en miniature´ (Fig. 3 B).

While constructing and maintaining the burrows the animals constantly processed sediment. Excavated sediment was brought to the blow-out chamber and ejected. Coarse material which could not be expelled was transported to deeper burrow compartments and was used to construct chamber walls (Fig. 4 C).

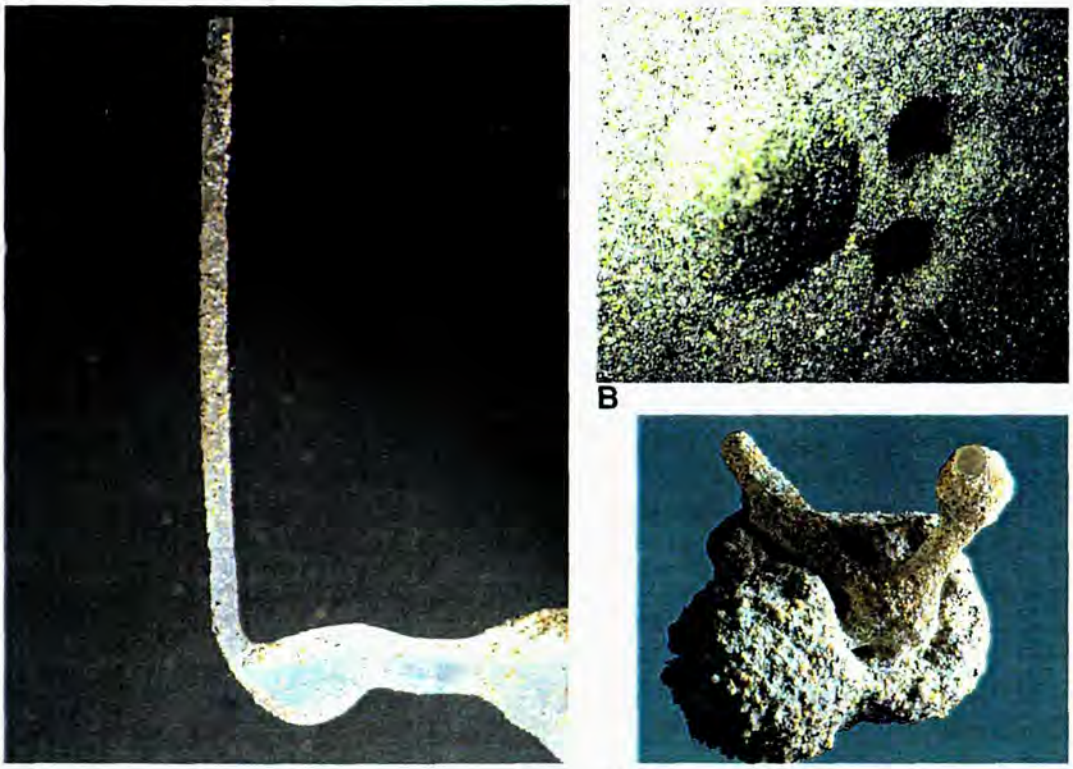

Fig 4. Characteristic burrow features. **A**) Blow-out chamber **B**) One mound and two funnels at the sediment surface **C**) Chamber with coarse chamber wall.

Particle transport

While the shrimps were constructing and maintaining their burrows they were processing large amounts of sediment. They loosened sediment in one part of the burrow, gleaned the particles for nutrition and carried packages of unwanted material upward from gallery to gallery to be ejected. Other material was mixed with mucus and used to construct walls. Coarse sand grains were used for chamber walls, while the shafts were built with finer material. Thus the three-dimensional burrow system was a semi-permanent structure slowly `migrating´ through the sediment column while the sediment is sorted and transported vertically. This could also be seen in the sediment core with layers of stained sand grains (Fig 5 A). The particles were moved upward and packages of excavated material were found in higher levels. Finally the grains were deposited at the sediment surface. This bioturbation also changed the redox conditions in the sediment. This was apparent in a reduced sediment core where a shrimp was allowed to construct a burrow. The reduced black material is transported to the surface where it was oxidised (Fig. 5 B). An estimation of sediment transport by this tracer method was not made, because the fluorescent particles were randomly mixed with natural particles and an extrapolation of total transported amount of sediment was therefore difficult. The direct entrapment method of ejected

sediment resulted in an average sediment dry weight of 2,75 g per mound and hour (n = 30 ; SD = 2.4). Assuming a density of 120 ind. m^{-2} this would amount to 7.92 kg m^{-2} day^{-1}.

The grain-size analysis of ejected sediment in comparison with ambient sediment showed a significant shift to smaller grainsize fractions. While the median grain-size of the ambient sediment consisted of sediment with a median grain-size of 350 µm, the collected sediment from the traps had a median grain-size of 200 µm. The selective ejection of fine grained sand and the use of coarse material for the construction of the burrow altered the grain size distribution and increased the bulk sediment permeability in the inhabited area and resulted in distinct layers of coarse sand at the depths where burrow galleries are constructed because of the uniform architecture and the high densities of burrows. Thus facilitating pore water transport.

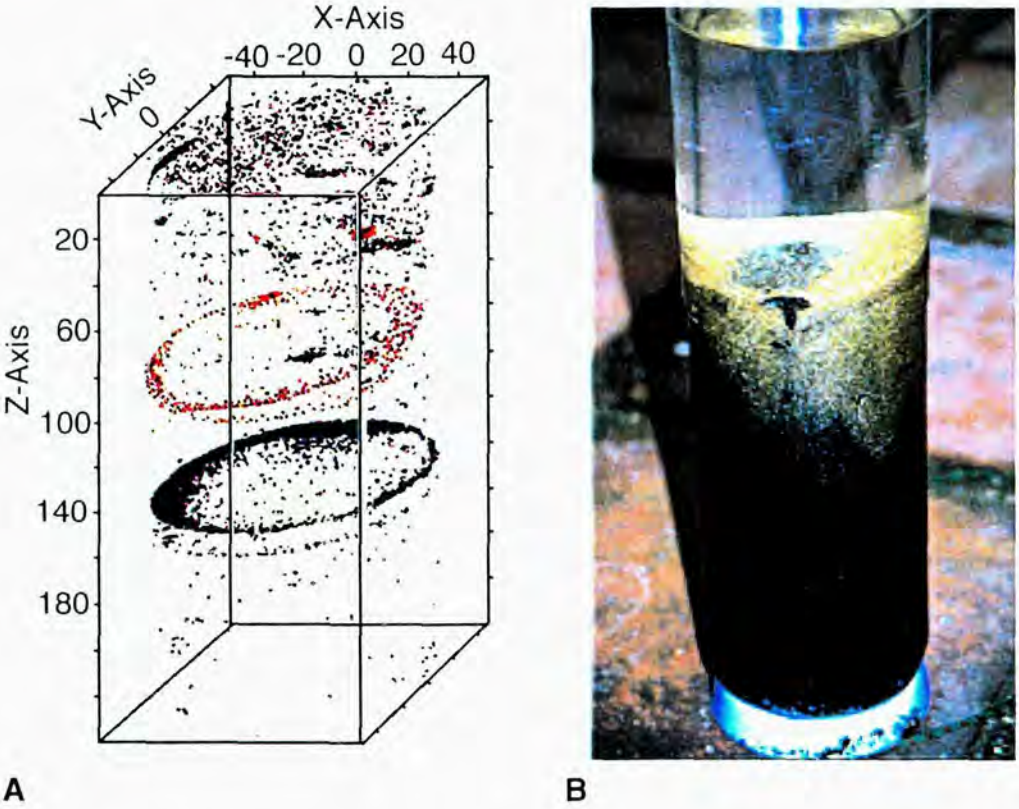

Fig. 5. A Sediment core prepared with two layers of stained sand grains (luminophores), demonstrating particle transport. **B.** Reduced sediment core where C. truncata was allowed to construct a burrow.

Fluid transport

To eject sediment through the exhalant shaft considerable high animal-generated flow velocities (1.3 cm s^{-1}) were produced (Fig. 6, event A). The outflow induces a compensatory inflow at the two opposite inhalant openings thus the funnels are being formed. Once established the funnels represent stabile surface structures functioning as sediment traps. Organic particles, mainly seagrass fragments, transported in the near-bottom horizontal flow are hydrodynamically caught in these funnels. Experiments with stained seagrass fragments showed that the trapped material was transported by the shrimps into deeper parts of the burrow. Decaying sea grass was often found in blind-ending chambers. Analyses of the gut content revealed that the animals either feed directly on the sea grass or on the bacteria growing on the organic material.

In addition to the active irrigation a passive ventilation of the upper burrow compartment is induced by the deflection of the horizontal bottom current at the mound (Vogel 1987, Huettel & Gust 1993, Ziebis 1996). Velocities of passive ventilation measured in a laboratory set-up similar to the one used by Allanson et al. (1992) showed an induced water flow of 0.3-0.4 cm s^{-1} in the inhalant shafts and 0.7 cm s^{-1} in the thin shaft ending in the mound, at a current speed of 10 cm s^{-1} of the bottom current.

The pumping of water through the burrow system by the shrimp (Fig. 6) recorded in an aquarium set-up revealed a distinct ventilation pattern by *C.truncata* . Six different ventilation categories could be distinguished according to the flow speeds (A-F). By a rhythmic beating of the pleopods the flow speeds could be maintained for periods of up to 120 s, although the frequency of the long duration events of each category were less than the shorter periods, they were important for the total volume of water transported through the burrow. With the diameter of the shaft being 4 mm, the calculated total volume of exchanged water was 36 cm^3 per h. Considering a density of 120 burrows per m^2 this would amount to 4 litre of water being exchanged between sediment and water column per hour and one 1 m^2 sediment surface. The longest recorded gap between ventilations was 2.5 min. Thus the shrimp was 22 minutes of one hour or 35 % of the recorded time actively irrigating its burrow.

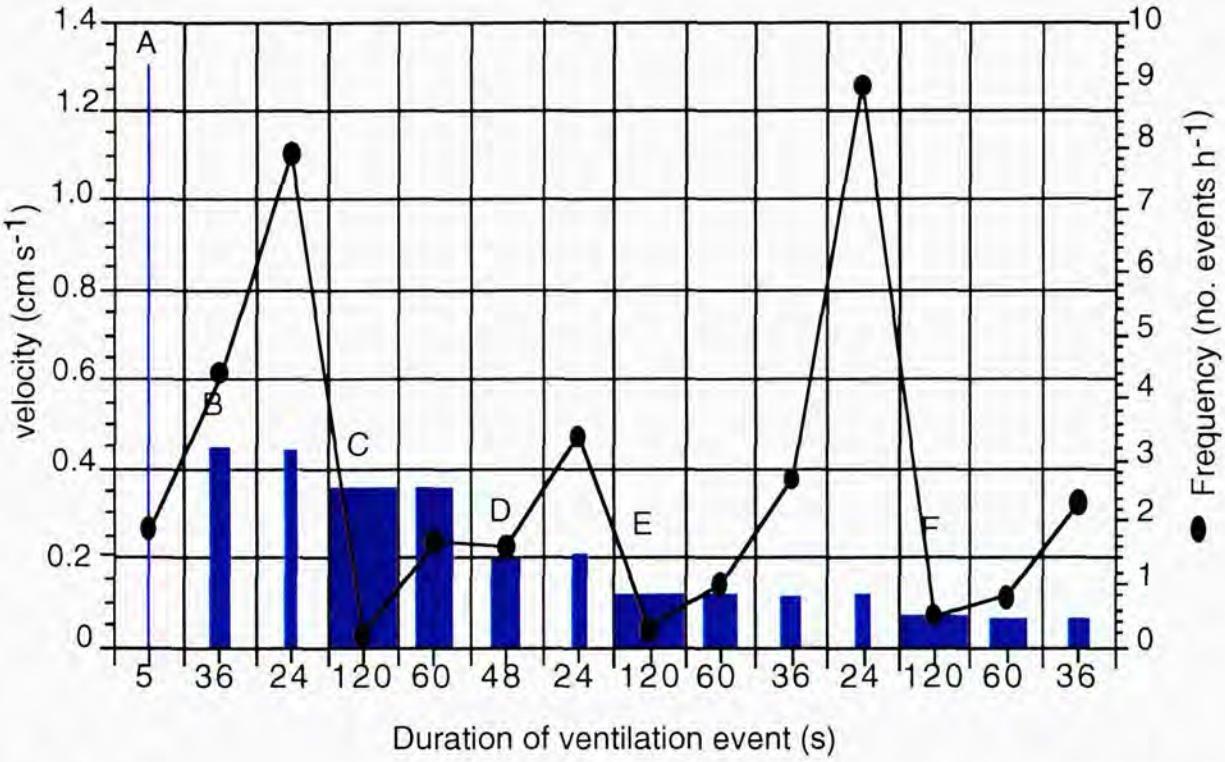

Fig. 6. The active ventilation of a burrow system recorded for a period of 11 h. 6 different ventilation events (A-F) could be distinguished according to the flow velocity. These events lasted up to 120 s. The shorter events were more frequent in each category.

Burrow water chemistry and effect on the surrounding sediment

The supply of oxygen to deeper sediment layers by the Bio-pumping of the shrimp was studied in-situ and is reported in detail elsewhere (Ziebis et al. 1996, Ziebis et al. 1997). Oxygen was recorded in 26 cm and 48 cm sediment depth in intact burrow systems. The oxygen concentrations were maintained at 3-12 % and 10-40 % of air saturation in the respective depths. Oxygen penetrated through the more permeable chamber walls 6-7 cm into the surrounding sediment whereas through the finer grained shaft walls penetration depth was 3-4 mm. Enhancement of bacterial ammonium oxidation was investigated in the burrow water and the surrounding sediment (Fig. 7)

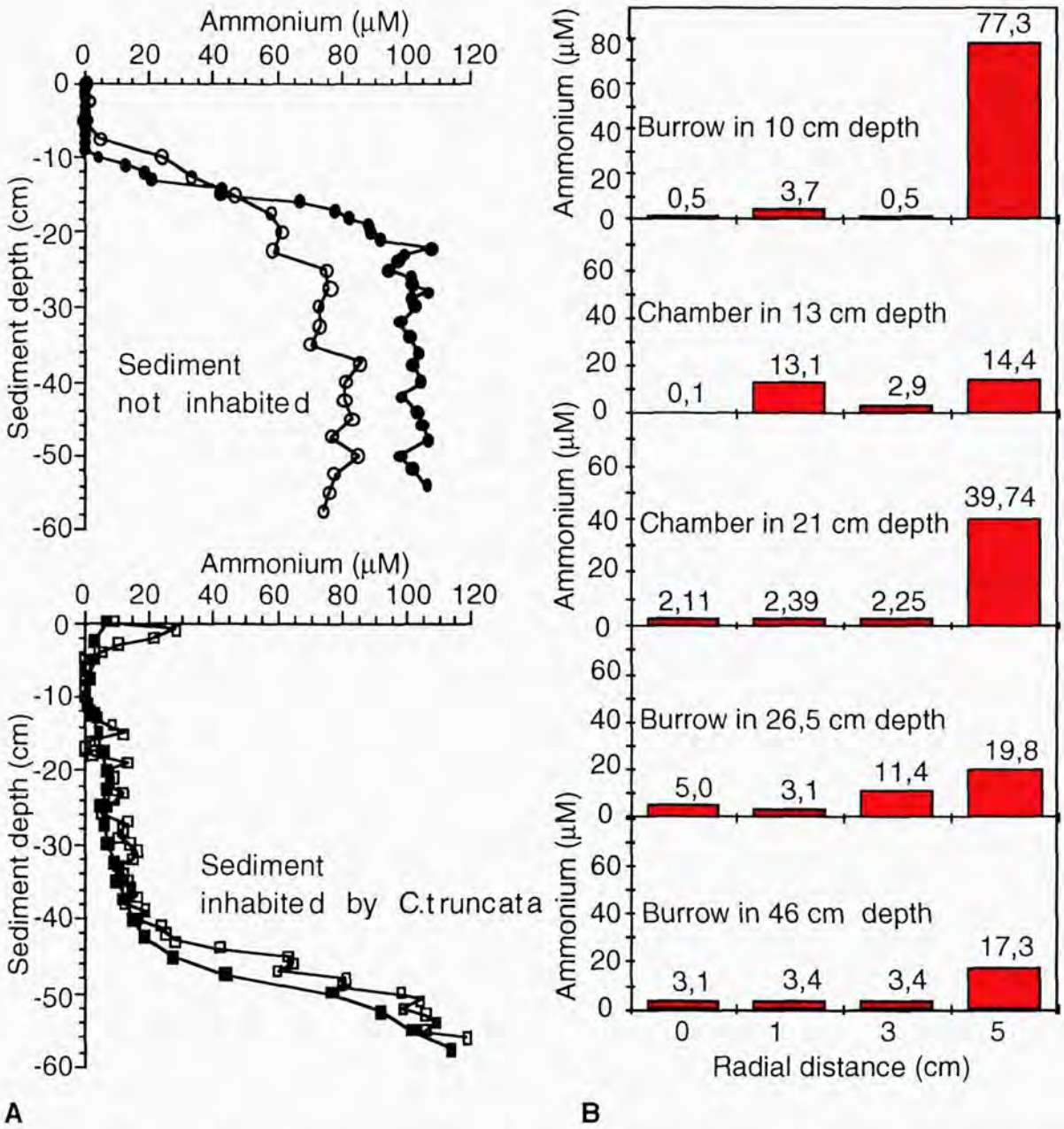

Fig. 7. A Ammonium profiles in bulk sediment inhabited by C. truncata (upper graph) and in non inhabited sediment (lower graph). Two profiles each were measured, one in vertical distances of 1 cm, the second in 2. 5 cm distances. **B** Samples for Ammonium analyses were taken from the burrow lumen and in radial distances from the pore water of the surrounding sediment.

In the uninhabited sediment ammonium increased below 10 cm sediment to concentration between 80 and 100 µM, whereas ammonium concentrations in the bulk sediment bioturbated by *C. truncata* were low (< 20 µM) to a depth of 45 cm. Inside the burrow systems (0) ammonium was found in concentrations of less than 10 µM to a depth of 46 cm. The surrounding sediment was depleted of ammonium to a distance of 3-5 cm. Down to a sediment depth of at least 50 cm the burrow system is surrounded by oxic sediment and ammonium depleted zones extending 4-5 cm into

the surrounding sediment, illustrated in Fig. 8. A sediment column with a diameter of 10 cm is thus influenced by a single shrimp. At the observed density of 120 individuals per m^2 the geochemistry of the entire sediment is affected by these only 2-cm small, burrowing decapods.

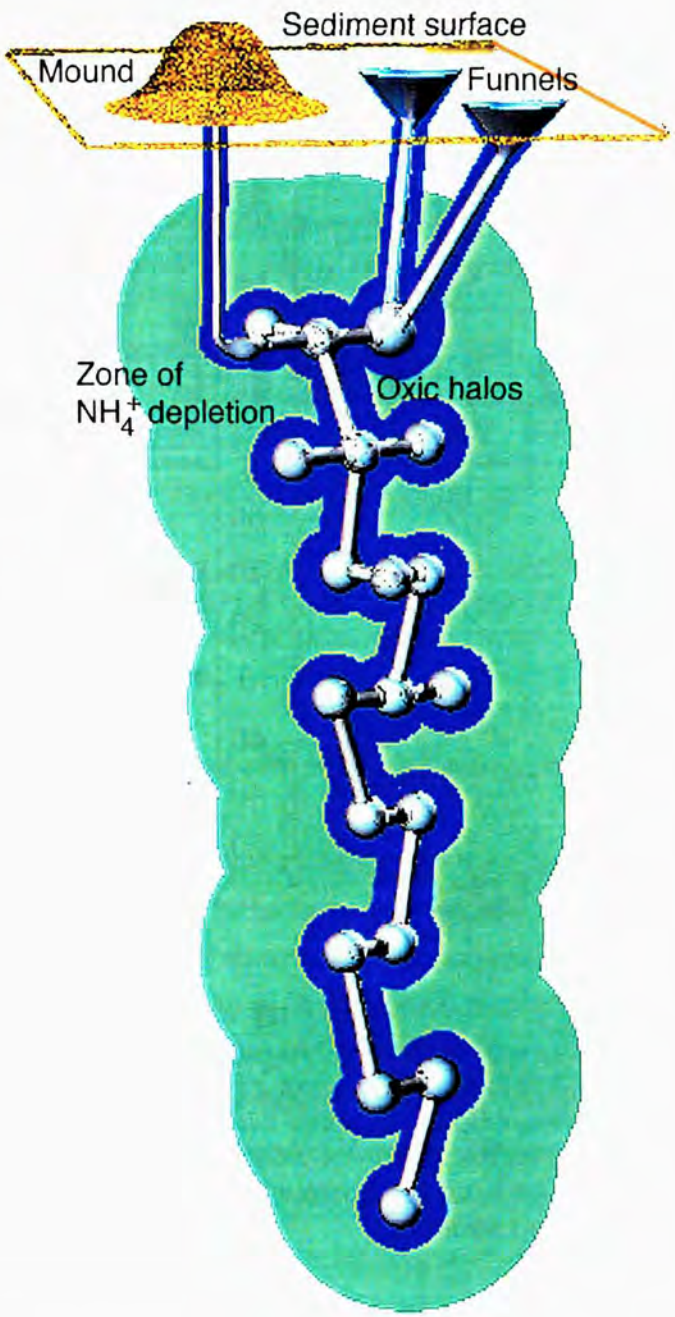

Fig. 8. Generated 3-D computer model of the burrow structure of *C. truncata* with the oxic sediment volumes and ammonium depleted zones illustrated.

DISCUSSION

Although the species *C. truncata* occurs in high densities in coastal environments it has often been overlooked due to its deep reaching burrows and the difficulty to collect these fast moving animals by traditional sampling methods. Most ecological studies on Thalassinids have been carried out in intertidal regions. The investigation of the ecological significance of these often dominant macrofauna organisms of sublittoral environments has been carried out mainly in laboratory set-ups. But the difficulty in providing appropriate laboratory conditions to observe the behaviour of these shrimp that sometimes burrow below 2 m depth (Pemberton et al 1976) has hindered ecological studies. The interpretation of burrow morphology and feeding modes was often not clear because the burrow casting depth was restricted by the microcosms used for the investigations (Nickell & Atkinson 1995). It was also observed that the intra-specific burrow morphology shows some plasticity depending on the densities of individuals, the sediment structure as well as the bottom current conditions. Thus in-situ investigations are the preferable method to gain detailed information on the ecology and biology of these wide-spread and often dominant macrofauna organisms in soft sediments.

A number of behavioural factors are crucial for the biologically mediated transport of fluids across the sediment-water interface into the sediment and the particle processing in the bioturbated sea beds. The pumping rate and its frequency determine the flow of supernatant oxygen-rich water through the burrow system and into the surrounding sediment, affecting processes and geochemical conditions also in the bulk sediment. This effect is even more pronounced in permeable sea floors. The burrow construction and maintenance have a strong impact on the structuring of the sediment. The selective sorting for smaller grain sizes, which has been also observed for other callianassids (Suchanek 1983) can alter the grain size composition of the sediment layer reworked and can have a strong effect on the permeability of the sediment thus promoting pore-water transport. The question to what amount the bioturbating activity by *C. truncata* in the bay of Campese contributed to the composition of the well sorted permeable sediment can only be assumed, because bottom currents in this shallow bay might have a greater effect on the sediment sorting of the upper sediment layer. But the selective ejection of small grains and the use of the coarse-grained material for the construction of deeper burrow compartments influenced at the observed densities the permeability of distinct sediment layers and enhanced solute exchange. The observation that also other callinassids tend to pump the finer sand fractions into the water column also have an

effect on the remobilisation and redistribution of other elements, for example radionuclids (Colin et al. 1986).

The increase of the surface area by the number and depth of burrows per m^2 enhances sediment-water exchange processes. The increase by 400 % for the investigated area is relatively high compared to findings of other species. *Callianassa subterranea* , a larger species, enlarged the sediment interface to 1.5 m^2 per m^2 sediment surface (Witbaard & Duineveld 1989). Higher values, a 7 -9 fold increase of the interface, were reported by Ott et al. (1976) for *Upogebia pussilla*. The amount of particle ejection was relatively high compared to other investigations. Although a comparison is difficult due to the different methods that have been used (Rowden & Jones 1993). The direct particle entrapment method was discussed to be the best method for comparable investigations. It was estimated that *Callianssa truncata* ejects roughly 8 kg sediment dw m^{-2} day^{-1}. Witbaard & Duineveld (1989) reported for *C. subterranea* that 3.5 kg sediment dw m^{-2} day^{-1} were ejected.

The exchange of solute between sediment and water column is not only dependant by the increased surface area but more significantly by the flushing of the burrow with supernatant water. While it has been described for other Thalassinids that they are able to withstand hypoxic conditions for longer periods of time, *C. truncata* seems to have a higher oxygen demand. This is epressed in the high frequency of ventilation and the transport of oxygen also in deep regions of the burrow system. Long-term measurements have documented that the frequent pumping of the shrimp keeps the oxygen concentration within a certain limit even in 0.5 m sediment depth. The calculated amount of 4 litre fluid exchanged per m^2 and hour is also a comparable high value. It is comparable to species of *Upogebia* that are known to suspension feed in their burrows by the ventilation current. At low oxygen levels ammonium produced by the degradation of organic material may accumulate in the burrows of macrofauna organisms. For instance found Koike & Mukai (1983) an increase by the factor of 10 in the ammonium concentrations in the burrows of *C. japonica*. The frequent flushing of the burrow by C. truncata kept the NH_4 concentrations very low, throughout the entire burrow system, due to the transport of ammonium to the overlying water and the oxygen dependant ammonium oxidation. In the permeable sediment oxygen penetrated also into the surrounding and ammonium was oxidised. This suggests that also other bacterial activities in the sediment down to the depth of burrowing activity are influenced by the irrigation behaviour of the decapods. It could be demonstrated that at the observed densities the entire sediment column down to a depth of at least 0.5 m is affected. These favour-able conditions play also a very important role for the distribution of micro-

fauna and meiofauna communities in these sediments (Branch & Pringle 1987). 30-100% increase in bacterial numbers compared to surrounding environment have been observed in sediments adjacant to deep reaching burrows.

The species-specific burrow architecture has been used to predict trophic modes and thus the significance of the burrows to the environment (Griffis & Suchanek 1991). Attempts have been made to classify different species by the burrow morphology and their feeding modes (Nickell & Atkinson 1995). Althoug difficulties in interpretation have been encountered due to the variability of burrow systems depending on the physical environment. Feeding modes have been distinguished by direct observations and laboratory investigations and different groups have been classified as `seagrass harvesters´ or `omnivorous scavengers´, deposit feeders and suspension feeders in order to make assumptions on the significance of organic matter transport and remineralisaton influenced by the different groups. This classification seems to be difficult for some species.It is also an interesting question how the energy demand can be fulfilled for these deep burrowing animals by the nutrition provided. It was observed that *Callianassa truncata* is deposit feeding by processing large amounts of sediment, gleaning sandgrains or scraping the burrow walls for bacteria. This mining yields only low amounts of energy. Whereas the culturing of bacteria on decaying sea grass stored in chambers, also referred to as ´gardening´, yields a higher nutritional value. The organic material caught in the sediment trap-like funnels serves also directly as food. This can be of plant (sea-grass harvester) or animal origin (omnivorous scavengers). The ventilation current transports organic particles directly into the burrow system and it is likely that *C. truncata* also suspension feeds on the offered material. Thus the feeding mode is variable and it is difficult to use it for a classification. But it also demonstrates that the different path ways of organic matter input to the sediment contribute significantly to the cycling of matter in the inhabited environments.

By the mode of burrow construction, ventilation, particle processing , organic material entrainment and enhancement of degradation by supplying oxygen to deep sediment layers *C. truncata* is a very important factor for the ecology of coastal sea beds.

ACKNOWLEDGEMENTS: Thanks are due to Adelbert Niemeyer for help in sediment sampling and processing, Thomas Pillen for assistance in burrow casting and Christoph Humborg for help in underwater field work. The members of the Giglio Diving and Research Team are thanked for their help during several dives. Greatly is acknowledged the support and supervision of the project by Stefan Forster and Markus Huettel. This study was financed partly by the Max-Planck-Society.

LITERATURE CITED

Allanson BR, Skinner D, Imberger J (1992) Flow in Prawn burrows. Estuarine Coastal and Shelf Science 35: 253-266

Aller AC (1980) Quantifying solute distributions in the bioturbated zone of marine sediments by defining an average microenvironment. Geochim

Aller AC (1983) The importance of the diffusion permeability of animal burrow linings in determining marine sediment chemistry. J Mar Res 41:299-322

Aller RC, Dodge RE (1974) Animal-Sediment relations in a tropical lagoon, Discovery Bay, Jamaica. J Mar Res 32: 209-232

Aller RC (1982) The effects of macrobenthos on chemical properties of marine sediment and overlying water. In: McCall PL,Tevesz MJS (eds) Animal-sediment relations (2): Topics in Geobiology. Plenum Press, New York, pp 53-96 Cosmochim Acta 44:1955-1965

Aller RC, Yingst RE, Ullmann WJ (1983) Comparative biogeochemistry of water in intertidal Onuphis (Polychaeta) and Upogebia (Crustacea) burrows: temporal patterns and causes. J Mar Res 41:571-604

Aller RC (1984) The importance of relict burrow structures and burrow irrigation in controlling sedimentary solute distributions. Geochim Cosmochim Acta 48:

Aller RC (1990) Bioturbation and manganese cycling in hemipelagic sediments. Phil Trans R Soc Lond A 331:51-68

Aller RC, Blair NE (1996) Sulfur diagenesis and burial an the Amazon shelf: Major control by physical sedimentation processes. Geo-Mar Lett 16:3-10

Alve E, Bernhard JM (1995) Vertical migratory response of benthic Foraminfera to controlled oxygen concentrations in an experimental mesocosm. Mar Ecol Prog Ser 116:137-151

Andersen FO, Helder W (1987) Comparison of oxygen microgradients, oxygen flux rates and electron transport system activity in coastal marine sediments. Mar Ecol Prog Ser 37:259-264

Atkinson RJA, Chapman CJ (1984) Resin casting: a technique of investigating burrows in sublittoral sediments.

Batchelor GK (1967) An introduction to fluid dynamics. Cambridge University Press, Cambridge

Bedford KW, Abdelrhman M (1987) Analytical and experimental studies of the benthic boundary layer and their applicability to near-bottom transport in lake Erie. J Great Lakes Res 13:628-648

Berner RA (1971) Principles of Chemical Sedimentology B. McGraw-Hill, New York, 240 pp

Berner RA (1980) Early diagenesis - a theoretical approach. Princeton University Press Princeton, New Jersey

Bernhard JM (1989) The distribution of benthic Foraminfera with respect to oxygen concentration and organic carbon levels in shallow-water Antarctic sediments. Limnol Oceanogr 34:1131-1141

Bernhard JM, Reimers CE (1991) Benthic foraminiferal populations related to anoxia Santa Barbara Basin. Biogeochemistry 15:127-149

Berninger UG, Epstein S (1995) Vertical distribution of benthic ciliates in response to the oxygen concentration in an intertidal North Sea sediment. Aquat Microb Ecol 9: 229-236

Blackburn TH (1987) Microbial foodwebs in sediments. In: Sleigh MA (ed) Microbes in the sea. Wiley Chichester pp 39 - 57

Boudreau BP, Guinasso NL (1982) The influence of a diffusive sublayer on accretion dissolution and diagenesis of the sea floor. In: Fanning KA, Mannheim FT (eds) The dynamic environment of the ocean floor. Lexington, pp 115-145

Boudreau BP (1994) Is burial velocity a master parameter for bioturbation ? Geochim Cosmochim Acta 58:1243-1249

Boudreau BP (1996) The diffusive tortuosity of fine-grained unlithified sediments. Geochim Cosmochim Acta 60:3139-3142

Branch GM, Pringle A (1987) The impact of the sand prawn *Callianassa kraussi* Stebbing on sediment turnover and on bacteria, meifauna, and benthic micoflora. J exp Mar Biol Ecol 107:219-235

Bowmann GT, Delfino JJ (1980) Sediment oxygen demand techniques: a review and comparison of laboratory and in-situ systems. Water Res14:491-499

Brendel PJ (1995) Development of a mercury thin film voltammetric microelectrode for the determination of biogeochemically important redox species in porewaters of marine and freshwater sediments. PhD thesis University of Delaware

Brendel PJ,Luther III GW (1995) Development of a gold amalgam voltammetric microelectrode for the determination of dissolved Fe Mn O-2 and S(-II) in porewaters of marine and freshwater sediments. Environ Sci Technol 29:751-761

Burdige DJ, Nealson KH (1986) Chemical and microbiological studies of sulfide-mediated manganese reduction. Geomicrobiol J 4:361-387

Burdige DJ (1993) The biogeochemistry of manganese and iron reduction in marine sediments Earth-Science Reviews 35:249-284

Cadée GC (1976) Sediment reworking by Arenicola marina on tidal flats in the Dutch Wadden Sea. Neth J Sea Res 10:440-460

Callender E, Hammond DE (1982) Nutrient exchange accross the sediment-water interface in the Potomac river estuary. Estuarine Coastal and Shelf Science 15:395-413

Canfield DE, Jørgensen BB, Fossing H, Glud RN, Gundersen J, Ramsing NB Thamdrup B, Hansen JW, Nielsen LP, Hall POJ (1993a) Pathways of organic carbon oxidation in three continental margin sediments. Mar Geol 133:27-40

Canfield DE ,Thamdrup B, Hansen JW (1993b) The Anaerobic Degradation of Organic Matter in Danish Coastal Sediments - Iron Reduction Manganese Reduction and Sulfate Reduction. Geochim Cosmochim Acta 57: 3867-3883

Chao TT, Zhou L (1983) Extraction techniques for selective dissolution of amorphous iron oxides from soils and sediments. Soil Sci Soc Am J 47: 225-232

Colin PL, Suchaned TH, McMurtry G (1986) Water Pumping and particulate resuspension by callinassids (Crustacea:Thalassinidea) at Enewetak and Bikini Atolls, Marshall islands. Bull Mar Sci 38:19-24

Crank J (1983) The mathematics of diffusion. Clarendon Press, Oxford

Dade WJD, Davis PD, Nichols D, Nowell ARM, Thistle M, Trexler B, White DC (1990) Effects of bacterial exopolymer adhesion on entrainment of sand Geomicrob J 8:1-16

Darcy H (1856) Les Fontaines Publiques de la Ville de Dijon. Dalmont

Davies AM (1993) A bottom boundary layer resolving 3-dimensional tidal model - a sensitivity study of eddy viscosity formulation. J Phys Oceanogr 23:1437-1453

Deuser WG, Ross EH, Anderson RF (1981) Seasonality in the supply of sediment in the deep Sargasso Sea and implications for the rapid transfer of matter to the deep ocean. Deep-Sea Res 28:495-505

Driscoll M, Tucholke BE (1983) Seafloor zonation in sediment texture and benthic megafauna in the Hebble (High Energy Benthic Boundary Layer Experiment) area. EOS Trans Am Geophys Union 64:729-735

Dworschak PC (1983) The biology of Upogebia pusilla (PETAGNA) (Decapoda Thalassinidea) I The burrows. Mar Ecol Naples 4:19 -43

Dobbs FC, Guckert JB (1988) Callinassa trilobata (Crustacea:Thalssinidea) influences abundance of meiofauna and biomass, composition, and physiologic state of microbial communities within its burrow. Mar Ecol Progr Ser 45:69-79

Fenchel T (1969) The ecology of marine microbenthos IV Structure and function of the benthic ecosystem its chemical and physical factors and the microfauna communities with special reference to the ciliated protozoa. Ophelia 6:1-182

Fenchel T, Blackburn TH (1979) Bacteria and mineral cycling. Academic press, London

Fenchel T, Finlay BJ (1995) Ecology and evolution in anoxic worlds. Oxford University Press, Oxford

Forster S, Graf G (1992) Continuously measured changes in the redox potential influenced by oxygen penetrating from burrows of Callianassa subterranea. Hydrobiolgia 235/236:527-532

Forster S, Graf G (1995) Impact of irrigation on oxygen flux into the sediment: intermittent pumping by Callianassa subterranea and 'piston-pumping' by Lanice conchilega. Mar Biol 123:335-346

Forster S, Huettel M, Ziebis W (1996) Impact of boundary layer flow velocity on oxygen utilization in coastal sediments. Mar Ecol Prog Ser 143:173-185

Froelich PN, Klinkhammer GP, Bender ML, Luedtke NA, Heath GR, Cullen D Dauphin P, Hammond D, Hartman B, Maynard V (1979) Early oxidation of organic matter in pelagic sediments of the eastern equatorial Atlantic: suboxic diagenesis. Geochim Cosmochim Acta 43:1075-1090

Gehlen M, Malschaert H, Van Raaphorst WR (1995) Spatial and temporal variability of benthic silica fluxes in the southeastern North Sea. Cont Shelf Res 15:1675-1696

Giere O (1993) Meiobenthology: The microscopic fauna in aquatic sediments. Springer-Verlag, Berlin

Giles RV (1976) Theory and problems of fluid mechanics and hydraulics. McGraw-Hill, Duesseldorf

Glud RN, Forster S, Huettel M (1996) Influence of radial pressure gradients on solute exchange in stirred benthic chambers. Mar Ecol Prog Ser 141:303-311

Glud RN, Gundersen JK, Jørgensen BB, Revsbech NP, Schulz HD (1994) Diffusive and total oxygen uptake of deep-sea sediments in the eastern South Atlantic Ocean: in situ and laboratory measurements. Deep-Sea Research 41:1767-1788

Graf G (1992) Benthic-pelagic couppling: a benthic view. Oceanogr Mar Biol Ann Rev 30:149-190

Graf G, Schulz R, Peinert R, Meyer-Reil L-A (1983) Benthic response to sedimentation events during autumn to spring at a shallow-water station in the western Kiel Bight. Mar Biol 77: 235-246

Grasshoff K, Ehrhardt M, Kremling K (1983) Methods of Seawater Analysis. Verlag Chemie

Griffioen J (1994) Uptake of phosphate by iron hydroxides during seepage in relation to development of groundwater composition in coastal areas. Environ Sci Technol 28 675-681

Griffis RB, Suchanek TH (1993) A model of burrow architecture and trophic modes in thalassinidean shrimp (Decapoda: Thalassinidea). Mar Ecol Prog Ser 79:171-183

Grundmanis V, Murray JW (1977) Nitrification and denitrification in marine sediments from Puget Sound. Limnol Oceanogr 22(5):804-813

Gundersen JK, Jørgensen BB (1990) Microstructure of diffusive boundary layers and the oxygen uptake of the sea floor. Nature 345:604-607

Hall POJ, Hulth S, Hulthe G, Landen A, Tengberg A (1996) Benthic nutrient fluxes on a basin-wide scale in the Skagerrak (north-eastern North Sea). J Sea Res 35:123-137

Hall POJ, Aller RC (1992) Rapid small-volume flow injection analysis for Σ CO_2 and NH_4^+ in marine and freshwaters. Limnol Oceanogr 37:1113 -1119

Hallbeck L, Pedersen K (1995) Benefits associated with the stalk of *Gallionella ferruginea* evaluated by comparison of a stalk-forming and a non-stalk-forming strain and biofilm studies in situ. Microbial Ecology 30:257-268

Hansen LS, Blackburn TH (1992) Effect of algal bloom deposition on sediment respiration and fluxes. Mar Biol 112:147-152

Hao OJ, Richard MG, Jenkins D (1983) The half-saturation coefficient for dissolved oxygen: a dynamic method for its determination and its effect on dual species competition. Biotechnol Bioeng 25: 403-416

Hargrave BT (1976) The central role of invertebrate feces in sediment decomposition. In: MacFayden A, Anderson J M (eds) The role of terrestrial and aquatic organisms in decomposition processes. Blackwell, p 301-321

Harvey RW, Kinner N pp 301-321, ED, MacDonald D, Metge W, Bunn A (1993) Role of heterogeneity in the interpretation of small-scale laboratory and field observations of bacteria microbial-sized microsphere and bromide transport through aquifer sediments. Water Resour Res 29:2713-2721

Heezen BC, Hollister CD (1971) The face of the deep. Oxford University Press, Oxford

Houot S, Berthelin J (1992) Submicroscopic studies of iron deposits occurring in field drains formation and evolution. Geoderma 52:209-222

Howe JA, Humphery JD (1995) Photographic evidence for slope-current activity Hebrides Slope NE Atlantic Ocean. Scot J Geol 31:107-115

Huettel M (1988) Zur Bedeutung der Makrofauna für die Nährsalzprofile im Wattenmeer. Ph D dissertation, Christian-Albrechts-University Kiel

Huettel M (1990) Influence of the lugworm Arenicola marina on porewater nutrient profiles of sand flat sediments Mar Ecol Progr Ser 89:253 - 267

Huettel M, Forster S, Klöser S, Fossing H (1996 a) Vertical migration in the sediment-dwelling sulfur bacteria Thioploca spp in overcoming diffusion limitations. Appl Environm Microbiol 62:1863-1872

Huettel M, Gust G (1992) Impact of bioroughness on interfacial solute exchange in permeable sediments. Mar Ecol Progr Ser (89):253-267

Huettel M , Gust G (1992a) Impact of bioroughness on interfacial solute exchange in permeable sediments. Mar Ecol Prog Ser 89: 253-267

Huettel M, Gust G (1992b) Solute release mechanisms from confined sediment cores in stirred benthic chambers and flume flows. Mar Ecol Prog Ser 82:187-197

Huettel M, Ziebis W, Forster S (1996 b) Flow-induced uptake of organic matter in permeable sediments. Limnol Oceanogr 41: 309-322

Hylleberg J, Henriksen K (1980) The central role of Bioturbation in sediment mineralization and element recycling. Ophelia 1:1-16

Iversen N, Jørgensen BB (1993) Diffusion coefficient and methane in marine sediments. Geoch Cosmochim Acta 75:571-578

Jahnke RA, Marinelli RL, Eckmann JE, Nelson JR (1996) Pore water nutrient distributions in non-accumulating sandy sediments of the South Atlantic Bight continenetal shelf. EOS76:202

Jeffrey SW, Humphrey GF (1975) New spectrophotometric equations for determining chlorophylls a b c1 and c2 in higher plants algae and natural phytoplankton. Biochem Physiol Pflanzen 167: 191-194

Jenness MI, Duineveld GCA (1985) Effects of tidal currents on chlorophyll a content of sandy sediments in the southern North Sea. Mar Ecol Prog Ser 21:283-287

Jensen P (1987) Feeding ecology of free-living aquatic nematodes. Mar Ecol Prog Ser 35:178-196

Johnson MA, Stride AH (1969) Geological significance of North-Sea sand transport rates. Nature 224: 1016-1017

Jørgensen BB, Revsbech NP (1985) Diffusive boundary layers and the oxygen uptake of sediments and detritus. Limnol Oceanogr 30:111-122

Jørgensen BB, Sørensen J (1985) Seasonal cycles of O_2 NO_3 and SO_4 reduction in estuarine sediments: the significance of an NO_3 reduction maximum in spring. Mar Ecol Prog Ser 24:65-74

Jørgensen BB, Revsbech NP (1989) Oxygen uptake bacterial distribution and carbon-nitrogen-sulphur cycling in sediments from the Baltic Sea-North Sea transition. Ophelia 31:29-49

Jørgensen BB, Bang M, Blackburn TH (1990) Anaerobic mineralization in marine sediments from the Balthic Sea- North Sea transition . Mar Ecol Prog Ser 59: 39-54

Jørgensen BB, Des Marais DJ (1990) The diffusive boundary layer of sediments: Oxygen microgradients over a microbial mat. Limn Oceanogr 35(6): 1343-1355

Jørgensen BB (1996) Material flux in the sediment. In Eutrophication in coastal marine ecosystems. pp 115-135 AGU

Keil RG, Tsamakis E, Fuh CB, Giddings JC ,Hedges JI (1994) Mineralogical and textural controls of the organic composition of coastal marine sediments - hydrodynamic seperation using split-fractionation. Geochim Cosmochim Acta 58:879-893

Kersten M, Dicke M, Kriews M, Naumann K, Schmidt D, Schulz M, Schikowski M, Steiger M (1988) Distribution and fate of heavy metals in the North Sea. In: Salomons W Bayne BL Duursma EK Förstner U (eds) Pollution of the North Sea - An Assessment. Springer, Heidelberg pp 36-58

Kostka JE, Luther III GW (1995) Seasonal cycling of Fe in saltmarsh sediments Biogeochemistry 29:159-181

Kostka JE, Luther III GW (1994) Partitioning and speciation of solid phase iron in saltmarsh sediments. Geochim Cosmochim Acta 58:1701-1710

Kristensen E (1985) Oxygen and inorganic nitrogen exchange in a Nereis virens (Polychaeta) bioturbated sediment-water system. J Coast Res 1:109-116

Kristensen E, Jensen MH, Andersen TK (1985) The impact of polychaete (Nereis virens Sars) burrows on nitrification and nitrate reduction in estuarine sediments. J exp mar Biol Ecol 85:75-91

Krom MD, Berner RA (1981) The diagenesis of phosphorus in a nearshore marine sediment. Geochim Cosmochim Acta 45:207-216

LaBarbera M, Vogel S (1976) An inexpensive thermistor flowmeter for aquatic biology. Limnol Oceanogr 21:750 -756

Lindeboom HJ, Sandee AJJ, de Klerk-van der Driessche HAJ (1985) A new bell jar/microelectrode method to measure changing oxygen fluxes in illuminated sediments with a microbial cover. Limnol Oceanogr 30:693-698

Lohse L, Epping EHG, Helder W, Vanraaphorst W (1996) Oxygen Pore Water Profiles In Continental Shelf Sediments Of the North Sea - Turbulent Versus Molecular Diffusion. Mar Ecol Prog Ser 145:63-75

Lovley DR, Phillips EJP (1987) Rapid assay for microbially reducible ferric iron in aquatic sediments. Appl Environ Microbiol 53:1536-1540

Lovley DR, Phillips EJP (1988) Novel mode of microbial metabolism: organic carbon oxidation coupled to dissimilatory reduction of iron and manganese. Appl Environ Microbiol 54:1472-1480

Lovley DR (1995) Microbial reduction of iron manganese and other metals. In: Advances in Agronomy Vol 54 (ed Sparks DL) pp 175-231 Academic Press Inc

Luther III GW, Nuzzio DB, Wu J (1994) Speciation of manganese in Chesa-peake Bay waters by voltammetric methods. Anal Chim Acta 284: 473-480

Mackin JK, Swider KT (1989) Organic matter decomposition pathways and oxygen consumption in coastal marine sediments. Jour Mar Res 47:681- 716

Madigan MT, Martinko J, Parker M, Brock J (1997) Biology of Microorganisms. Prentice Hall International Inc.

Malan DE, McLachlan A (1991) In -situ benthic oxygen fluxes in a nearshore coastal marine system: a new approach to quantify the effect of wave action. Mar Ecol Prog Ser 73:69-81

Marinelli RL, Jahnke RA, Craven DB, Eckman JE (1997) Benthic microalgal production and sediment nutrient inventories on the south atlantic bight (sab) shelf: the relative importance of nutrient regeneration uptake by bioirrigation and advection. Aquatic Sciences Meeting February 10-14 1997 Santa Fe New Mexico 232

Marinelli RL (1994) Effects of burrow ventilation on activities of a terebellid polychaete and silicate removal from sediment pore waters. Limnol Oceanogr 39(2):303-317

Martin GN, Noonon MJ (1977) Effects of domestic wastewater disposal by land irrigation on groundwater quality of central Canterbury plains. Water Soil Tech Publ 7

Mayer LM (1989) The nature and determination of non-living sedimentary organic matter as a food source for deposit-feeders. In: Lopez G, Taghon G, Levinton J (eds) Ecology of Marine Deposit Feeders. Springer, New York p 98-113

Mayer LM, Macko SA, Cammen L (1988) Provenance concentrations and nature of sedimentary organic nitrogen in the Gulf of Maine. Mar Chem 25:291-304

Mayer LM, Raheim PT, Guerin W, Macko SA, Watling L, Andersen FE (1985) Biological and granulometric controls on sedimentary organic matter of an intertidal mudflat. Estuar Coastal Shelf Sci 20:491-504

McCave IN (1984a) Size-spectra and aggregation of suspended particles in the deep ocean. Deep-Sea Res 31: 329-352

McCave IN (1984b) Mechanics of deposition of fine-grained sediments from nephloid layers. Geo-Mar Lett 4: 243-245

Mcmanus J, Hammond DE, Berelson WM, Kilgore TE, Demaster DJ, Ragueneau OG, Collier RW (1995) Early diagenesis of biogenic opal: Dissolution rates kinetics and paleoceanographic implications. Deep Sea Res Pt II-Top St Oce 42 871-903

Means RE, Parcher JV (1964) Physical properties of soils. Constable, London

Meyer-Reil L, Faubel A, Graf G, Thiel H (1987) Aspects of a benthic community structure. In: Rumohr J, Walger E Zeitschel B (eds) Seawater-sediment interactions in coastal waters-an interdisciplinary approach. Springer, Heidelberg, p 69 - 110

Meyer-Reil LA (1986) Measurements of hydrolytic activity and incorporation of dissolved organic substrates by microorganisms in marine sediments. Mar Ecol Prog Ser 31:143-149

Middleton GV, Southard JB (1984) Mechanics of sediment movement. SEPM Short course number 3

Millward GE, Moore R M (1982) The adsorption of Cu Mn and Zn by iron oxyhydroxide in model estuarine solutions. Water Res 16:981-985

Moncharment (1979) Notizie biologiche e faunistiche sui crostacei decapodi del Golfo Napoli. Annario dell'Istituto e Museo di Zoologia dell`Universita di Napoli 23

Morgan JJ , Stumm W (1964) Colloid-chemical properties of manganese dioxide. J Colloid Sci 19:347-359

Morse JW (1974) Calculation of diffusive fluxes across the sediment-water interface. J Geophys Res 79(33):5045-5048

Moss VA (1993) MacStereology Version 28, Ranfurly Microsystems

Mullin MM (1965) Size fractionation of particulate organic carbon in the surface waters of the western Indian. Ocean Limnol Oceanogr 10:459-462

Murray J W (1975) The interactions of metal ions at the manganese dioxide solution interface Geochim Cosmochim Acta 39 505-519

Myers CR, Nealson KH (1988) Microbial reduction of manganese oxides: interactions with iron and sulfur. Geochim Cosmochim Acta 48:1237-1247

Nedwell DB, Parkes RJ, Upton AC, Assinder DJ (1993) Seasonal fluxes across the sediment-water interface and processes within sediments. Phil Trans R Soc Lond Ser A 343:519-529

Nickell LA, Atkinson RJA (1995) Functional morphology of burrows and trophic modes of three thalssinidean shrimp species, and a new approach to the classification of thalassinidean burrow morphology. Mar Ecol Prog Ser 128: 181-197

Nielsen LP, Christensen PB, Revsbech NP, Sørensen J (1990) Denitrification and oxygen respiration in biofilms studied with a microsensor for nitrous oxide and oxygen. Microb Ecol 19:63-72

Nittrouer CA, Wright DL (1994) Transport of particles across continental shelves. Rev Geophys 32:85-113

Ott JA, Fuchs B, Fuchs R, Malasek (1976) Observation on the biology of Callianassa stebbingi Borradaille and Upogebia litorales Risso and their effect upon the sediment. Senckenbergiana Marit 8: 61-79

Palmer MA, Molloy RM (1986) Water flow and the vertical distribution of meifauna: a flume experiment. Estuaries 9:225-228

Pamatmat MM (1971) Oxygen consumption by the sea bed - IV Shipboard and laboratory experiments. Limnol Oceanogr 16:536-550

Pemberton SG, Risk MJ, Buckley DE (1976) Supershrimp: Deep bioturbation in the Strait of Canso, Nova Scotia. Science 192: 790-791

Phillips EJP, Loveley DR (1987) Determination of Fe(III) and Fe(II) in oxalate extracts of sediments. Soil Sci Soc Am J 51:938-941

Purcell EM (1977) Life at low Reynolds number. Am J Phys 45: 3-11

Rajagopalan R, Tien C (1976) Trajectory analysis of deep-bed filtration with a sphere-in-cell porous media model J AIChE 22: 523-533

Rasmussen H, Jørgensen BB (1992) Microelectrode studies of seasonal oxygen uptake in a costal sediment: role of molecular diffusion. Mar Ecol Prog Ser 81:289-303

Ray AJ, Aller RC (1985) Physical irrigation of relict burrows: implications for sediment chemistry. Mar Geol 62: 371-379

Redfield AC (1934) On the proportions of organic derivatives in sea water and their relation to the composition process of plankton. In: James Johnstone memorial volume. Liverpool University Press, Liverpool

Reimers C, Smith KL jun. (1986) Reconciling measured and predicted fluxes of oxygen across the deep sea sediment - water interface. Limnol Oceanogr 31: 305-318

Reimers CE, Glenn SM, Creed EL (1996) The dynamics of oxygen uptake by shelf sediments. EOS 76:202

Reineck HE (1967) Layered sediments of tidal flats beaches and shelf bottoms of the North Sea. In: Lauff G (ed) Estuaries. American Association for Advancement of Science, Washington DC, pp 191-206

Revsbech NP, Jørgensen BB, Blackburn TH (1980) Oxygen in the sea bottom measured with a microelectrode. Science 207:1355-1356

Revsbech NP, Jørgensen B (1986) Microelectrodes: their use in microbial ecology. In: Marshall KC (ed) Advances in microbial ecology. Plenum Press New York pp 293-352

Revsbech NP (1989) An oxygen microsensor with a guard cathode. Limnol Oceanogr 34:472-276

Riedl R, Huang N, Machan R (1972) The subtidal pump a mechanism of intertidal water exchange by wave action, Mar Biol 13:210-221

Riedl RJ, Machan EA (1972) Hydrodynamic patterns in lotic intertidal sands and their bioclimatological implications. Mar Biol 13:179-209

Riley GA (1956) Oceanography of Long Island Sound 1952-1954 IX Production and utilization of organic matter. Bull Bingham Oceanogr Collect 15:324-343

Risk MJ, JS Moffat (1977) Sedimentological significance of fecal pellets of *Macoma baltica* in the Minas Basin Bay of Fundy. J Sediment Petrol 47: 1425-1436

Rönner U (1985) Nitrogen transformations in denitrification counteracts. Ambio 14 (3): 134-138

Rowden AA, Jones MB (1995) The burrow structure of the mud shrimp *Callianassa subterranea* (Decapoda: Thalassinidea) from the North Sea. Journ Nat Hist 29: 1155-1165

Rumohr J, Walger E., Zeitzschel B (1987) Sea-water-Sediment Interactions in Coastal waters (An interdisciplinary Approach). Lecture Notes on Coastal and Estuarine Studies. Springer Verlag , Heidelberg

Rutgers van der Loeff MM (1980) Nutrients in the interstitial waters of the southern bight of the North Sea. Netherlands Journal of Sea Research 14: 144-171

Rutgers van der Loeff MM (1990) Oxygen in pore waters of deep-sea sediments. Phil Trans R Soc Lond A 331:69-84

Savant SA, Reible DD, Thibodeaux LJ (1987) Convective transport within stable river sediments. Water Resour Res 23: 1763-1768

Savant SA, Reible DD, Thibodeaux LJ (1987) Convective transport within stable river sediments. Water Resour Res 23:1763-1768

Schink DR, Guinasso NLJr, Fanning KA (1975) Processes affecting the concentration of silica at the sediment-water interface of the Atlantic Ocean. Journal of Geophysical Research 1975 80(21):3013-3031

Schlichting H (1987) Boundary layer theory. 7th ed MacGraw-Hill, New York

Schmidt WD, Overbeck J (1994) Iron bacteria In Microbial ecology of Lake Plussee. Overbeck J (ed) Springer-Verlag, New York, pp 326-336

Schmidt-Nielsen K (1983) Animal Physiology: adaptation and environment. Cambridge University Press Cambridge

Schwertmann U, Fitzpatrick RW (1992) Iron minerals in surface environments In Biomineralization processes of iron and manganese: modern and ancient environments. Skinner HCW, FitzpatrickRW (eds) Catena Verlag, pp 7-31

Seibold E, Berger WH (1982) The Sea Floor - an introduction to marine geology. Springer, Berlin

Sharp JH (1973) Size classes of organic carbon in seawater. Limnol Oceanogr 18: 441-447

Shimeta J (1993) Diffusional encounter of submicrometer particles and small cells by suspension feeders. Limnol Oceanogr 38:456-465

Shum KT, Sundby B (1996) Organic matter processing in continental shelf sediments - The subtidal pump revisited. Mar Chem 53:81-87

Sinton LW (1980) Investigations into the use of the bacterial species Bacillus stearothermophilus and Escherichia coli (H_2S positive) as tracers of ground water movement. Water Soil Technol Publ 17

Skinner HCW, Fitzpatrick RW (1992) Iron and manganese biomineralization. In: Biomineralization processes of iron and manganese: modern and ancient environments. Skinner HCW, Fitzpatrick RW (eds) Catena Verlag, pp 1-7

Slomp CP, Vandergaast SJ, Vanraaphorst W (1996) Phosphorus binding by poorly crystalline iron oxides in North Sea sediments. Mar Chem 52:55-73

Smetacek V, von Bröckel K, Zeitschel B, Zenk W (1978) Sedimentation of particulate matter during a phytoplankton spring bloom in relation to the hydrographical regime. Mar Biol 47:211-226

Smith KL, Kaufmann RS, Wakefield WW (1993) Mobile megafaunal activity monitored with a time-lapse camera in the abyssal North Pacific. Deep-Sea Res 40: 2307-2324

Stolzenbach KD, Newman KA, Wong CS (1992) Aggregation of fine particles at the sediment-water interface. J Geophys Res 97: 17889- 17898

Stookey LL (1970) Ferrozine - A new spectrophotometric reagent for iron. Analytical Chemistry 42 779-781

Straub KL, Benz M, Schink B, Widdel F (1996) Anaerobic nitrate-dependent microbial oxidation of ferrous iron. Appl Environ Microbiol 62:1458-1460

Stumm W, Morgan J J (1981) Aquatic Chemistry. John Wiley and Sons

Suchanek TH (1983) Control of seagrass communities and sediment distribution by Callianssa (Crustacea, Thalassinidea) bioturbation J Mar Res 41: 281-298

Suchanek TH (1985) Thalassinid shrimp burrows: ecological significance of the species-specific architecture. Proceedings of the 5th international coral reef congress Tahiti Antenne museum-PHE Moorea French Polynesia p 205-210

Suess E (1973) Interaction of organic compounds with calcium-carbonate-II Organo-carbonate association in recent sediments. Geochim Cosmochim Acta 37:2435-2447

Sun MY, Aller RC, Lee C (1994) Spatial and temporal distribution of sedimentary chloropigments as indicators of benthic processes in Long Island Sound. J Mar Res 52:149-176

Thamdrup B, Fossing HB, Jørgensen BB (1994a) Manganese iron and sulfur cycling in a coastal marine sediment Aarhus Bay, Denmark. Geochim Cosmochim Acta 58:5115-5129

Thamdrup B, Glud RN, Würgler Hansen J (1994b) Manganese oxidation and in situ manganese fluxes from a coastal sediment. Geochim Cosmochim Acta 58: 2563-2570

Thessalou-Legakis M (1984) Preliminary data on the occurrence of Thalssinidea (Crustacea, Decapoda) in the greek seas. Biologia Gallo-hellenica 12:181-187

Thibodeaux LJ, Boyle JD (1987) Bed-form generated convective transport in bottom sediment. Nature 325(6102):341-343

Van Raaphorst W, Kloosterhuis HT (1994) Phosphate sorption in superficial intertidal sediments. Mar Chem 48:1-16

Van Raaphorst W and Malschaert J F P (1996) Ammonium adsorption in superficial North Sea sediments. Cont Shelf Res 16:1415-1435

van Duyl FC, Kop AJ, Kok A, Sandee AJJ (1992) The impact of organic matter and macrozoobenthos on bacterial and oxygen variables in marine sediment boxcosms. Neth J Sea Res 29:343-355

van Duyl FC, Raaphorst W, van Kop AJ (1993) Benthic bacterial production and nutrient sediment-water exchange in sandy North Sea sediments. Mar Ecol Prog Ser 100:85-95

Van Cappellen P, Wang YF (1996) Cycling of iron and manganese in surface sediments: A general theory for the coupled transport and reaction of carbon oxygen nitrogen sulfur iron and manganese. Amer J Sci 296:197-243

Van Weering TC, Berger EGW , Okkels E 1993 Sediment transport resuspension and accumulation rates in northeast Skagerrak. Mar Geol 111:269-288

Vogel S (1983) Life in moving fluids. Princeton University Press, New Jersey

Wallmann K, Hennies K, Koenig I, Petersen W, and Knauth H-D (1993) New procedure for determining reactive Fe(III) and Fe(II) minerals in sediments. Limnol Oceanogr 38:1803-1812

Walsh JJ (1991) Importance of continental margins in the biogeochemical cycling of carbon and nitrogen. Nature 350:53-55

Wang XC, Lee C (1993) Adsorption and desorption of aliphatic amines, amino acids and acetate by clay minerals and marine sediments. Mar Chem 44:1-23

Webb JE, Theodor JL (1972) Wave-induced circulation in submerged sands. J Mar Biol Assoc: 52

Webb JE, Theodor J (1968) Irrigation of submerged marine sands through wave action. Nature 220: 682-685

Webster IT, Norquay SJ, Ross FC, Wooding RA (1996) Solute exchange by c onvection within estuarine sediments Estuarine Coastal Shelf Sci 42:171-183

Webster IT (1992) Wave enhancement of solute exchange within empty burrows. Limnol Oceanogr 37:630-643

Webster IT, Taylor JH (1992) Rotational dispersion in porous media due to fluctuating flow .Water Resources Research 28:109-119

Williams RE, Lewis MS (1986) Stream model of benthic nitrification-denitrification. Journ of Environm Engin - ASCE 112(N2): 367- 386

Williams J, Elder SA (1989) Fluid physics for oceanographers and physiscists. Pergamon Press

Witbaard R, Duineveld GCA (1989) Some aspects of the biology and ecology of the burrowing shrimp Callianassa subterranea (Montagu) (Thalassinidea) from the southern North Sea. Sarsia 74:209-219

Wollast R (1991) The coastal organic carbon cycle: fluxes, sources and sinks. In: Ocean Margin Processes in Global Change. Mantoura RFC, Martin J-MR Wollast R (eds) John Wiley & Sons, London, pp 365-382

Yager PL, Nowell ARM, Jumars PA (1993) Enhanced deposition to pits: a local food source for benthos. J Mar Res 51:209-236

Yallop MLB, de Winder D, Paterson M, Stal LJ (1994) Comparative structure primary production and biogenic stabilization of cohesive and non-cohesive marine sediments inhabited by microphytobenthos Estuarine Coastal Shelf Sci 39: 565-582

Ziebis W, Forster S, Huettel M, Jørgensen BB (1996a) Complex burrows of the mud shrimp Callianassa truncata and their geochemical impact in the sea-bed. Nature 382:619-622

Ziebis W, Huettel M, Forster S (1996b) The impact of biogenic sediment topography on oxygen fluxes in permeable seabeds. Mar Ecol Prog Ser 140:227-237

SUMMARY

The investigated marine coastal area in the Mediterranean Sea (Giglio Island, Italy) was characterised by a permeable sand (5.1×10^{-11} m^2) which was densely populated (120 individuals per m^2) by the thalassinidean shrimp *Callianassa truncata* (Crustacea, Decapoda). These macrofauna organisms construct deep reaching burrows (80 cm) in the sea bed. In the course of burrowing, discarded sediment is ejected at the sediment surface forming sediment mounds (average height 4 cm). Thus, the topography of the sea floor is dominated by the high number of these biogenic structures (120 mounds per m^2) which are exposed to horizontal bottom water currents. The interaction of sea bed topography and boundary layer flows in permeable sediments was investigated in laboratory flow channels. The horizontal flows are deflected at the obstacles and the induced velocity differences generate pressure gradients that are the driving forces for advective transport of solutes and particles across the sediment-water interface.

Advective transport of oxygen from the water column into the sea bed was investigated with oxygen microelectrodes. At a smooth surface oxygen penetration depth did not exceed 4 mm, independent of flow velocity. In contrast, the topography-induced oxygen transport increased with current speed. At a current speed of 10 cm s^{-1} oxygen was transported locally down to 40 mm sediment depth at a 1-cm high mound. This increased the oxic sediment volume by a factor of 4.8. The effect of advective transport was dependent on the permeability of the sediment. In a less permeable sediment (5.4×10^{-12} m^2) from the North Sea, the effect could still be demonstrated but was less pronounced. In long-term measurements the high spatial and temporal variability of oxygen penetration in coastal sediments could be demonstrated.

The total oxygen uptake (TOU) of the sediment was also a function of flow velocity. TOU increased by 91% in coarse sand when the flow velocity was increased from 3 to 14 cm s^{-1}. An addition of algae material stimulated TOU to a larger extent in coarse sand than in fine sand, suggesting that flow-enhanced oxygen utilisation is potentially effective in permeable beds of coastal and shelf regions. This is in contrast to the situation in cohesive sediments, where the supply of oxygen is limited by diffusion.

Parallel to the advective transport of solutes across the interface particles suspended in the bottom flows are transferred from the boundary layer into the upper strata (4 cm) of permeable sediments. The transport is again driven by pressure gradients

generated when bottom flows encounter small surface structures. Increased pressure up- and downstream of small mounds (2.5 cm) drove water 5 cm into the sediment carrying suspended particles (1 µm) to 2.2-cm sediment depth within 10 h. Simultaneously pore-water fluid was drawn upward from deeper layers (10 cm) in the low pressure areas at the downstream slope of the mounds. The friction within the sediment reduced the velocity of the particulate tracers, resulting in size fractionation and layers of increased particle concentration. The results suggest that bedform-induced interfacial flows are important for the uptake of particulate organic matter into permeable shelf sediments.

In subsequent laboratory flume experiments it could be demonstrated that advective pore water flows produce biogeochemical reaction zones in permeable sediments causing specific and reproducible patterns of iron, manganese and nutrient distribution. Distinct zones of enhanced nitrification and ferric iron precipitation were generated. This inflow was balanced by ammonium-rich pore water ascending from deeper sediment layers thereby creating an anoxic channel where dissolved ferrous iron and Mn^{2+} reach the sediment surface. While a sediment with a smooth surface was a sink for metals and nutrients, the sediment with mounds revealed to be a source for these substances. The experiments showed that in permeable sands with an oxidised surface layer reduced metal species can be released to the water column by flow-topography-interactions. It is concluded that advective transport processes induced by the interaction of sediment topography and bottom water flows constitute an important process controlling biogeochemical zonations and fluxes in permeable sea beds.

The conspicuous mounds and funnels covering the sediment surface at an average density of 120 m^{-2} are the surface structures of elaborate burrow system of the thalassinidean shrimp *Callianassa truncata* (Crustacea, Decapoda). Polyester resin casts made in-situ revealed that the intricate burrows have a uniform architecture of horizontal galleries interconnected by vertical shafts reaching down to 80 cm sediment depth. At the observed abundances, the extensive burrows with a mean volume of 60 cm^3 (+/- 5 cm^3, n = 14) increased the total area of the sediment-water interface by roughly 400 %. The animals consolidated their burrows with particles cemented by mucus. In the course of burrowing, fine-grained sediment was selectively excavated and ejected to the sediment surface through the thin shaft in the mound. Roughly 7 kg sediment dw m^{-2} day^{-1} were ejected. Coarse grains, possibly too heavy to be ejected, are transported downward and are used for the construction of the chamber walls at deeper burrow levels. The selective ejection of fine grained sand into the overflowing sea water increased the bulk sediment

permeability of the whole inhabited area. As the depth intervals of galleries were very regular for all burrows, the accumulation of coarse sand grains in chamber walls resulted in distinct horizontal layers of highly permeable coarse sand.

A diver observatory was deployed in the sea floor allowing direct measurements and sampling in intact burrow systems to assess the geochemical impact of the shrimps on the sedimentary environment. The decapods produce a water current through their burrow system by a regular beating of their pleopods flushing their burrow systems with oxygen rich water. Oxygen microelectrodes were inserted horizontally into the burrows and the surrounding sediment though silicone-filled ports in the walls of the observatory. Continuous oxygen measurements at 26 cm and 48 cm sediment depth revealed that *C. truncata* maintained burrow-water oxygen concentrations at 10-40 % and 3-12 % of air saturation, respectively at the two depths. Horizontal oxygen profiles measured perpendicular to the burrow showed that oxygen penetrated 6-7 mm through the highly permeable chamber walls into the ambient sediment, whereas oxygen penetration out from the vertical shafts was only 3 mm. An oxic sediment environment of 12-25 mm diameter thus surrounded each burrow. Given the population density of 120 individuals per m^2, each 10 cm x 10 cm area of the sea bed thus contained one complex structure, some centimetres wide, of oxic sediment penetrating down at least half a meter. The flushing with oxygenated sea water also enhanced the bacterial ammonium oxidation. Ammonium concentrations measured inside the burrows were thus low (2 -14 µM) down to a depth of 60 cm. In the porewater of the surrounding sediment ammonium was depleted to < 15 µM at a distance of up to 3 - 4 cm as compared with 100 µM in surrounding sediment not inhabited by *C. truncata*. The ammonium concentration was thus kept low in the entire sediment down to at least 50 cm depth.

The laboratory investigation showed that the biogenic topography created by *Callinassa truncata* has a strong effect on interfacial transport processes and the biogeochemistry in the upper sediment. The *in-situ* studies revealed that these only 2-cm long crustaceans construct unique burrows of extreme architectural and functional complexity that influence the sediment structure and geochemistry of the entire sea bed down to a depth of 0.5 m. Burrowing crustaceans of the group Thalassinidea occur worldwide, except for the pole regions, in coastal areas. Because of their high abundances and their often deep reaching burrows they greatly influence the sediment water exchange processes and the biogeochemistry in coastal areas.

DANKSAGUNG

Ich danke Herrn Prof. Bo Barker Jørgensen für die Betreuung dieser Arbeit und die wissenschaftliche und menschliche Hilfestellung während der verschiedenen Projekte.

Ich möchte Herrn Prof. Horst Schulz danken für die Übernahme des Zweitgutachtens und der freundlichen Hilfe bei der endgültigen Fertigstellung dieser Arbeit.

Markus Huettel und Stefan Forster danke ich sehr für die nette Zusammenarbeit, Betreuung und Unterstützung, die diese Arbeit erst möglich machten.

Olaf Eckhoff, Georg Herz, Gerhard Kothe und Volker Meyer halfen bei vielen großen und kleinen technischen Problemen, die oft auch ganz schnell und in letzter Minute gelöst wurden. Ein großer Dank gilt ebenfalls Anja Eggers, Gaby Eickert, Anni Glud und Vera Hübner, die wunderbare Elektroden hergestellt haben und bei vielen technischen Fragen halfen. Susanne Menger und Martina Schütte sei herzlich gedankt für die Unterstützung und der Mithilfe bei vielen Arbeiten in der flume group.

Den Mitgliedern des Giglio Diving and Research Teams (Knut Eichstaedt, Joan Hass, Christian Lott, Thomas Pillen und Boris Unger) sei gedankt für die Unterstützung bei der Unterwasserarbeit auf der Insel Giglio.

Meinen Kollegen, Kolleginnen und allen Freunden sei ganz herzlich gedankt für die Hilfe und Unterstützung, die dazu beitrugen, die einzelnen Hürden bis zur Fertigstellung dieser Arbeit zu überwinden. Auch wenn hier nicht alle genannt werden können, bedanke ich mich ganz besonders bei allen, die mir mit Rat und Tat zur Seite standen und mich auch in schwierigen Zeiten immer wieder ermutigten. Meiner Freundin Bine möchte ich sehr danken für ihre uner-müdliche Hilfe.

Nicht zuletzt gilt mein ganz besonderer Dank meiner Familie, die mir in allen Situationen sehr geholfen hat. Ohne die Unterstützung meiner Eltern hätte ich diese Arbeit nicht duchführen können.